Gauri Misra *Editor*

Introduction to Biomolecular Structure and Biophysics

Basics of Biophysics

Springer

Introduction to Biomolecular Structure and Biophysics

Gauri Misra

Editor

Introduction to Biomolecular Structure and Biophysics

Basics of Biophysics

Springer

Editor
Gauri Misra
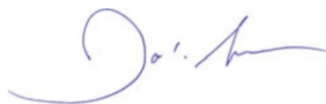Amity University
Noida, Uttar Pradesh
India

Dedicated to
The lotus feet of Shri Radha Krishna
and
Goverdhannathji

Foreword by Prof. Joel L. Sussman

Receiving is not always important; however, giving back to society can be incredibly significant. This book, *Introduction to Biomolecular Structure and Biophysics: Basics of Biophysics*, is an excellent volume of Dr. Gauri Misra to present the fundamentals and advances in the field of Biophysics to the scientific community. A journey beginning from the basic macromolecular structure, their functioning, interactions transcending to the methodology that includes the classical and new approaches makes this effort incredibly worthwhile. Contribution from the experts in the field enhances the quality of the content. Reading about new folds and structures, e.g., the Roadblock and Longin folds, is fascinating and will clearly stimulate the reader from neophyte through expert.

The book goes from classical biochemistry, e.g., amino acids, primary through quaternary structures, to very recent discoveries such as intrinsically disordered proteins. New discoveries and creative thought process keep the flame of scientific curiosity ignited. The magnitude of work done to bring forth the new advancements in the field makes the book unique. The principles of the most complex of techniques, e.g., the latest developments of cryoEM and their impact on structural biology, are explained in a very clear manner so that the student's enthusiasm remains intact while reading. This book will be useful to people working not only in biophysics but also in other scientific disciplines from chemistry through life sciences. The text is strengthened enormously by beautiful diagrams.

I strongly believe this book will be a reader's delight providing comprehensive understanding of macromolecular structure and functioning. It will be an excellent introduction for students towards biophysics and will clearly help them to develop a wider perspective of the field.

Department of Structural Biology   Joel L. Sussman
Weizmann Institute of Science
Rehovot, Israel

Foreword by Shekhar C. Mande

I am pleased to write this foreword on the book edited by Dr. Gauri Misra. Having browsed through the book, I am very happy to note that the book addresses several important aspects of modern Biophysics. Dr. Misra herself is a well-trained biophysicist; therefore she is in a good position to edit such a book. The field of Biophysics has seen several important developments in recent years, such as the advent of cryo-electron microscopy for determining high-resolution structures of proteins and macromolecular assemblies, super-resolution microscopy for high-end imaging of biological systems, hydrogen deuterium exchange, etc. For the students, to keep up with these developments is difficult, unless guided by trained biophysicists in these areas. Dr. Misra has clearly attempted to do so by bringing together experts in different fields and writing chapters on these aspects. Moreover, the fundamentals of biophysics have been well covered so that students do not miss the basics while trying to understand the modern developments. This book also provides insights into different kinds of biomolecules, including polypeptides, nucleotides, membranes, lipids, etc., in sufficient details. The structural insights into functioning of various macromolecules are explained with the help of several illustrations. Moreover, many useful resources are included as part of chapters. This book covers areas, such as protein folding, higher-order nucleic acid structures, new protein folds, conformational aspects of proteins with functional implications, thermodynamics of protein/DNA stability, etc. Dr. Misra's creative contribution as an author on the chapter on protein structure is worthy of appreciation. Thus, a good blend of fundamental biophysics, structural biology, and modern developments in biophysics has been achieved in this book. This book has attempted to provide basic understanding of simple and complex experimental and theoretical aspects of biophysics. I am therefore sure that students of biophysics at the under-graduate, postgraduate, and doctoral levels will find this book very useful.

Director, National Centre for Cell Science   Shekhar C. Mande
Pune, India

Preface

The present book is the beginning of a new chapter in my academic journey. A successful accomplished research career ignited within me the desire to disseminate the knowledge to young students which are desirous of building a career in science. I joined the university structure and started teaching biophysics and structural biology to the undergraduate, postgraduate, and doctoral students. Interaction with the students introduced me to the reality that they have an inherent apprehension for these subjects as the available resources for most of the underlying concepts in these subjects were either research articles or academic reviews. They expressed their desire to have a reference book which could encompass a comprehensive collection of basic principles in biophysics and recent research developments in the concerned field. This was the driving force behind the conception of this book.

The last few decades have evidenced tremendous growth in the macromolecular data supported by advances in technology and methodology. This upsurge in the information about proteins, DNA, and lipid structure along with fundamentals of various classical and advanced biophysical techniques used in drug discovery process needs to reach out to students in a language that is elucidating and does draw extensively upon academic jargon. This underlying motive is being attempted at in the treatment of ideas, concepts, and experiences presented in this book. There are nine chapters that form the framework of this book. The idea to encompass knowledge spanning from what is known to what is unknown in the writings from the experts in the field resulted in a concerted effort to justify the various topics. We sincerely hope our efforts will be embraced by students with appreciation and enthusiasm for learning.

Organization of the Book

I would like to present an overview of ideas that inform the organization of this book. In doing this, I would also like to foreground the salient and novel features that might draw the attention of readers and make it interesting and engaging. The book is structured in nine chapters that bring to students interesting dimensions of human understanding that relate to the subject in focus.

The first chapter highlights the fundamentals of protein structure and functioning with emphasis on the role of various structural folds and motifs. The recent research findings involving a new fold have now enhanced our knowledge in the field. The newer discovery and some implications from this work have been incorporated.

The second chapter elaborates the basic process of protein folding which is responsible for attributing them with the multitude of functions. An additional information on the computational understanding of this process including the various intermediates involved is being explained.

The third chapter navigates through the basics of DNA and RNA structure with underlying structural principles and properties. A brief outline toward the various methods used for the identification of these structures is presented in the last section of this chapter.

The fourth chapter extends the basic knowledge of nucleic acid structure to higher-order structures considering the latest developments in this domain that involves the exhaustive details of various higher-order structures, chemical principles in higher-order structural organization, thermodynamic parameters, therapeutic usage, and other biological applications of these structures.

The fifth chapter discusses the various aspects of macromolecular interactions, binding energetics, models, and other structural aspects of these interactions.

The sixth chapter deals with lipids and their classification and structural organization, various lipid assemblies, and techniques used for studying these structures with implications in various cellular processes and human health.

The seventh chapter specifically addresses the biophysical concepts in membrane biology. It highlights the different membrane parameters relating to their functioning. The physiological and metabolic relevance of various membrane-associated transport processes is also discussed.

The eighth chapter explains in detail the techniques that are commonly used in biophysics. The principle behind these techniques and the brief outline of instrumentation, recent advances in the field, and biological applications are elaborated.

The ninth chapter adds a new dimension to this book that intricately provides the knowledge about new biophysical techniques that have been recently gaining popularity to gain new perspectives of macromolecular structure, functioning, and interactions.

The understanding of science is incomplete without the aid of visuals that help us envision and mentally model the structures and processes involved. In this book, there has been a consistent effort from all the authors to include beautiful and informative illustrations and visuals for explaining the various structures and processes. The text has been kept simple, concise, and easy to understand. An effort is made to use a lucid language without compromising on the content of scientific concepts and the rationalities in order to match the expectations of its prospective target audience.

Amity University, Noida, India   Gauri Misra

Acknowledgments

Contents

About the Editor

Dr. Gauri Misra is currently working as Assistant Professor at Amity University, Noida (U.P.), India. Before joining Amity University, she has worked as Assistant Professor at Hygia Institute of Pharmaceutical Education and Research, Lucknow (U.P.), India. From 2010 to 2011, she worked as a postdoctoral fellow at CHUL Research Centre, Quebec, Canada. As a postdoctoral fellow, she focused towards understanding the role of androgen receptor in the growth and proliferation of breast cancer cells using structural biology approaches. She also contributed successfully in various collaborative projects. During her Doctoral studies at the Central Drug Research Institute, Lucknow (U.P.), India, she made an innovative contribution toward understanding the structural and functional characterization of proteins that are involved in the transit peptide-mediated pathway from *Plasmodium falciparum*. She has been the recipient of many awards including the Eli-Lilly Asia Outstanding Thesis Award (first prize) in 2009 and best oral presentation award at the "National Seminar on Crystallography-37," held in Jadavpur University, Kolkata, from 6–8th February 2008. She has been an outstanding performer receiving gold medals and honors at various stages of her academic journey. Previously, she had been selected as visiting Scientist under the INSA bilateral exchange program to visit the Israel Structural Proteomics Center situated at Weizmann Institute of Science, Rehovot, Israel, in 2014.

She is serving as reviewer for various prestigious international journals. Furthermore, she is member of many scientific societies including the Indian Biophysical Society, Indian Science Congress Association and Indian Crystallographic Association. She has also delivered invited talks at various prestigious platforms. Till date, she has authored and co-authored 12 articles in peer-reviewed journals. During the past 6 years, she has been actively involved in both research and teaching graduate and postgraduate students from diversified background of biological science, engineering, and pharma programs.

Principles of Protein Structure and Function

Juliana Helena Costa Smetana and Gauri Misra

Abstract

The present chapter highlights the structural properties of amino acids and organization of proteins into primary, secondary, tertiary, and quaternary structures. The concept of dihedral angles and Ramachandran plot is given to provide an understanding of the thermodynamically feasible protein conformations. The biophysical concepts of structural hierarchy are explained with the help of suitable examples. A deep understanding of various folds and motifs is provided to clear the theoretical aspects of protein structure and its functional implications including the recently discovered novel fold. Besides thermodynamic parameters of structural organization, various covalent and noncovalent interactions that play an important role in protein structure are explained. The important globin-containing proteins, namely, hemoglobin, myoglobin, cytochromes, and lysozyme, have been discussed with respect to their structural features responsible for their functioning. Further, the structural aspects of integral and peripheral membrane proteins are elaborated.

Keywords

Protein structure • Amino acids • Alpha helix • Beta sheet • Protein folding

J.H.C. Smetana

Brazilian Biosciences National Laboratory (LNBio), Brazilian Center for Research in Energy and Materials (CNPEM), 13083-970 Campinas, Sao Paulo, Brazil
e-mail: juliana.smetana@lnbio.cnpem.br

G. Misra (✉)
Amity University, Noida, Uttar Pradesh, India
e-mail: kamgauri@gmail.com

1.1   Structure, Classification, and Properties of Amino Acids

Proteins are the result of polymerization of **L-α-amino acids** by **peptide bonding** (Fig. 1.1). This, however, is also true for any polypeptide or small peptide. As an additional information to define what a protein is, one needs to consider that proteins, different from other polymers made of L-α-amino acids, are products of biological evolution. They have a biological function which is defined by their unique three-dimensional structures (Kyte 1991; Branden and Tooze 1999; Petsko and Ringe 2004).

Intrinsically unfolded proteins do not display a rigid structure, yet they still have a biological function which depends on their structural properties. These proteins usually adopt different conformations depending on which interaction partner is associated with them, and when free in solution they explore an ensemble of different conformations.

Amino acids are **zwitterionic** molecules, meaning that they have both acidic (carboxylate) and basic (amino) groups and have neutral net charge. However, in addition to the amino and acid groups, amino acids have a **radical group** (or side chain) covalently linked to a central carbon, the **α-carbon**. If this side chain is not neutral then the resulting molecule will be charged. There are only 20 **proteinogenic** amino acids (the ones found in natural proteins), and each one of them is specifically designated by one or more codons in the **genetic code**.
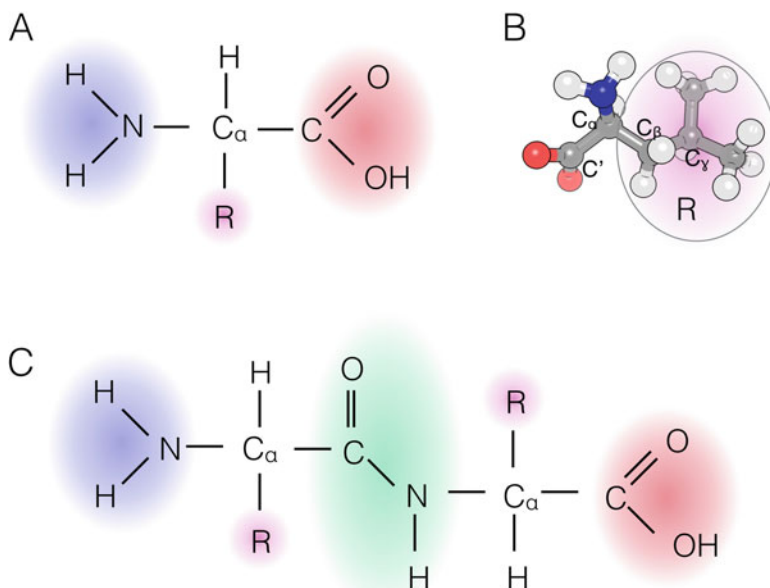

Fig. 1.1 Amino acids and peptide bond (**a**) Illustration of the general structure of alpha-amino acid R: radical group. (**b**) Example of amino acid structure (L-Leucine) in ball and stick representation. (**c**) Illustration of the peptide bond (highlighted in *green*)

The α-carbon is **chiral** and all life on earth has evolved to use only **L-amino acids** in proteins. There are only a few exceptions to this rule, such as peptidoglycans made of D-amino acids which are found in bacterial cell walls. Experiments have shown that artificial, synthetic proteins made of D-amino acids are the exact mirror images of their natural counterparts made of L-amino acids and their substrate specificity reflects this inverted chirality. The reason for the almost exclusive presence of L-amino acids in naturally occurring proteins is not well understood and might have been favored by chance.

Incorporation of an amino acid in protein results in the loss of both the amino and acidic groups due to peptide bonding; hence it is no longer called an amino acid but "amino acid residue" instead – or, for simplicity, "residue." The peptide bond is catalyzed by the ribosome in living cells and is accompanied by loss of a water molecule. The nature of the peptide bond is of a **partial double bond**, or resonance, implying that the bond is not free to rotate and the four atoms involved in this bond are **coplanar** (Fig. 1.2).

Therefore, the conformational flexibility of the backbone derives from the remaining bonds which are able to rotate around their axes: the N–Cα bond and the Cα–C bond which define, respectively, the **torsion angles phi (φ)** and **psi (ψ)** (Fig. 1.3). These angles are dihedral angles defined three-dimensionally as the angles between planes. There is a limited rotation range for each of these angles in proteins due to steric clashes. A two-dimensional plot of phi and psi angles, the **Ramachandran plot** (Fig. 1.4), (Ramachandran et al. 1963) categorizes the information about possible combinations for these angles in protein structures, highlighting regions that are allowed. Glycine behaves differently because its side chain consists of a hydrogen atom, and its allowed range of phi and psi angles is considerably broader than those of other amino acids. Repetitive patterns of these torsion angles result in secondary structure elements.

Because proteins are not circular, they have extremities which are defined by the presence of unbound amine or carboxyl groups. The amino group defines the amino-terminal or **N-terminal** which is the first to appear during ribosomal translation and usually contains the **initiator methionine**. The carboxyl group defines the carboxy terminus or **C-terminus** of the protein, the last segment to be translated. Therefore, proteins display N- to C-terminal **polarity**.

The side chain atoms are labeled with Greek letters. The atom closer to the α-carbon is β, the next one is labeled γ, and so on. The chemical bonds connecting each of these atoms define dihedral angles in the same way as the phi and psi angles of the main chain. Glycine and alanine are devoid of any degrees of freedom in their side chains; therefore only one **rotamer** exists for each of them. All the remaining amino acids can be found in different conformations or rotamers. The aromatic side

Fig. 1.2 Resonance in the peptide bond

	Distance (Å)
Cα – Cα (adjacent residues)	3.8
C' – N (peptide bond)	1.32
N – Cα (same residue)	1.45
Cα – C' (same residue)	1.52
C' – O (same residue)	1.23
N – H (same residue)	1.05
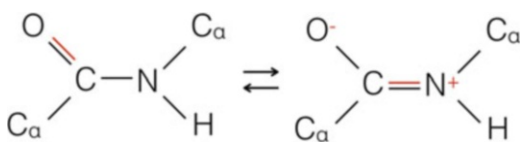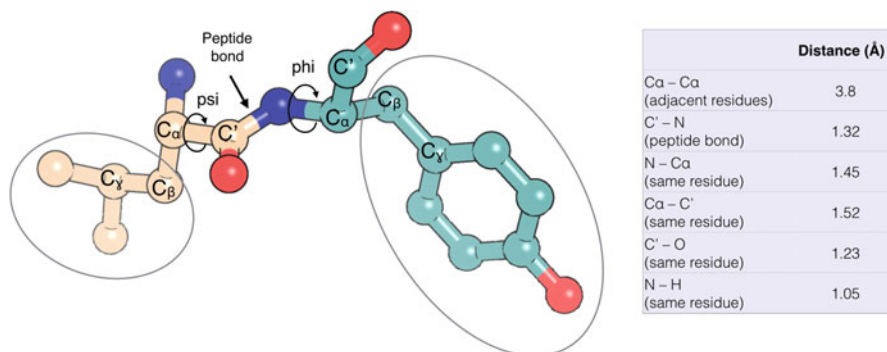
Fig. 1.3 Peptide bond and torsion angles are highlighted in the structure of a Leu–Phe bond. The table summarizes bond lengths and Cα–Cα distance (Adapted from Withford D)

white regions-sterically disallowed for all amino acids except glycine.

blue regions-allowed regions namely the α-helical and β-sheet conformations.

yellow areas-outer limit
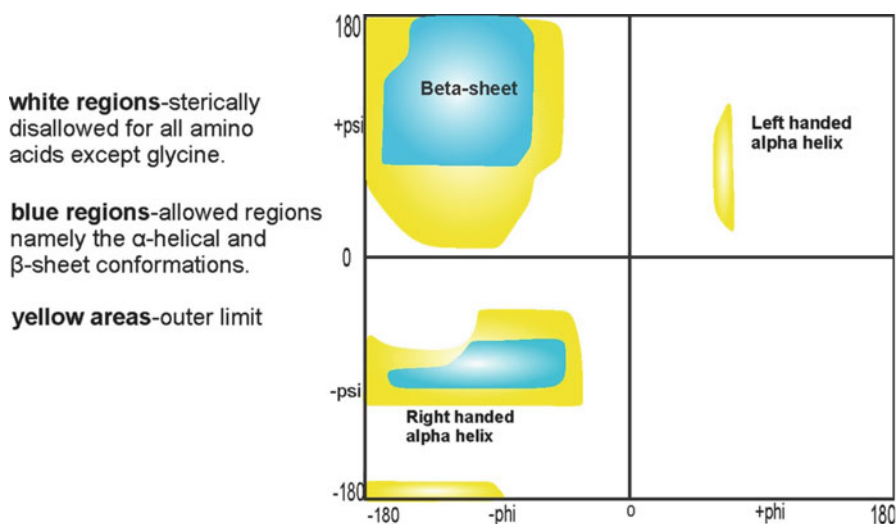
Fig. 1.4 Ramachandran plot

chains are restricted by the rigidity of double bonds, the aromatic rings are planar, and the rotational freedom is reduced. For each amino acid, some rotamers are common while others are highly unusual, and this depends on the energetics of each configuration. In general, **staggered conformations** are favored for tetragonal carbons, and *trans* are usually favored over *cis* conformations. The only way to accurately determine the conformation of one given amino acid within a protein is experimentally, usually by X-ray crystallography. The most common softwares for X-ray structure refinement are equipped with rotamer libraries to facilitate the fitting of amino acid side chains to electron density.

The proteinogenic amino acids can be **classified** in different ways according to the nature of their side chains (Fig. 1.5). In a broader way, they can be grouped as

	One letter code	Three letter code	Chemical classification	Functional group in side chain	Elements in side chain (except hydrogen)
Glycine	G	Gly	-	-	-
Alanine	A	Ala	apolar, aliphatic	alkyl (methyl)	C
Isoleucine	I	Ile	apolar, aliphatic	alkyl	C
Leucine	L	Leu	apolar, aliphatic	alkyl	C
Methionine	M	Met	apolar, aliphatic	thioether	C, S
Proline	P	Pro	apolar, aliphatic	imino acid	C
Valine	V	Val	apolar, aliphatic	alkyl	C
Phenylalanine	F	Phe	apolar, aromatic	phenyl	C
Tryptophan	W	Trp	aromatic, amphipatic	indole	C, N
Tyrosine	Y	Tyr	aromatic, amphipatic	phenol	C, O
Aspartate (Aspartic acid)	D	Asp	polar, charged (negative)	carboxylic acid	C, O
Glutamate (Glutamic acid)	E	Glu	polar, charged (negative)	carboxylic acid	C, O
Histidine	H	His	polar, charged (positive)	imidazole	C, N
Lysine	K	Lys	polar, charged (positive)	amine	C, N
Arginine	R	Arg	polar, charged (positive)	guanidine	C, N
Cysteine	C	Cys	polar, uncharged	sulpydryl (thiol)	C, S
Asparagine	N	Asn	polar, uncharged	amide (carboxamide)	C, N, O
Glutamine	Q	Gln	polar, uncharged	amide (carboxamide)	C, N, O
Serine	S	Ser	polar, uncharged	hydroxyl	C, O
Threonine	T	Thr	polar, uncharged	hydroxyl	C, O

Fig. 1.5 Classification of amino acids

hydrophobic, polar, and charged. Glycine is the simplest amino acid which is usually grouped with the hydrophobic amino acids, but due to its unique properties it is often considered to form a separate group. The **polar** amino acids can be further classified into **charged** and **uncharged**. The charged amino acids are the ones whose side chains can be fully ionized in neutral pH. They can be either positively (histidine, lysine, and arginine) or negatively charged (aspartate and glutamate). The side chains of uncharged, polar amino acids display different chemical groups: hydroxyl groups are present in serine and threonine (as well as tyrosine), sulfhydryl (thiol) is found in cysteine, and carboxamide is in asparagine and glutamine. Each chemical group endows them with unique properties: for example, cysteine is the only side chain that can form covalent bonds by means of disulfide bridges, and hydroxyl groups are frequent sites of posttranslational modifications such as phosphorylation. **Hydrophobic**, apolar amino acids can be further classified into **aromatic** and **aliphatic** side chains. Amino acids with aromatic side chains include phenylalanine, which has a benzene group as side chain, tyrosine, and tryptophan, the bulkier amino acid. Together, the aliphatic amino acids leucine, isoleucine, and valine constitute the **branched-chain amino acids** (**BCAA**), defined as aliphatic amino acids with a branch point in their side chains.

1.2 Structural Levels of Proteins

1.2.1 Primary Structure

Linear amino acid sequence in a protein joined together by the peptide bonds defines its primary structure. In essence, the sequence defines the structure and function of the protein, as we will see in the coming sections. It can be represented by the one-letter or three-letter codes for amino acids. For example, both M-A-E-D (one-letter code) and Met-Ala-Glu-Asp (three-letter code) describe the same stretch of residues in a protein, i.e., a stretch of its primary sequence. The primary structure is represented from N-terminus to C-terminus, compatible with the 5′ to 3′ orientation of the DNA and RNA sequences that codify proteins. It can be inferred from the DNA or RNA sequence using the genetic code table. The usual amino acid residue found in the N-terminal extremity of the primary structure in natural proteins (i.e., those expressed in a cell, as opposed to those produced synthetically) is **methionine**, which is specified by the **ATG start codon**. In bacteria, **formyl-methionine** is used as the initiator residue instead of methionine.

1.2.2 Secondary Structure

The repetitive patterns of phi and psi angles of the polypeptide backbone define what is known as **secondary structure**. The classical regular secondary structure elements frequently found in proteins are the **α-helix**, **β-strand**, and the **reverse turns,** in addition to **loop regions** characterized by the lack of a repetitive pattern.

In the Ramachandran plot, each type of secondary structure corresponds to one of the allowed regions in the graphic.

The **α-helix** was predicted by Linus Pauling based on the known chemical structure of polypeptides, including the fact that the peptide bond is planar and the C–N distance within this bond is 1.32Å (Pauling et al. 1951). Using a piece of paper, he drew an extended polypeptide chain and folded it in a way that would maximize the noncovalent interactions. The model, a "hydrogen-bonded helical configuration of the polypeptide chain," was published in PNAS in 1951 along with a second helical model. The structure of myoglobin, the first three-dimensional protein structure to be solved, was composed mostly by α-helices showing the exact geometry predicted by Linus Pauling.

The geometry of the α-helix is defined by the repetitive phi and psi angles found in this structural element, which are, respectively, $-57°$ and $-47°$. These angles are found in the bottom left quadrant of the Ramachandran plot. This combination of angles results in a favorable geometry where all the main-chain N and O atoms are connected by hydrogen bonding. The α-helix has 3.6 residues per turn, and the hydrogen bonds are formed between C′=O of one residue and N–H of another residue, skipping three positions: C′=O of residue 1 pairs with N–H of residue 5, residue 2 with 6, and so on (Fig. 1.6). The α-helices found in proteins are **right-handed** because they are made of L-amino acids.

There are other possible helical elements of secondary structure in proteins which are, however, very rare and energetically unfavorable. The 3_{10}**-helix** is formed when a residue N makes a hydrogen bond with residue N + 3, and the **π-helix** occurs when residue N connects in such a way with residue N + 5. The name of the 3_{10}-helix derives from the fact that it has exactly three residues per turn and ten atoms between the hydrogen bond donor and acceptor. Using the same logic, an α-helix would be a 3.6_{13}-helix, although this nomenclature is not usual. The top view of a 3_{10}-helix is triangular (Fig. 1.7).

The definition of a **π-helix** implies that if a single amino acid insertion occurs in the middle of an α-helix, it could be accommodated by locally adopting the dihedral angles of a π-helix. In fact, these insertions are the proposed evolutionary origin of π-helices, and these are usually found as short elements within α-helices, frequently close to functional sites, rather than as isolated structural elements (Cooley and Karplus 2010).

β-strands, also predicted by Linus Pauling, (Pauling and Corey 1951) are extended structures stabilized by hydrogen bonds between the amide N–H and C=O groups from the main chain (Fig. 1.8). They are usually represented as arrows in schematic representations of protein structures. These groups protrude laterally, making connections with the same kind of groups from an adjacent strand. Two or more β-strands connected in this way form a **β-sheet**. These connections can be either parallel or antiparallel. The amino acid side chains protrude up and down from the β-sheets in an alternating pattern. Typical geometric parameters in β-sheets are the distance of 3.3 Å between consecutive residues and the phi and psi angles which are $-130°$ and $125°$, respectively. They are also characterized by a pronounced **right-handed twist** originating in steric effects attributed to the
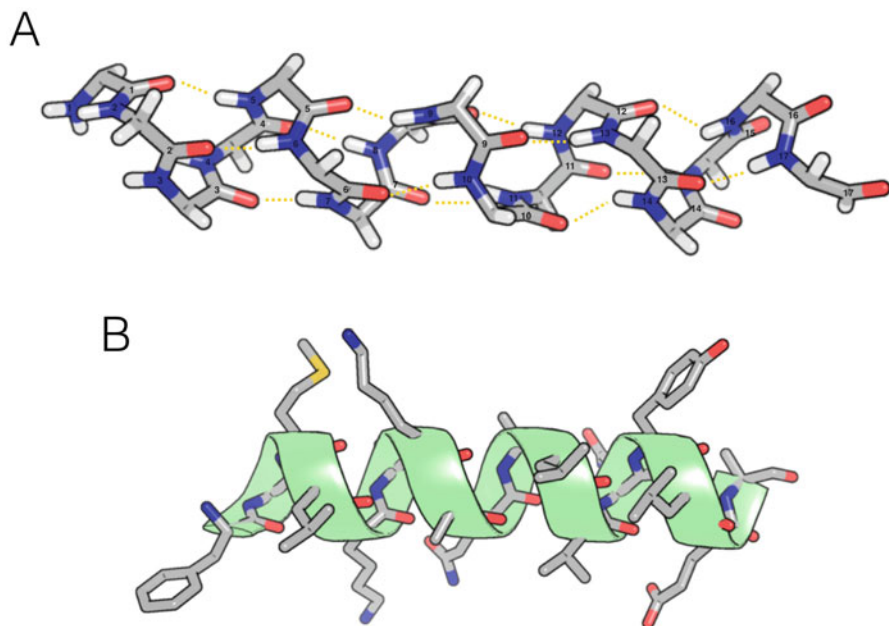
Fig. 1.6 Secondary structure: alpha helix. (**a**) Representation of an alpha helix shown here in stick representation (upper panel). The amino acid side chains were omitted. Hydrogen bonds are represented as dashed lines, and the amino acid residues are numbered. (**b**) Illustration of an alpha helix combining sticks and cartoon representation. Carbon, *gray*; Nitrogen, *blue*; Oxygen, *red*; Hydrogen, *white*; Sulfur, *yellow*

presence of L-amino acids; this twist allows them to form saddlelike structures and closed, circular structures.

Both α-helices and β-sheets can be **amphipathic** or **hydrophobic.** Amphipathic helices and sheets are found on the surfaces of proteins, allowing one of the sides to engage in hydrophobic interactions with other structural elements inside the protein's core, while another side is polar and exposed to solvent. β-sheets formed exclusively by hydrophobic amino acids are often found in the interior of proteins, particularly when they form parallel sheets. Hydrophobic antiparallel β-sheets as well as hydrophobic α-helices are typically found as transmembrane structures, in the form of β-barrels and single-span helices, respectively.

Loop regions are stretches of irregular structure (the angles phi and psi do not follow regular patterns) connecting helices, sheets, and other regular elements, and they are usually localized at the surface of proteins. These regions are frequent sites of insertions and deletions as their irregular structures are more amenable to accommodate changes than regular secondary structure elements. Loops are also functionally important elements in active sites of enzymes, antigen-binding sites of antibodies, and in protein–protein and protein–small molecule interfaces. Charged and polar residues are common in loops, and both their side chains and main chains (C′=O and NH groups) are involved in hydrogen bonding with solvent or ligands.
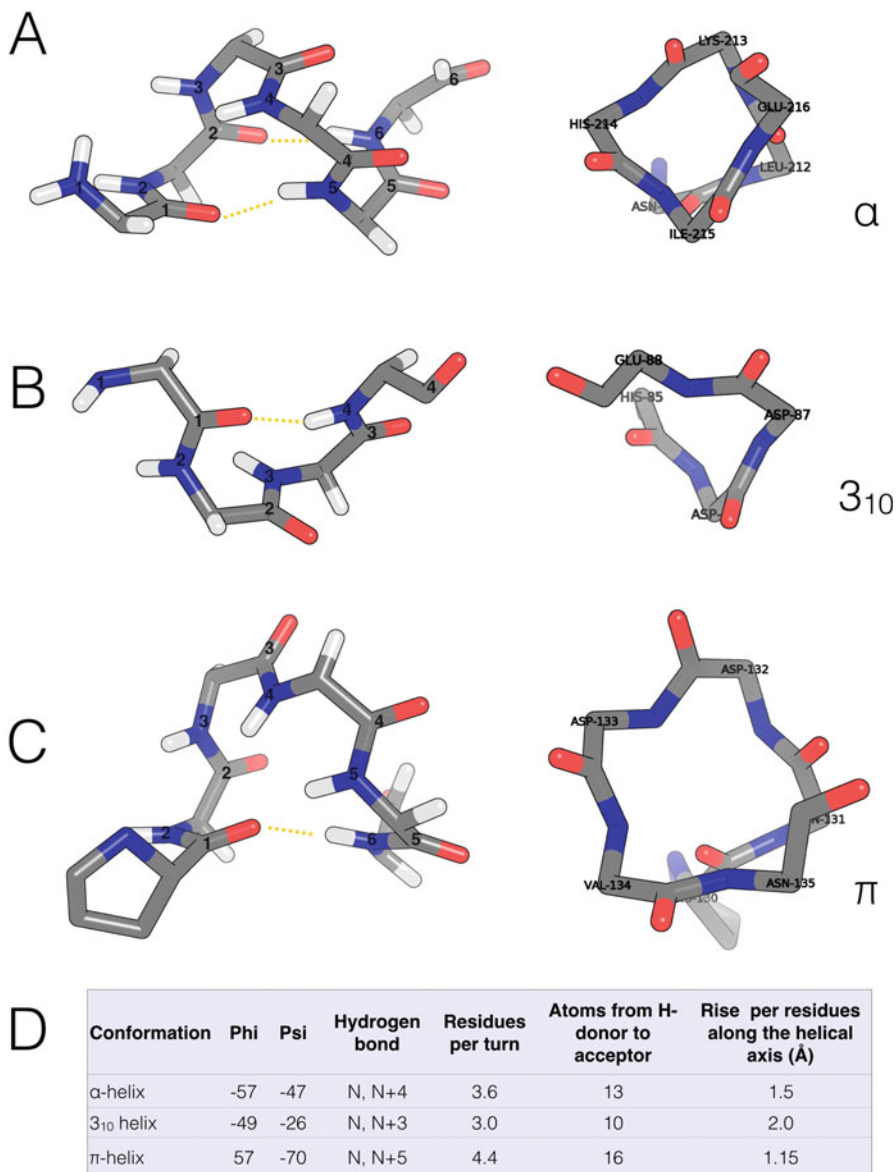
Fig. 1.7 Secondary structure: helical elements. Stretches of amino acid residues adopting α-helical (**a**), 3_{10} (**b**), or π-helical (**c**) configurations were extracted from the structure of fumarase C (PDB: 1FUO). The left panels show side views and the numbering of residues is relative. Side chains are omitted for clarity, except for proline. The *right panels* show upper views where the amino acid residues are labeled according to the original PDB file. Side chains (except proline) and hydrogen atoms are omitted. Carbon, *gray*; Nitrogen, *blue*; Oxygen, *red*; Hydrogen, *white*. Figure adapted from Weaver, 2000. (**d**) Summary of the properties of the α-helix, 3_{10}-helix, and π-helix (Adapted from Petsko and Ringe)

Table (panel D):

Conformation	Phi	Psi	Hydrogen bond	Residues per turn	Atoms from H-donor to acceptor	Rise per residues along the helical axis (Å)
α-helix	-57	-47	N, N+4	3.6	13	1.5
3_{10} helix	-49	-26	N, N+3	3.0	10	2.0
π-helix	57	-70	N, N+5	4.4	16	1.15

Fig. 1.8 Secondary structure: antiparallel beta-sheet. (**a**) A stretch of amino acids in β-sheet connected by a β-hairpin structure/type I turn, shown here in stick representation (*upper panel*). The amino acid side chains were omitted (they would be protruding above and below the plane of the figure). The same peptide is shown below in cartoon representation. (**b**) In beta-sheets, the amino acid side chains protrude up and down in an alternating fashion

The length of loops in proteins is variable, ranging from two to around 20 residues in the majority of proteins, although there is no upper limit for their size. Long loops account for a protein's mobility, as their irregular structure allows them to adopt variable conformations, sometimes in a regulated fashion responding to stimuli. Short loops of only two to four residues are more rigid. **Hairpin loops** are short loops connecting adjacent antiparallel β-strands. **Turns** are also considered to be a special type of short loop with defined characteristics. The terms hairpin loop, beta turn, and reverse turn are often used interchangeably.

The constraints for polypeptide chain reversal by turns were established by Venkatachalam in 1968 (Venkatachalam et al. 1968). **Reverse turns** are stretches of four amino acid residues in which the peptide chain undergoes a nearly 180° reversal, forming a hydrogen bond between the C=O group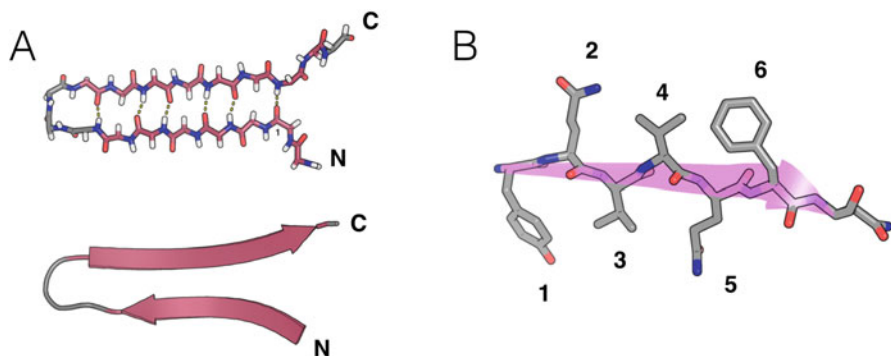 of residue N and the NH group of residue N+3. Considering the possible conformations of residues in turns, Venkatachalam identified three types of reverse turns based on their allowed dihedral angles. In **type I turns**, φ_2, ψ_2, φ_3, and ψ_3 are −60°, −30°, −90°, and 0°, respectively. In **type II turns**, these angles are −60°, 120°, 80°, and 0° (Fig. 1.9). **Type III turns** display the angles −60°, −30°, −60°, and −30°, which are actually identical to the **3_{10}-helix**. If all the signs of these dihedral angles are reversed, the turns are classified as types I′ II′, and III′, respectively, which are also allowed conformations. There is a tolerance of about 15° for each of these angles (Crawford et al. 1963).

Some amino acids are more likely to be found in α-helices, while others in β-sheets, turns, or loops. Long side chains, such as those of Leu, Met, Gln, are frequently found in α-helices, while branched-chain amino acids (Val, Ile) and bulky side chains like Trp, Tyr, and Phe are usually found in β-sheets. Proline and glycine have a strong preference for turns because of their unique conformations. Proline is favored at the second position in both type I and type II turns, while it is
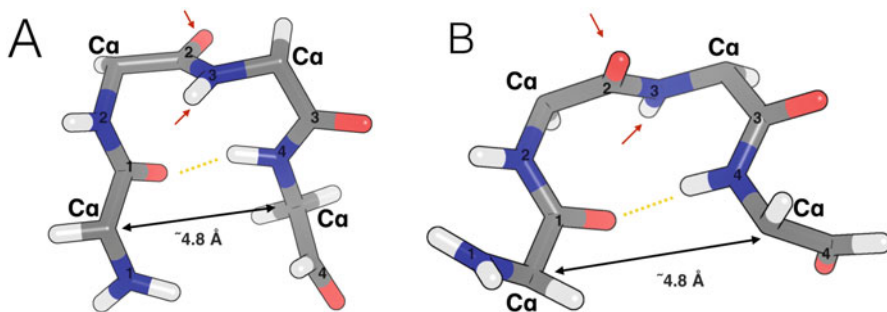
Fig. 1.9 Secondary structure: reverse turns. Examples of residues adopting the indicated conformations were taken from the lysozyme structure (PDB: 193L) and carboxypeptidase A structure (PDB: 5CPA) according to their classification by Crawford et al. (1972). (**a**) Type I turn (residues 41–44 of carboxypeptidase A; sequence: Ser-Tyr-Glu-Gly). (**b**) Type II turn (residues 17–20 of lysozyme, sequence: Leu-Asp-Asn-Tyr). Residues are numbered from one to four according to their positions in the turn. The double-headed arrows indicate the distance between Cα carbons of the first and last residues. The red arrows indicate the major differences between type I and type II turns, located in the relative positions of C=O (second residue) and NH groups (third residue). In type I turns, the oxygen atom is projecting to the back, and the hydrogen is projecting to the front in the orientation shown in the figure. In type II turns, these positions are inverted. Side chains are omitted for clarity. Carbon, *gray*; Nitrogen, *blue*; Oxygen, *red*; Hydrogen, *white*

not allowed at the third position in type I turns. However, as a rule, no amino acid is forbidden in any type of secondary structure – even proline can participate in α-helices where it causes a distortion of the hydrogen bond pattern that sometimes can be accommodated with a small kink.

Secondary structure can be inferred with high accuracy from primary structure using bioinformatics tools. Experimentally, the global secondary structure content can be determined spectroscopically using circular dichroism or infrared spectroscopy.

1.2.3 Tertiary Structure

A **fold** is characterized both by the relative position of secondary structure elements and by the arrangement of their connections. **Topology** refers to the interconnections among secondary structure elements. The usual topological representation of proteins depicts α-helices as cylinders and β-sheets as arrows in a flat projection of secondary structure elements and their connections. Alternatively, flat representation of protein topology can be depicted as if the observer is looking at the secondary structure elements from top to bottom. In this case, α-helices are represented as circles and β-strands as triangles which point up or down to indicate the direction of the strand.

Examples of different folds showing similar structural elements but different topologies are the roadblock and longin folds (Levine et al. 2013) (Fig. 1.10). These
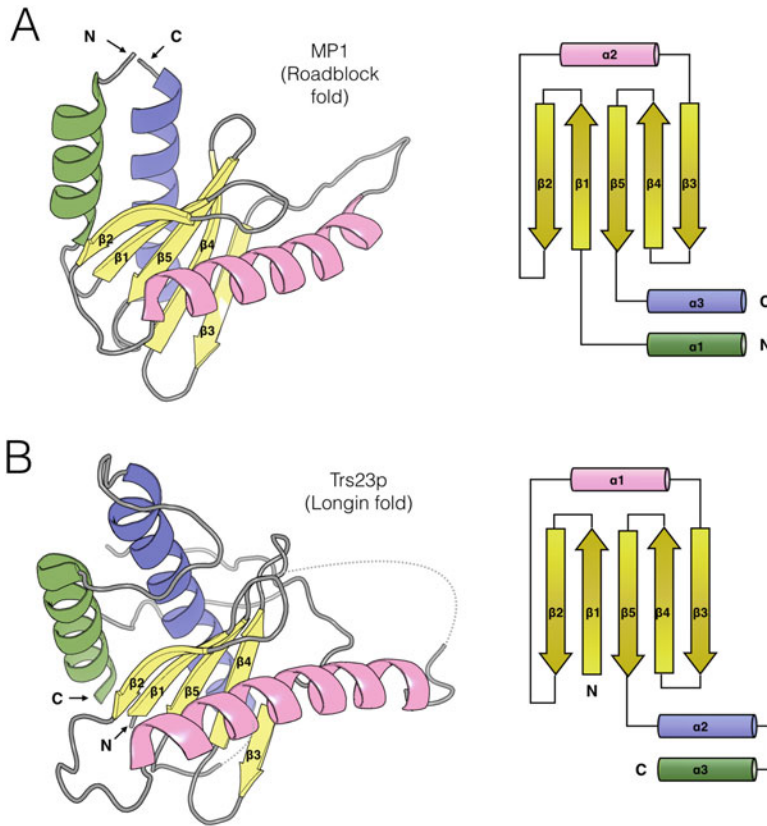
Fig. 1.10 Different topology results in different fold. (**a**) MP1 adaptor protein, a roadblock fold protein (PDB 1VET, chain B). (**b**) Yeast protein Trs23p, a longin fold (PDB 3CUE)

folds are present in adaptor proteins involved in vesicle trafficking, motility, and GTPase regulation. The relative three-dimensional positions of the secondary structure elements in roadblock and longin folds are very similar: both are α/β domains of three α-helices organized around a core of five antiparallel β-strands. However, one of these α-helices is positioned N-terminally in the roadblock fold, while it is located C-terminally in the longin fold. This is likely the result of an ancient event of circular permutation from a common ancestor fold.

The number of protein folds in nature is large but finite. As more and more protein structures become available, it becomes increasingly rare to find novel folds. Several efforts have been made to categorize and explore the wealth of structural information currently available. The major resources dedicated to categorize protein folds and structures are the online **databases CATH** and **SCOP**. CATH is an acronym for Class, Architecture, Topology/fold and Homologous superfamily. According to the latest census available in the CATH database, there are 2737 superfamilies. In SCOP (Murzin et al. 1995), domains are defined

as structurally and functionally independent evolutionary units that can either fold in a single-domain protein on their own or recombine with others to form part of a multidomain protein. Figure 1.11 illustrates an example of a recently described protein fold. The human TIPRL structure reported by Scorsato et al. (2016) displays two layers of antiparallel β-sheet surrounded by α-helices and the rare 3_{10}-helices as well as a considerable amount of random loops in a completely novel architecture. This structure is likely the representative of the conserved Tip41/TIPRL family fold, belonging to regulatory proteins that modulate the activity of type 2A serine/ threonine phosphatases.

Protein domains are classified in families according to the types of secondary structure present in them. α-domains are made exclusively of α-helices and β-domains exclusively of β-sheets, and there are two types of mixed structures: α/ β domains and α + β domains. All of these also have elements of random structure (loops) connecting the helices and sheets. Additionally, some protein domains are stabilized by disulfide bridges and coordination of metal ions rather than secondary structure elements; these are known as crosslinked domains.

Multidomain proteins are, by definition, constituted by more than one domain in a single, continuous polypeptide chain. They evolve by gene duplication, divergence, and fusion. Each domain in a protein can fold and function independently, while still suffering influences from the other domains. The relative independence of protein domains is illustrated by the fact that isolated domains from multidomain proteins can be expressed in heterologous systems, characterized biochemically and functionally, and even crystallized. In fact, this is often the only way to get high resolution information on some large multidomain proteins which are frequently too flexible to be crystallized.

α-domains are fundamentally organized upon the relatively few possible ways to pack α-helices against each other. In soluble globular proteins, these helices are usually amphipathic, meaning that they have a polar side facing the solvent and a hydrophobic side facing another α-helix. Most of the helix–helix packing found in globular α-domain proteins can be explained by the "ridges in grooves" model (Fig. 1.12). The side chains in the surface of α-helices form ridges and grooves which interdigitate, forming connections that stabilize the interaction. There are two ways to trace imaginary parallel lines connecting the side chains in α-helices to define the ridges. If we pick the side chains which are four residues apart, these would form an angle of 25° relative to the direction of the helix. Instead, if we choose to pick side chains separated by three residues, the imaginary lines form an angle of −45°. If we try to pack two helices according to the 25° angles so that the ridges defined by these lines will interdigitate with the grooves in the other helix, we would have to turn one of the helices so that the angle between them is $25 + 25 = 50°$. Another possible scheme is combining the 25° lines in one helix with the −45° lines in another helix, which would result in an angle of $25° – 45° = −20°$. In fact, 50° and −20° are two of the most frequent angles found in helix–helix packing. The −20° angle is found in the **four-helix bundle**, a common structural motif characterized by four helices packed in a bundle which can be either parallel or antiparallel (Fig. 1.13). Some of the simplest α-domain proteins, such as the human
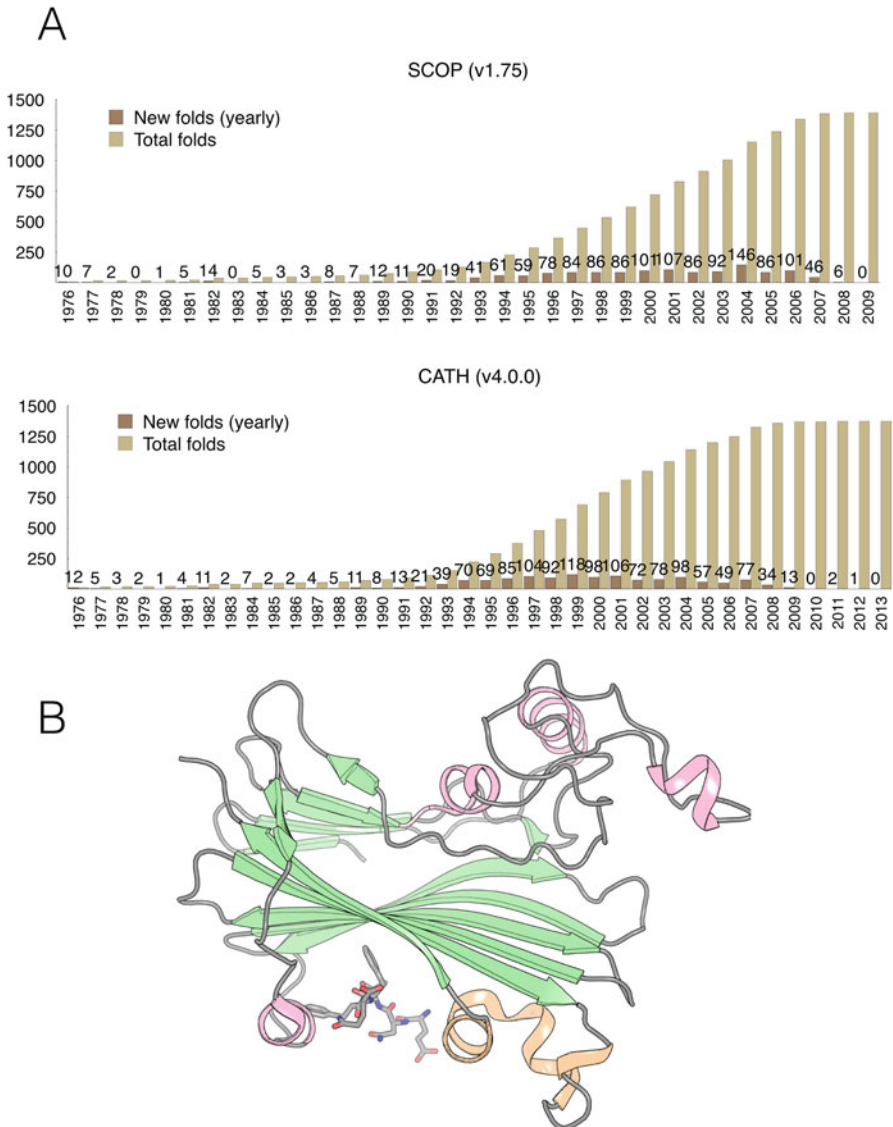
Fig. 1.11 The scarcity of novel folds. (**a**) The number of novel folds deposited on the PDB each year according to CATH (lower panel) and SCOP (*upper panel*). *Red lines* indicate the number of structures, and *blue lines* indicate the number of novel folds per year. (**b**) A recently described fold of a human protein: the TIPRL/hTip41 protein, a regulator of type 2A phosphatases (PDB 5D9G, released in 2016). The fold has a peptide-binding cleft which accommodates the extreme C-terminus of PP2Ac. The peptide is displayed as sticks
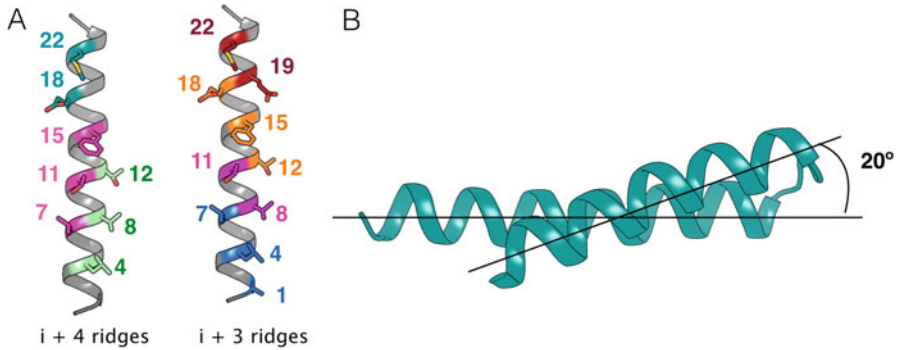
Fig. 1.12 The ridges-in-grooves model of helix packing. (**a**) The two ways to ridges (amino acid side chains) on the surface of alpha helices: the $i + 4$ model, forming parallel lines of 25°, and the $1 \neq 3$ model, forming parallel lines of −45°. Each ridge is formed by residues of the same color. (**b**) The $i + 4$ and $i + 3$ ridges/lines packing results in an angle of 20° between the packed helices
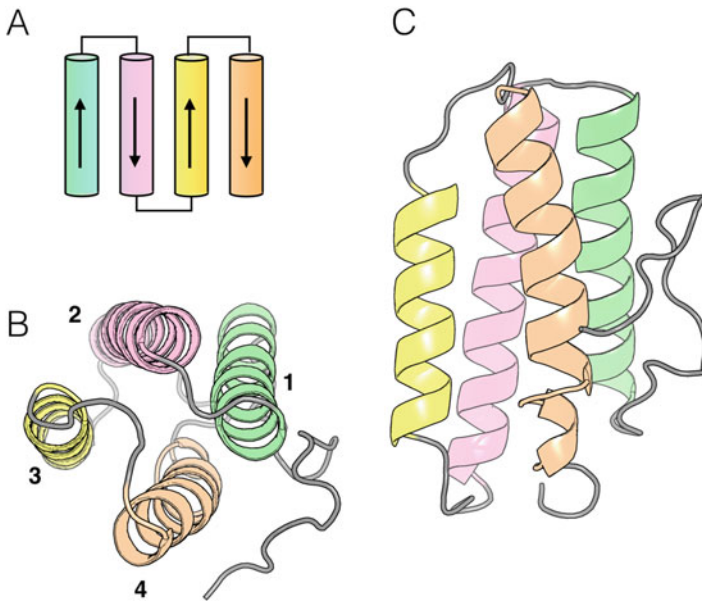
Fig. 1.13 α-domains: the 4-helix bundle of myohemerythrin (PDB 2MHR). (**a**) The up-and-down topology of the 4-helix bundle in myohemerythrin. (**b**) Top view of the 4-helix bundle. The helices are numbered from N- to C-terminus. (**c**) Side view of the 4-helix bundle

growth hormone, are formed only by the four-helix bundle. Another common α fold is the **globin fold**, in which the 50° packing angle is found between some of its eight helices.

In **β-domains**, the β-strands are arranged in antiparallel β-sheets because there are no helices to make the kind of connections observed in parallel β-sheets. There
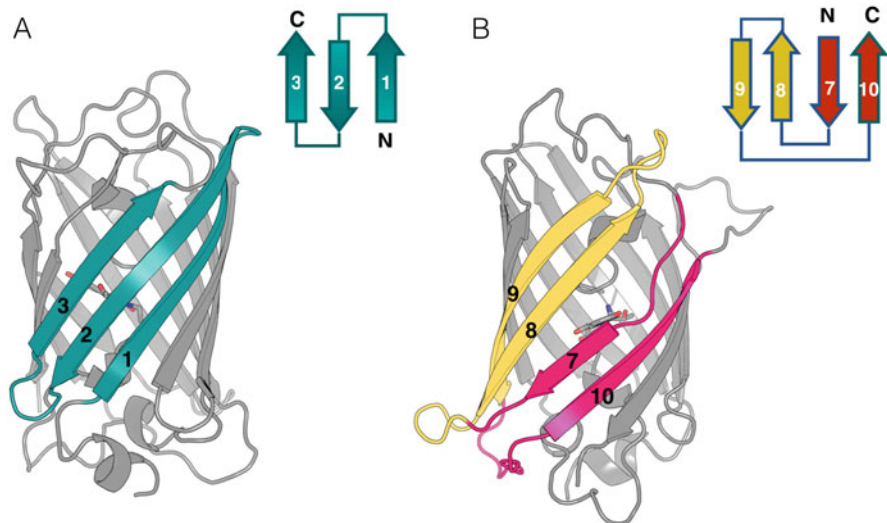
Fig. 1.14 Illustration of beta motifs in the structure of the green fluorescent protein (GFP), PDB: 1EMA. The structure is shown in cartoon representation, except for the chromophore, which is shown as sticks. The *top-right panels* illustrate the topologies of the highlighted motifs. (**a**) Strands 1–3 in the structure of GFP form an antiparallel up-and-down motif, as well as strands 4–6 (not shown). (**b**) Strands 7–10 in the structure of GFP form a Greek key motif

are two major types of connectivity in β-domains: up-and-down and Greek key motifs, both of which can be found in the two major types of β fold: the β-barrel and β-sandwich.

In the **up-and-down** motif, the β-strands go up and down as the name suggests, forming sequential antiparallel interactions. The **Greek key**, a structural motif of antiparallel β-sheets named after a common decorative element found in ancient Greek vases, is slightly more intricate than its up-and-down counterpart. To understand how a Greek key is organized, imagine a segment of four β-strands of similar size numbered from 1 to 4 (from N- to C-terminus). Then fold it in half between strands 2 and 3 forming a hairpin structure, so that strands 2 and 3 are hydrogen bonded in an antiparallel fashion, as well as strands 1 and 4. Finally, fold it again in half so that strands 3 and 4 also engage in antiparallel interactions. A single antiparallel β-domain can be formed by up-and-down motifs, Greek keys, or combinations of these motifs, such as in the green fluorescent protein (Fig. 1.14).

A **β-barrel** is a continuous antiparallel β-sheet where the first and last strands are hydrogen bonded to each other, closing the structure in the shape of a barrel. This kind of structure fulfills most if not all of the hydrogen bonding potential of the main chain within itself. This makes it especially suited for transmembrane proteins because no polar groups are left without hydrogen bonding, which would be unfavorable in the hydrophobic interior of membranes (considering that the side chains are all hydrophobic in the face exposed to lipids). In fact, transmembrane domains made of β-sheets often form barrels, which make good pores because they

can have a polar surface in the inner side of the barrel and a hydrophobic surface in the outside. β-barrels can also be found in soluble proteins, one such example is the green fluorescent protein (GFP) described above.

A **β-sandwich** is characterized by two β-sheets packed against each other, reminiscent of two slices of bread. These sheets usually display a polar surface exposed to solvent and a hydrophobic surface facing the other sheet, forming the hydrophobic core of the domain. In each of these interacting sheets, the strands located in the extremities have exposed polar groups in their main chains which can engage in hydrogen bonding with solvent or with side chains. The immunoglobulin fold is a typical example of β-sandwich fold.

α/β domains usually display variations on the theme of β-α-β structural motif. The β-sheets are either parallel or mixed. When they are parallel, the α-helix functions as a connectivity element between two strands. The connectivity of β-α-β structural motif can be either left-handed or right-handed, but due to the right-handed twist of the β-sheet, it is found to be right-handed in more than 95% of protein structures. α/β domains display two types of fold: the α/β barrel and the α/β twist.

The **α/β barrel** is formed by tandem repeats of the α-β-α motif forming a closed barrel-like structure. A minimum of four repeats is able to form this kind of structure, but the presence of eight strands in the barrel confers highest stability. The core of the barrel is formed by the parallel β-strands organized as a closed β-sheet, and the outer side is occupied by the connecting amphipathic α-helices which have a hydrophobic side packed against the sheet and an outer polar side facing the solvent. Although the α/β barrel might seem to have an inner hole when represented as cartoon, its core is usually filled with hydrophobic side chains from the β-strands. The eight-stranded version of this fold is called the **TIM barrel** because it is found in the enzyme triosephosphate isomerase (TIM). It is the most common fold, occurring in 10% of enzyme structures (Fig. 1.15). These enzymes, despite sharing a common fold, display a broad range of enzymatic activities.

Another common fold in α/β proteins is the **α/β twist**, also known as the **nucleotide-binding fold** because it is present in many nucleotide-binding proteins. It differs from the α/β barrel mostly because of its open structure. The core is formed by an open parallel β-sheet twisted in a saddlelike shape. A classical example of this category is Rossmann fold (Fig. 1.16) that consists of basic **β-α-β repeat** unit connected by loops. This is one of the most common folds present in most of the enzymes involved in nucleotide binding.

α + β domains are characterized by the presence of α-helices and β-sheets, but here these structural elements are found as segregated entities instead of the alternating pattern of helices and sheets found in α/β domains. This allows greater structural variability in these domains, because there are no special organizing principles underlying their structures. Winged helix domain is an example of α + β domain structure found in DNA-binding proteins. The domain is formed by an association of three alpha helices with three beta-sheets that interacts with the major groove of DNA. The two small winglike structures can interact with different regions on DNA. Several transcription factors such as LexA, arginine, or biotin
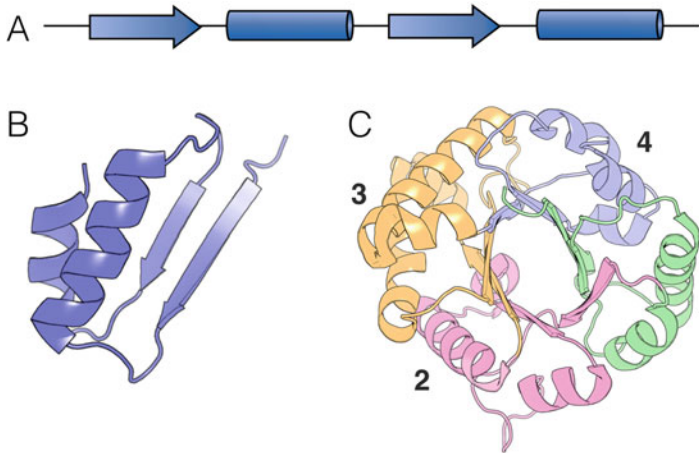
Fig. 1.15 α/β structures: the TIM barrel. (**a**) Schematic representation of a β-α-β-α motif. A TIM barrel fold is made of four tandem repeats of this motif. (**b**) Structure of the β-α-β-α motif of a TIM barrel from yeast. (**c**) The TIM barrel fold (PDB 1YPI). The motifs are numbered from N- to C-terminus

Fig. 1.16 Rossmann fold
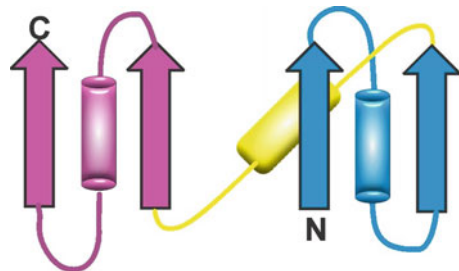
repressor proteins contain winged helix domain where it plays an important role in protein–protein interactions (Fig. 1.17).

1.2.4 Quaternary Structure

The arrangement of proteins in oligomeric supramolecular assemblies defines what we know as **quaternary structure**. These can be **homooligomers** (made of identical subunits) or **heterooligomers** (made of distinct subunits which can be structurally related or completely unrelated). There are specific names to reflect the number of subunits in the oligomeric assembly: dimer, trimer, tetramer, pentamer, and hexamer, indicating the presence of two, three, four, five, or six subunits, respectively. Oligomeric assemblies of proteins are also called **protein complexes**.
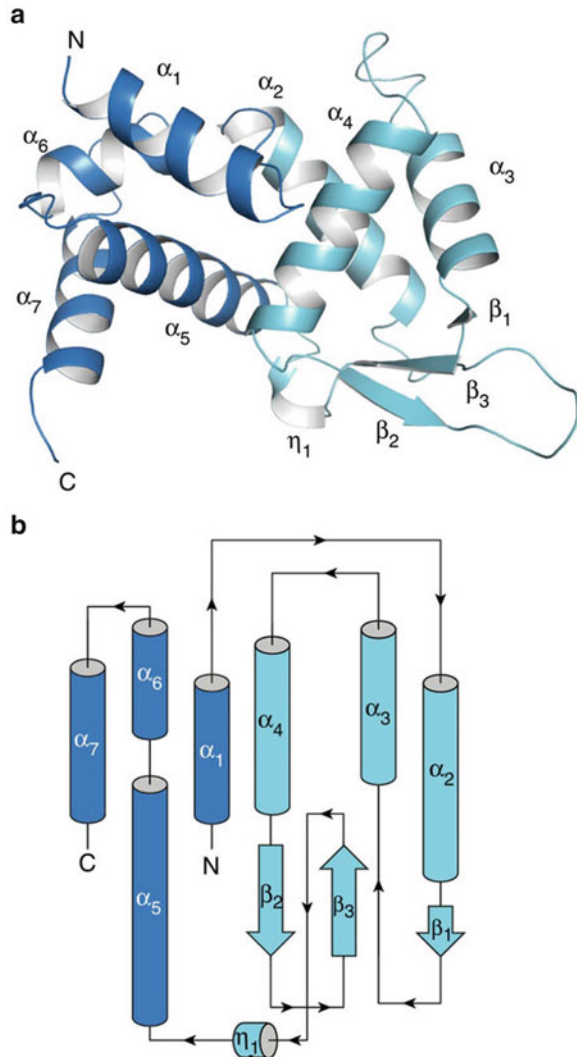
Many heterooligomers are made of structurally related subunits that sometimes do not display significant sequence similarity. Their evolutionary origin involves gene duplication and divergence. However, contrasting with the evolution of multidomain proteins, in the case of oligomers there is no gene fusion so the peptide chains remain as separate entities.

The forces that hold oligomers together are the same types of noncovalent forces that stabilize the tertiary structure. The subunits display complementary surfaces allowing them to engage in noncovalent interactions which stabilize the interfaces.

Fig. 1.18 Quaternary structure: example of a pseudosymmetric heterodimer, the MP1-p14 adaptor complex (PDB: 1VET). The subunits MP1 and p14 are shown separately (*above*) and then in the complex (*below*). Each one of them has a roadblock fold
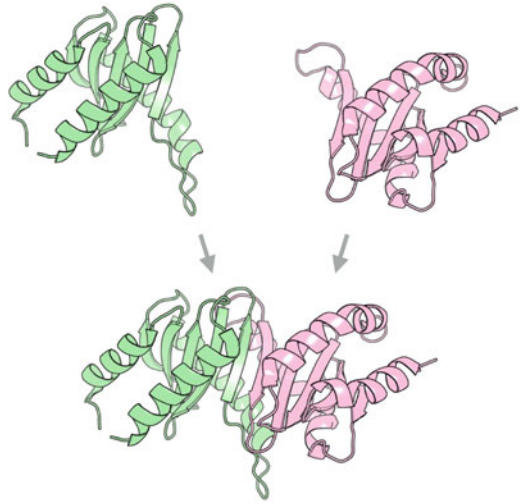
In extracellular and secreted proteins, disulfide bridges can help to stabilize the interfaces of oligomers.

The relative strength of binding between subunits of a complex is variable, and there are several ways to measure it. Whenever the high resolution structure of the complex is available, it is possible to measure the interface area with high accuracy, which is a strong predictor of the biological relevance of the interface. Some protein complexes have high dissociation constants and are found in equilibrium under normal temperature and pH, while others are virtually indissociable reflecting a small dissociation constant and tight packing of subunits.

Homooligomers have a strong tendency to form **symmetric structures**. Homodimers are always symmetrical and are able to form parallel or antiparallel arrangements (also known as head-to-tail dimers). Homotrimers usually have a central threefold rotation axis. Tetramers often form tetragonal structures, but they can also be arranged as a planar assembly with a central fourfold symmetry axis. Planar assemblies with central symmetry axis of the same order of the number of subunits are also frequently found in pentamers, hexamers, and heptamers. Another frequent way to assemble hexamer is a trimer of dimer with central three fold axis (Misra et al. 2009). In the case of heterooligomers of structurally related subunits, these symmetric arrangements have their **pseudosymmetric** counterparts. Hemoglobin, for example, is a pseudosymmetric tetramer made of two α and two β subunits which are nearly identical. Another example of pseudosymmetric quaternary assembly is the MP1–p14 adaptor complex, a dimer of two roadblock folds (Fig. 1.18) (Kurzbauer et al. 2004). Even protein complexes made of unrelated subunits, which are usually asymmetrical, can form symmetric assemblies if the entire unit repeats itself at least once around a symmetry axis.

1.2.5   Forces Stabilizing Protein Structures

Protein folding is the process by which an extended polypeptide chain adopts its native three-dimensional conformation. Although it is believed that a protein's primary sequence contains all the information necessary to define its fold, predicting a protein's structure ab initio with high accuracy is still a major unsolved problem in biophysics (Murphy 2001).

A landmark experiment performed by Christian B. Anfinsen (1973) is considered to be the fundamental demonstration that protein folding can occur spontaneously and that a protein can adopt its native conformation in the absence of any information other than its own primary sequence. In this experiment, he used the bovine pancreatic ribonuclease A (RNAse A) enzyme. The enzyme was denatured in the presence of 8 M urea (a chaotropic agent) and β-mercaptoethanol (a reducing agent to break the S–S bonds). Upon removal of the denaturing agents and addition of oxidizing agents to promote S–S bonds, the protein was able to fully recover its enzymatic activity. RNAse A has eight cysteine residues which form four S–S bonds in defined positions, which characterize the native state of this enzyme. Theoretically, these eight S–H groups could be reorganized in 105 different S–S pairs upon a cycle of reduction and oxidation; nevertheless, they go on to reconstitute exactly the same pairs which were originally present.

Thermodynamically, the simplest way to describe the folding process is to consider the existence of discrete native (N) and unfolded (U) states for a given protein which are in equilibrium. The folded state is energetically favored (displays a lower Gibbs energy) under appropriate conditions such as temperature, ionic strength, and pH, and this lower energetic state drives the folding reaction. The thermodynamic equilibrium hypothesis requires that the unfolding reaction is reversible, although, in practice, many proteins do not show this kind of behavior: instead, they aggregate or precipitate upon denaturation which renders the process irreversible.

By assuming the thermodynamic equilibrium between states, we can define an equilibrium constant for the unfolding reaction $\mathbf{K} = \mathbf{[U]/[N]}$ and then use this constant to calculate the Gibbs free energy involved in the transition from folded to unfolded states as $\mathbf{dG^{\circ} = -RT\ ln\ K}$, where R is the universal gas constant and T is the absolute temperature in Kelvin. The Gibbs free energy has both **enthalpic (H)** and **entropic (S)** contributions described by the equation $\mathbf{dG^{\circ} = dH^{\circ} - TdS^{\circ}}$.

In thermodynamics, **entropy (S)** is defined as the natural logarithm of the number of microscopic configurations of a system, multiplied by the Boltzmann constant (kB). According to this definition, the number of states in a system is directly proportional to its entropy. Intuitively, entropy can be understood as a measure of disorder. A system displaying an elevated degree of freedom is more entropic (disordered) than a comparable system in an ordered state. The **second law of thermodynamics** states that the entropy of an isolated system never decreases – it either increases over time or stays unchanged. In other words, spontaneous processes always involve a gain of entropy. This fundamental law underlies every process in the Universe and, not surprisingly, applies to biophysics as well.

A folded protein, even when some flexibility is allowed, is an ensemble of a relatively small number of configurations compared to an unfolded polypeptide chain, which samples large areas of conformational space. This means that, in terms of entropy, the folding of a protein is a largely unfavorable process because it forces the protein to restrict its conformational freedom, related to the rotation of main chain angles phi (φ) and psi (ψ) and side chains around χ angles. Obviously, it does not violate the second law of thermodynamics because the protein is immersed in solvent and the system "protein + solvent" always increases its entropy. However, there's an entropic cost which needs to be counteracted by other forces to allow a protein to fold.

The major drivers of protein folding, which counteract the negative effect of the loss of configurational entropy, are the **hydrophobic effect** and **hydrogen bonding**.

The noncovalent interactions which act to stabilize the structures of proteins can be explained in terms of electronegativity and polarity. **Electronegativity** is the tendency of an atom to attract electron density toward its nucleus. It depends both on the atomic number and the distance between the valence atoms and the atomic nucleus. In proteins, the most electronegative atom is oxygen, followed by nitrogen – their electronegativity values in the Pauling scale are 3.5 and 3.0, respectively. Hydrogen and carbon are more electropositive: their electronegative values are low (2.5 and 2.1, respectively) meaning that they are more likely to donate electron density to other atoms. For comparison, the most electronegative atom in the periodic table is fluorine (value = 4.0 in the Pauling scale). When a hydrogen atom is covalently bound to an atom with high electronegativity, this atom will affect the electrons around it generating a partial positive charge in the hydrogen atom. This effect, which applies to any covalent bond between atoms of different electronegativities, is the origin of **polarity**. The N–H and O–H groups are polar because the electron cloud is polarized toward the nitrogen or oxygen atom, which bears a partial negative charge, while the hydrogen atom displays a partial positive charge resulting in a **dipole**. In comparison, C–H groups are **apolar** because the electronegativities of C and H are both low, resulting in a more even distribution of the electron cloud.

Hydrogen bonds always involve a shared hydrogen atom between an atom to which it is covalently bonded (the donor) and another non-hydrogen atom which is negatively polarized (the acceptor). Both donor and acceptor are electronegative atoms, usually O and N in proteins. Hydrogen bonds allow the donor and acceptor atoms to be closer than they would be in the absence of such interaction. Whenever two non-hydrogen atoms are found less than 3.5 Å apart in a protein structure, it is assumed that they are involved in hydrogen bonding. The typical distance involved in hydrogen bonds is 3.0 Å, and the free energy ranges from 2 kJ/mole in water up to 21 kJ/mole if the donor or acceptor is ionized – in this case, it would be called a **salt bridge**, and the typical distance decreases to about 2.8 Å. A typical example of salt bridges in proteins involves the side chain of a positively charged residue such as lysine or arginine interacting with the side chain of negatively charged glutamate or aspartate.

Van der Waals interactions are weak electrostatic interactions involving induced dipoles in the fluctuating electron clouds of atoms or groups of atoms. They typically occur at a distance range of about 3.5 Å and drop rapidly with distance (r) following a $1/r^6$ dependence. These interactions are common among methyl groups in aliphatic, hydrophobic side chains such as leucine, isoleucine, and valine which are highly polarizable. The free energy involved in a Van der Waals interaction is small (only ˜4 kJ/mole), but the net effect of all these interactions in a single protein can be quite large, often reaching hundreds of kJ/mole.

The **hydrophobic effect** relates to the energetics involved in the solvation of hydrophobic side chains. The hydrophobic effect has both entropic and enthalpic contributions. When hydrophobic molecules are in contact with water, the water molecules are oriented around the hydrophobic groups in a way that results in a decrease of entropy compared to the state of water molecules in the absence of any hydrophobic groups. This "cage" of ordered water molecules around exposed hydrophobic groups can be experimentally observed in some high-resolution protein structures. Therefore, the system will spontaneously rearrange so that the hydrophobic molecules are grouped together reducing the area of interface between hydrophobic and polar molecules, so that the water molecules will be able to adopt a more disordered state, increasing the entropy of the system. In a protein, this translates as a tendency for the hydrophobic side chains to occupy the interior of globular proteins, while the polar and charged side chains are found in the solvent-exposed areas.

Energetically, protein stability results from a balance of both stabilizing and destabilizing forces. The difference between them is usually small and is strongly influenced by environmental factors such as temperature pH and ionic strength; this is the major reason why most proteins have narrow ranges of stability and are easily denatured.

1.3   Conformation of Globular Proteins

Globular proteins are formed by organizing their polar groups at protein's surface, and nonpolar groups are directed toward the center of the protein. The globular proteins containing polar side chains exhibit strong interactions toward other polar groups of atoms within the protein molecule as well as toward polar molecules in the protein's surroundings. Similarly, nonpolar side chains have attraction toward other nonpolar side chains within the protein. These proteins have high aqueous solubility that helps them perform diverse biological functions such as enzymatic catalysis, antibodies, DNA replication, and repair.

1.3.1   Hemoglobin

It is the most characterized protein present in red blood cells in humans. The structure was first determined by Max Perutz in 1959 (Perutz et al. 1960). The

Fig. 1.19 Hemoglobin structure
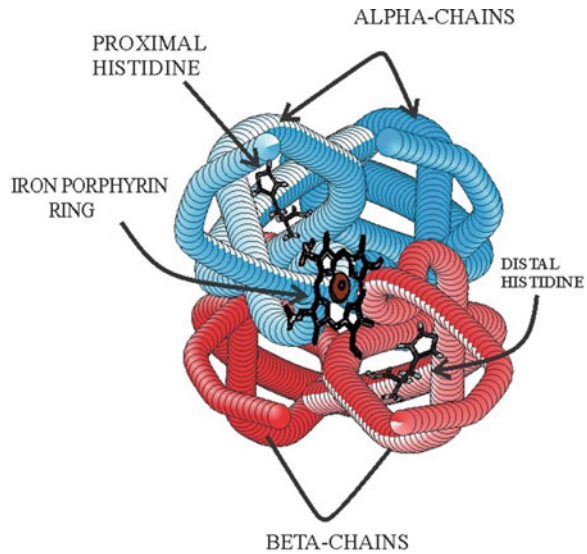
quaternary structure of hemoglobin consists of four polypeptide chains – two identical α-chains consisting of 141 amino acid residues and two identical β-chains consisting of 146 amino acid residues contributing toward a molar mass of 64,500. Hemoglobin is one of the members of the globin superfamily. The globin fold consisting of eight alpha helices is an example of all alpha fold. This fold dictates the functional properties of globin superfamily members including hemoglobin and myoglobin. In hemoglobin, this fold undergoes heterodimerization to form a tetramer with a centrally located iron-protoporphyrin IX ring coordinated to a heme prosthetic group (Fig. 1.19). The iron is in the physiological ferrous state coordinated to the four pyrrole nitrogen atoms in one plane, to an imidazole nitrogen atom of His 8 in the "F" helix, and to a gas atom opposite to this His residue. Each molecule of gas binds to these four ferrous ions in the globin chain respectively accounting for the transport of O_2, CO, and NO. Carbon dioxide, however, binds to amino-terminal of hemoglobin in place of iron atoms forming a weak carbamino complex and transported in blood. The oxygen binding to hemoglobin is represented by a sigmoidal curve (Fig. 1.20) defined by the following equation:

$$Y_{O_2} = \frac{(pO_2)^n}{(p_{50})^n + (pO_2)^n}$$

The sigmoidal curve indicates the presence of allosteric cooperativity in oxygen binding where one molecule of oxygen binding to one heme subunit induces conformational changes in other subunits thus promoting the binding of three more molecules of oxygen to the other three subunits of hemoglobin. The deoxy
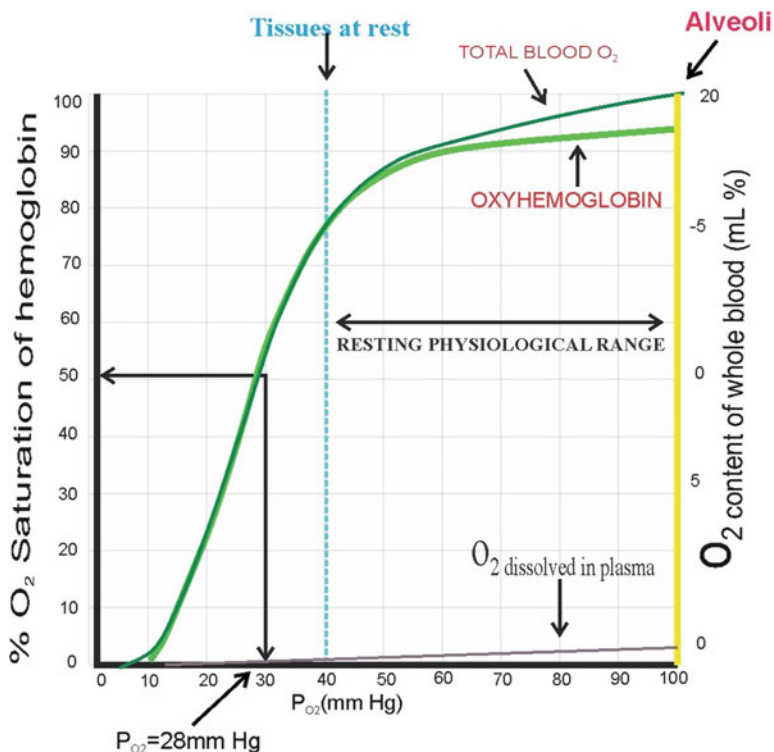
Fig. 1.20 Hemoglobin saturation curve

hemoglobin has heme present in the subunits in T (tensed) form which is the low affinity state for O_2 binding. Once the O_2 molecule binds to any of the subunits, there is a conversion of T to R (relaxed) form having high affinity for O_2 molecule.

There are significant tertiary and quaternary structure changes responsible for this conversion. $Fe + 2$ is pulled in to the plane of the porphyrin ring by 0.039 nm when oxygen binds with the help of His 8 in the "helixF." One alpha–beta pair moves relative to the other by 15° upon oxygen binding resulting in the breaking of ionic bonds in alpha chains and in beta chains in the R-state decreasing pK's of sidechains that releases protons. Release of oxygen in tissues is further regulated by the allosteric binding of 2,3-bisphosphoglycerate to the beta chain of hemoglobin that has more affinity for deoxy hemoglobin. The Hill coefficient for the oxygen binding to hemoglobin is 2.8–3, emphasizing the binding cooperativity. The functioning of hemoglobin is further described by Bohr's effect which postulates that when hemoglobin binds O_2 there is a release of protons.

$$Hb\,(O_2)n\,Hx + O_2 == Hb(O_2)n + x[H+].$$
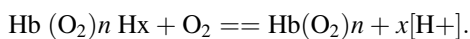
When the oxygenated blood reaches tissues, there is a release of oxygen because there is low pH in cells due to high concentration of protons. The increased respiratory activity inside the cells results in the increase in the concentration of CO_2. The enzyme carbonic anhydrase present in red blood cells converts CO_2 to carbonic acid which further dissociates to form bicarbonate ions and protons, thus resulting in the release of oxygen from hemoglobin.

There are different types of hemoglobin based on the type of chains comprising the hemoglobin molecule. In erythrocytes of normal human adults, hemoglobin A ($\alpha 2\beta 2$) is majorly present (97%) in blood, hemoglobinA2 with $\alpha 2$ $\delta 2$ (2%) and hemoglobin F or fetal hemoglobin with $\alpha 2\gamma 2$ chains (1%). Hemoglobin binds oxygen in lungs at high PO_2 of100 mm Hg, which is the high affinity state for oxygen and releases it to metabolically active cells at a lower PO_2 of 30 mm Hg that signifies the low affinity state for oxygen in tissues. Besides, its main role of oxygen transport hemoglobin also binds carbon dioxide (CO_2), carbon monoxide (CO), and nitric oxide (NO).

1.3.2 Myoglobin

Myoglobin is the heme containing protein found in vertebrate skeletal and cardiac muscle. This is the first protein crystal structure determined using X-ray crystallography by John Kendrew and colleagues in 1958. It has a single polypeptide chain consisting of 153 amino acid residues that binds and stores oxygen in skeletal muscles from blood and is the source of continuous oxygen supply to active muscle groups during respiration. A high degree of conservation is observed in the tertiary and ligand binding regions of myoglobin and other globin specifically the hydrophobic heme pocket; the distal pocket containing distal H64 and proximal H93 along with four other pockets spanning from Xe1 to Xe4 is conserved across species (Fig. 1.21). Presence of the porphyrin ring in the plane of the heme pocket is characteristic of the globin proteins. Noncovalent interactions involving hydrophobic interactions with nonpolar amino acids and electrostatic interactions between the heme propionic sides with polar amino acids near the cavity including H97, R45, and S92 stabilize the structure of the myoglobin. The backbone structure of myoglobin is stable, whereas the side chains exhibit conformational dynamism required for binding oxygen and other ligands. The proximal histidine H93 is covalently bound to the iron at the center of the heme, while the distal histidine H64 is known for stabilizing the oxygen–heme bond. The distal pocket is the gap adjacent to the heme iron, and the distal histidine serves as a gate allowing the heme to bind oxygen and other ligands. The variations observed in globin structure are responsible for the differential binding of oxygen. It has high oxygen affinity which reaches saturation at low PO_2 (2 mm Hg). The partial pressure of oxygen in capillaries is 30 mm Hg where myoglobin easily binds oxygen beyond saturation. However, it releases oxygen in metabolically active cells where $PO_2 < 2$ mm Hg. The oxygen binding curve of myoglobin is hyperbolic (Fig. 1.22) defined by the following equation:
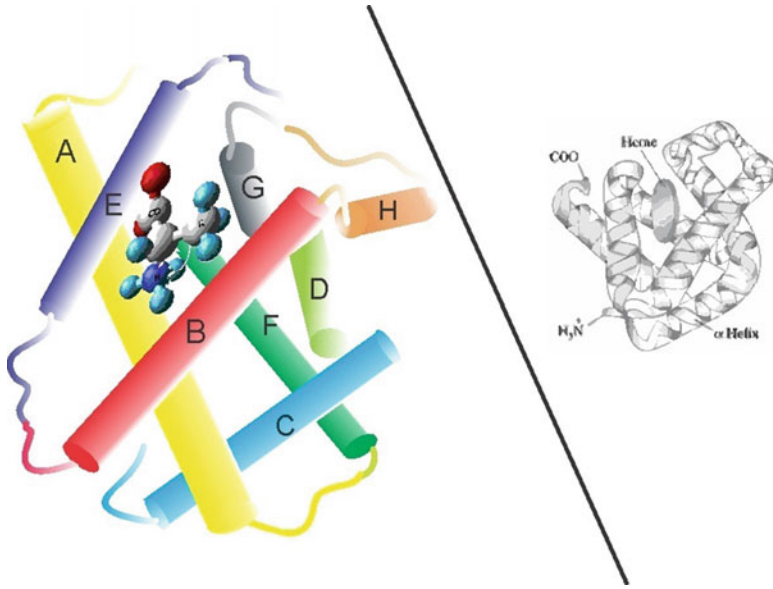
Fig. 1.21 Myoglobin structure
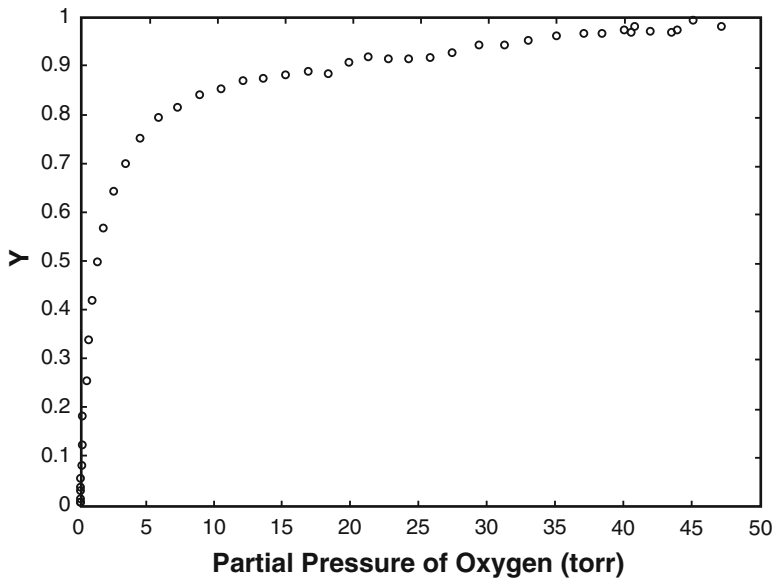
Fig. 1.22 Myoglobin saturation curve (Barlow et al. 1992)

Fig. 1.23 Lysozyme
structure
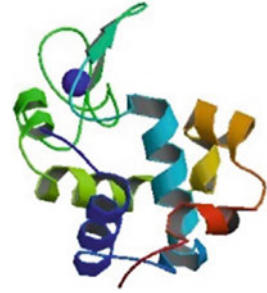
$$Y_{O_2} = \frac{(pO_2)}{p_{50} + (pO_2)}$$

Scientific research has provided insights related to other roles of myoglobin. It regulates the intramuscular bioavailability of nitric oxide (NO), thereby influencing mitochondrial respiration. The oxygen availability in the intracellular milieu is responsible for the transitioning of myoglobin from NO scavenger (at high PO_2) to a NO producer as PO_2 decreases.

1.3.3 Lysozyme (1,4-β-N-Acetylmuramidase)

This is the widely studied protein to understand the effect of various factors on protein structure. It consists of a single polypeptide chain with 129 amino acids (Fig. 1.23). It folds into a compact three-dimensional structure with a long cleft present on the surface under physiological conditions. It is present across species ranging from plants, animals, and humans. The mucous lining of the nasal cavity, tear ducts, kidney tissue, milk, leukocytes, saliva, etc. are some of the places where lysozyme is expressed. The main function of this enzyme is the hydrolysis of the bond linking N-acetylglucosamine (NAG) and N-acetylmuramic acid (NAM) resulting in the increase of bacterial cell wall permeability. This has important implications in the prevention of various bacterial infections.

1.3.4 Cytochromes

Cytochromes belong to a class of hemoproteins involved in the transport of electron or proton transport by reversibly changing the valency of iron atom present in the heme group. There are different types of cytochromes, namely, a, b, c, and d, depending on their spectrochemical characteristics. The existence of different variants of these basic types of cytochromes has been reported in bacteria, green plants, and algae (e.g., cyt f is a variant of cyt c). The mitochondrial system of

Fig. 1.24 Cytochrome structure
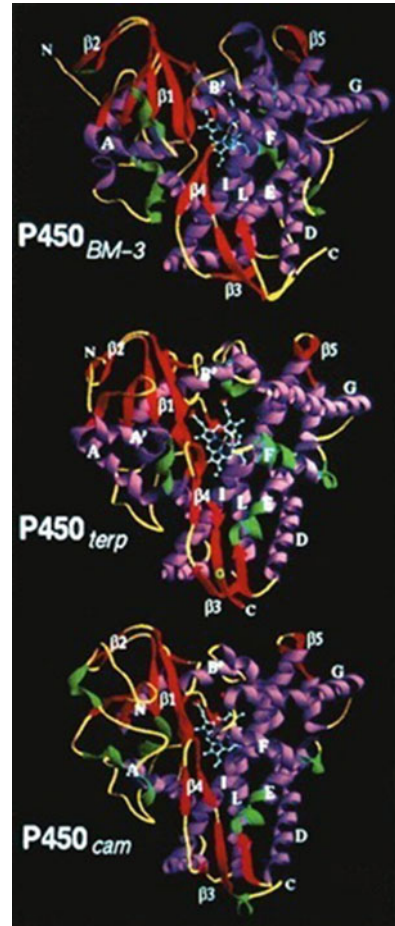
cytochromes provides electron transport through cytochrome c oxidase to molecular oxygen as the terminal electron acceptor (respiration). Cytochromes P450 belonging to the superfamily of heme thiolate enzymes have been extensively characterized. Despite a significant difference in the primary sequence of various P450 enzymes, the functional tertiary fold is conserved. This P450 fold contains 13 α-helices (A, B, B′, and C-L) and five β-sheets (31–135) (Fig. 1.24). They are involved in a variety of functions including biosynthesis of steroids, fats, bile acids, monooxygenation of hydrophobic substrates, hydroxylation of bicyclic monoterpene camphor, drug and xenobiotic metabolism, etc. They have been classified as class I and class II P450s based on their sequence similarity and the nature of electron donor which is iron–sulfur proteins in case of class I and FAD/FMN-containing reductase proteins in class II enzymes.
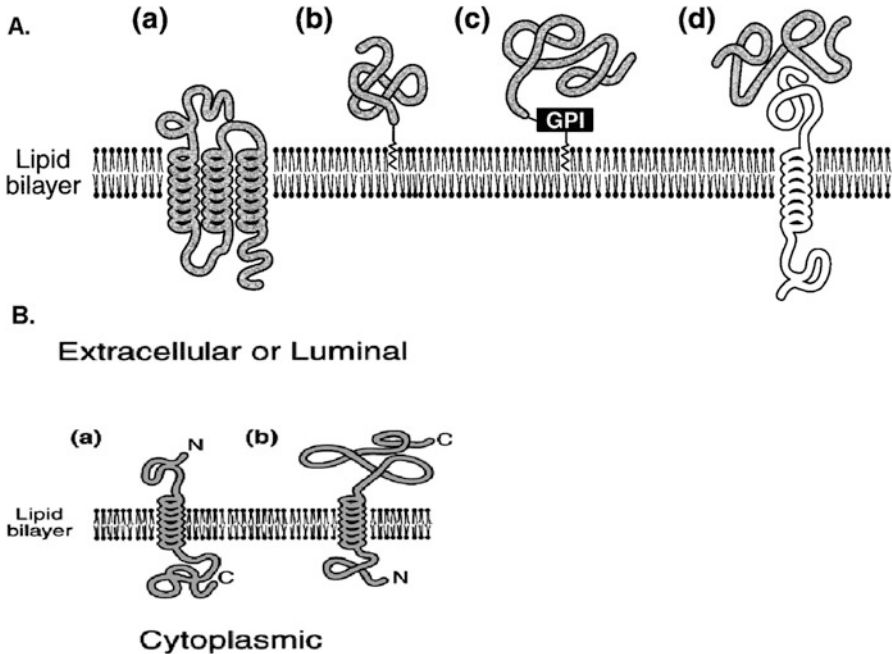
Fig. 1.25 Integral and peripheral membrane proteins (Chou et al. 1999)

1.4 Membrane Proteins

All the eukaryotic cells and their constituent organelles are enclosed within the plasma membrane. The structural organization of this membrane is a lipid bilayer interspersed with membrane proteins. These proteins have key functional roles spanning from cell signaling to ion transport. Membrane proteins undergo extensive oligomerization to enhance their stability and genetic efficiency, e.g., cytb6f. These membrane proteins are classified as integral or peripheral proteins depending upon the strength of their association with the plasma membrane (Fig. 1.25).

1.4.1 Integral Proteins

These proteins pass the lipid bilayer either once (single pass proteins) or multiple times (multiple pass proteins). The single pass proteins are classified as type I proteins having extracellular (or luminal) amino terminus and cytosolic carboxy terminus. The multiple pass proteins are also referred to as type II with luminal carboxy terminus and cytosolic amino terminus. Thus, they are capable of functioning on both sides of the lipid bilayer, e.g., ion channels (Chou et al. 1999). The

integral proteins are enriched in alpha helical content as their presence in lipid bilayer facilitates the intrachain hydrogen bonding characteristic of alpha helix. These proteins are majorly composed of hydrophobic residues. Many transmembrane motifs such as four-helix bundle and beta barrel are the predominant super secondary structures present in these proteins. The classical example of all alpha helical membrane protein is bacteriorhodopsin with serpentine receptor (seven helices spanning the lipid bilayer). Another protein, namely, porin, is an example of all beta strand structure. Most of the channel proteins are made up of antiparallel beta strands forming the beta-sheet where the surface-exposed residues are mostly hydrophobic, and the hydrophilic residues are present inside the channel where water molecules are present (Rees et al. 1989).

There is also a class of proteins termed as anchored proteins which are covalently linked to the bilayer by either fatty acid/ lipid chains having prenyl groups (lipid anchored) or by glycosylphosphatidylinositol (GPI anchored). There are sequence-specific features of such anchored proteins having isoprenylation at carboxy terminus with CAAX consensus motif, myristoylation at the amino terminus with conserved GXXXS/T motif, or palmitoylation at the same terminus at specific cysteine residue. However, GPI-anchored proteins have a GPI residue attached at the carboxy terminus with a hydrophobic tail (Chou et al. 1999).

1.4.2   Peripheral Proteins

These proteins are attached through noncovalent interactions either to the hydrophobic head of the lipid or to the domains of integral proteins exposed to the surface. In the former case they are referred to as amphitropic proteins. They do not have any significant consensus sequences and can be disrupted using detergents or change in pH unlike the integral proteins. Many proteins such as synucleins, several annexins, enzymes, namely, lipoxygenases, etc., are included in this category.

References

Anfinsen CB (1973) Principles that govern the folding of protein chains. Science 181:223–230
Barlow CH, Kelly KA, Kelly JJ (1992) Simultaneous determination of hemoglobin and myoglobin oxygen binding curves by spectral curve fitting. Appl Spectrosc 46(5):758–763
Branden C, Tooze J (1999) Introduction to protein structure, 2nd edn. Garland Publishing Group, New York
Chou K-C, Elrod DW (1999) Prediction of membrane protein types and subcellular locations. Proteins 34:137–153. doi:10.1002/(SICI)1097-0134(19990101)34:1<137::AID-PROT11>3.0.CO;2-O

Cooley RB, Arp DJ, Karplus PA (2010) Evolutionary origin of a secondary structure: π-helices as cryptic but widespread insertional variations of α-helices that enhance protein functionality. J Mol Biol 404:232–246

Crawford JL, Lipscomb WN, Schellman CG (1963) The reverse turn as a polypeptide conformation in globular proteins. Proc Natl Acad Sci U S A 70:538–542

Kurzbauer R et al (2004) Crystal structure of the p14/MP1 scaffolding complex: how a twin couple attaches mitogen-activated protein kinase signaling to late endosomes. Proc Natl Acad Sci U S A 101:10984–10989

Kyte J (1991) Structure in protein chemistry. Garland Publishing Group, New York

Levine TP et al (2013) Discovery of new longin and roadblock domains that form platforms for small GTPases in ragulator and TRAPP-II. Small GTPases 4:62–69

Misra G, Aggarwal A, Dube D, Zaman MS, Singh Y, Ramachandran R (2009) Crystal structure of the Bacillus anthracis nucleoside diphosphate kinase and its characterization reveals an enzyme adapted to perform under stress conditions. Proteins Struct Funct Bioinform 76:496–506

Murphy KP (2001) Chapter 1: Stabilization of protein structure in protein structure, stability, and folding. In Methods in molecular biology, vol 168. Humana Press

Murzin AG, Brenner SE, Hubbard T, Chothia C (1995) SCOP: a structural classification of proteins database for the investigation of sequences and structures. J Mol Biol 247:536–540

Pauling L, Corey RB (1951) The pleated sheet, a new layer configuration of polypeptide chains. Proc Natl Acad Sci U S A 37:251–256

Pauling L, Corey RB, Branson HR (1951) The structure of proteins; two hydrogen-bonded helical configurations of the polypeptide chain. Proc Natl Acad Sci U S A 37:205–211

Perutz MF, Rossmann MG, Cullis AF, Muirhead H, Will G, North AC (1960) Structure of haemoglobin: a three-dimensional Fourier synthesis at 5.5-Å. Resolution, obtained by X-Ray analysis. Nature 185:416–422

Petsko GA, Ringe D (2004) Protein structure and function. New Science Press

Ramachandran GN, Ramakrishnan C, Sasisekharan V (1963) Stereochemistry of polypeptide chain configurations. J Mol Biol 7:95–99

Rees DC, DeAntonio L, Eisenberg D (1989) Hydrophobic organization of membrane proteins. Science 245(4917):510–513

Scorsato V et al (2016) Crystal structure of the human Tip41 orthologue, TIPRL, reveals a novel fold and a binding site for the PP2Ac C-terminus. Sci Rep 6:30813

Venkatachalam CM (1968) Stereochemical criteria for polypeptides and proteins. V. Conformation of a system of three linked peptide units. Biopolymers 6:1425–1436

Protein Folding

Smriti Shrivastava

Abstract

Proteins are macromolecular structures, functionally active in their three-dimensional state, and their entire machinery depends on involvement of number of polypeptides. A perceptive insight of protein folding mechanism is a remarkable task, and various studies in protein structure and function have investigated mechanism of determining protein's three-dimensional details. Apart from understanding basic energy forces and molecules operational behind protein folding, various computational models have also been designed that outline essential aspects of protein folding mechanism. In the present chapter, we have exercised to bring all aspects of protein folding under one roof with all essential components affecting protein folding, which include major driving forces, mechanisms, folding pathways, thermodynamics, kinetics, effect of chemical reagents, pH, temperature, and computational model to analyze protein folding mechanisms. Reliable prediction of protein folding process allows deducing its appropriate function, and we believe that present chapter will prove a step forward in the respective study.

2.1 Introduction

Physical process by virtue of which proteins acquire their three-dimensional structure is protein folding. It broadly occurs at four levels, i.e., formation of primary, secondary, tertiary, and quaternary structures (Fig. 2.1). Peptide group majorly

S. Shrivastava (✉)
Amity Institute of Biotechnology, Amity University, Sector: 125, Noida, Uttar Pradesh, India
e-mail: sshrivastava1@amity.edu
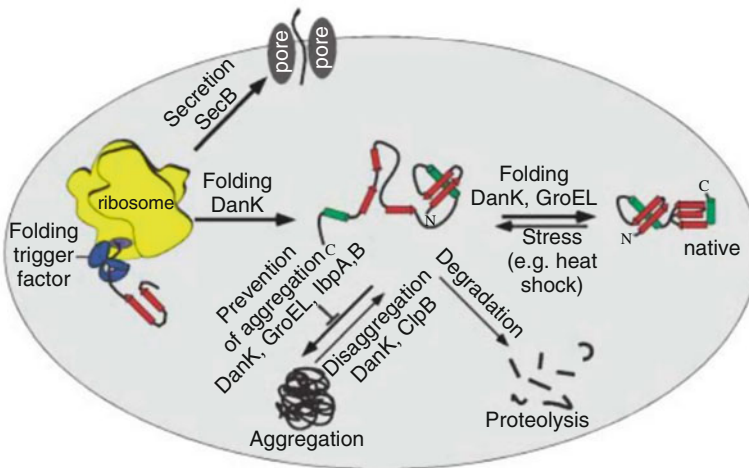
Fig. 2.1 Protein folding cycle inside the cell shows location of protein synthesis (ribosomes), its folding to native structure, molecular chaperones (prokaryotic homologues shown), and probable secondary structures of protein (beta strands and alpha helices) (Mogk et al. 2002)

consists of six atoms, and peptide bond conformations are restricted to *trans* and *cis* configurations with a highly stable trans configuration. Polypeptides fold into characteristic functional three-dimensional structure from random coils (Alberts et al. 2002). Protein folding provides functional capability to proteins in reproducible manner. Unfolded proteins and random coils lack stable three-dimensional structures, thus signifies the need for a properly defined three-dimensional structure. Protein folding initiates during translation of polypeptides, and interaction of amino acids with each other confirms a three-dimensional structure at native state. Amino acid sequence and primary structure are major determining factors behind three-dimensional structure and are termed as Anfinsen's dogma (Anfinsen 1972). Folding pathway through which unfolded proteins assuming its native state (stable structure) is described by energy landscape. Protein structures are also broadly influenced by codon for amino acids (Saunders and Deane 2010). Berg et al. in the year 2002 reported that an accurate three-dimensional structure is essential for protein to function and also suggested that even in functional proteins some part may remain unfolded, in order to maintain protein dynamics. It was studied that failure to fold into native structure leads to formation of inactive proteins, and in certain cases misfolded proteins can even have a modified or toxic function. Broadly termed as proteopathies or proteinopathies, protein conformation disorders or protein misfolding diseases include Parkinson's disease, Alzheimer's disease, prion disease, Creutzfeldt-Jakob disease, etc. (Walker and LeVine 2000; Luheshi et al. 2008; Chiti and Dobson 2006, Friedrick 2006; Spinner 2000; Carrell and Lomas 1997; Westermark et al. 2007). Various other disorders including neurodegenerative disorders are also results of misfolded proteins which lead to accumulation of amyloid fibrils (Selkoe 2003). Incorrect protein folding may also lead to

various kinds of allergies as immune system does not produce antibodies for these antigens (Alberts et al. 2010).

2.2   Driving Forces in Protein Folding

Protein folding is not dependent upon energy inputs from nucleoside triphosphates and is chiefly supported by intramolecular electrostatic interactions, van der Waals forces, and hydrophobic interactions. It was also understood quite early that protein folding is opposed by conformational entropy (Essential Biochemistry 2016). Limitation to protein folding abilities of a protein is in general restricted to bending angles or possible conformations. Three major components that determine the geometrical structural validation are protein backbone conformation (ϕ and ψ angles), side-chain rotamers, and Cα geometry (Lovell et al. 2003). The above study also reported that Cα is significant for evaluating distortion of covalent geometry in protein structure; it joins backbones and also responds to compatibility between protein structure and backbone. They believed ϕ and ψ angles are central for structural validation as they encapsulate all information of the backbone conformation. Basis of these studies on geometrical structural validation is the Ramachandran plot analysis which plots ϕ versus ψ conformational angles for each protein residue and shows experimental scatter plots of the conformations of known 3D structures, that show contour of calculated energies or steric criteria as a function of ϕ and ψ for a dipeptide (Ramachandran and Sasisekaran 1968). Basically protein folding takes place on its own, but this process majorly also depends on the presence of solvent-like water molecule or lipid bilayer (Van den Berg et al. 2000), salt concentration, pH and temperature of surrounding medium, presence of cofactors, and molecular chaperones facilitating protein folding. Though co-translational process of folding of N-terminus of protein while C-terminus of protein is still under synthesis marks the beginning of protein folding, protein folding may also be a spontaneous process after biosynthesis. Levinthal's paradox of protein folding states randomly searching native folded state of protein through permutation and combination of varied possible configurations can be a lengthy process. Protein folding is a very fast process, and mathematical analysis of simple model, of order of few kT, can reduce Levinthal's time significantly.

2.2.1   Electrostatic Interactions and Hydrogen Bond

Electrostatic interactions generated by charge surface residues or ionic bonds (salt bridges) play significant role in protein folding (Fig. 2.2). Ionic bonds form the outer layer of hydrophobic core of proteins and are rarely seen in protein interior, and if found at the core, they are strong electrostatic attractions. Electrically charged amino acids, present on surface of protein, help in its suitable folding by interacting with water molecules. Water develops as shield around charged surface residues and helps in stabilizing the protein structure.

Fig. 2.2 Intermolecular
ionic bonds
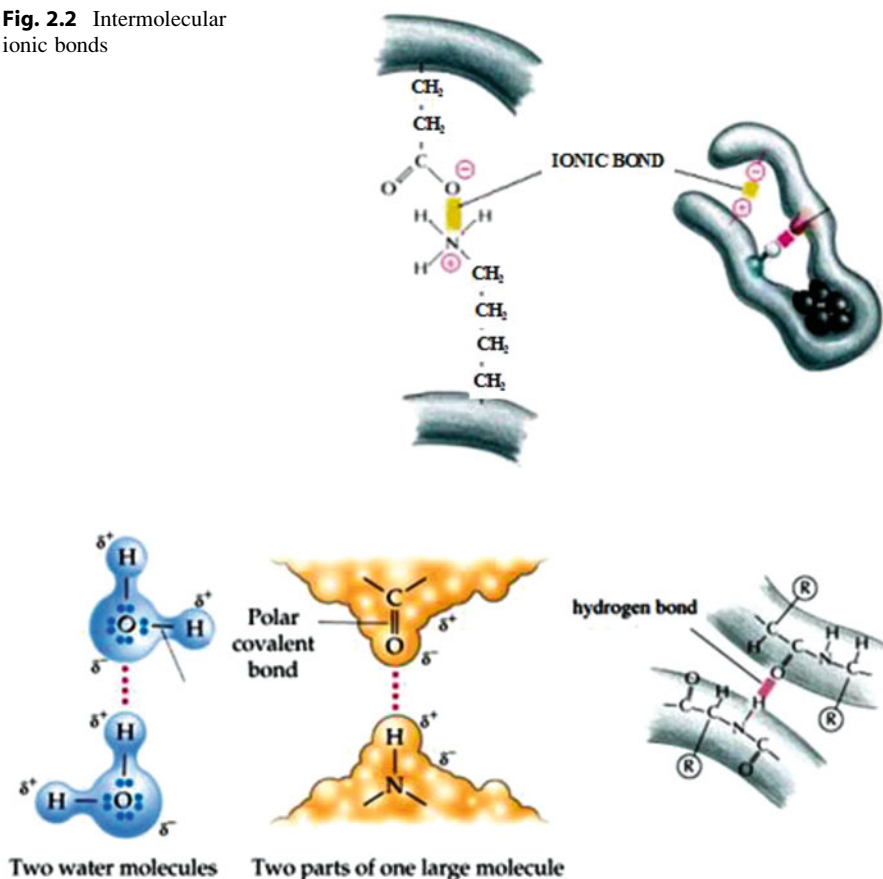
Fig. 2.3 Intermolecular hydrogen bonds

Interaction of hydrogen atom covalently bonded to an electronegative donor atom with another electronegative acceptor atom leads to formation of hydrogen bond, which confers directional interactions strengthening protein folding and structure and its molecular identification. Secondary structure of proteins, α helix and β sheet, makes the core of protein structure. Interaction of corresponding hydrogen-bonding groups of von interacting surfaces gives specific molecular recognition to a protein. Hydrophobic core of protein is formed due to intramolecular hydrogen bond (Fig. 2.3) formed between main chain polar molecules. Protein, nucleic acid, substrates, enhancers, and inhibitors of proteins are major ligands which provide directionality and specificity to protein, which make the primary facet of protein molecular recognition. In order to allow rapid sampling to confer stability and specificity to protein structure, energetic and kinetics of hydrogen bonding need to be optimized (Hubbard and Haider 2010). Most frequently observed hydrogen bond is of less than 2.5 Å, in general 1.9 Å with donor acceptor angle between 90 and 180°.

Fig. 2.4 Inter-chain hydrogen bonding in collagen where amide H of glycine in one chain is hydrogen bonded to C=O in another chain
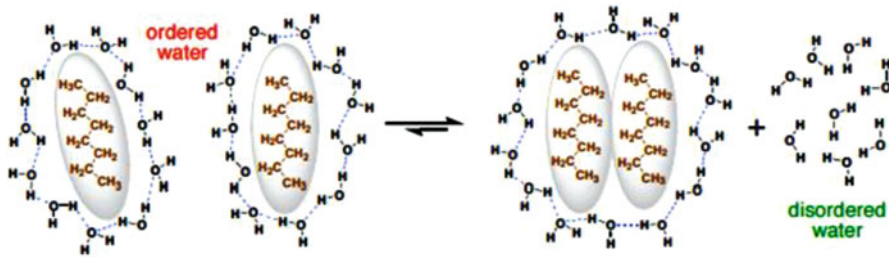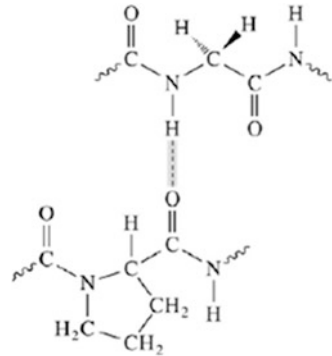
Fig. 2.5 Hydrophobic effects

Studies on hydrogen bonding patterns have suggested that compact helices have lesser number of residues per turn, and if the number of residues per turn is two, it is difficult to control them in same chain and then eventually forms β pleated sheets. Beta sheets are formed when chains are formed when chains are folded in an accordion-like fashion from one α carbon atom to another α carbon atom, and each residue is rotated by 180° with respect to the previous one followed by formation of hydrogen bond between adjacent chains. As discussed in Chap. 1, β strands in a sheet are parallel and antiparallel, where parallel β sheets run in same N- to C-terminal direction with distorted H bonds and antiparallel runs in opposite N- to C-terminal directions with perpendicular H bonds making the structure more stable. Hydrogen bonding of protein is not restricted within or between polypeptide chains, but also with surrounding aqueous medium. Figure 2.4 depicts inter-chain H bonding in collagen.

2.2.2 Hydrophobic Bonds

Another chief force activating appropriate protein folding is hydrophobic bonds (Fig. 2.5). They minimize energy loss caused due to interruption of amino acids into water molecule and bring hydrophobic side chains side by side; as a result of which,

Fig. 2.6 Amino acids containing hydrophobic and hydrophilic side chains
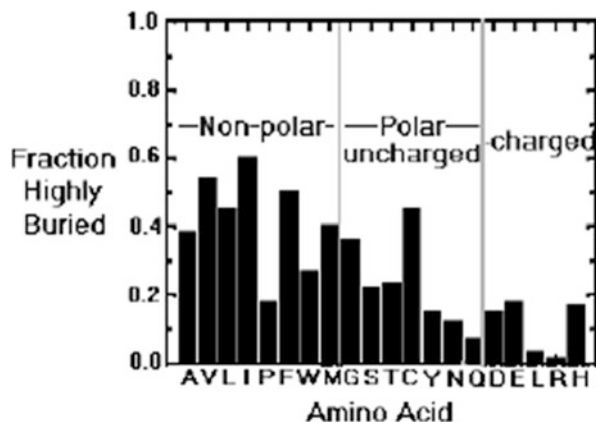
Table 2.1 Thermodynamic parameters of protein folding of some globular proteins at 25°C in aqueous solution

Protein	ΔG (kJ/mol)	ΔH (kJ/mol)	ΔS (J/K.mol)
Ribonuclease	−46	−280	−790
Chymotrypsin	−55	−270	−720
Lysozyme	−62	−220	−530
Cytochrome c	−44	−52	−27
Myoglobin	−50	0	+170

Data adapted from Privalov and Khechinashvili (1974)

an interior hydrophobic protein core is developed where maximum hydrophobic side chains are present in close association and protected from interaction with solvent water (Brandon and Tooze 1991; Dressler and Potter 1991). Pro[198], Val[200], Leu[209], and Trp[207] are major hydrophobic amino acids present in the interior of proteins. Amino acids with hydrophobic side chains are also seen on the polypeptide surface, and when these amino acids (e.g., Pro[24] and Phe[71]) are exposed to polar water solvents, they exhibit extensive hydrophobic bonds.

The shape of protein structure is majorly determined by hydrophilic and hydrophobic side chains of amino acids (Fig. 2.6) and nature of interaction of various R groups with aqueous environment.

Thermodynamic parameters, entropy, enthalpy, and free energy for protein folding, vary from one globular protein of which few are listed in Table 2.1. They play an important role in folding of globular protein.

2.2.3 Van der Waals Forces

Weak electrical attraction between two atoms is van der Waals attraction. Fluctuation in electric cloud of each atom yields temporary dipole, and the transient dipole
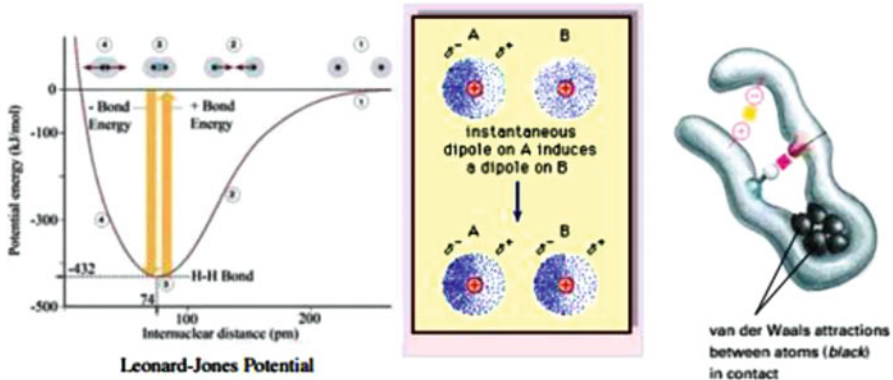
Fig. 2.7 Van der Waals forces

that is generated in one atom induces a complementary dipole on another if they are in close proximity. This leads to weak electrostatic attraction, van der Waals forces (Yennawar et al. 1994). Whenever two atoms are in close proximity, repulsive forces also come into play as a result of negatively charged electrons (caused due to electron cloud overlapping between two adjacent atoms); thus, appropriate distance required for van der Waals (Fig. 2.7) depends upon van der Waals radius (size of electron cloud). These attractions play an important role in protein structure determination because of their number (Harel et al. 1991) and also are important in protein-protein recognition when complementary shapes are involved.

2.2.4 Disulfide Bonds

Disulfide bonds, bond between sulfur of cysteine molecules, give higher level stabilization to already existing three-dimensional protein structures, and they are thermodynamically linked to protein folding (Marnathambika and Bardwell 2008; Creighton 1990) (Fig. 2.8). According to Anfinsen's principle, protein sequence is based on oxidative refolding of a protein with disulfide bonds, and it plays vital role in determining protein structure. Qin et al. in 2015 found that efficient folding of broad class of single domain protein is a result of formation of specific collapsed native structures of proteins. In general protein disulfide bond stabilizes native conformation by virtue of decreasing entropy of unfolded forms (to destabilize denatured form) (Thornton 1981), and they affect the rate of protein folding. As per studies the increase in stability of native structures imparted by disulfide bonds is proportional to the number of residues between linked cysteines (Flory 1953; Pace et al. 1988). Relative location of disulfide bonds to folding nucleus affects kinetics of protein folding, and it has been reported that if the disulfide bond is in or nearer to folding nucleus, it accelerates protein folding, and if it is elsewhere, it can decelerate folding by up to three times (Abkevich and Shakhnovich 2000). The whole
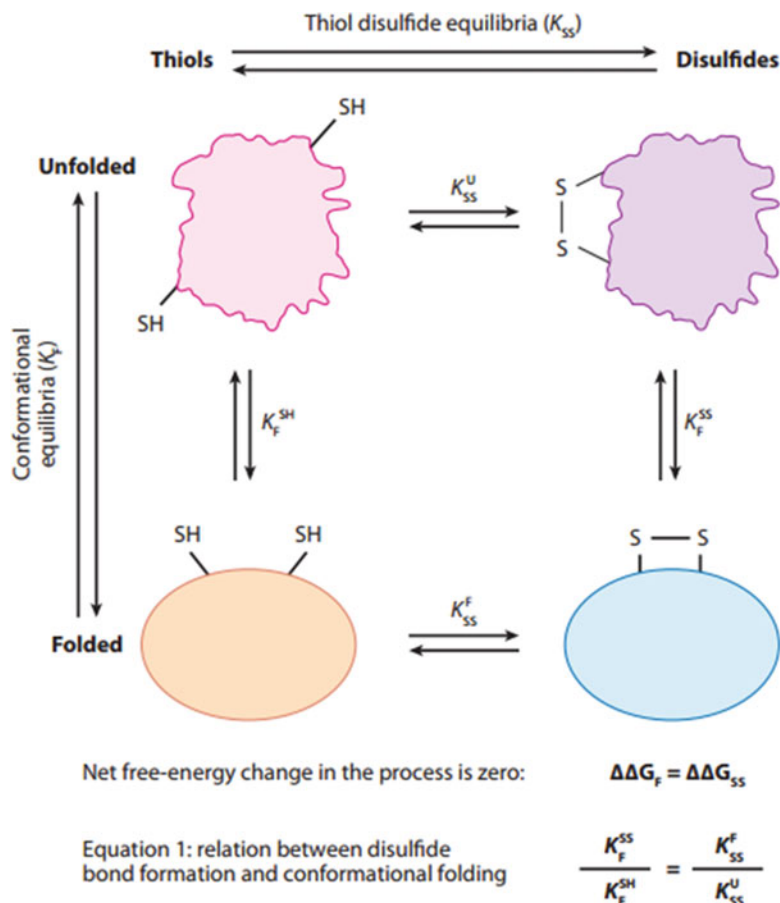
Fig. 2.8 Effect of disulfide bond formation on protein conformation. The figure shows protein with two cysteine residues in its unfolded and folded conformations. Stability is conferred by disulfide bonds, and conformation is given by equilibrium constants K_{SS} and K_F, respectively. The equilibrium constants for folding with and without the disulfide bond are given by K_F^{SS} and K_F^{SH}, respectively. The stability of the disulfide bond in the folded and unfolded states is given by K_{SS}^F and K_{SS}^U, respectively. Equilibrium constants (Eq. 2.1) are linked to net free energy change and that should be maintained to zero. Folded conformation affects the stability of the disulfide bond to the same extent to which the disulfide bond affects the stability of conformation (Creighton 1990)

equilibrium constant (K_{eq}) for thiol-disulfide exchange reaction is a measure of protein folding stability and can range from a value of 3 to 105 (Darby and Creighton 1993). A minor population of disulfide bonds also provides functional capability, which can be broadly classified as catalytic disulfides and allosteric disulfides. Catalytic disulfide is found at the active sites of enzymes mediating thiol-disulfide exchange (e.g., oxidoreductases), and allosteric disulfides regulate function non-enzymatically through making alterations in protein structure (Hogg 2003; Schmidt et al. 2006).

2.2.5 Chaperones

Chaperonins are molecular machinery working in protein folding, unfolding, and disaggregation and also prevent protein misfolding. They are present in high concentration in all cells from bacteria to human and are varied families of proteins having multi-domain that helps in providing native folds to nascent protein. They protect protein subunits from heat shock during their assembly.

Increased expression of chaperones at the time of stress is an important factor in maintaining health of cell. Contrasting to enzymes (having precise and specific active sites), chaperones are multifunctional molecules that can operate on wide range of substrates. Understanding of structural basis of their mechanism of action involves substantial displacements of 20–30 kDa domains over distances of 20–50 Å and rotation up to 100° (Saibil 2013). Chaperones are also known as heat shock proteins as their production is induced by heat shock. Chaperone families (Table 2.2) have derived its name from molecular weight of its corresponding main representative. Members of the Hsp60 (recognized as GroEL in *Escherichia coli*), Hsp70 (recognized as DnaK in *E. coli*), Hsp90 (recognized as HptG in *E. coli*), and Hsp100 (recognized as ClpA and ClpB in *E. coli*) families (the number indicates the molecular mass of each Hsp subunit) interact either with aggregation-prone, non-native polypeptides or with proteins tagged for degradation. Hsp70 acts by managing cellular functions by directing substrates for unfolding, disaggregation, degradation, or refolding. Hsp90 helps in the integration of signaling functions, is active at later stage of folding, and is important in cellular signaling and targeting substrates for proteolysis, and on the other hand, Hsp60 acts at early stages of folding. Hsp60 forms complex that is symmetrical and self-contained where substrate and nucleotide-binding sites are located inside cavities and Hsp70 exposes regulatory surfaces, linking with varied binding proteins to redirect its activity (Saibil 2013).

2.3 Protein Folding Mechanism

After emerging from the ribosome, all proteins exist as a linear chain of amino acid residues. They must fold to their active native conformation. During the process, the amino acids interact with each other and fold into their characteristic and functional three-dimensional structure, which is determined by the amino acid sequence (Anfinsen's dogma). An example of this was seen in experiments carried out by Christian Anfinsen in the 1950s. When purified ribonuclease (124-residue single-chain protein) was exposed to concentrated urea solution (8M) containing reducing agent (2-mercaptoethanol), it was completely denatured, and its four disulfide bonds cleaved to yield an inactive protein. However, removing the urea and reducing agent completely restored the enzymatic activity of ribonuclease as it refolded into the correct tertiary structure. This was the first evidence that all the information required for correct folding of a protein is contained in its amino acid sequence, which was later confirmed when similar results were obtained using

Table 2.2 Chaperone families: structures and functions

Chaperone family	Structure	ATP	Examples Prokaryote	Eukaryote	Co-chaperone	Function
Hsp100	6 – 7-merr	+	ClpB			Disaggregation together with Hsp70
			ClpA			Proteolysis together with the ClpP protease
				Hsp104		Thermotolerance disaggregation together with Hsp70
Hsp90	Dimer	+	HtpG			Tolerance to extreme heat shock
				Hsp90	Hop, p23, CDC37	Stress tolerance control of folding and activity of steroid hormone receptors, protein kinases, etc.
Hsp70	Monomer	+	DnaK		DnaJ, GrpE	de novo protein folding prevention of aggregation of heat-denatured proteins solubilization of protein aggregates together with ClpB regulation of the heat shock response
				Hsp70, HSC70	Hsp40, Bag 1, Hip, Chip, Hop, HspBP1	de novo protein folding prevention of aggregation of heat-denatured proteins solubilization of protein aggregates together with Hsp104 regulation of the heat shock response regulation of the activity of folded regulatory proteins (such as transcription factors and kinases)
Hsp60	14-mer, 16-mer	+	GroEL		GroES	de novo protein folding prevention of aggregation of heat-denatured proteins
				CCT/TRiC	Prefoldin	de novo folding of actin and tublin

sHsp	8 – 24-mer		IbpA, IbpB		Prevention of aggregation of heat-denatured proteins binding to inclusion bodies
				Hsp25 (crystalline)	Prevention of aggregation of heat-denatured proteins component of the lens of the vertebrate eye
Trigger factor	Monomer		Trigger factor		Ribosome-associated potential function in de novo protein folding
NAC	Heterodimer		NAC		Ribosome-associated potential function in de novo protein folding
SecB	Tetramer		SecB		Protein secretion
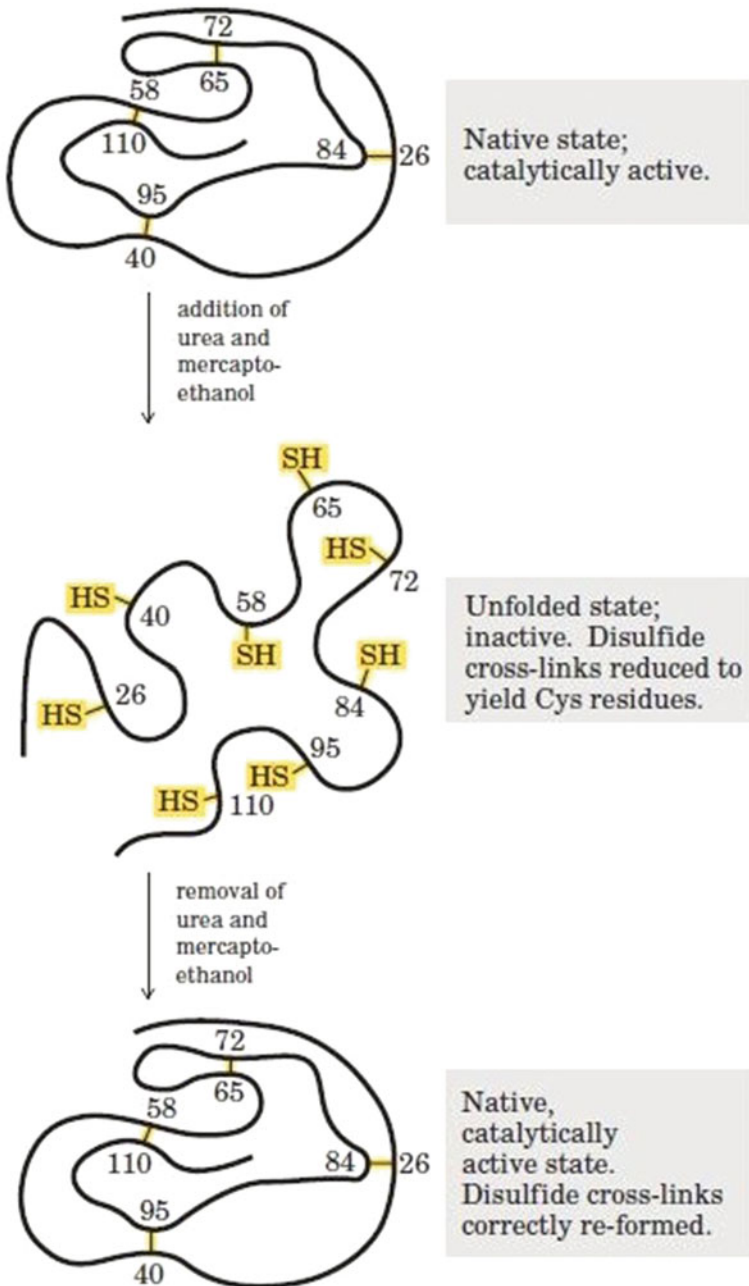
Fig. 2.9 Renaturation of unfolded, denatured ribonuclease. Urea is used to denature ribonuclease and mercaptoethanol (HOCH$_2$CH$_2$SH) to reduce and thus cleave the disulfide bonds to yield eight Cys residues. Renaturation involves reestablishment of the correct disulfide cross-links (Nelson and Cox 4 ed. Chapter 4, p. 148, 2005)

chemically synthesized ribonuclease which was also catalytically active. The process is difficult and dangerous as its success and failure determine the biological health and disease, respectively (Fig. 2.9).

2.3.1   Protein Folding Pathways

Protein folding is a highly complex process, and several models have been proposed in order to explain the pathways for the same. In one model, protein folding is seen as a hierarchical process. First local secondary structures are formed with certain amino acid sequences folding readily into α helices or β sheets followed by formation of stable supersecondary structures. In an alternative model, hydrophobic forces among the nonpolar residues initiate the folding by a spontaneous collapse of the polypeptide into a compact state (molten globule) having high content of secondary structures. A protein may fold by incorporating the features of both of the pathways. The process of protein folding can be seen as a folding funnel. The unfolded state (top of the funnel) has a higher degree of entropy and free energy. Progress of folding is accompanied by a decrease in the number of states present, thereby reducing the entropy and free energy and increasing the amounts of native-like structures of the protein. Small depressions along the sides of the funnel represent semi-stable intermediates which might slow the folding process (Fig. 2.10).

2.3.1.1 Secondary and Tertiary Structure Formation

Protein folding is initiated by formation of secondary structure. The simplest secondary structure, α helix, is a rodlike structure in which the polypeptide backbone is tightly coiled forming the inner part of the rod with side chains (R groups) protruding outward in a helical manner. Hydrogen bonds are formed between the CO group of each amino acid with the NH group of the amino acid that is situated four residues ahead in the sequence. All amino acids within the α helix are hydrogen bonded except for the ones near the end. Approximately 3.6 amino acid residues are found per turn of the helix. Both right-handed (clockwise) and left-handed (counterclockwise) α helices are allowed conformations in the Ramachandran plot. However, right-handed helices are energetically more favorable due to less steric hindrance among the side chains and the backbone. Essentially right handed α helices are found in all proteins. Stability of α helix depends on electrostatic force, weight of adjacent R group, interaction between R groups spaced close (3–4 residues apart) to each other, occurrence of proline and glycine residues, the interaction between amino acid residues at the end of helical segment, and the electric dipole inherent to the α helix. The tendency of a given segment of a polypeptide chain to fold up as α helix therefore depends on the identity and sequence of amino acid residues within the segment (Fig. 2.11).

In the β pleated sheet or β strand, the polypeptide chain extends in a zigzag manner, arranged side by side (hence the name) with R groups protruding in opposite directions. In this structure, the hydrogen bonds are formed between the

Beginning of helix formation and collapse
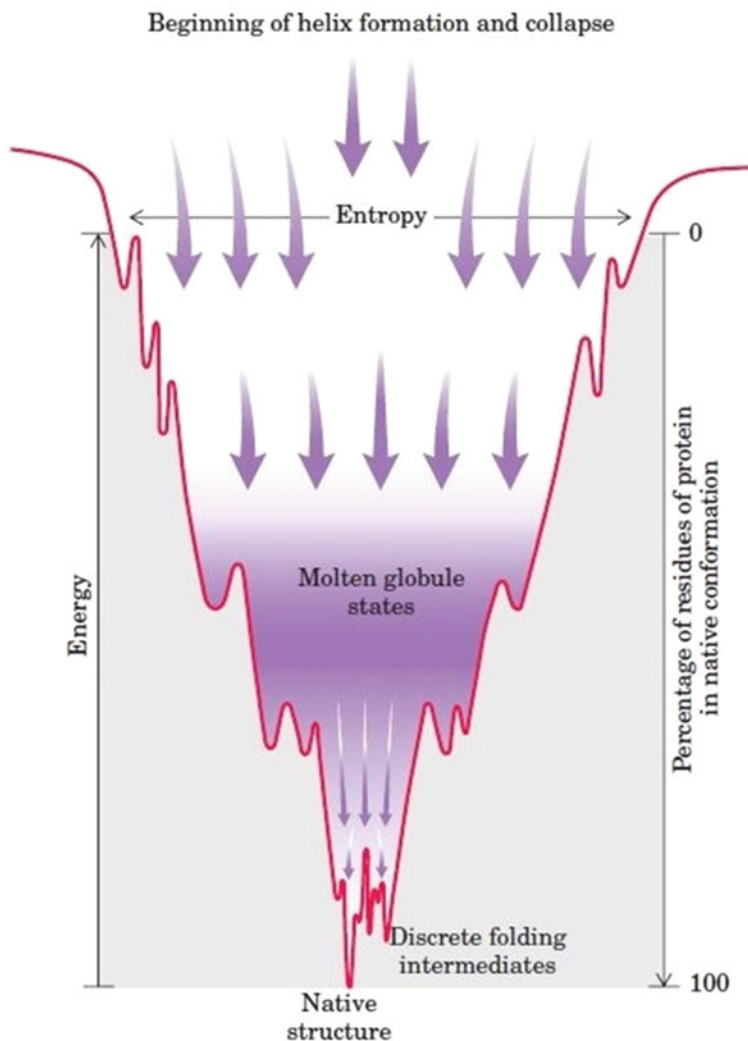
Fig. 2.10 The thermodynamics of protein folding depicted as a free-energy funnel (Nelson and Cox 4 ed. Chapter 4, p. 149, 2005)

adjacent residues in the polypeptide chain. Amino acids along a β strand lie approximately 3.5 Å to each other. The adjacent chains can either run in opposite, i.e., antiparallel direction or in the same, i.e., parallel direction (having the opposite or same amino-to-carboxyl orientations, respectively). In the antiparallel confor- mation, the NH group and the CO group of each amino acid, respectively, bond with the CO group and the NH group of another amino acid on the adjacent chain.
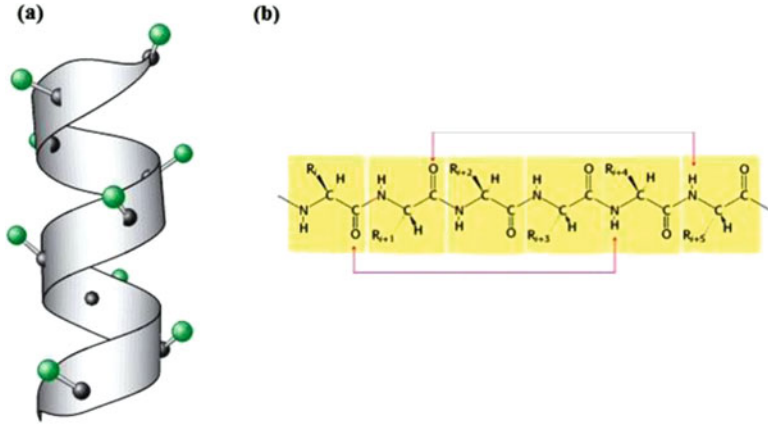
Fig. 2.11 Structure of the α helix. (**a**) A ribbon depiction with the a-carbon atoms and side chains (*green*) shown. (**b**) Hydrogen bonding scheme for an α helix, the CO group of residue *n* forms a hydrogen bond with the NH group of residue *n* + 4 (Stryer 5 ed. Chapter 3, p. 105, 2002)
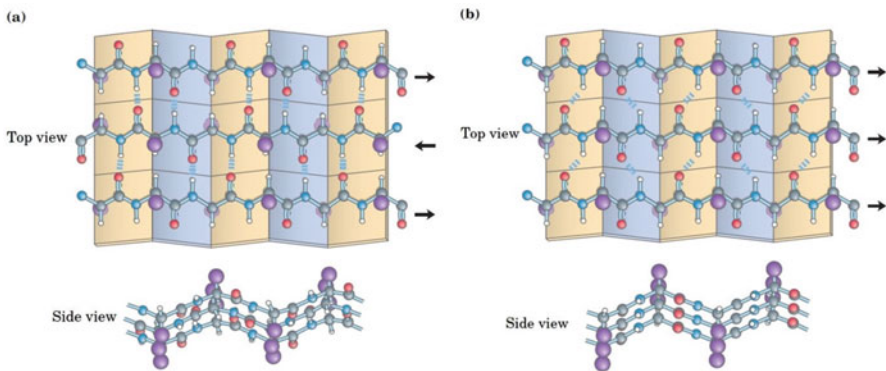
Fig. 2.12 The β conformation of polypeptide chains (Nelson and Cox 4 ed. Chapter 4, pp. 123, 2005) (**a**) Antiparallel (**b**) Parallel

In the parallel conformation, for each amino acid, the NH group is bonded to the CO group of one amino acid on the adjacent strand, whereas the CO group is bonded to the NH group on the amino acid two residues farther along the chain (Fig. 2.12). Many β strands combine to form a β sheet. The β sheets are significant elements in many proteins such as fatty acid-binding proteins which are important for lipid metabolism.

In more compact globular proteins, polypeptide chain reverses direction, accomplished by common structures called reverse turn (β turn or hairpin bend). These structures act like connecting elements, linking the successive α helix or β conformation. The structure of β turn comprises of four amino acid residues, with the CO
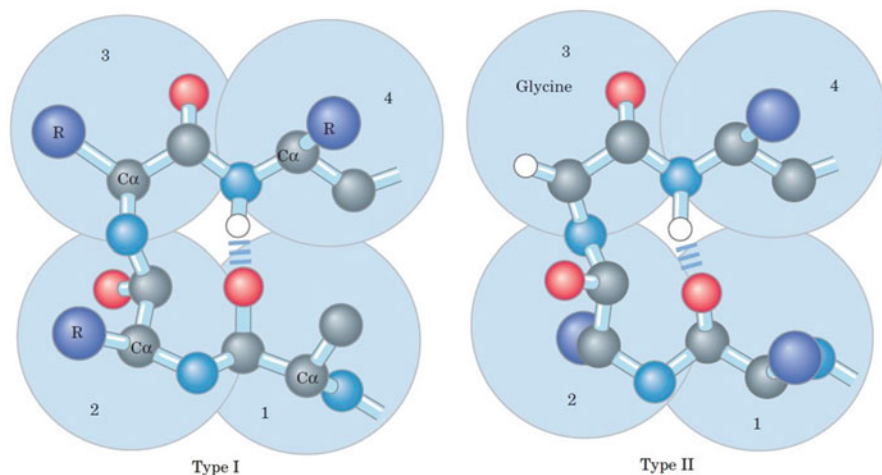
Fig. 2.13 Structures of β turns. Type I and type II β turns are most common; type I turns occur more than twice as frequently as type II. Type II β turns always have Gly as the third residue (Nelson and Cox 4 ed. Chapter 4, p. 124, 2005)

group of the first residue hydrogen bonded to the NH group of fourth residue, all arranged in a 180° turn. Other structures called Ω loops (omega loops) are also responsible for reversals in the chain. These are well defined and rigid, but do not have regular, periodic structures. Turns and loops are responsible for interactions between proteins and other molecules. The distribution of α helices, β strands, and turns along a protein chain is often referred to as its secondary structure (Fig. 2.13).

The overall three-dimensional arrangement of all atoms in a protein is referred to as the protein's tertiary structure. Amino acids residing far apart and in different types of secondary structure may interact within the completely folded structure of a protein. Amino acids such as Pro, Thr, Ser, and Gly determine the location, direction, and angle of the bends in the polypeptide chain. The tertiary structure is stabilized by hydrophobic interactions, like covalent bonds such as disulfide cross-links between two cysteine residues. Tertiary structure may give way to quaternary structure, which involves the arrangement of two or more already folded protein subunits (identical or different) in three-dimensional complexes.

2.3.1.2 Role of Water in Protein Folding

The properties of water dominate the interactions of biological molecules. Since water is a polar molecule, hydrophobic residues in a polypeptide chain have a strong tendency to reject water. In an aqueous environment, the proteins fold in such a way that the hydrophobic (nonpolar) side chains are buried inside and its polar (hydrophilic) charged chains remain on the surface. The α helices and β sheets contain hydrophilic and hydrophobic portions (i.e., amphipathic nature) which aid in the formation of tertiary structures and hence assist in the folding of the proteins.

Water-filled
hydrophilic channel

Largely hydrophobic
exterior
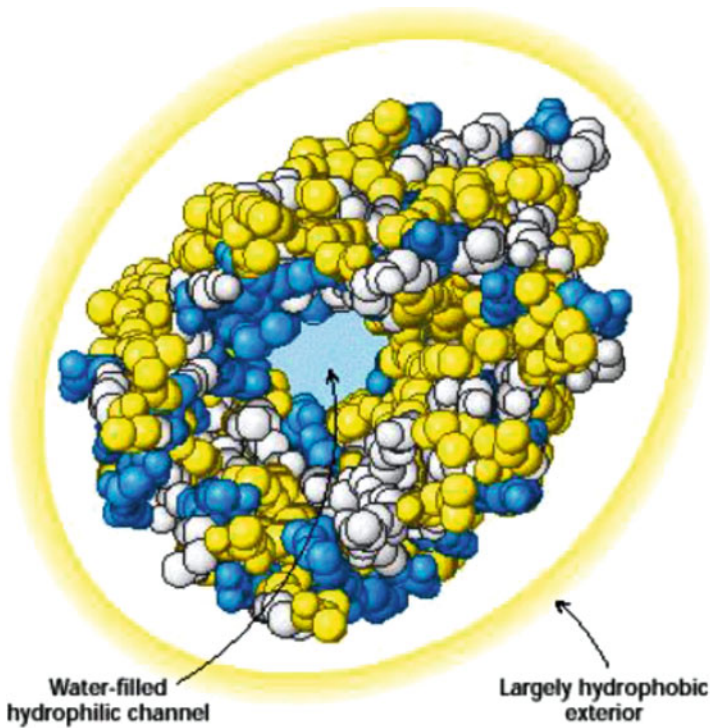
Fig. 2.14 "Inside Out" amino acid distribution in porin (Stryer 5 ed. Chapter 3, p. 114, 2002)

The utmost purpose of such formation is to increase the stability of the protein. The polypeptide backbone is buried inside so that all the carbonyl and amino groups are paired by hydrogen bonding. Van der Waals interactions between tightly packed hydrocarbon side chains also contribute to the stability of proteins. Exceptions to this rule are found in bacterial membrane proteins called porins. The permeability barriers of membranes are built largely of alkane chains that are quite hydrophobic. Thus, porins are covered on the outside largely with hydrophobic residues that interact with the neighboring alkane chains (Fig. 2.14).

2.3.2 Folding/Unfolding M-Values

Proteins undergo unfolding in aqueous solution upon addition of certain reagents (denaturing agents). One of the primary ways of comparing the stabilities of mutant proteins with normal proteins is by means of measuring their conformational stability in the presence of denaturants. These denaturants alter the equilibrium between the folded (native) and unfolded (denatured) states of the proteins and hence the free energy. The free energy of the unfolding reaction can be stated as:

$\Delta G = -RT \ln(U/F)$. F and U are the concentrations of protein in the folded and unfolded conformation, respectively, at a particular denaturant concentration and can be determined by spectral studies of protein conformations. The free energy of unfolding is plotted against denaturant concentration in the transition region.

Urea and guanidinium hydrochloride are commonly used denaturants. Their interaction with proteins shows a linear dependence of free energy of unfolding on the molar concentration of denaturant, and thus this linear extrapolation method is used widely to estimate the conformational stability of the protein. Through this method two parameters were obtained: the free energy of unfolding at zero denaturant concentration (represented by ΔG^{H_2O}, the intercept) and the dependence of free energy on denaturant concentration (represented by the symbol m, the slope) (Myers et al. 1995). Variation in solvent accessible area of hydrophobic residues may be a reason for varied M-values, and this value depends upon the cooperation during transition in protein structure.

2.3.3 Models of Protein Folding

The framework or hierarchic model (Fig. 2.15) proposed that folding starts with amino acid residues forming the secondary structure, which then interacts to form an intermediate. As the folding proceeds, side chains are packed in a specific manner. Several folding intermediates are formed during the process of complete protein folding and it is assumed that elements of secondary structure are independent of tertiary structure. The diffusion-collision model (Fig. 2.16) is based on the assumption that protein is composed of several highly unstable microdomains which comprise of nascent secondary structure or hydrophobic clusters. In order to gain stability these elements diffuse and collide, successfully adhering and coalescing to form a more stable entity and hence give the tertiary structure (Karplus and Weaver 1994).

The hydrophobic-collapse model is based on the fact that the native state of a protein consists of a hydrophobic core of nonpolar amino acid residues in the protein's interior. The model hypothesizes that this hydrophobic core would collapse rapidly before the formation of secondary structures and then can be restructured from restricted conformational space occupied by the intermediate.

The nucleation condensation model is based on the assumption that protein folding is analogous to crystallization and nucleus formation being the limiting step in the process. It is the fusion of both hydrophobic collapse and framework mechanism. This model postulates that folding starts with the formation of weak local nucleus, i.e., some neighboring residues in the sequence form native secondary structure (nucleus), which is further stabilized by interactions leading to a more extended nucleus. The native structure would propagate from this nucleus in a stepwise manner. Thus, the tertiary structure would form as a necessary outcome of the secondary structure (Ahluwalia et al. 2012).
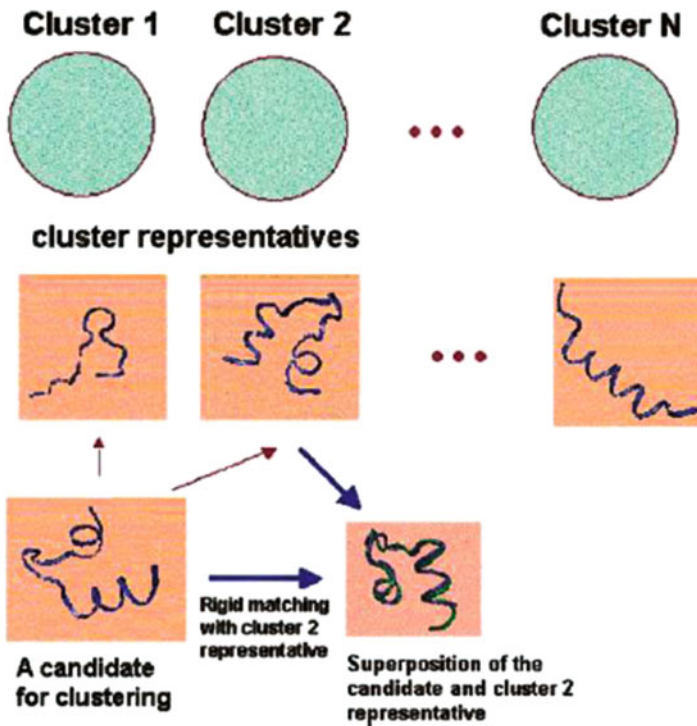
Fig. 2.15 Illustration of the clustering process. Circles at the top represent the clusters, and building blocks below them are their representatives. In this figure there are three clusters. The bottom left building block is a candidate for clustering. It is a trial matched against the representatives of the clusters until a match is found (in this case, a match is obtained with the representative building block of cluster 2). The match is shown in the square at the bottom center. Consequently, the candidate building block is joined to cluster 2 and is not tested against the other cluster representatives (Haspel et al. 2003)

2.3.4 Protein Misfolding

Cooperative structural unit of native proteins is known as foldons, and these are under the process of continuous folding and unfolding. In order to function appropriately, protein must first achieve a proper conformation and get packed within the cell. As discussed in Sect. 2.2.5, multiple chaperone systems are required for correct folding of proteins. Degradation pathways for destruction of improperly folded proteins also work parallel, but particulars of multisystem process provide plenty of opportunities for error. In addition to general misfoldings, mutations may also cause misfolding, nonfunctional proteins to accumulate.

Nonfunctional proteins lead to various pathological conditions (proteopathology). Improper degradation, mislocalization, dominant-negative mutations, and structural alterations are few phenomena which lead to novel toxic functions and amyloid accumulation. Some examples are CFTR (cystic fibrosis
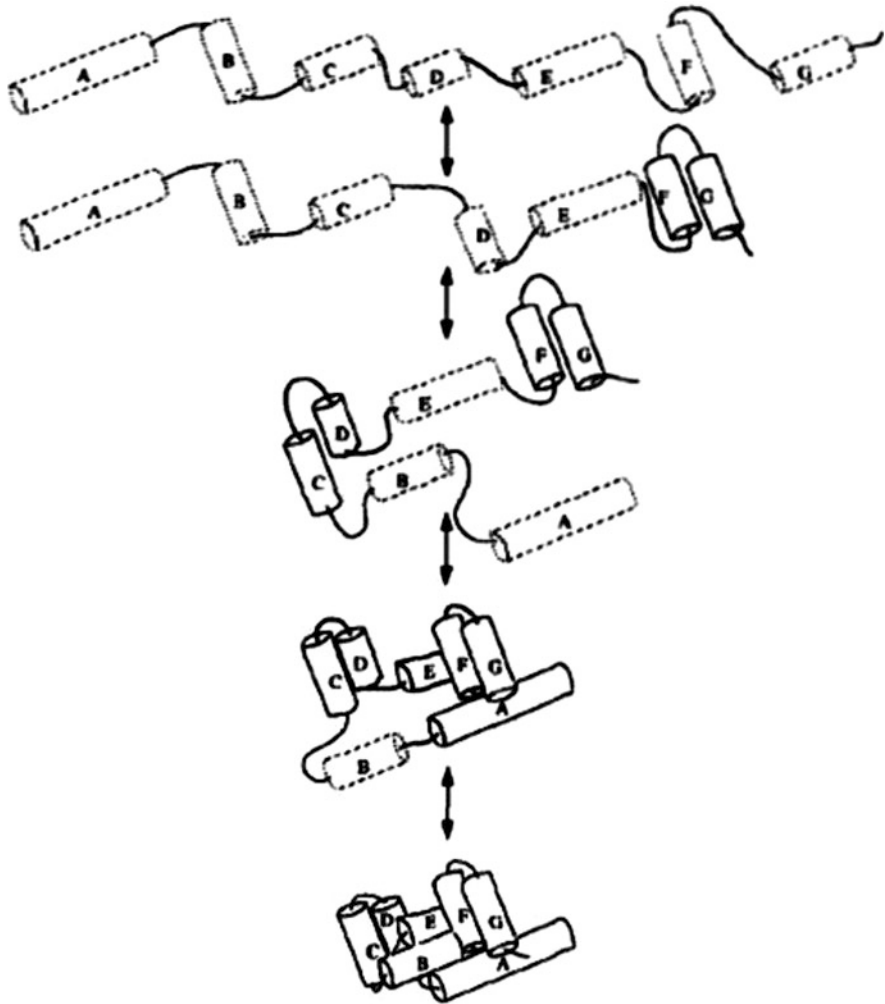
Fig. 2.16 A cartoon showing five "snapshots" of the diffusion-collision folding kinetics of a multimicrodomain protein or protein domain. The time line of the kinetics runs from the top down. The system starts in the "random coil" set of conformations. The microdomains (**A–G**) are individually unstable (indicated by dashed outlines) and transiently occupy folded secondary structure conformational states (probably native or near native). Diffusive encounters, when a pair of microdomains is transiently folded, lead to more stable coalescence intermediates (denoted by solid outlines) held together by hydrophobic interactions. Multimicrodomain intermediates collide and coalesce into a loosely folded, more stable structure (Karplus and Weaver 1994)

transmembrane conductance regulator, caused due to mutation leading to its misfolding in endoplasmic reticulum), Alzheimer's disease, Parkinson's disease, Huntington's disease, and prion disease caused due to aggregation of diverse set of peptides and proteins associated with the conversion to amyloid-like fibrillar

assemblies. The function of chaperones in these processes has encouraged efforts to chemically modulate systems, with the objective of providing global protection against protein misfolding (Valastyan and Lindquist 2014).

2.4 Protein Structure and Stability

Stability of protein structure is defined as tendency of protein to maintain its native structure. Native proteins are only marginally stable entities under physiological conditions. The proteins have a stable structure due to the balance among the various non-covalent forces, to which it is subjected—ionic and dipolar interactions, hydrogen bonding, and hydrophobic forces. Protein stability is the free energy change between the correctly folded structure of a protein and the unfolded or denatured state. The equilibrium constant, $K_{eq} = $ [native]/ [denatured], is large for the folding reaction which indicates that the protein is stable. Proteins can be denatured by lowering the pH, increasing the temperature, or adding detergents.

2.4.1 Effect of Charged Ions and Chemical Reagents

Salts have varying effects on the protein structure. Some stabilize the protein structure; some have no effect, while others destabilize it. Various ions affect the protein stability in a specific order (Hofmeister series) which also corresponds to their capacity to salt out proteins. The ions in the Hofmeister series that tend to denature proteins, I^-, SCN^-, Li^+, Mg^{2+}, Ca^{2+}, and Ba^{2+}, are said to be chaotropic. Chaotropic agents disrupt the hydrophobic forces by increasing the solubility of nonpolar substances in water. On the other hand, protein stabilizing agents strengthen the hydrophobic interactions, thus increasing the tendency of water to expel proteins and salt them out (salting out). Urea and guanidinium ion (Gu^+) increase the solubility of the hydrophobic side chains in water. Detergents and miscible organic substances, such as aliphatic alcohols or acetone, interfere with the hydrophobic interactions perturbing the stability of protein structures through formation of their own hydrophobic interactions with water.

2.4.2 Effect of pH and Temperature

The stability of protein structure highly depends upon the pH and temperature of their environment. Variations in pH alter the ionization states of amino acid side chains thereby changing the net charge distribution on the protein, causing differences in the electrostatic forces and disruption of some of the hydrogen bonds. Temperature changes primarily affect the weak interaction in a protein. When the temperature of a protein in solution is increased, its conformationally sensitive properties, such as viscosity, optical rotation, and UV absorption, change

abruptly over a narrow temperature range. Loss of structure or unfolding in one part of the protein destabilizes the remaining parts suggesting that unfolding is a cooperative process. The temperature at the midpoint of this process is known as the protein's melting temperature (T_m). Thermophilic microorganisms produce highly stable proteins that can function at the temperature of hot springs. The structural stability of these proteins is still unknown, yet they show slight difference in their structure from those proteins derived from mesophilic microbes.

2.4.3 Thermodynamic Linkage Between Protein Structure Stability and Function

Protein stability is proportional to the difference in the Gibbs free energy (ΔG) between the folded and the unfolded states of the protein. Stability of protein is affected by relative free energies of the folded (G_f) and the unfolded (G_u) states (Eq. 2.1).

$$\Delta G = G_u - G_f \qquad (2.1)$$

Gibbs free energy (G) is related to enthalpy (H) and entropy (S) by the following Eq. 2.2:

$$G = H - TS \qquad (2.2)$$

where T is the temperature in Kelvin.

For a globular protein, the folding free energy difference, ΔG_u, is typically small (5–15 kcal/mol) as compared to, say, a covalent bond which is around ~30–100 kcal/mol. During a reaction, the free energy change depends on the equilibrium constant. For favorable and downhill reactions, the free energy of the product is lower than that of the reactant, hence ΔG is negative. Very downhill reactions have very large equilibrium constants.

2.5 Conclusions

By virtue of pooling all facts related to protein folding in this review, it was found through various studies that possible trajectories channelized through global free energy minimum are responsible for protein folding. Decisive interactions among side chains of amino acids, various thermodynamic factors, and environment are responsible for protein folding, and limited range of protein scaffolds is available which influence protein folding pathway making backbone of protein. Understanding of protein folding mechanism helps us to understand cellular regulations in an improved way, gives opportunity to design proteins with novel functions, and helps in genomics studies and therapeutics. Similarly better understanding of proteopathies is an essential trait to combat various protein folding linked diseases.

We believe that bringing all factors associated with protein folding together will be of substantial help to readers.

References

Abkevich VI, Shakhnovich EI (2000) What can disulfide bonds tell us about protein energetics, function and folding: simulations and bioinformatics analysis. J Mol Biol 300:975–985

Ahluwalia U, Katyal N, Deep S (2012) Models of protein folding. J Prot Proteo 3(2):85–93

Alberts B, Johnson A, Lewis J, Raff M, Roberts K, Walters P (2002) The shape and structure of proteins. Molecular biology of the cell, 4th edn. Garland Science, New York/London. ISBN 0-8153-3218-1

Alberts B, Bray D, Hopkin K, Johnson A, Lewis J, Raff M, Roberts K, Walter P (2010) Protein structure and function. Essential cell biology, 3rd edn. Garland Science, New York, pp 120–170. ISBN 978-0-8153-4454-4

Anfinsen CB (1972) The formation and stabilization of protein structure. Biochem J 128 (4):737–749. doi:10.1042/bj1280737. PMC 1173893 PMID 4565129

Berg JM, Tymoczko JL, Stryer L (2002) Protein structure and function. Biochemistry. W. H. Freeman, San Francisco. ISBN 0-7167-4684-0

Brandon C, Tooze J (1991) Introduction to protein structure. Garland Publishing, New York/London

Carrell RW, Lomas DA (1997) Conformational disease. Lancet 350(9071):134–138. doi:10.1016/S0140-6736(97)02073-4

Chiti F, Dobson CM (2006) Protein misfolding, functional amyloid, and human disease. Annu Rev Biochem 75(1):333–366. doi:10.1146/annurev.biochem.75.101304.123901

Creighton TE (1990) Protein folding. Biochem J 270:1–16

Darby NJ, Creighton TE (1993) Dissecting the disulphide-coupled folding pathway of bovine pancreatic trypsin inhibitor: forming the first disulphide bonds in analogues of the reduced protein. J Mol Biol 232:873–896

Dressler D, Potter H (1991) Discovering enzymes. W.H. Freeman, New York/Oxford

Essential Biochemistry (2016) www.wiley.com

Flory P (1953) Principles of polymer chemistry. Cornell University Press, Ithaca

Friedrich O (2006) Critical illness myopathy: what is happening? Curr Opin Clin Nutr Metab Care 9(4):403–409. doi:10.1097/01.mco.0000232900.59168.a0

Harel M, Su CT, Frolow F, Silman I, Sussman JL (1991) Gamma-chymotrypsin is a complex of alpha-chymotrypsin with its own autolysis products. Biochemist 30:5217

Haspel N, Tsai CJ, Wolfson H, Nussinov R (2003) Hierarchical protein folding pathways: a computational study of protein fragments. Prot Struc Func Genet 51:203–215

Hogg PJ (2003) Disulfide bonds as switches for protein function. Trends Biochem Sci 28(4):210–214

Hubbard RE, Haider MK (2010) Hydrogen bonds in proteins: role and strength. University of York, York. doi:10.1002/9780470015902.a0003011.pub2

Karplus M, Weaver DL (1994) Protein folding dynamics: The diffusion-collision model and experimental data. Prot Sci 3:650–668

Lovell SC, Davis IW, Arendall WB III, de Bakker PIW, Word JM, Prisant MG, Richardson JS, Richardson DC (2003) Structure validation by C_α geometry: φ/ψ and C_β deviation. Prot Struc Func Genet 50:437–450

Luheshi M, Crowther DC, Dobson CM (2008) Protein misfolding and disease: from the test tube to the organism. Curr Opin Chem Bio 12(1):25–31. doi:10.1016/j.cbpa.2008.02.011

Marnathambika BS, Bardwell JC (2008) Disulfide-linked protein folding pathways. Annu Rev Cell Dev Biol 24:211–235

Mogk A, Mayer MP, Deuerling E (2002) Mechanisms of protein folding: molecular chaperones and their application in biotechnology. Chem Bio Chem 3(9):807–814

Myers JK, Pace CN, Scholtz JM (1995) Denaturant m values and heat capacity changes: relation to changes in accessible surface areas of protein unfolding. Protein Sci Publ Protein Soc 4(10):2138–2148

Pace CN, Grimsley GR, Thomson JA, Barnett BJ (1988) Conformational stability and activity of ribonuclease T1 with zero, one, and two intact disulfide bonds. J Biol Chem 263:11820–11825

Privalov PL, Khechinashvili NN (1974) J Mol Bio 86:665–684

Schmidt B, Ho L, Hogg PJ (2006) Allosteric disulfide bonds. Biochemistry 45(24):7429–7433

Qin M, Wang W, Thirumalai D (2015) Protein folding guides disulfide bond formation. PNAS 112(36):11241–11246

Ramachandran GN, Sasisekaran V (1968) Conformation of polypeptides and proteins. Adv Prot Chem 23:284–438

Saibil H (2013) Chaperone machines for protein folding, unfolding and disaggregation. Nat Rev Mol Cell Biol 14(10):630–642. doi:10.1038/nrm3658

Saunders R, Deane CM (2010) Synonymous codon usage influences the local protein structure observed. Nucl Acids Res 38(19):6719–6728. doi:10.1093/nar/gkq495

Selkoe DJ (2003) Folding proteins in fatal ways. Nature 426(6968):900–904. doi:10.1038/nature02264

Spinner NB (2000) CADASIL: notch signaling defect or protein accumulation problem? J Clin Invest 105(5):561–562. doi:10.1172/JCI9511

Thornton JM (1981) Disulphide bridges in globular proteins. J Mol Biol 151:261–287

Valastyan JS, Lindquist S (2014) Mechanisms of protein-folding diseases at a glance. Disease Mod Mech 7:9–14. doi:10.1242/dmm.013474

Van den Berg B, Wain R, Dobson CM, Ellis RJ (2000) Macromolecular crowding perturbs protein refolding kinetics: implications for folding inside the cell. EMBO J 19(15):3870–3875. doi:10.1093/emboj/19.15.3870

Walker LC, LeVine H III (2000) The cerebral proteopathies: neurodegenerative disorders of protein conformation and assembly. Mol Neurobiol 21(1–2):83–95. doi:10.1385/MN:21:1-2:083

Westermark P et al (2007) A primer of amyloid nomenclature. Amyloid 14(3):179–183. doi:10.1080/13506120701460923

Yennawar NH, Yennawar HP, Farber GK (1994) X-ray crystal structure of gamma-chymotrypsin in hexane. Biochemistry 33:7326

Nucleic Acid Structure and Function

3

Jyotika Rajawat

Abstract

This chapter deals with the in-depth knowledge about nucleic acid types, structure, function, and properties. Deoxyribonucleic acid (DNA) and ribonucleic acid (RNA) consist of three major constituents, namely, nitrogen base, pentose sugar, and phosphate group. The major difference between DNA and RNA component is the presence of different sugars and also the difference in nitrogen base where uracil is present in RNA instead of thymine. Both DNA and RNA have different conformations in a living cell with varying structures. The groundbreaking work included the deduction of double-helical DNA structure proposed by Watson and Crick, and later tRNA structure was explained in detail by Robert W. Holley and then Alexander Rich. We have also focused on the significance of major and minor grooves of DNA in regulating various functions of DNA. These grooves are promiscuous binding sites for proteins required during replication and transcription. The chapter also includes various forces like bonds, geometrical conformations, base pairing, and base stacking, which regulate the nucleic acid geometries and contribute in the stability of DNA structure. Besides the regular Watson-Crick pairing, Wobble base pairing has been discussed which provides different contextual functions to several proteins. We also highlight the unique properties of nucleic acids and the various ways to fractionate them. This chapter also contains several other functions of nucleotides, other than the genetic storehouse of the cell, where nucleotides function as energy carrier, chemical messengers, and cofactors of enzymes.

J. Rajawat (✉)

Cell Death Research Laboratory, Endocrinology Division, CSIR-Central Drug Research Institute, B.S. 10/1, Sector-10, Jankipuram Extension, Lucknow 226031, Uttar Pradesh, India
e-mail: jrajawat@gmail.com

3.1 Components of Nucleic Acids

Nucleic acids (DNA and RNA) are large organic molecules in cells and are genetic storehouse of the body.

3.1.1 Nucleosides and Nucleotides

Nucleotides are building block or monomeric units, which join together to form polymeric DNA or RNA. Each nucleotide has three characteristic components:

1. Nitrogen base/organic base
2. Pentose sugar (five carbon)
3. Phosphate group

Molecule without phosphate group, containing only nitrogen base and pentose, is called nucleoside. Structural unit of DNA is deoxyribonucleotide (deoxyribonucleoside-5′ monophosphate) and of RNA is ribonucleotide (ribonucleoside-5′ monophosphate). Nucleic acids with 50 nucleotides or less are known as oligonucleotide, and longer nucleic acid is called polynucleotide.

3.1.2 Purine and Pyrimidine Bases

Nitrogen bases are derived from two parent compounds, pyrimidines (single-ring structure) and purines (two-ring structure). Five different nitrogen bases are components of DNA and RNA, of which two are major purine bases, adenine (A) and guanine (G), present in both nucleic acids and three pyrimidine bases. Cytosine (C) is common in both nucleic acids, but the second pyrimidine in DNA is thymine (T) and is uracil (U) in RNA. Free purine and pyrimidine bases have weak basic nature and are highly conjugated molecules. Conjugating property of bases is responsible for the change in several properties of nucleic acids such as structure, electron distribution, and light absorption. The ring structure provides resonance to bases imparting partial double-bond character, and also existence of tautomers depends upon pH change. Uracil occurs in three tautomeric forms, lactam, lactim, and double lactim, based on pH change. All nucleotide bases absorb UV light at 260 nm due to resonating structures. Hydrophobic nature of organic bases imparts them insoluble property at neutral pH, and with the change in pH, the bases get charged, hence increasing the solubility.

Fig. 3.1 Nucleotides structure with the hydrogen bonds in nucleic acids
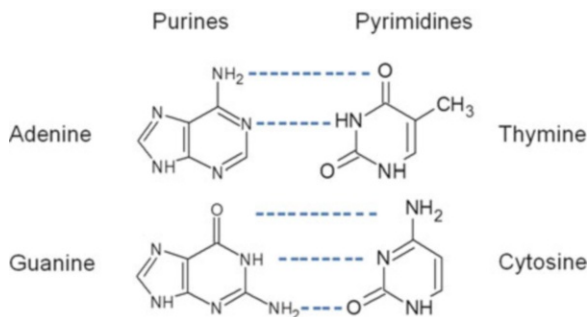
Some minor unusual bases are also present in nucleic acids which regulate and protect the genetic information. Some unusual bases include 5-methylcytidine reported in DNA of higher plants and certain animal species, N6-methyladenosine in bacterial DNA, 5-hydroxymethylcytidine in phage-infected bacterial DNA, N2-methylguanosine in RNA duplex and G-tetraplex, and 7-methylguanosine. Some minor bases found in tRNA are inosine, pseudouridine, and 4-thiouridine. Inosine contains hypoxanthine as base, and pseudouridine has uridine.

3.1.3 Pentose and Phosphate

There are two types of pentose in nucleic acids. $2'$-deoxy-D-ribose is a component of deoxyribonucleotide units of DNA, while D-ribose is a constituent of ribonucleotide units of RNA. Pentose ring is in puckered conformation.

Nitrogen base is covalently joined through hydrogen ($-H$) at pyrimidine N1 or purine N9 by N-β glycosyl bond to the hydroxyl group ($-OH$) at C1 of pentose sugar with the removal of a water molecule forming O-glycosidic bond (Fig. 3.1). Phosphate group is esterified to the carbon 5 (C5) of pentose and is always ionized with pKa of 1.0.

Successive nucleotides are linked covalently via phosphate group bridges where $5'PO_4$ group of one nucleotide is linked to $3'OH$ group of the next nucleotide through phosphodiester linkage. Thus nucleic acid backbone consists of alternating phosphate and pentose, while nitrogen bases constitute side groups. Phosphodiester linkages impart polarity due to similar orientation along the chain and also distinct ends to each strand of nucleic acids. Hydroxyl group of pentose provides hydrophilic nature to nucleic acid backbone.

Cells also contain nucleotides with phosphate group at different positions than $5'C$ such as ribonucleoside $2'3'$-cyclic monophosphate and ribonucleoside $3'$-monophosphate which are formed during RNA hydrolysis catalyzed by ribonuclease. Adenosine $3'5'$-cyclic monophosphate (cAMP) and guanosine $3'5'$-cyclic monophosphate (cGMP) are regulatory molecules with PO_4 group at different positions than usual.

3.2   Structure of Nucleic Acids

3.2.1   Double-Helical Structure of DNA

DNA is a double-helical structure which stores genetic information. DNA was first accidentally identified in human white blood cells by Swiss scientist Friedrich Miescher and termed it as "nuclein." Miescher's work was unrecognized for more than 50 years. Later Russian biochemist Phoebus Levene first discovered the major components of a nucleotide along with their order. He puts forth the model of "polynucleotide" for yeast nucleic acid. Levene proposed that each nucleotide is composed of single nitrogen base, a phosphate group, and either deoxyribose (in DNA) or ribose (in RNA). Further, nucleotides were arranged as tetranucleotide repeats to constitute nucleic acid. Levene's work was carried forward by Erwin Chargaff, who proposed Chargaff's rules for DNA composition and properties in species. Chargaff's rules and Levene's work laid the foundation for Watson and Crick to deduce the crystal structure of DNA and to propose double-helical structure. DNA fibers were first analyzed in detail by Rosalind Franklin and Maurice Wilkins through X-ray diffraction. Their inference includes helical form of DNA molecule along with two periodicities at the long axis, primary being 3.4 Å between two base pairs and secondary with 34 Å involving ten base pairs. Just before Watson and Crick's proposal, Linus Pauling also predicted the three-dimensional structure of DNA based on the bond length and bond angles, but his prediction for DNA structure proved to be incorrect. Later in 1953, Watson and Crick postulated 3D model of DNA whereby right-handed double helix is formed when two helical chains in DNA interwound along the long axis. The two strands are antiparallel and complementary to each other, and pairing of these strands generates grooves on the duplex surface, known as major and minor groove. Nucleotides are connected through phosphate groups which link $3'$ end of one sugar to $5'$ end of the next. Hydrophilic backbone of deoxyribose and phosphate groups is toward the outer side of helix, and nitrogen bases are stacked inside, being perpendicular to long axis. To account for two periodicities observed, it was proposed that the vertically stacked bases are 3.4 Å apart and second periodicity accounted for 10.5 base pairs per turn of the helix. Two major forces responsible for holding double helix involve a hydrogen bonding between bases of antiparallel strands and another being intrastrand hydrophobic base-stacking interaction. Base-stacking interaction is a major force responsible for DNA stability. Thus this model provided the evidence for self-replication of DNA (Fig. 3.2).

3.2.2   Helix Parameters

Helical analysis of DNA was first described from techniques of Dickerson and colleagues. The helical axis of DNA is perpendicular to its plane and passes through the center. DNA attains helical structure due to twisting of the stacked bases to increase the hydrophobic interactions. Each dinucleotide combination in B-DNA
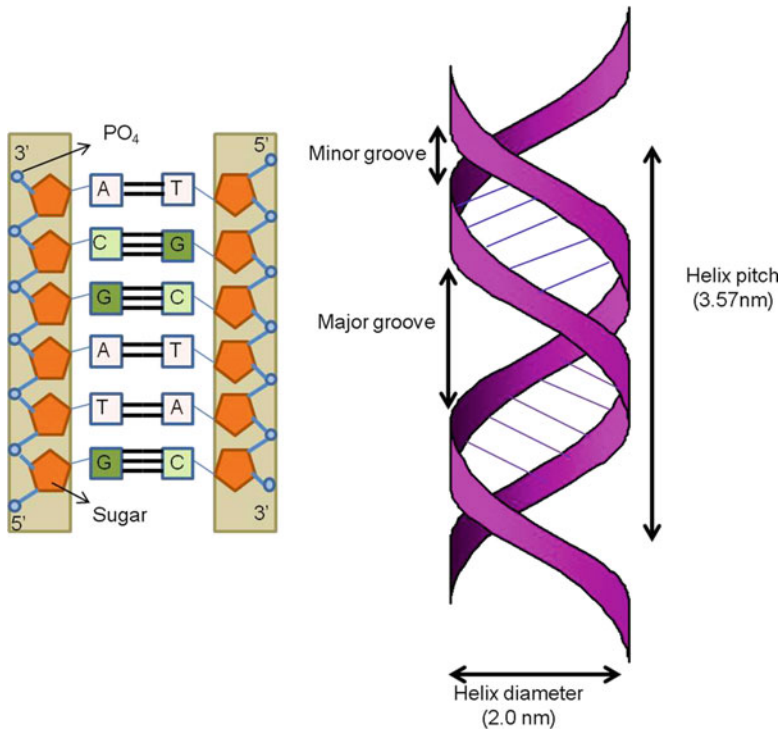
Fig. 3.2 Double-helical B-DNA structure proposed by Watson and Crick

has different twist angle and propeller twist accompanied with varying stacking energies. Moreover, the helical parameters vary for all conformations including, A-, B-, and Z-DNA (Table 3.1).

3.2.3   DNA Supercoiling and Gyrase

DNA is interwound or twisted causing supercoiling of the helix. In eukaryotes DNA is wrapped around octamers of histones, while in prokaryotes DNA is under torsional strain. DNA when twisted in helix direction generates positive supercoiling where bases are tightly held, while when twisted in opposite direction, bases come apart more easily, generating negative supercoils. DNA compaction and gene regulation are few such biological processes that involve supercoiling. Conformational variability in DNA largely arises due to supercoiling. Moreover, the presence of unpaired bases and distortions relieve torsional strain, thus further adding to the variability. Mostly DNA is maintained in negative supercoiled state, and positive state is transiently formed during replication and transcription. The degree of supercoiling is defined or measured by linking number, twist, and writhe. Linking number (denoted as Lk) is defined as the number of times a DNA strand

Table 3.1 Helical parameters in different conformations of DNA

Parameters	A-DNA	B-DNA	Z-DNA
Helix direction	Right handed	Right handed	Left handed
Base pairs/turn	11	10.5	12
Helix pitch	28°	34°	45°
Tilt (per base pair)	20°	−6°	7°
Twist angle	33°	36°	−30°
Helix diameter (nm)	2.3	2.0	1.8

winds around the other strand and is represented as an integer. The number of revolutions about the double helix is twist (Tw), and the number of turns a double helix takes around other duplex is known as writhe (Wr). It is a superhelical twist. Thus the degree of supercoiling is numerically expressed as:

$$Lk = Length\ of\ DNA(bp)/10.5$$

$$Lk = Tw + Wr$$

Linking number is equal to twist in a relaxed DNA (Lk = Tw) (Cruz 2012).

Supercoiled DNA can exist in two forms – toroidal and plectonemic (interwound). One start tight left-handed turn produces toroid, and two start right-handed helices with terminal loops generate plectonemes. Supercoiled DNA is wrapped as toroid in nucleosome core particles, while plectoneme is the dominant form in bacteria (Travers and Muskhelishvili 2007). Sometimes for larger molecules a hybrid structure containing both toroid and plectonemic loop is seen.

Topology of DNA in both prokaryotes and eukaryotes is maintained by topoisomerases. In most prokaryotic DNA, topoisomerase I acts on negative supercoil, where it introduces nick in one DNA strand and removes a negative supercoil one at a time. This is an energetically favored reaction which occurs without the expense of ATP. Since growing DNA fork generates positive supercoil, topoisomerase II (DNA gyrase) comes in action. Topoisomerase II introduces nicks in both strands of DNA and further reseals the cut by ATP hydrolysis, thus linking (catenation) and unlinking (decatenation) the two strands of double-helical molecule (Lodish et al. 1995).

3.2.4 Intercalation

A large number of ligands/molecules interact with DNA, and there are three modes of DNA association with metal complexes or ligands – external binding, groove binding, and intercalation.

External binding is electrostatic in nature where positively charged metal ions Ru or Mg^{2+} interact with negatively charged DNA phosphate sugar backbone. There is adsorption of molecules in the DNA grooves held by van der Waals

force, while hydrophobic and hydrogen bonding provide stability to this complex upon groove binding.

Intercalation is an insertion of planar aromatic compound between stacked base pairs, and binding is stabilized by hydrophobic stacking interactions. Intercalated molecule induces shape and flexibility change of DNA and increases the viscosity. In addition, intercalation engenders lengthening and unwinding of the DNA helix (Sinden 2012).

3.2.5 Structure of RNA

Single-stranded RNA assumes a right-handed helical conformation, dominated by base-stacking interactions. The presence of complementary sequences form double-stranded A-form right-handed helix. Z-form of RNA is observed only in a laboratory under high concentration of salt or high temperature condition, while B-form is still to be found. The following structures are commonly seen in RNA:

(a) Bulges/internal loops – These are breaks in A-form helix due to mismatched bases in one or both strands. They form double-helical segments.
(b) Hairpin stems/loops – They are formed between nearby self-complementary sequences. They are the commonly observed secondary structures in RNA. Specific short sequences of base-like UUCG are frequently seen at the ends of hairpins which form tight and stable loops. Additional structural contributions are credited to hydrogen bonds that are different from regular Watson-Crick base pairs.

RNA has no regular secondary structure, but it varies with types.

tRNA Structure
After the discovery of DNA structure, tRNA was discovered by Robert W. Holley and team in 1964; further L-shaped tertiary structure was proposed by Alexander Rich in 1973. DNA and tRNA structures are among the most widely studied macromolecules. tRNA has cloverleaf structure due to four base-paired stems consisting of 70–90 nucleotides. It contains three non-base paired loops, namely, D loop, anticodon, and TψC loop. 3′end of tRNA always terminates with CCA sequence whose 3′OH of the terminal "A" ribose mediates the point of covalent attachment for amino acid. D loop acts as a recognition site for aminoacyl tRNA synthetase and contains dihydrouridine. TψC loop contains pseudouridine bases and is a ribosomal-binding loop. Variable loop, an extra arm, varies from tRNA to tRNA. The tertiary structure of tRNA is a compact L-shaped structure stabilized by base pairing and base stacking, where double helix is formed by anticodon stem and acceptor stem (Fig. 3.3).

Fig. 3.3 Cloverleaf model of transfer RNA (tRNA)
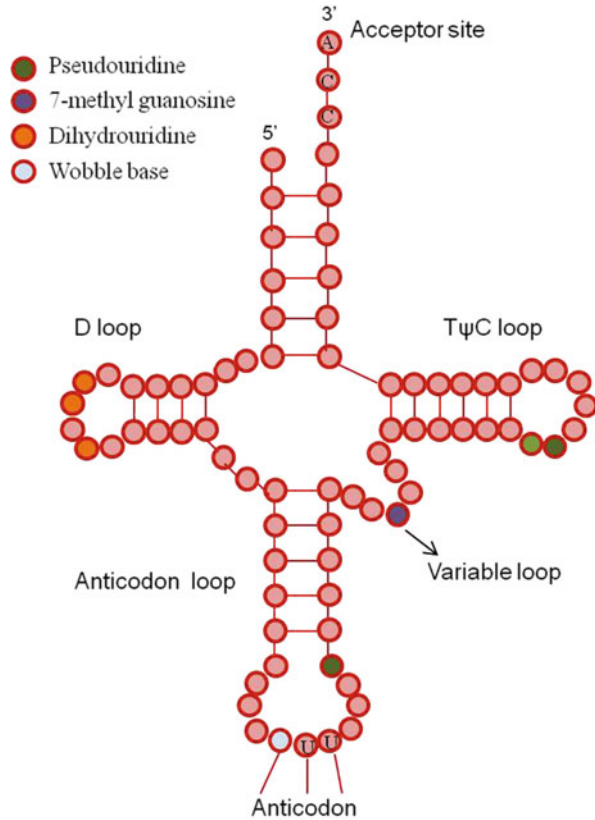
mRNA Structure

mRNA has 5′cap of modified guanine nucleotide (m7G) and poly (A) tail at 3′end that protects mRNA from degradation. mRNA is not a mere sequence of codons, but it is folded into a complex secondary structure consisting of stems and loops, which can affect its stability and translational fidelity. mRNA stable structure as well as the presence of specific arrest sequence in nascent polypeptides on mRNA are prime causes of ribosomal stalling or pause. mRNA folding is inversely related to translation, whereby secondary structural elements in mRNA reduce the speed of translation. High stable structures of mRNA affect the translation rate and also influence protein folding and compactness. Thus mRNA contains another layer of information besides coding proteins, supporting the hypothesis where RNA folding energy correlates with protein compactness (Faure et al. 2016).

rRNA Structure

In prokaryotic cell, 5S, 16S, and 23S rRNA consist of 120, 1540, and 2900 nucleotides, respectively. Mitochondrial rRNA exhibits variability in the size and lacks 5S rRNA.

16S rRNA molecule is composed of three major structural domains and one minor domain. Each domain is defined with helix of particular nucleotide range, separated from each other by several loops and bridges. Multiple G-U pairs and A-G juxtapositions are found in the helices of 16S rRNA. rRNA structure is formed of multiple short helices rather than long ones, creating a complex 3D structure (Noller 1984). 23S rRNA has compact double-helical configuration with seven domains, where six domains are rooted around the core central domain. The central core domain termed as domain 0 is highly conserved and is the basis for 23S rRNA structural integrity. Over 100 helices are present in these domains. The central single-stranded region of 23S rRNA comprises of helix26a made up of non-canonical base pairs (Petrov et al. 2013) and flanked by Watson-Crick base pairs. This helix lies within the loop E motif parameters. Helix26a is found to be conserved over the phylogeny in both 23S and 28S rRNA and is critical for ribosomal structure and function. Many single and double-base bulges are observed as seen in 16S. 5S rRNA in three-dimensional structure is placed in close proximity to helix39 in domain 2 (Petrov et al. 2014).

Thus the overall secondary structure of rRNA is found to be phylogenetically conserved, although the length of helices may vary between species. Furthermore, tertiary folding is seen in rRNA due to interstrand cross-links. In 5S rRNA secondary structural cross-links have been identified in stem regions along with tertiary cross-links between helices (Brimacombe and Stiege 1985).

3.3 Different Forms of DNA

Three major differences lead to structural variation in DNA. These are:

(a) Possible deoxyribose conformations
(b) Contagious bond rotation that constitutes DNA backbone
(c) C-1-N′-glycosyl bond rotation

Purines with respect to deoxyribose have two stable conformations, known as "syn" and "anti," while pyrimidines exist only in "anti" form due to stearic hindrance present in sugar and pyrimidine carbonyl O at C2. Besides the above criteria, three conditions can change the conformation of DNA. These include hydration or ionic environment, DNA sequences, and presence of proteins. In a living cell, DNA is mostly found in a mixture of A- and B-DNA, while only small regions (<10%) form Z-DNA.

Three major forms of DNA known are as follows.

3.3.1 A-DNA

A form has a right-hand helix and is the broadest among all DNA with diameter of 26 Å. It has 11 bases per helix turn with a distance of 2.6 Å between two bases.

Nitrogen bases are not exactly stacked on top of each other but are somewhat off-center and thus impart less stability and more rigidity to A-DNA. Major groove is more deepened, while minor groove becomes shallower due to tilting of A-DNA along helical axis. Presence of A-DNA is uncertain in cells and is highly favorable in water devoid of solutions or dehydrating conditions. Although certain stretches of purine bases (AAAA) favor A-form even in hydrating environment. Double-stranded RNA and DNA-RNA hybrid commonly have α helix, credited to the presence of hydroxyl group of ribose sugar which does not fit in the tightly coiled B-DNA.

3.3.2   B-DNA

The most stable structure of DNA in cells is B-form and is dependent strongly on the sequence. B-DNA has right-handed helix, consisting of 10.5 bp per helical turn with α helix rise of 3.4 Å/bp. Two chains run antiparallel. Major and minor grooves represent the front and back sides of DNA. Major groove is wide and shallow, characterized by exposing the hydrogen bonding faces of purines including Hoogsteen face. Contrarily, minor groove is narrow containing water and cations. Sequences in B-form are placed strategically so that it can perform different functions smoothly. Those sequences which can melt easily like TATA are mostly found in open reading frame to initiate transcription readily. Rigid sequences are favorable sites for binding of proteins and in formation of complexes.

3.3.3   Z-DNA

Left-handed, irregular, zigzag helical DNA formed transiently in a cell is Z-DNA. It appears more slender and elongated with short stretches found in eukaryotes as well as prokaryotes. DNA backbone is zigzag and has narrow and deep minor groove, while major groove is barely apparent. Certain DNA sequences, more specifically alternating purine and pyrimidine tracts, form Z-DNA. Even some methylated CpG islands are also known to attain Z conformation. To form left-handed helix, purine residues adopt syn conformation alternating with anti-conformation of pyrimidine residues. The reorganization brought phosphate group in closer proximity, resulting in electrostatic repulsion pushing the molecule back to B-DNA conformation (Rich and Zhang 2003).

Certain conditions favor transition from B-DNA to Z-DNA including:

(a) Alternate purine-pyrimidine sequence (specially poly(dGC)$_2$)
(b) Negative supercoiling
(c) High salt concentration
(d) Cations like spermine and spermidine

A-DNA   B-DNA   Z-DNA
Right handed   Right handed   Left handed
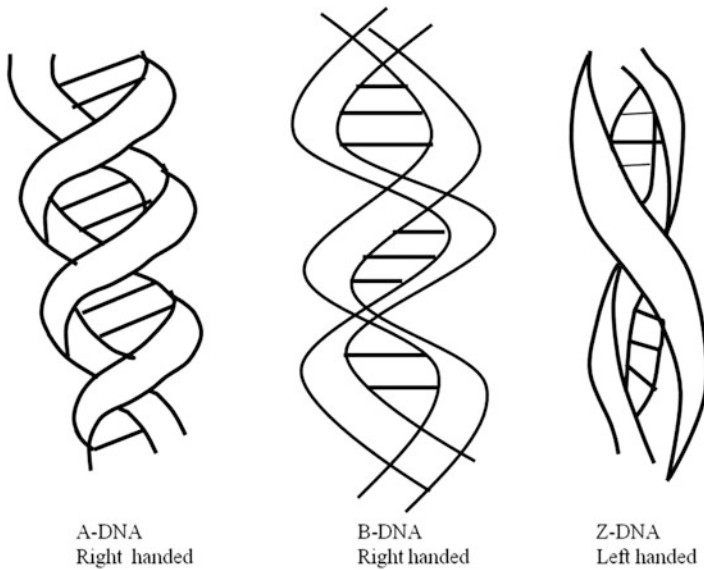
Fig. 3.4 Different conformations of DNA

B-to-Z junction box is formed during such transition from B- to Z-DNA. DNA needs to unwind at sites where DNA is being copied to RNA, and during this process of negative supercoiling, left-handed helical Z-DNA is formed. Recently it was reported that Z-DNA is formed on nucleosomes by the addition of SWI/SNF (protein for remodeling nucleosomes) and ATP (Rich and Zhang 2003). Few instances of biological significance are reported now, but more detailed studies need to be done to establish its biological role (Fig. 3.4).

3.3.4   Circular DNA

Two independent research groups Dulbecco and Vogt and Weil and Vinograd in 1963 discovered closed circular DNA in polyomavirus. Circular DNA is characteristic of bacterial and cytoplasmic DNA in animals. Extrachromosomal circular, single-stranded rings and covalently closed duplex rings are types of circular DNA found in eukaryotes and prokaryotes. Furthermore, higher organisms comprising of large DNA molecules organized into loop-like structure, which resembles closed circular DNA (Cohen and Segal 2009). Topological state of closed circular DNA is not easily altered by conformational rearrangements. Circular DNA exhibits supercoiling, and there is transition of conformation induced by negative supercoiling depending on the ionic conditions. Supercoiling plays a biological role in protein binding to double-helical DNA, where the binding of protein can induce twist and writhe resulting in change in supercoiling free energy. This free energy affects the DNA-protein binding constant.

3.4   Different Forms of RNA

3.4.1   tRNA

tRNA is small in size (4S) and has peculiar sequence and structure. tRNA serves as an adaptor molecule in protein synthesis with twofold function, where it binds to tRNA synthetase and accepts and recognize the correct amino acid, followed by binding to codon on mRNA-ribosome complex to transfer the respective amino acid. tRNA contains some minor or rare variant bases other than regular four bases. These rare base modifications restrict certain base pairings, finally affecting the tRNA tertiary structure.

3.4.2   mRNA

It is also known as cellular RNA or coding RNA and constitutes 1–3% of total RNA. mRNA is a blueprint molecule coding for polypeptide chain with codon triplet sequences. One or several polypeptide chain can be coded from a single mRNA. mRNA can be monocistronic when it codes for single polypeptide chain and polycistronic when two or more polypeptide chains are coded. Mostly mRNAs in eukaryotes are monocistronic, while prokaryotic mRNA is polycistronic.

3.4.3   rRNA

It constitutes more than 80% of total RNA and is a major component of ribosomes. rRNA is the most stable form of RNA. 18S and 28S rRNA are found in small 40S and large 80S ribosomal subunits, respectively, of eukaryotes, while bacteria and archaea consist of 5S, 16S, and 23S rRNAs. 16S is the only rRNA component of small ribosomal subunit, while 5S and 23S constitute large subunit components. rRNA function remains the same throughout the species, but the nucleotide sequence does vary among the species. Variations in rRNA are attributed to three key features:

(a) rRNA molecule in ribosome folds into a complex three-dimensional shape that is conserved between species, but the primary sequence may change without affecting the 3D shape of molecule.
(b) Sequence divergence during evolution is very slow in rRNA; nonetheless the structure and function remain the same.
(c) Genes encoding rRNA have evolved in a unique way, making them as markers to trace phylogeny during evolution and thus as powerful tool to detect species from sequencing data.

3.5 Structural and Biological Significance of Major and Minor Groove of DNA

The periodicity of helical structure of DNA gives rise to grooves. Double-helical B-DNA has two asymmetric grooves, larger major and smaller minor grooves. Major and minor grooves resulted from the Watson-Crick base-pairing geometry due to the angles formed by glycosidic bonds. This configuration forces the base pairs to attach at obtuse angle of $120°$ and another into acute angle, resulting in the formation of major and minor grooves. Major groove is the region where the backbones are at a distance, and minor groove is formed in the region where backbones are in close proximity. The edge of bases is exposed due to grooves and thus helps in determining the base sequence of a specific region in DNA molecule. A-DNA has minor and major grooves of almost equal size, and in Z-DNA, major groove does not exist while minor groove is deep and narrow (Ussery 2002).

The grooves have important role in binding of proteins involved in replication and transcription. Recognition α helix of the protein makes base-specific contacts in major grooves of DNA which further determines the binding mode with DNA (dimer or multimeric), while in minor groove, proteins bind non-specifically through their β strand. Major groove provides distinctive pattern of hydrogen bases and thus helps α helix of protein to recognize base pair and fit perfectly in DNA. Several factors contribute to this protein-DNA binding and its stability; this includes energy, hydration water, and cations. DNA molecule is strongly associated with water molecules which occupy hydration sites in major and minor grooves of DNA in a specific pattern. In minor groove water is present as one-water and two-water bridges, while major groove is enriched with two- and three-water bridges. Structural water in the grooves is a major factor responsible for the stability of DNA conformation. "Spine of hydration" hypothesis postulates that A-tract in B-DNA is surrounded by a large amount of bound water as compared to alternating AT sequence. Greater enthalpy is required to remove water hydrating the minor groove of AT-rich DNA than major groove, and thereby larger entropy is provided for binding. Association of DNA-binding domain of protein with DNA is energetically driven, where binding with major groove is an enthalpic reaction, while minor groove association is characterized by favorable entropy and unfavorable enthalpy (Privalov et al. 2007). Difference in energetic profile is contributed by distinct hydration pattern of both grooves, wherein the water present in AT-rich minor groove is in high-ordered state, and water removal upon ligand binding results in favorable entropy. Thus binding in minor groove involves higher affinity and sequence specificity. Intrinsic energetic differences exist among the grooves which are primary determinants in binding of DNA-interacting proteins. Dimensional difference and favorable enthalpy imply major groove as binding site for proteins, while small non-peptidyl molecules favorably bind to minor groove.

The minor groove also contributes in transition of DNA from one form to another. The functional groups of minor groove stabilized DNA helix and A/B equilibrium in a cooperative manner. The equilibrium is shifted from B to A form in

the absence of functional groups of adenine and thymine residues, and surrounding water and associated metal ions in minor groove stabilize the B conformation of DNA helix (Woods et al. 2003).

Divalent cations specifically Mg^{2+} bound to the ApG of major groove and influence its conformation. ApG in major groove generates sufficient electrostatic potential that bonds with Mg^{2+}. Cations preferentially anchor at N7 adenine and O6/N7 guanine of purines. Strong electronegative potential of AT residues imparts capability to minor groove to bind cations despite its steric hindrance. DNA bends have been observed when divalent cations bridge guanine residues in CpG, thus compressing the major groove, while effect on minor groove is still controversial (Gueroult et al. 2012).

3.6   Chargaff's Rule

Phoebus Levene proposed that DNA was composed of tetrameric repeats of GACT, but later it was disproved. Erwin Chargaff first showed that the percentage of guanine is identical to cytosine, and adenine is equal to thymine. He proposed the following rules for DNA:

(a) Number of adenosine = thymine and guanine = cytosine. Thus the sum of purine and pyrimidine residues is equal, i.e., A + G = T + C.
(b) Base composition does not change within tissues of same species.
(c) Age or nutritional state does not affect base composition in a particular species.
(d) Base composition varies from species to species.

Chargaff's theory also laid foundation for Watson and Crick's double-helical DNA structure.

3.7   Nucleic Acid Geometrics/Forces Stabilizing Nucleic Acid Structures

The precise dimensions and geometries of the helix vary with conformations and the environment. Biological function of nucleic acids is critically dependent on the specific folded structure a nucleic acid adopts in a cell. Geometries and conformations of sugar ring and phosphate group determine the overall conformation of nucleic acids. Nucleotide geometries are mainly influenced by phosphodiester torsional angles, sugar puckering, and planar base stacking.

3.7.1   Glycosidic Bond, Rotational Isomers, and Sugar Puckering

Glycosidic bond is a covalent bonding between C1 anomeric carbon of sugar and N9 of purine or N1 of pyrimidine. Nitrogen base pair geometries regulate conformational parameters based on the probability of homo or hetero base pairs combination. The following parameters determine the base pair geometry:

(a) Propeller twist – an angle between two base planes along the joining axis. Larger propeller twist is observed in hetero than homo pairs, with purine-pyrimidine pairs exhibiting the larger twist than homo pairs.
(b) Buckle – a dihedral angle formed between planes of two bases after propeller twist becomes zero.
(c) C1′–C1′ distance – is a distance between 1-substituted pyrimidines and 9-substituted purines.
(d) Hydrogen bond – hydrogen bond number, bond angle, and bond distance determine the base geometry and pairing, furthermore the local helix geometry.

These parameters are of utmost importance in determining the helix geometry and biological function of double-helical DNA (Wilson 1988).

The geometry of a base pair with respect to preceding pair (base stacking) is characterized by six coordinates categorized into two groups, rotation and translation. Thus spatial position of base pair $n + 1$ is regulated by six degrees of freedom and is derived relative to local coordinate axis of base pair "n." Three rotational angles include, twist (rotation of $n + 1$ around the helical z-axis of n), roll (y-axis), and tilt (x-axis). Three coordinates of translation are rise (displacement along the helix, z-axis), slide (displacement directed from one strand to another), and shift (displacement directed from minor to the major groove). These six geometric parameters help in determining the global rotation matrix of each base pair (Rn) (Drendel et al. 2011).

The geometry of an individual base pair consists of six coordinates in rotation and six in translation (Table 3.2).

Translation coordinates of a base pair geometry are stagger (Sz), stretch (Sy), shear (Sx), rise (Dz), slide (Dy), and shift (Dx). The coordinate values of nucleotides also contribute in secondary structure of nucleic acids, and under physiological conditions, only few values are permitted.

The pentose sugar in nucleic acid contains five carbon atoms, out of which at least one atom lies out of the plane creating puckered conformation. Puckering is a phenomenon when furanose rings of sugar are twisted out of the plane to minimize the non-covalent interactions in its substituents. When all ring carbon atoms of a pentagon arrange in eclipsed conformation, ribose pucker ring arises despite shifting of 108° pentagon angle in close proximity to 109.5° carbon tetrahedral angle. Sugars adopt two major conformations depending on whether the ring puckers at C2′ or C3′ or to both. B-form DNA adopts C2′endo while A-form DNA and RNA adopt C3′endo conformation where the designated carbon atoms

Table 3.2 Individual base pair geometry: rotation

S.No.	Coordinate frames	Axis	Nature of rotation
1.	Buckle	Rotation about short *x* axis	
2.	Propeller twist	Long *y*-axis	Rotation of one base with respect to other
3.	Opening		
4.	Inclination	*x*-axis	Rotation of a base pair to overall helix axis
5.	Tip	*y*-axis	
6.	Pitch		Base pairs/turn of the helix

lie out of the plane to provide flexibility to the structure. Deoxyribose sugars have greater conformational flexibility than ribose sugars. C2′ endo structures have more variable puckering amplitude that resulted in more flattering in deoxyribose than the ribose sugars. C3′ endo pucker resulted in shorter distance between phosphate groups in a backbone leading to a compact conformation than C2′ endo pucker. There can be S or N twist in the puckered ring depending upon the orientation of the zigzag structure. The steric hindrance of ribose sugar in eclipsed conformation is relieved due to puckering resulting in slight deviation from tetrahedral bond angle (Gelbin et al. 1996).

Geometry of the phosphodiester linkage including the torsion angles, bond length, and valence angles also determines the conformation. The valence geometry relies on the conformation of sugar. Bond length varies significantly for sugars in C2′ conformation, while in C3′ endo conformation, only C1–C2 bond length is different for both sugars.

3.7.2 Base Pairing

Two nitrogen bases of nucleic acid strands are held together by hydrogen bonding between amino group and carbonyl group of two bases. Watson and Crick first defined the bonding pattern, where adenine and thymine/uridine were held by two hydrogen bonds and guanine and cytosine with three bonds. Although single hydrogen bonding is energetically and entropically unfavored, base pairing is favored by other entropic effects. The favorable entropy is observed in freed water molecules; furthermore, second and third hydrogen bondings have less penalty on rotational entropy (Kool 2001). Steric constraint allows only purine-pyrimidine pairing, but exceptional unusual base pairing is also seen as G-form bonds with U/T. DNA containing high G–C content is more stable than low G–C. Base pairing provides specificity and periodicity to the structure and also contributes in the stability of nucleic acids.

3.7.3   Base Stacking

Several non-covalent forces interact to provide stability to base stacking. It is the major force responsible for the stability of nucleic acid helical structure. Aromatic bases of the same plane overlap geometrically and lead to hydrophobic stacking interactions. Stacking mainly involves a dipole effect aligning partial positive charge at the edge of bases in face-to-face offset orientation and pi electrons at the center. This polarization of N–H and C=O groups result in stacking of bases. Base pair overlaying determines the base-stacking interaction and the energy. Base-stacking energy varies with the type of overlap, as G–C overlaying C–G is not similar to C–G overlaid G–C, and hence the degree of overlap changes with different helical arrangements. Base stacking contributes more than half of free energy of the total base pair. It might be possible that stacking and pairing energies contribute to the greater cooperativity and rigidity in helix center. Several forces including van der Waals dispersive force, electrostatic effect, and solvation effect stabilize base stacking. Van der Waals forces are predominant forces in stabilizing base stacking followed by solvation-driven forces and then electrostatic influence of one base to another (Kool 2001).

Stability of RNA secondary and tertiary structures is also dependent on base stacking as seen in RNA stem-loop. Besides, stacking also influences DNA polymerase activities.

3.8   Wobble Base-Pairing and Its Correlation with Genetic Diseases

3.8.1   Introduction

Wobble base pair is seen in tRNA where two nucleotides pairing deviate from Watson-Crick base pairing. G–U pair is a common wobble base pair seen in tRNA. It was first identified in yeast tRNA[ala] and later in tRNA[Phe] G–U pair is a prime determinant in amino acid acceptor identity of a molecule. G–U pair is now seen in most of the functional RNA and has varied roles to play in cell depending on the unique properties of wobble base pair. Wobble pair in tRNA[ala] is conserved in all living organism identifying its importance in evolution and thus possessing some unique features not observed with other base pairs.

3.8.2   Wobble Hypothesis

Wobble hypothesis was proposed by Francis Crick which states that base-pairing rules are relaxed at the third position of the codon, so that a base can pair with more than one complementary base. Thus U and C present at third position may be read by G in the anticodon.

3.8.3 tRNA Base-Pairing Schemes

The conformational flexibility of the tRNA anticodon loop is the reason for the wobbling at the first base in anticodon. The third base is less discriminatory compared to the first two due to degeneracy of the genetic code.

3.8.4 Biological Importance

G–U pair has expanded the in-depth knowledge of double-stranded RNA and unique recognition sites for various functions due to its conformational and accessible properties. G–U pair provides different contextual functions as it provides unique recognition tag/site to proteins like aminoacyl tRNA synthetases, ribosomal proteins, RNA enzymes, RNAs, and divalent metal ions:

(a) RNA catalysis – the cleavage site of ribozymes contains G–U pair in self-splicing introns, and replacement of this wobble pair compromised reactivity and fidelity of ribozymes. Sequence context of wobble base location and binding factor directs the unique conformation of individual G–U pair. The sequence context has prime importance in determining the catalytic function of G–U pair and also the structural diversity of A-RNA. The distinctive structure of G–U pair acts as anchor point providing high specificity in recognition or catalytic function, distinguishing between cognate and non-cognate substrates/ligands.

(b) Functional amino groups of Watson-Crick base pairs are projected into the major groove differently than wobble base pair. There exist differences in the orientation of bases also between them. These differences lead to divalent metal ion binding with more affinity to major groove of G–U pair, and this affinity further becomes stronger with side-by-side presence of two G–U pairs.

(c) G–U pair has high thermodynamic stability approaching to Watson-Crick base pairs compared to other mismatch pairs. G–U pair also provides stability to backbone turns, as in tRNA where G–U pair is frequently seen at sharp turns in T helix and V loop. This stability provides G–U pair to functionally substitute Watson-Crick base pair in double-helical rRNA, other RNAs, and ribozymes.

(d) G–U wobble pair also provides a distinctive structure to A-form RNA due to dissimilar glycosidic bond angles of G ($40°$) and U ($65°$); hence substitution with Watson-Crick pair would cause structural perturbation. While this is not the case with Watson-Crick base pair as the bond angle is approximately $54°$ for all nucleotides, thus four strand base pairs can be interchanged without compromising the helix parameters.

(e) Conformational flexibility of G–U pair is dependent upon the chemical and structural environment, and thus wobble pair provides a site where double-helical RNA conformation can be altered easily, making an appropriate model for induced fit (Varani and McClain 2000).

3.8.5 Correlation Between the Wobble Base Pairing with Genetic Disease

Several mitochondrial diseases in humans are associated with point mutations or deletions in mitochondrial (mt) tRNA genes. Mutations in mitochondrial tRNAs could possibly impair posttranscriptional modifications leading to mitochondrial diseases. Deficiency or absence of posttranscriptionally modified wobble base pair in mitochondrial tRNAs due to point mutations is associated with two mitochondrial encephalomyopathic diseases, MERRF (myoclonus epilepsy associated with ragged red fibers) and MELAS (mitochondrial myopathy, encephalopathy, lactic acidosis, and stroke-like episodes). Two taurines containing modified uridines, namely, 5-taurinemethyluridine and 5-taurinomethyl2-thiouridine at the wobble site, were lacking in mitochondrial tRNA of mitochondrial diseases MELAS and MERRF (Kirino and Suzuki 2005). These two disorders are the first reported disorders of RNA modification dysfunction, and there are possibilities of occurrence of other RNA modification disorders in human.

3.9 Properties of Nucleic Acids

3.9.1 DNA Polymorphism

The differences in sequences of DNA occurring in coding or noncoding region are termed as polymorphism. DNA polymorphism is the basis which led to the genetic variability in human population from African to European race. Polymorphism can be seen in either coding (exons) or noncoding (introns) regions of DNA. Polymorphic sites in human genome consist of variable times of repeated short DNA sequence known as tandem repeat sequences. This variation (tandem repeats or microsatellite regions) is unique and specific to each individual and hence is used in individual identity and paternity testing. The variation involving a difference of single base pair is termed as single nucleotide polymorphism (SNP) which constitutes 90% of genetic variations in a population. Mostly SNPs do not lead to functional change but can be used as markers for certain genetic diseases predisposition.

Polymorphism is an evolutionary process, heritable and modified by natural selection. Genetic variation, biodiversity, and adaptation lead to polymorphism. The variations in a population are attributed to polymorphism. Occurrence of two different types of individuals within the same organism is due to polymorphism. Rare variations and mutations are not classified as polymorphisms, but the criterion for polymorphism is that the new mutation should be more than 1% in a population. Polymorphism is associated with the adaptation of the species in an environment whereby there is a change in the color, predation, and food supply, ultimately leading to higher speciation rate.

The term "polymorphism" was initially used to describe "phenotypic variations" that distinguished an individual within a species from each other. But with the

passage of time and advancement in science, it was termed as "genetic polymorphism" which describes differences in DNA sequence, making each human genome unique. The changes in DNA sequence is basically "functionally silent." Genetic polymorphism is the occurrence of mutation in the same population of two or more alleles that are at least 1% in frequency. These genetic polymorphisms are conserved in a population steadily by natural selection. The phenotype fitness is denoted by its variable frequency relative to other phenotypes in a population and varies spatially and temporally.

Polymorphism can be controlled by alleles localized on single locus as in human ABO blood groups, whereas the complex polymorphisms are controlled by several tightly linked genes known as "supergenes" on a single chromosome, but this is still a debatable issue, and further research is in progress. Several genetic polymorphisms are maintained in human population by means of balancing selection. The common human polymorphisms are discussed here as under:

(a) Human blood groups – The ABO blood group is the most familiar example of genetic polymorphism. The blood group phenotypes A, B, AB, and O are present in human population with varying proportions in different regions globally. The blood group phenotypes are regulated by multiple alleles at single locus and can never be eliminated due to natural selection. To maintain a balance, the "pleiotropic" effect of the genes is opposed by selective forces.

(b) Sickle cell anemia – Sickle cell anemia is mostly found in the population predominant in the tropical regions of Africa and India where homozygous individual with recessive sickle hemoglobin has shorter life expectancy in comparison to the "heterozygote" and "dominant homozygote." This is the major reason for the large number of deaths associated due to malarial parasite in these regions of the world.

(c) MHC molecules – "Major histocompatibility complex" (MHC) genes are highly polymorphic coding for various "T cells." The diversity of MHC genes acts as a medium for resistance to the pathogens.

(d) Glucose-6-phosphate dehydrogenase (G6PD) – Glucose-6-phosphate dehydrogenase (G6PD) is an important human polymorphism where G6PD alleles are implicated in malarial resistance especially in African and Indian sun continent.

3.9.2 Hyperchromicity

Change or increase in absorbance of DNA after denaturation (single stranded) is coined hyperchromic effect, which resulted due to base unstacking. Conversely, decreased in absorption upon annealing or renaturation (double stranded) is termed hypochromic effect. Resonance of aromatic ring of bases in double helix is restricted by hydrogen bond, thus leading to decrease in absorbance. This decrease is termed as hypochromic effect. This difference in absorption accounts up to 40% higher in single-stranded than double-stranded DNA. Higher delocalization of
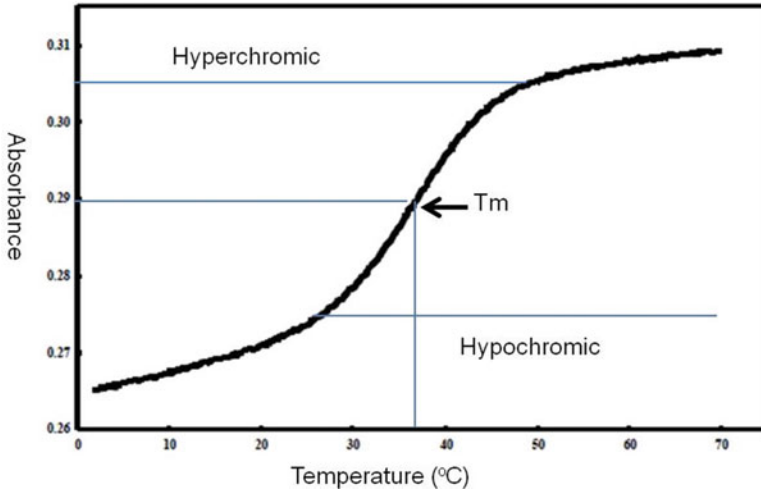
Fig. 3.5 Melting curve for DNA

excitonic states upon denaturation as compared to double-stranded DNA results in hyperchromicity (D'Abramo et al. 2013). Hyperchromicity is recorded during the melting curve when double-stranded DNA undergoes conformational transition to single-stranded form upon chemical or physical change. A typical melting curve records the change in absorbance with increase in temperature. The transitional midpoint of melting curve is termed as melting temperature (Tm), an indicator of duplex thermal stability. Melting temperature depends on the length and nucleotide sequence of DNA. The increase in UV absorption is credited to strand separation due to heat or change in pH or the presence of denaturant like salts, etc. Multiple factors like, nucleic acid sequence, length, base-pairing fidelity, higher-order structures, salt concentration, and pH affect the stability of nucleic acids (Doktycz 2002) (Fig. 3.5).

3.9.3 Cot Curve

Cot analysis also coined as DNA renaturation kinetics was developed by Eric Davidson and team to study DNA renaturation kinetics. The rate of reassociation of a denatured genomic sequence is proportional to its occurrence in the genome. Britten and Kohn in 1968 first showed the redundancy in eukaryotic genome based on Cot analysis technique. Reassociation of heat-denatured DNA with time provides cot values, calculated as
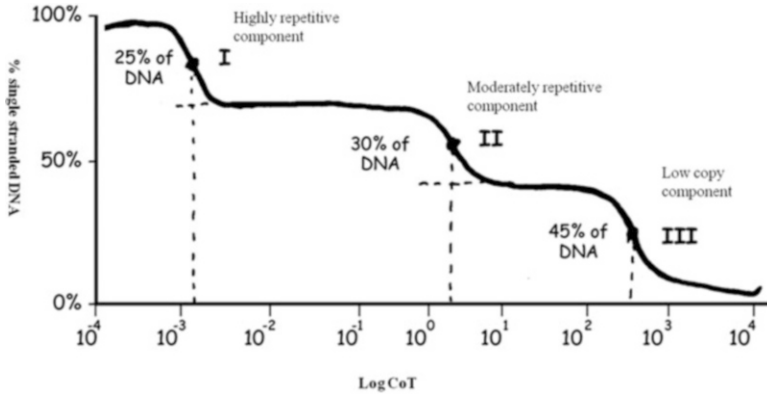
Fig. 3.6 Cot curve analyses

$$\text{Cot value} = \text{DNA conc (mol/L)} \times \text{renaturation time (sec)}$$
$$\times \text{ buffer factor based upon the cation concentration}$$

With the increase in time and concentration, single-stranded DNA reanneals and virtually completely reanneals at a high cot value. The total amount of reassociation does not change at a given cot value. Cot ½ value is the point where half of the DNA is still single stranded. Cot ½ value is proportional to genomic size and thus is a measure of genome complexity, which is the base pair numbers in repeating unit. Cot curve measures the % single-stranded DNA at various time points (Fig. 3.6).

Earlier studies have estimated genome size, % single copy, and presence of repetitive components, and later kinetics of DNA was determined by Cot curve analysis. It has also provided insight into evolution of eukaryotic genome along with the structural changes (Peterson et al. 2002).

3.9.4 C-Value Paradox

The constant amount of nonreplicating haploid DNA content per nucleus of a species is termed as C value, typically expressed in picograms. Different cell types of an organism have the same C value. Organisms at similar morphological complexity presume to have similar genomic content and, nevertheless, have DNA content with same order of magnitude; this paradox is termed as C-value paradox. Paradox in DNA constancy within species and profound variation in genome size among species is expressed as C value. Not only paradox is observed in different species but few similar species also have different genomic sizes (Eddy 2012). Besides, there exists paradox in DNA content and number of genes. The genome size does not correlate with organismal complexity nor does it reflect gene number in eukaryotes. Single-celled protists have much larger genome than humans, and

salamanders also contain 40 times more DNA than humans. Furthermore, human genome comprises of only 2% protein coding regions.

Scientists have come up with several explanations for extra DNA which was earlier termed as junk DNA. Junk DNA was proposed to be the reason for larger genome unrelated to gene number. Later it was reported that not all junk DNA is useless, but it is noncoding (introns). However, noncoding genome harbors certain sequences, which were involved in gene-regulating function. With regard to introns, there is a pronounced difference between animal and plant species. The size of genome and introns might be apparently related in animal species, but such kind of relationship seems to be absent in plants. Another theory proposed the existence of selfish DNA elements including transposons which replicate at the expense of host genome and thus contributes to the pool of junk DNA leading to paradox. Although it is termed as junk DNA, its presence in genome indicates its significance in evolution where it might be useful someday for the organism. The transposable elements invade in our DNA constituting around 45% of the genome, which ultimately with time die and decay. Larger genomes constitute larger neutrally decayed fraction of transposon relics (Eddy 2012). Until recently, genomic insertions were obvious mechanisms for the increase in size of genome; however, evidences of the decrease in genomic size have led to the idea of DNA loss or deletion due to mutations. Thus mutational load might be another strategy adapted for genomic survival during evolution (Gregory 2005).

3.10 Other Functions of Nucleotides

Nucleotides have other functional role in cell besides the carrier of genetic information.

3.10.1 Energy Carriers

Nucleoside triphosphates are intermediates of energy, used in variety of biochemical reactions as a source of chemical energy. Most commonly used agent is adenosine triphosphate (ATP), but GTP, UTP, and CTP are also used in particular reactions. ATP is a major energy currency of a cell and GTP as driving force in protein synthesis.

3.10.2 Chemical Messengers

Nucleotide is often a second messenger, most common being adenosine $3',5'$-cyclic monophosphate (cyclic AMP or cAMP), synthesized from ATP via adenylate cyclase located in the inner plasma membrane. cAMP is a regulatory molecule involved in many signaling pathways. Guanosine $3',5'$-cyclic monophosphate (cGMP) also acts as regulatory molecule in certain reactions. ppGpp, a regulatory

nucleotide in bacteria, inhibits rRNA and tRNA synthesis, preventing the wastage of nucleic acids.

3.10.3 Enzyme Cofactor Components

Adenosine constitutes an important component of enzyme cofactors, like acetyl coenzyme A (CoA), nicotinamide adenine dinucleotide (NAD), and flavin adenosine dinucleotide (FAD) in the form of adenosine diphosphate (ADP). It does not participate directly in the function, but its removal drastically affects the function of coenzyme. Removal of adenosine phosphate from acetyl CoA reduces its activity by a factor of 106 for its enzyme β-ketoacylCoA transferase. UDP acts as an intermediate in sugar metabolism and CDP in lipid metabolism.

ATP and GTP are allosteric regulators of many metabolic enzymes, where ATP activates certain enzymes like glycogen phosphorylase and AMP inactivates it. Furthermore, ATP-dependent phosphorylation activates several enzymes like phosphorylase and inactivates few enzymes such as glycogen synthase.

3.11 Nucleic Acid Fractionation

Nucleic acids occur in association with polysaccharides, proteins, and lipoproteins, and fractionation of DNA is also required to study several molecular biology aspects. Such separation can be achieved based on following techniques.

3.11.1 Precipitation

DNA can be fractionated or separated based on size by selective precipitation using polyethylene glycol (PEG). Amount of PEG required for precipitation decreases with the increase in size and asymmetry of macromolecule. Hence, homogenous class of macromolecule differing in molecular mass is separable by precipitating at different concentrations of PEG. Thus, DNA with different sizes can be separated at different PEG concentrations. DNA with lower molecular weight precipitates at higher PEG concentration and vice versa. Double-stranded DNA in the range of 100–50,000 base pairs (3–5×10^7 daltons) can be separated using PEG precipitation. This method is convenient, cost-effective, and high capacity and has applicability over broad range of conditions. However, there are several limitations, which include the following: it is less efficient for DNA concentrations less than 10 ug/ml, and the degree of resolution is low as it can resolve two fragments only if the size difference is of factor two and above. Besides PEG concentration, several other factors regulate the fractionation like, salt concentration, presence of divalent ions, pH, temperature, and centrifugal force. These conditions have to be optimized for proper separation of nucleic acids (Lis and Schleif 1975). Further application of DNA separated by PEG precipitation requires removal of PEG and thus adds an

additive and limiting step in process. Mostly researchers prefer electrophoresis for separation of DNA fragments.

3.11.2 Electrophoresis

Electrophoresis is a technique applied to separated nucleic acids based on molecular mass and charge. Agarose gel electrophoresis is used for the separation of nucleic acids and negatively charged molecules that are separated in an electric field, where nucleic acids migrate toward positive charge anode. Small molecular-weight nucleic acid migrates faster than larger molecules. Increasing the concentration of agarose and reducing the voltage decrease the migration and increase the sharpness of resolution. Nucleic acid is visualized on gel by DNA-binding dye ethidium bromide (EtBr) which fluoresces upon UV-light illumination. SyBr green dye can also be used for visualization, but it is an expensive dye compared to EtBr. If desired band has to recover from gel, then exposure to UV should be minimized as longer exposure may degrade the DNA. Another advantage of agarose gel electrophoresis is recovery, extraction, and purification of DNA band of interest for further application. Electrophoresis is a widely popular technique as it has varied applications. Agarose gel electrophoresis is employed to resolve circular DNA having varied supercoiling topology, to purify fragments for cloning, and to analyze PCR products.

For separation of small nucleic acids (<100 bp), polyacrylamide gel electrophoresis (PAGE) is used which has high resolving capacity and can separate nucleic acids with <10 bp size. Nucleic acids on PAGE can be visualized with more sensitive stain known as silver nitrate stain. It is 100 times more sensitive and can detect very low base pair of DNA.

3.11.3 Chromatography

Specific nucleic acids can be purified by affinity chromatography or column chromatography, where an oligomer is immobilized in a column, wherein its compliment will bind to oligomer from a pool of nucleic acid mixture. The best application of affinity chromatography is the binding of eukaryotic mRNA containing poly (A) tails to oligo (dT)-cellulose matrix columns, separating mRNA from total RNA of a cell. For efficient binding and stabilizing of the nucleic acid duplexes, high salt containing chromatographic buffer has to be used as few dT-A base pairs hybridize. Elution of bound mRNA is then carried out using low salt concentration in buffer.

Another type of chromatography implied for nucleic acid purification is anion exchange chromatography, where negatively charged polyanions (DNA) interact with positively charged diethylaminoethyl (DEAE) cellulose of resins. Different classes of nucleic acids are fractionated from the column using elution buffers of different pH and concentration.

3.11.4 Ultracentrifugation

Nucleic acids can be separated by ultracentrifugation using CsCl gradient. Cesium and rubidium salts are used exclusively for isopycnic separations, and high-density solutes such as nucleic acids are separated using these salts. Isopycnic centrifugation separates molecules based on equilibrium position or densities, where each molecule moves to the position where its density matches with the CsCl solution density. However, intra- and intermolecular bonds can be disrupted at high concentrations attributed to their high ionic strength and osmolarity. Usually EtBr-CsCl gradient is used for concentration of nucleic acids, and EtBr upon intercalation alters the density of the molecule. Covalently closed circular DNA incorporates less EtBr and hence accumulates at lower density as compared to linear DNA. Density-gradient centrifugation is less common as it is time-consuming, expensive, and laborious compared to other purification methods.

3.11.5 Solid Phase Extraction/Chaotropic Agents

Nucleic acid extraction using solid phase is more efficient than conventional methods and is based on principle of adsorption. This technique is based on conditioning of column with buffers of particular pH and salt concentration. Silica matrices are commonly used as solid phase where positively charged silica particles selectively bind to negatively charged nucleic acids. Silica materials, namely, silica particles, microfibers, glass powder, and diatomaceous earth have been used for nucleic acid purification. Nitrocellulose and polyamide matrices also bind to nucleic acids, but the specificity is low (Tan and Yiap 2009).

Purification of nucleic acid (DNA/RNA) using chaotropic agents, guanidinium thiocyanate, and guanidinium hydrochloride enhances the binding of nucleic acids with silica particles or diatoms. This technique can separate double-stranded form from single-stranded DNA due to differential binding to silica particles in the presence of chaotropes (Beld et al. 1996; Boom et al. 1990).

References

Beld M et al (1996) Fractionation of nucleic acids into single-stranded and double-stranded forms. Nucleic Acids Res 24:2618–2619

Boom R et al (1990) Rapid and simple method for purification of nucleic acids. J Clin Microbiol 28:495–503

Brimacombe R, Stiege W (1985) Structure and function of ribosomal RNA. Biochem J 229:1–17

Cohen S, Segal D (2009) Extrachromosomal circular DNA in eukaryotes: possible involvement in the plasticity of tandem repeats. Cytogenet Genome Res 124:327–338

Cruz B (2012) Supercoiling: linking number, twist, and writhe

D'Abramo M et al (2013) On the nature of DNA hyperchromic effect. J Phys Chem B 117:8697–8704

Doktycz MJ (2002) Nucleic acids: thermal stability and denaturation. eLS

Drendel J et al (2011) Geometry of the DNA double helix. Math 474, Spring 2011

Eddy SR (2012) The C-value paradox, junk DNA and ENCODE. Curr Biol 22:R898–R899

Faure G et al (2016) Role of mRNA structure in the control of protein folding. Nucleic Acids Res 44:10898–10911

Gelbin A et al (1996) Geometric parameters in nucleic acids: sugar and phosphate constituents. J Am Chem Soc 118:519–529

Gregory TR (2005) The C-value enigma in plants and animals: a review of parallels and an appeal for partnership. Ann Bot 95:133–146

Gueroult M et al (2012) Mg^{2+} in the major groove modulates B-DNA structure and dynamics. PLoS One 7:e41704

Kirino Y, Suzuki T (2005) Human mitochondrial diseases associated with tRNA wobble modification deficiency. RNA Biol 2:41–44

Kool ET (2001) Hydrogen bonding, base stacking, and steric effects in dna replication. Annu Rev Biophys Biomol Struct 30:1–22

Lis JT, Schleif R (1975) Size fractionation of double-stranded DNA by precipitation with polyethylene glycol. Nucleic Acids Res 2:383–389

Lodish H et al (1995) Molecular cell biology. Scientific American Books, New York

Noller HF (1984) Structure of ribosomal RNA. Annu Rev Biochem 53:119–162

Peterson DG et al (2002) Integration of cot analysis, DNA cloning, and high-throughput sequencing facilitates genome characterization and gene discovery. Genome Res 12:795–807

Petrov AS et al (2013) Secondary structure and domain architecture of the 23S and 5S rRNAs. Nucleic Acids Res 41:7522–7535

Petrov AS et al (2014) Secondary structures of rRNAs from all three domains of life. PLoS One 9: e88222

Privalov PL et al (2007) What drives proteins into the major or minor grooves of DNA? J Mol Biol 365:1–9

Rich A, Zhang S (2003) Timeline: Z-DNA: the long road to biological function. Nat Rev Genet 4:566–572

Sinden RR (2012) DNA structure and function. Elsevier

Tan SC, Yiap BC (2009) DNA, RNA, and protein extraction: the past and the present. J Biomed Biotechnol 2009:574398

Travers A, Muskhelishvili G (2007) A common topology for bacterial and eukaryotic transcription initiation? EMBO Rep 8:147–151

Ussery DW (2002) DNA Structure: A-, B- and Z-DNA Helix Families. eLS

Varani G, McClain WH (2000) The G × U wobble base pair. A fundamental building block of RNA structure crucial to RNA function in diverse biological systems. EMBO Rep 1:18–23

Wilson CC (1988) Analysis of conformational parameters in nucleic acid fragments. II Co-crystal complexes of nucleic acid bases. Nucleic Acids Res 16:385–393

Woods KK et al (2003) The role of minor groove functional groups in DNA hydration. Nucleic Acids Res 31:1536–1540

Higher-Order Nucleic Acid Structures

4

Preeti Arivaradarajan

Abstract

The nucleic acids are capable of organizing in variety of noncanonical structures. In this chapter we will highlight the different structures adopted by nucleic acids, forces stabilizing these structures, and their biological significance. The ability of DNA and RNA to organize into three-stranded structures has been utilized in various therapeutic applications. Also the four-stranded structures assumed by G- and C-rich nucleic acid sequences have been exploited in nanotechnology. A special focus has been laid here on the nature of telomeric DNA and its role in cancer and aging. We have further discussed the biophysical approaches to measure the thermodynamic parameters determining the stability of triplex and quadruplex structures. The chapter also describes the RNA tertiary interactions such as coaxial stacking, tetraloop–receptor interactions, A-minor motifs, and ribose zippers responsible for folding, stability, and maintenance of RNA three-dimensional structure. Finally, the interactions responsible for higher-order chromatin structures assumed by eukaryotic and bacterial DNA are presented here.

P. Arivaradarajan (✉)
Amity University, Sector-125, Gautam Buddha Nagar, Noida 201 313, Uttar Pradesh, India
e-mail: preetirajan_2005@yahoo.co.in

4.1 Tertiary Structure of Nucleic Acid

4.1.1 Triple-Stranded Nucleic Acid Structures

Three-stranded nucleic acid structures also known as triplexes are formed either by association of a homopurine–homopyrimidine duplex with a single-stranded oligonucleotide (such as triplex-forming oligonucleotide, TFO) or by folding of one of the two strands of a homopurine–homopyrimidine duplex. The duplex part of the triplex is held by Watson and Crick base pairing, and the associated or the folded third strand is held to the duplex by Hoogsteen or reverse Hoogsteen hydrogen bonds. In Hoogsteen base pairing, the pyrimidine uses its Watson–Crick surface to pair with the N1, C6, N7 side of the purine base, whereas in reverse Hoogsteen base pairing the pyrimidine is rotated 180° with respect to the other base (Fig. 4.1).
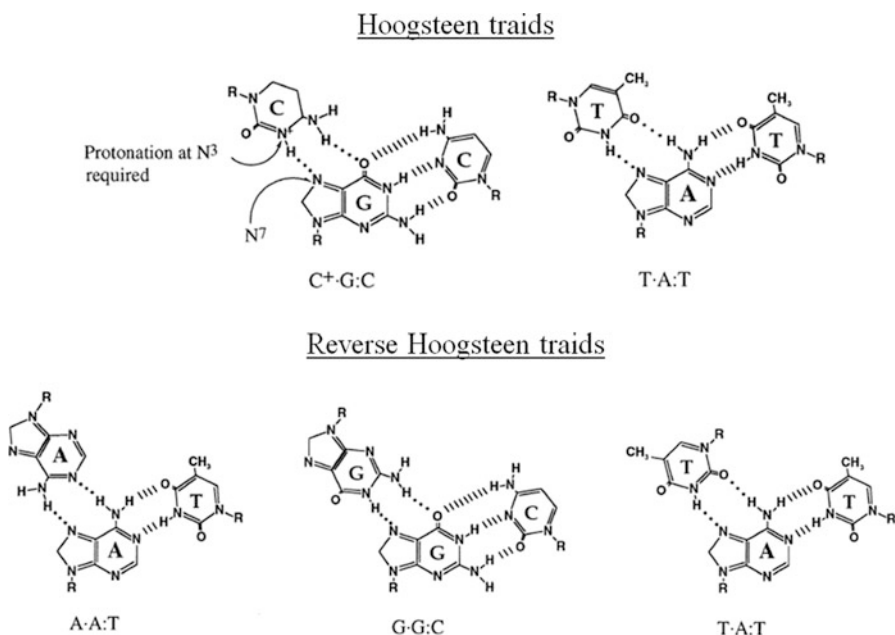
Fig. 4.1 Hoogsteen and reverse Hoogsteen base pairing scheme in the DNA triplexes
C^+ represents protonated cytosine
Reprinted from (Mirkin 2001)

4.1.2 DNA Triplexes

The triple-helical structure formed between a DNA duplex and a third DNA strand is referred to as DNA triplex. Depending on the origin of the third strand, DNA triplexes are classified into two types: intermolecular triplex and intramolecular triplex (Fig. 4.2). An intermolecular triplex is formed when the third strand originating from another DNA entity (such as TFOs) rests in the major groove of DNA duplex forming hydrogen bonds with the purine-rich strand of the duplex.

An intramolecular triplex or H-DNA structure is formed when the third strand is contributed by one of the strands of the target duplex DNA molecule at a homopurine–homopyrimidine tract with a mirror repeat. The mirror repeat is a DNA sequence that has same base reading in both 3′ and 5′ directions, from a central point. A half of either the homopurine or the homopyrimidine strand pairs as the third stand and complementary strand of the corresponding region remain unpaired. The resulting third strand lays in the major groove of duplex, whereas its complementary unpaired strand exists as a single strand. The third stand can be provided by either the 5′ or 3′ half of a homopurine or the homopyrimidine resulting in four isomers of intramolecular triplexes.

Based on the composition and binding orientation of the third strand with respect to the purine-rich strand of the target duplex, two configurations exist. In the first configuration, the pyrimidine-rich third strand binds in parallel orientation to the purine-rich strand of the duplex via Hoogsteen hydrogen bonding, whereas in the second configuration the purine-rich third strand binds in an antiparallel orientation to the purine-rich strand of the duplex via reverse Hoogsteen hydrogen bonds.
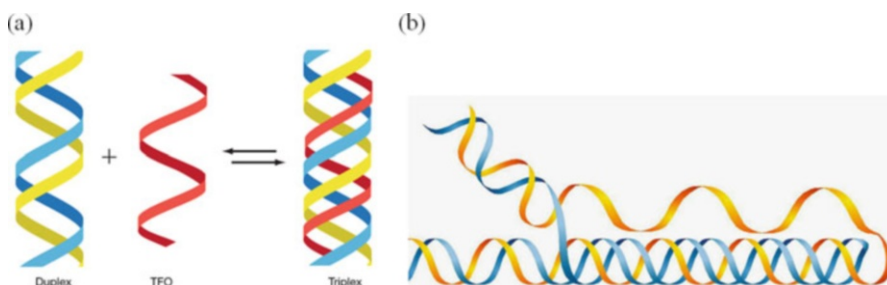
Fig. 4.2 Schematic representation of triplex formation
(**a**) An intermolecular triplex formation: the target duplex consists of a purine-rich (shown in *blue*) and a pyrimidine-rich (shown in *yellow*) strand. The TFO (shown in *red*) positions in the major groove of the duplex and binds to its purine-rich strand to form the triplex structure
(**b**) An intramolecular triplex formation: in the homopurine–homopyrimidine tract with mirror repeat symmetry, half of one strand (shown in *blue*) folds back and forms triplex structure while its complementary segment (shown in *yellow*) remains unpaired
Reprinted from Jain et al. (2008)

4.1.3 RNA Triplexes

The triple-helical structure formed between an RNA duplex and a third RNA strand is referred to as RNA triplex. Similar to DNA triplex, both intramolecular and intermolecular RNA triplexes are formed. The third RNA strand may be accommodated in either the major groove or the minor groove of an RNA duplex, resulting in a major groove RNA triplex and a minor groove RNA triplex, respectively. The triplex formation does not disrupt the preformed RNA duplex structure. In isolation a major groove RNA triplex structure is stabilized by forming successive major groove base triples such as U·A-U and C^+·G-C (lines represent Watson–Crick pairs and dots represent non-Watson–Crick pairs). The major groove triplex observed in H-type pseudoknot structure found in human telomerase RNA is critical for telomerase activity. However, minor groove triplex structure is usually not stable in isolation. It is often formed within large structured RNAs and RNA–protein complexes (Devi et al. 2015). For example, the A-minor motif, a minor groove RNA triplex structure, is a recurrent motif present in almost all large RNAs, including group I intron and group II intron, riboswitches, ribosomal RNAs, and the mRNA–tRNA–ribosomal RNA complex structure.

In addition to DNA and RNA triplex, the triplex formed between DNA and RNA called DNA–RNA triplex also performs a wide array of biological activities in the cell. For example, the noncoding RNA transcripts associate with genomic DNA to form biologically active RNA–dsDNA triplex structures that mediate gene silencing.

4.1.4 Role of Triplexes in Therapeutics

4.1.4.1 Antireplicative Agents: Oligonucleotide Clamps

An oligonucleotide clamp or "oligonucleotide–loop–oligonucleotide" (OLO) is a composite oligonucleotide consisting of two oligonucleotides covalently linked by either a hexaethylene glycol linker or an oligonucleotide sequence (Fig. 4.3). One
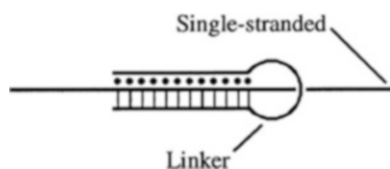
Fig. 4.3 Representation of triple helix formation on a single-stranded nucleic acid with an oligonucleotide clamp. The two oligonucleotide domains of an oligonucleotide clamp interact with the single-stranded target by Watson–Crick and Hoogsteen base pairing. The domains are covalently linked by a linker that allows the oligonucleotide clamp to fold back on itself resulting in a triplex structure
Reprinted from Chan and Glazer (1997), Copyright (1997), with permission from Springer

of the oligonucleotides forms Watson–Crick base pairs with the single-stranded homopurine or homopyrimidine target, while the other oligonucleotide binds with the target via Hoogsteen base pairing, thereby forming a triple-helical complex. The oligonucleotide clamps form more stable triple helices with a single-stranded target than either the corresponding trimolecular triplex or the duplex formed by individual unlinked strands alone.

To further enhance the stability of oligonucleotide clamp triplex, a psoralen derivative is attached to the 5′ end of the oligonucleotide clamp. The psoralen derivative becomes covalently linked to all three segments of the triplex, rendering the oligonucleotide clamp irreversible.

Studies have shown that *in vitro* replication of single-stranded DNA templates by DNA polymerases such as T7, Taq, and Vent in the presence of oligonucleotide clamps conjugated with or without psoralen is inhibited at the chain elongation step. Mostly the viruses either have single-stranded DNA/RNA as genetic material or during replication they form single-stranded DNA intermediate. These are perfect target sites for oligonucleotide clamps. As oligonucleotide clamps targeted to single-stranded viral sequence may function to inhibit viral replication.

4.1.4.2 Targeted DNA-Damaging Agents

The triplex-forming ability of TFOs is used to direct site-specific DNA damage and thus stimulate replication-independent DNA repair synthesis at the specified site. It has been demonstrated that the efficacy of the anticancer nucleoside analog gemcitabine in human breast cancer cells can be improved significantly when used in combination with TFOs. TFOs targeted to the c-*myc* oncogene stimulate repair synthesis in the presence of gemcitabine, to increase its incorporation into DNA thereby inhibiting the growth of human breast tumor cells.

4.1.4.3 Triplex-Mediated Mutagenesis and Recombination

Triplex-mediated site-directed mutagenesis relies on the ability of a TFO to place a tethered mutagen adjacent to a specific base pair. The TFO conjugated to psoralen (or any mutagen) mediates a site-specific intercalation of psoralen into the DNA. Subsequent exposure to UVA radiation in the presence of psoralen results in covalent cross-linking of thymines on both strands. In mammalian cells DNA repair and/or bypass replication of the induced lesion leads to T/A to A/T transversions.

The triplex-mediated site-directed mutagenesis potentially could be used to repair point mutations or knockout gene function in cells ex vivo, thereby opening new avenues for treatment of single gene disorders, such as cystic fibrosis and sickle cell anemia.

Unlike simple point mutations, gene defects such as deletions, insertions, and other mutations cannot be repaired by site-directed mutagenesis. Correction of these defects requires replacement of large DNA fragments which could also be mediated by triplex-stimulated homologous recombination. Three pathways have been proposed for resolution of triplex-directed DNA damage. Firstly the DNA damage can be processed by nucleotide excision repair. Either the repair is followed by errorprone gap-filling repair synthesis. Or alternatively, prior to gap-filling repair, the strand exchange with a nearby homologous gene can provide a damage-free template. Lastly,

the psoralen–TFO adduct could also provoke a double-stranded DNA break at a site flanking the triplex. Subsequent exonuclease activity can reveal homologous single strands, which anneal to form a heteroduplex intermediate. Resolution of this intermediate by DNA mismatch repair produces apparent crossover recombinants.

This site-specific exchange of genetic information mediated by triplex-induced recombination may possibly be used for clinical applications.

4.1.4.4 Transcriptional Inhibitor

Triplex-mediated antigene approach relies on the ability of TFOs to inhibit gene transcription. The TFO binding at or downstream of gene promoters results in triplex formation at the binding site. Triplex formation at gene promoter induces a conformational change in DNA that prevents the assembly of transcription machinery. It has been demonstrated that triplex formation at a promoter can block the binding of various transcription factors, such as SP1, bacteriophage T7 RNA polymerase, and nuclear factor κB, thereby inhibiting transcription. Triplex formation in an open reading frame stalls RNA polymerase thereby preventing transcriptional elongation.

Gene promoters of many clinically important genes such as human c-*myc*, human Ha-*ras*, dihydrofolate reductase, murine c-*pim*-1, rat *HER2*/*neu*, human epidermal growth factor, and the mouse insulin receptor have been targeted in vitro by the triplex-mediated antigene approach.

4.1.4.5 A Diagnostic Tool

CyGene Inc. (Alachua, FL, USA) has devised a diagnostic tool called target protection assay (TPA) based on triplex formation to locate low-copy disease-related genes in DNA and RNA. The TPA procedure has an edge over PCR because of its ability to detect low abundance targets that can be missed by sampling error in PCR. The crucial step in TPA is the selection of an appropriate target nucleotide sequence from the infectious agent of interest and designing a TFO directed to it. Figure 4.4 describes the TPA procedure in detail.

Briefly, the technique involves isolation of DNA/RNA from blood, tissue, or body fluid of the infected organism. From the isolated DNA (or RNA), the target sequence along with some upstream and downstream sequence is excised using restriction enzymes and protected by target-specific TFO. After triplex formation, the 3′ ends of the duplex part are digested till the triplex boundary. The remaining triplex DNA is bound to magnetic beads, washed and detected using a fluorescent probe.

TPA provides an opportunity for identification of target sequence during early days of infection (when load of infectious agent is low), increasing the prospect of early treatment.
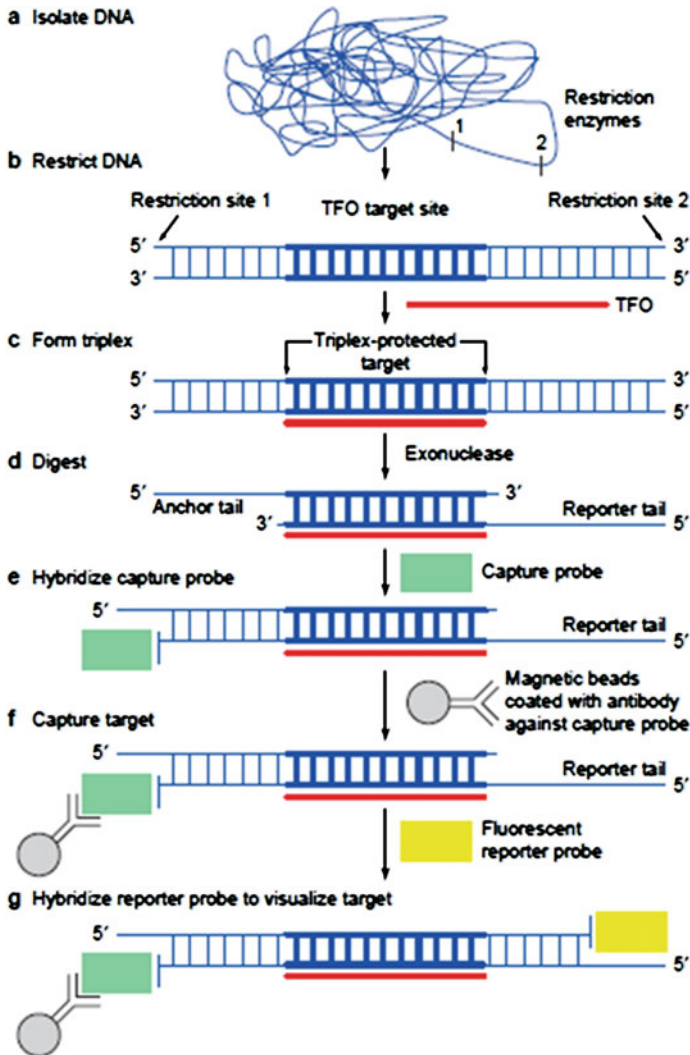
Fig. 4.4 The procedure of target protection assay

(**a**) DNA/RNA is isolated from sample such as blood, tissue, or body fluid. (**b**) Using restriction endonucleases the target along with its upstream and downstream sequence is excised from the DNA. (**c**) A target-specific TFO is added to the excised DNA, which hybridizes with the target sequence forming a triplex molecule. (**d**) Upon addition of exonuclease III, the duplex DNA is degraded in the $3'$ to $5'$ direction. However, as the exonuclease reaches the triplex structure, the enzyme falls off because the third strand positioned in the major groove of duplex DNA blocks the advancement of the enzyme. This results in a triplex-protected target with two $5'$ ends. (**e**) One of the $5'$ tails is hybridized to a "capture probe," containing a "biochemical hook." (**f**) The triplex-protected target is then bound to a magnetic bead coated with antibody directed to the biochemical hook. The beads are then washed to remove nonspecific DNA/RNA binding. (**g**) The captured complex is visualized using a reporter probe. The reporter probe is conjugated to a fluorescent probe such as fluorescein isothiocyanate (FITC) and specifically attached to the other $5'$ tail. The degree of fluorescence allows quantification of the target and thereby determines the extent of infection

Reprinted from Fricker (1998), Copyright (1998), with permission from Elsevier

4.2   Four-Stranded Nucleic Acid Structures

The G-rich and C-rich nucleic acid sequences assume four-stranded higher-order structures referred as G-quadruplex and i-motif, respectively.

4.2.1   Quadruplexes

The four-stranded structure adopted by guanine-rich RNA or DNA is known as guanine quadruplexes (alternatively referred to as G-quadruplexes, or tetraplexes, or G4 structures). The basic building block of G-quadruplexes is the guanine tetrad (also known as guanine quartet or simply G-quartet). The guanine tetrad is a square coplanar array of four guanine bases associated into a cyclic Hoogsteen hydrogen bonding arrangement that involves N1, N7, O6, and N2 of each guanine base. Two or more planar guanine tetrads stack on top of each other to form a G-quadruplex (Fig. 4.5). The formation and stability of G-quadruplexes is cation dependent (especially monovalent cations such as Na$^+$ and K$^+$). The cation is located within the central channel of the guanine tetrad stack, created by the guanine O6 atoms.

In general, G-quadruplex structure contains a core of two or more stacked G-tetrads, which are held together by loops arising from mixed-sequence nucleotides that are not usually a part of G-tetrad. The topological polymorphism in G-quadruplex is attributed to the number of G-rich strands, the polarity of the strands, and the location and length of the loops (Lane et al. 2008; Rhodes and Lipps 2015; Simonsson 2001).
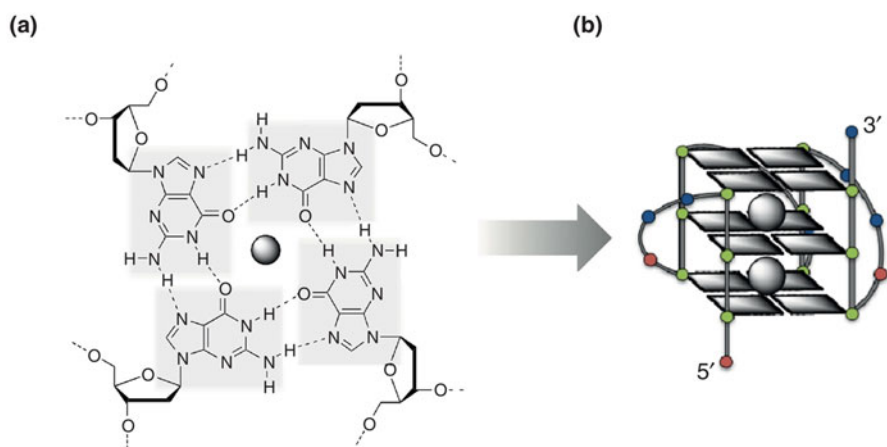
Fig. 4.5 G-quartets and G-quadruplexes
(**a**) The guanine quartet stabilized by Hoogsteen hydrogen bonding. (**b**) The planar G-quartets stack on top of one another, forming four-stranded helical structures, G-quadruplexes
Reprinted from Murat and Balasubramanian (2014), Copyright (2013), with permission from Elsevier
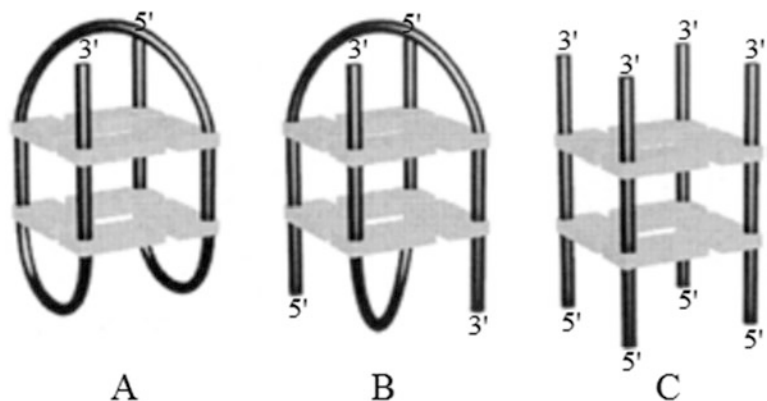
Fig. 4.6 Strand stoichiometry variations in G-quadruplex structures
(**a**) Unimolecular quadruplex, a one-stranded structure. (**b**) Bimolecular quadruplex, a two-stranded structure. (**c**) Tetramolecular quadruplex, a four-stranded structure
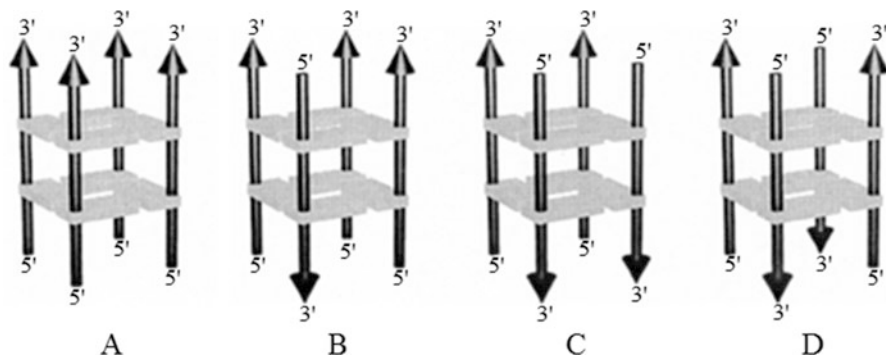
Fig. 4.7 Strand polarity variations in G-quadruplex structures
(**a**) All strands parallel. (**b**) Three parallel strands and one antiparallel strand. (**c**) Two pairs of adjacent parallel strands. (**d**) Alternating antiparallel strands

The strand stoichiometry variation results in intramolecular and intermolecular quadruplexes (Fig. 4.6). The formation of intramolecular or unimolecular quadruplex requires the presence of four or more G tracts in one strand. The G tracts can be of unequal length, and if one of the short G tracts is longer than the others, some of the extra G residues will be located in the loop regions. However, intermolecular quadruplex result from association of two (bimolecular quadruplex) or four (tetramolecular quadruplex) G-rich strands. Also, the length of different G-rich strands in an intermolecular quadruplex may or may not be equal.

The relative orientations of adjacent backbones in G-quadruplex give rise to four configurations: all parallel, three parallel and one antiparallel, adjacent parallel, or alternating antiparallel (Fig. 4.7). These structures are irrespective of whether adjacent backbones are part of the same nucleic acid molecule or not.

The loops that connect guanine tracts participating in the formation of G-quadruplexes are positioned in different ways. The parallel quadruplex have propeller-type loops wherein the loop regions are positioned to the sides of the quadruplex. In antiparallel quadruplex topology the loops are either diagonal, joining two diagonally opposite tracts of guanine bases, or lateral, joining two adjacent tracts of guanines.

4.2.2 i-Motif

i-Motifs are four-stranded structures formed by DNA sequences containing stretches of cytosines. Stabilized by acidic conditions, they are comprised of two parallel-stranded DNA duplexes zipped together in an antiparallel orientation by forming intercalated hemiprotonated cytosine–cytosine base pairs. The building block of i-motif structure, the $C \cdot C^+$ base pair, is stabilized by the formation of three hydrogen bonds (Fig. 4.8).

i-Motifs formed by folding of a single strand containing four tracts of cytosines separated by stretches of other bases are known as monomeric or intramolecular i-motif. Alternatively i-motif structures are also possible with two, or four independent C-rich DNA strands known as the bimolecular or tetramolecular i-motifs, respectively (Fig. 4.9). The DNA sequences that connect the adjacent cytosine stretches form the loops that play an important role in determining the conformations and stability of the i-motif structure. i-Motifs with longer loops are more stable than ones with shorter loops, because of extra stabilizing interactions within the longer loop regions.
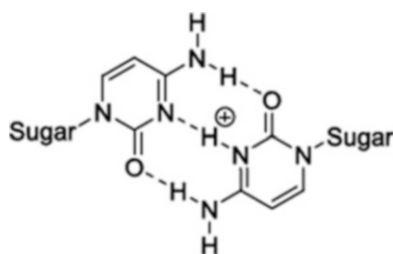
Fig. 4.8 A hemiprotonated base pair involving one neutral (deprotonated) cytosine and one positively charged (protonated) cytosine at the N_3 position
Reprinted from Day et al. (2014), Copyright (2014), with permission from Elsevier
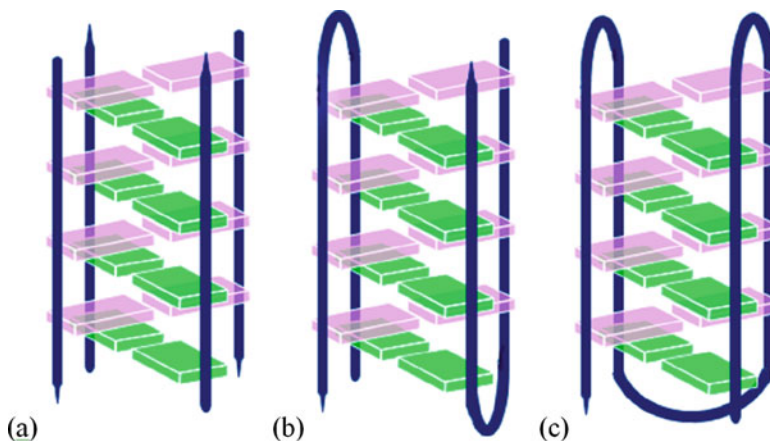
Fig. 4.9 Schematic representation of i-motif conformations
(**a**) tetramolecular i-motif structure, (**b**) bimolecular i-motif structure, (**c**) intramolecular i-motif structure
Adapted with permission from Dong et al. (2014). Copyright (2014) American Chemical Society

4.2.3 Role of G-Quadruplex and i-Motif in Nanotechnology

The tetrameric structure of G-quadruplex and i-motif has diverse nanoscale applications.

The fact that the folding and unfolding of G-quadruplex is responsive to environmental stimulus finds manifold application of G-quadruplex in nanotechnology, for example, stimulus-responsive G-quadruplex and its combination with nanopore systems, small ligand-responsive G-quadruplex stabilization for drug screening, nanomaterial-responsive G-quadruplex reformation, and target-triggered continuous formation of G-quadruplex by DNA nanomachine.

The stimulus could be small metal ions such as K^+, Cs^+, Pb^{2+}, etc., which have been proven to stabilize the structure of G-quadruplex. Also, small molecules such as ATP, cocaine, etc. and biomolecules such as DNA, protein, etc. may act as stimulus.

Figure 4.10 illustrates stimulus-responsive nanochannel fabricated by immobilization of conformation- switchable G-quadruplex DNA onto the inner surface of a synthetic nanopore. The underlying principle of this nanochannel system is the positive correlation between the G-quadruplex DNA conformational change and potassium ion concentration. The G-quadruplex DNA immobilized in a synthetic nanopore undergoes a potassium-responsive conformational change which induces reduction in the effective pore size of the nanopore. The responsiveness of this system is regulated by adjusting potassium concentration which in turn governs the stability of G-quadruplex structure. The responsive ion transport property of this nanopore G-quadruplex system is determined by measuring the ionic current across the nanochannel.
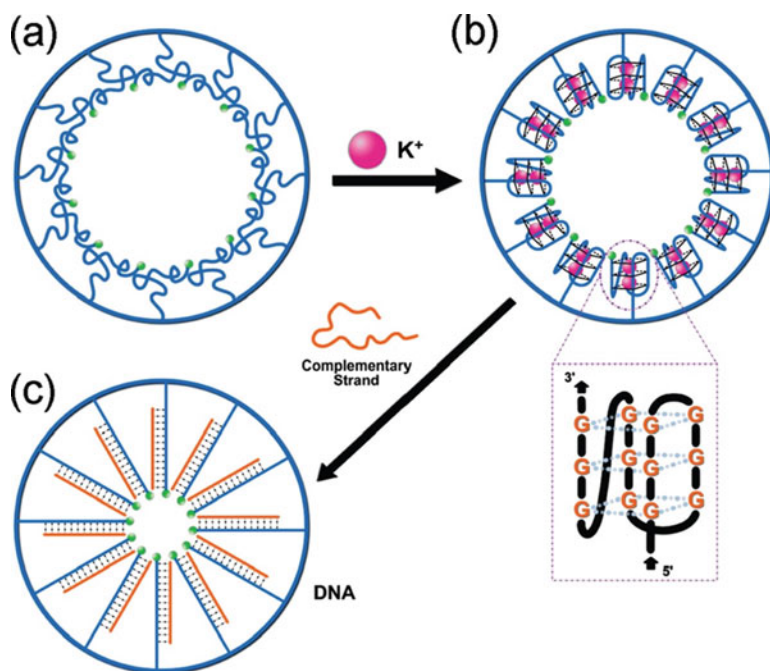
Fig. 4.10 Stimulus-responsive nanochannel
A G-quadruplex DNA labeled with a fluorescent group BODIPY 493/503 (*green circle*) at 3′ end is immobilized onto the inner surface of a single nanopore. (**a**) In the absence of K^+, the G-quadruplex DNA assumes a loosely packed single-stranded structure. (**b**) In the presence of K^+, the G-quadruplex DNA folds into a quadruplex structure which partially reduces the effective pore size of the nanopore. (**c**) Upon addition of complementary DNA strands, G-quadruplex DNA forms a closely packed arrangement of double-stranded DNA on the single nanopore
Adapted with permission from Hou et al. (2009). Copyright (2009) American Chemical Society

The immobilization of G-quadruplex DNA in a single nanopore closely resembles the in vivo situation of the G-rich telomere overhang attached to the ends of the chromosome. Therefore, this biomimetic nanochannel system will pave a way to study conveniently conformational changes in biomolecules in a confined space by current measurement.

Similar to G-quadruplex structures, i-motif structures are also used in nanotechnology. The formation of stable i-motif structures in vitro compulsorily requires a protonated cytosine in its building block. This feature allows pH-dependent reversible folding and unfolding of i-motif structures resulting in its immense applications in DNA nanotechnology. One of the applications is the pH-driven DNA molecular motors based on i-motif.

Molecular motors are molecular assemblies that can perform movements upon stimulation and translate energy into mechanical movements or other energy forms. i-Motif structures have been used to fabricate molecular motors driven by pH changes.
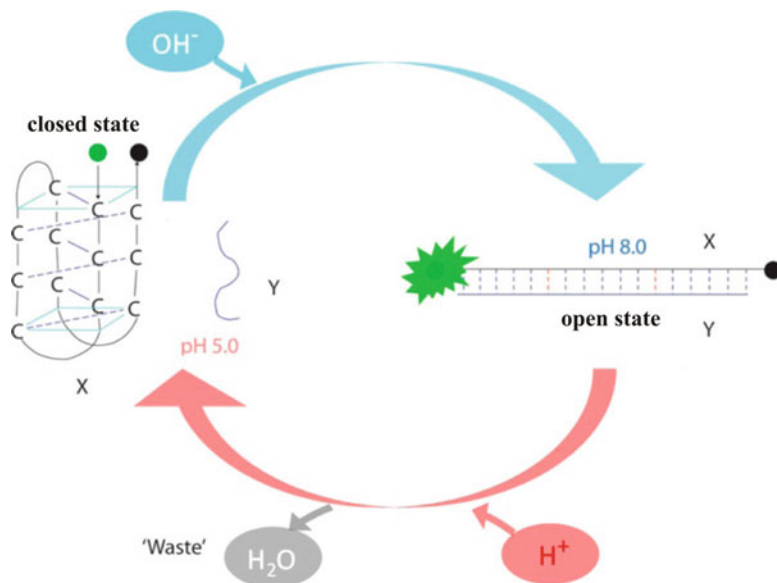
Fig. 4.11 DNA molecular motor based on i-motif structures

At pH 5.0, X strand folds into the i-motif structure (*the closed state*), and the complementary Y strand adopts a random-coil conformation. When pH is increased to 8.0, X strand unfolds and is hybridized to Y strand resulting in a duplex structure (*the open state*). Interconversion of closed and open states of the DNA molecular motor is simply mediated by alternating addition of H^+ and OH^-

Adapted with permission from Dong et al. (2014). Copyright (2014) American Chemical Society

As shown in Fig. 4.11, the pH-driven DNA molecular motor consists of a 21-mer single-stranded sequence X containing four CCC stretches and a 17-mer single-stranded sequence Y partially complementary to X. A slight acidic pH triggers sequence X to fold into an intramolecular i-motif structure with its 3′ and 5′ ends close to each other, representing the motor's "closed" state. However, changing the pH to slight basic conditions results in unfolding of the i-motif structure and formation of the duplex XY, representing the motor's "open" state. The by-products of the pH changes are only salt and water, which do not affect the DNA secondary structures. Also, the operating speed of this pH-driven DNA molecular motor is only determined by the intramolecular chain movement, which can occur at milliseconds to seconds.

The DNA molecular motor based on the i-motif structure has been widely used for fabrication of intelligent reversibly switchable surfaces, controllable release devices, and molecular logic gates.

4.2.4 Telomeric DNA

4.2.4.1 Discovery

In 1961 Leonard Hayflick and his colleague Paul Moorhead discovered that cultured human somatic cells have a limited capacity to divide, after which they stop growing and become enlarged. The Russian gerontologist Alexey Olovnikov in 1973 recognized shortening of daughter DNA strand with respect to the template during somatic cell division. On the basis of Leonard Hayflick's and his observation, Olovnikov proposed a theory of marginotomy to explain the shortening of DNA. He suggested that DNA sequences are lost with each cell cycle until the loss reaches a critical level, at which the cell division halts.

The first experimental answer to the shortening of DNA ends came in 1978 when the then postdoctoral fellow Elizabeth Blackburn and Joseph Gall observed that chromosome ends from *Tetrahymena thermophila* contain the six base sequence 5′-TTGGGG-3′ repeated 20–70 times.

In 1982 Blackburn and Jack Szostak successfully demonstrated the transfer of telomeric function from one organism (*Tetrahymena*) to another (*Saccharomyces cerevisiae*). Further, Blackburn and Carol Greider (1985–1989) identified a terminal transferase capable of extending telomeric sequences. This enzymatic activity was identified to be a part of a ribonucleoprotein with essential RNA and protein components and was termed "telomerase." Since the RNA component was complementary to the telomeric repeat sequence, they suggested that it was acting as a template for telomere repeat addition.

The 2009 Nobel Prize in Physiology or Medicine was jointly awarded to Elizabeth H. Blackburn, Carol W. Greider, and Jack W. Szostak for the discovery of how chromosomes are protected by telomeres and the enzyme telomerase.

4.2.4.2 Nature and Function

The telomere is a nucleoprotein complex located at the terminal ends of linear chromosomes. The nucleic acid component of telomere commonly referred as telomeric DNA is a noncoding DNA. In all eukaryotic cells, telomeric DNA is double stranded for most of its length, culminating in a 3′ single-stranded overhang. Telomeric DNA consists of tandem repeats of short guanine-rich sequences in the 5′→3′ strand with complementary cytosines on the other strand. The guanine-rich repeats of telomeric DNA endow it with the capability to form stable hydrogen-bonded nonduplex structures, the G-quartet, while the corresponding cytosine-rich regions adopt i-motif structures. The sequence and length of a tandem repeat are species specific, such as d(TTAGGG) in *Homo sapiens*, d(TTTAGGG) in *Arabidopsis thaliana*, and d(GGGGTCTGGGTGCTG) in *Candida glabrata*.

The protein component of telomere consists of telomere-specific proteins that bind to the telomeric DNA. The mammalian telomeric protein complex called shelterin consists of six proteins, TRF1 (telomeric repeat-binding factor 1), TRF2 (telomeric repeat-binding factor 2), RAP1 (repressor/activator protein 1), TIN2 (TRF1-interacting protein 1), TPP1 (TINT1/PIP1/PTOP 1), and POT 1 (protection of telomeres 1). The double-stranded telomeric repeats are bound by TRF1 and
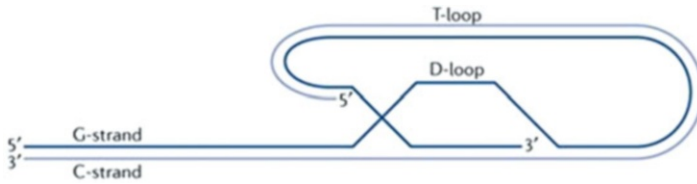
Fig. 4.12 The structures of T-loop and D-loop
Adapted with permission from Macmillan Publishers Ltd.: *Nature Reviews Molecular Cell Biology* (Nandakumar and Cech 2013), Copyright (2013)

TRF2, whereas POT1 attaches to the single-stranded overhang. These DNA-binding modules are further bridged by TPP1 and TIN2.

The telomeric proteins interact along with many other factors that transiently localize to telomeres and assist in sequestration of the single-stranded 3′ telomeric overhang into the duplex part of the telomeric DNA, thereby leading to the formation of two loops: the telomeric loop (T-loop) and the displacement loop (D-loop) (Fig. 4.12). A T-loop is a lariat structure formed as the telomeric DNA loops back on itself. The closed configuration of the T-loop provides a protective cap at chromosome ends that prevents the natural ends of linear chromosome from being recognized as sites of DNA damage. A D-loop is a single-stranded DNA loop, resulting from the invasion and pairing of a 3′ DNA end into homologous double-stranded sequences. Maintenance of telomeric DNA in loop structure serves to protect the vulnerable ends of linear chromosomes.

The T-loop is formed at the 3′ termini as the telomeric DNA folds back on itself to form a large loop. The D-loop is formed by base pairing of 3′ strand overhang with homologous double-stranded sequences, displacing the normal complementary chain. The loop structure provides end protection to linear chromosomes.

4.2.4.3 Alternative Length of Telomere

The ends of linear chromosomes shorten with each round of DNA replication due to the end-replication problem. In human somatic cells, each cell division results in the progressive shortening of telomeric DNA. Excessive telomere shortening triggers replicative senescence, after which no further replication takes place. This is considered as an intrinsic mechanism to limit the proliferative life span of somatic cells. However, in stem and germ line cells, telomeric DNA at chromosome ends are replenished to prevent replicative senescence. This telomere stabilization is accomplished by activation of telomerase in the late S phase of cell cycle.

The telomerase is a ribonucleoprotein complex composed of two main subunits: an RNA component called telomerase RNA (TR), which serves as the template for telomere synthesis, and a catalytic protein, the telomerase reverse transcriptase (TERT). In addition to its two major subunits, the telomerase is associated with several other proteins that are classified into three classes: firstly, the H/ACA-like proteins which stabilize the RNA component; secondly, the heterogeneous nuclear ribonucleoproteins which facilitate recruitment of the telomerase complex to its

substrate by interacting with double- or single-stranded telomeric repeats; and finally, the chaperon protein necessary for normal telomerase activity.

The sequence of telomerase RNA is complementary to the $5' \rightarrow 3'$ telomere repeat sequence. For instance, the RNA component of human telomerase contains the sequence $3'$-AATCCC-$5'$, which is complementary to the $5'$-TTAGGG-$3'$ human telomere repeat sequence. The function of telomerase is to counterbalance the trimming of telomere ends by elongation of the G-rich telomere strand and by its subsequent complementary replication. Basically, telomerase binds to the guanine-rich $3'$ end of telomeric DNA and by reverse transcription synthesizes the addition of further telomeric repeat sequence onto the end using its own RNA as template.

4.2.4.4 Role of Telomere in Cancer and Aging

The onset of cancer is a multistep process characterized by stepwise accumulation of genetic and molecular abnormalities, and selection of clonal cells with uncontrolled growth capacities. During the carcinogenic selection process, the tumor cells acquire immortality by dysfunction of p53/pRb (tumor suppressor protein) and upregulation of telomerase activity.

As somatic cells divide, telomeres shorten because of the end-replication problem. In cells lacking telomerase, excessive telomere attrition elicits DNA damage responses that trigger p53/pRb-dependent cell arrest/senescence. Cells with p53/pRb mutation bypass senescence and continue to divide until critically shortened telomeres initiate crisis (a period of complete replicative senescence, chromosome end-to-end fusions, chromosomal instability, and extensive cell death). However, during crisis some rare cells escape cell death and accumulate genetic alterations that cause upregulation or activation of telomerase or alternative mechanisms of maintaining telomeres, resulting in proliferative immortality. These immortal cells maintain stable but usually shortened telomere.

Telomerase is an attractive target for the development of effective therapeutics against cancer as it plays a major role in driving the growth of cancer cells. Also, the fact that normal human cells including stem cells have lower telomerase expression and generally maintain long telomeres compared to cancer cells ensure that anti-telomerase therapeutics will selectively induce cell death in cancer cells while minimizing the effects on normal cells. Various approaches adopted to achieve telomerase-based anticancer therapy include antisense gene therapies targeting TR, TERT-based immunotherapy, small-molecule inhibitors targeting TERT or TR, and development of ligands that stabilize telomere G-quadruplex structures.

The telomere system consisting of telomerase, telomeric repeats, and telomere-specific proteins that bind to the telomeric repeats also plays a crucial role in aging. The rate and progression of cellular aging varies depending on cell type. The number of times a cell can divide before senescence is constant for a particular cell growing under a specific set of conditions. This proliferative limit of a cell is largely ascertained by the telomere system.

Telomerase activity is absent in most normal human somatic cells because of the lack of expression of TERT. Without telomerase, telomere shortening eventually

limits the growth of cells, either by senescence or by crisis. To make up for the lost cells, stem cells exit from their niche, proliferate, differentiate, and repopulate the tissues as needed (Donate and Blasco 2011).

As previously mentioned, stem cell and germ line cells actively express telomerese. As stem cells proliferate their telomerase function to partially counterbalance the telomere shortening. In young or adult organisms, stem cell telomeres are long enough, whereas in old organisms, stem cell telomeres are too short. Critically short telomeres are recognized as sites of DNA damage, triggering a p53/pRb-mediated DNA damage signaling response that impairs stem cell mobilization, and, as a consequence, the tissue regeneration is suboptimal leading ultimately to organ failure.

The length of telomere is an indicator of cell's age and in turn an indicator of the organism's age/life span. Premature aging and disorders caused by early aging could be treated by boosting telomerase activity. Also telomerase-based cell therapy offers the possibility to slow down normal human aging. This has implications for considering telomerase as a potent antiaging intervention.

4.3 Coaxial Stacking

Coaxial stacking, also known as helical stacking, is a major determinant of three-dimensional structure in RNA. Coaxial stacking is the stacking of two base pairs at the termini of adjacent RNA helices, thereby aligning the two helices along a common axis (Fig. 4.13). Coaxial stacking is classified into two types: flush coaxial stacking, wherein no intervening unpaired nucleotides exist between the stacked helices, and mismatch-mediated coaxial stacking in which a single unpaired nucleotide occurs between the stacked helices. Coaxial stacking has been observed in higher-order structures of tRNA, rRNAs, and self-splicing group I and group II introns. This terminal base-stacking between the two RNA helices provides thermodynamic stability to the molecule as a whole (Laing et al. 2012).

Fig. 4.13 Two-dimensional representation of coaxial stacking in four RNA helices labeled 1–4
(**a**) mismatch-mediated coaxial stacking and (**b**) flush coaxial stacking
Adapted from Tyagi and Mathews (2007)
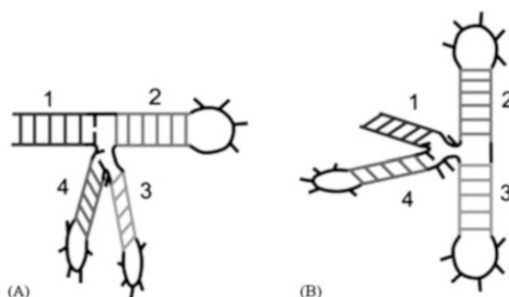
4.4   Thermal Melting of DNA Thermodynamic Parameters and Analysis

The thermodynamics of higher-order nucleic acid structures folding and unfolding provides an insight of their stability. The thermodynamic parameters are determined by analysis using two-state models. The model assumes that during unfolding of higher-order nucleic acid structures, only folded (fully associated) and unfolded (fully dissociated) states exist in equilibrium, and no intermediate states exist.

4.4.1   Monitoring Thermal Melting of Triplex and G-Quadruplex

The folding and unfolding of triplex and G-quadruplex can be monitored by thermal melting experiment. With increase in temperature of a solution containing a higher-order nucleic acid structure, the constituent strands denature or separate or melt. The experiment not only yields the temperature at the midpoint of this transition (T_m) but also provides important thermodynamic information, which helps to determine the stability of the higher-order nucleic acid structures and study their interaction with ligands. The melting transitions are recorded either by different types of spectroscopy (UV-visible, circular dichroism, fluorescence) or by calorimetry. However, the spectroscopic methods are preferred over calorimetric analysis.

4.4.1.1 UV Spectroscopy

The thermal denaturation of structured DNA molecule can be monitored by UV-visible spectrophotometer. Upon thermal denaturation, the structured nucleic acid melts, and the nucleobases become unstacked, causing an increase in absorbance (hyperchromicity). For duplex nucleic acids this change in absorbance is measured at 260 nm, and for quadruplex nucleic acids the same is measured at 295 nm. Conjunction of G-quadruplex thermal denaturation with UV spectroscopy is depicted as melting curves wherein absorbance at 295 nm is plotted as a function of temperature (Mergny and Lacroix 2009).

The melting curves are used to determine T_m values and thermodynamic parameters. The T_m value provides an estimation of the predominant form, i.e., at a temperature above the T_m, the nucleic acid structure is predominantly unfolded, and at a temperature below the T_m, the structure is predominantly folded. The notation $T_{1/2}$ is used instead of T_m when transition from folded to unfolded form is not reversible.

4.4.1.2 CD Spectroscopy

The melting temperature can also be measured by circular dichroism (CD) spectroscopy. To study the G-quadruplex conformation, the characteristic signals are measured at either 260 nm or 295 nm, which are reduced upon heat-induced denaturation. Also, at an appropriate wavelength, CD spectroscopy can be used to study the changes in melting temperature of G-quadruplex upon interaction with ligands. Measuring $T_{1/2}$ in the absence or presence of a ligand allows

Fig. 4.14 The schematic representation of change in melting temperature of G-quadruplex upon interacting with a stabilizing ligand, recorded by CD spectroscopy
Adapted from (Murat et al. 2011) with permission of The Royal Society of Chemistry
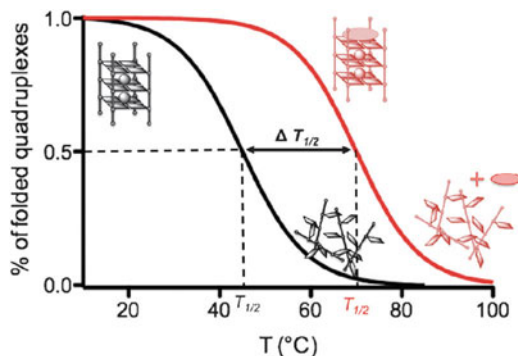
to determine whether the ligand under investigation stabilizes or destabilizes the G-quadruplex. As shown in Fig. 4.14, a stabilizing ligand will give a higher $T_{1/2}$ value.

4.4.1.3 Fluorescence Spectroscopy

A major drawback with UV and CD spectroscopic methods is low intensity signal variation, which results in imprecise melting curves. This limitation is overcome by fluorescence resonance energy transfer (FRET)-based method devised for measuring melting temperatures.

An intramolecular quadruplex forming oligonucleotide is labeled at 3' and 5' ends with a fluorophore and a quencher, respectively. As the oligonucleotide folds and forms quadruplex, the two opposite ends of the oligonucleotide come in vicinity, and the fluorescence is quenched because the quencher is in close proximity to the fluorophore. However, thermal denaturation of the quadruplex causes the fluorophore and quencher to move apart, and the fluorescence is restored. The hence obtained variation in fluorescence is recorded to obtain melting curves. As the change in fluorescence intensity is very high, the FRET-based method provides well-resolved melting curves. $T_{1/2}$ measurements in absence or presence of a ligand allow to quantify the effect of ligand under investigation.

4.4.2   Analyzing Thermodynamic Parameters of Triplex and G-Quadruplex

The stability of higher-order structures can be investigated by determining the thermodynamic parameters for their formation. The thermodynamic functions, namely, enthalpy change (ΔH), entropy change (ΔS), and Gibbs free-energy change (ΔG), can be evaluated via analysis of UV melting curves. The melting curves of duplexes exhibit single transition, whereas biphasic nature of most triplex melting curves adds to complication in their thermodynamic analysis. The two common measures of the melting temperature characterizing a heat-induced transition are T_m and T_{max}. T_m corresponds to the temperature at which the 50% transition

is complete, whereas T_{max} is the temperature corresponding to the maximum of the $dA/d(1/T)$ plot derived from the melting curves, where A is the absorbance (Shafer 1997).

For T_m measurement the absorbance versus temperature melting curve is converted to θ versus temperature, where θ is the fraction of strands in the dissociated state. This measurement requires baseline data at both high and low temperatures. However, T_{max} is directly determined from the maximum in the absorbance data, assuming that the absorbance of the two states (either fully associated or dissociated) depends linearly on temperature.

In biphasic triplex melting curves (triplex $\rightarrow$ duplex $\rightarrow$ single strands), the T_{max} method of analysis is applied, wherein each transition is treated separately. In such situations T_{max} depends on oligonucleotide concentration according to the equation

$$\frac{1}{T_{max}|} = \frac{R}{\Delta H} \ln C_t + \frac{\Delta S + b}{\Delta H}$$

where b is a constant ascertained by the strand stoichiometry, C_t is the total strand concentration, and R is the gas constant. ΔH and ΔS values are calculated from the slope and intercept of the straight lines obtained by fitting the data points on $1/T_{max}$ versus $\ln C_t$ plots by linear regression (Scaria et al. 1995). The above equation can be applied to the two maximums in the derivative melting curve, each corresponding to the two transitions, if they are well separated.

The quadruplex stability is evaluated by the thermodynamic relationships summarized below:

$$\Delta G = -RT \ln(K) = \Delta H - T\Delta S$$
$$\frac{\partial \Delta H}{\partial T} = \Delta C_p$$
$$\frac{\partial \Delta S}{\partial T} = \frac{\Delta C_p}{T}$$

where ΔG is the Gibbs free-energy change, T is the absolute temperature, K is the equilibrium constant, and ΔC_p is the change in heat capacity. Change in heat capacity is a more fundamental quantity than changes in enthalpy and entropy.

For intramolecular quadruplexes, the thermodynamic parameters are independent of oligonucleotide concentration, whereas for intermolecular quadruplexes, the entropy (and thus ΔG) does depend on oligonucleotides concentration.

4.5   Keto–Enol Tautomerization

4.5.1   Introduction

Commonly occurring bases can exist in at least two alternative chemical forms or tautomeric forms. Adenine and cytosine can exist in either amino (NH_2) or imino (=NH) forms, and guanine, thymine, and uracil can exist in either lactam

(keto, C=O) or lactim (enol, C–OH) forms. However, the keto and amino forms of the bases are highly favored. Tautomerization can reverse the polarity of hydrogen bonding sites resulting in base mispairs (Topal and Fresco 1976). For example, C (imino) = A (amino) and T (enol) ≡ G (keto).

4.5.2   Mechanism

Keto–enol tautomerism refers to the chemical equilibrium between a keto and an enol form. The two tautomers (structurally distinct compounds) are readily interchanged by migration of a proton within the molecule. The process is a slow process in neutral solution, and an acid or a base acts as a catalyst in the process. In the acid-catalyzed reaction, the keto form is first protonated on oxygen, and subsequent loss of the proton from alpha carbon results in enol form. However, in the base-catalyzed reaction, the base first removes the proton from alpha carbon, and then protonation of oxygen atom results in enol form. Since these reactions are catalytic, the catalysts, H^+ and OH^-, are regenerated at the end of the acid-catalyzed and the base-catalyzed mechanism, respectively.

4.5.3   Erlenmeyer Rule

The Erlenmeyer rule, formulated by Emil Erlenmeyer, states that alcohols with the hydroxyl group attached directly to a double-bonded carbon atom undergo tautomerization into the ketone or aldehyde form. This conversion occurs because the keto form, in general, has lower energy and hence higher stability compared to its enol tautomer.

4.5.4   Stereochemistry of Ketonization

The tautomerization of an enol with different R groups leads to a keto form with a new stereocenter formed at the alpha carbon. Depending on the nature of the R groups, the resulting stereoisomers would either be diastereomers or enantiomers. In a pair of enantiomer, one of two stereoisomers is a non-superposable mirror image of each other. While diastereomers are two or more stereoisomers of a compound with different configurations at one or more related stereocenters and are not mirror images of each other.

4.5.5   Phenols

Aromatic compounds such as phenol also exhibit keto–enol tautomerism. However, cyclohexadienone the keto tautomer of phenol is highly unstable compared to its enol form. The higher stability of the enol tautomer is attributed to its aromatic

character. Thus, at equilibrium only a tiny fraction of phenol exists as keto tautomer, while the majority exists in the enol form.

4.6   Tetraloop–Receptor Interactions

Tetraloops are RNA motifs composed of four loop nucleotides that form a compact and stable structure. RNA hairpins, the most common RNA secondary structure, are often capped by tetraloops. Tetraloops assist RNA-folding processes and provide sites RNA–RNA and RNA–protein interactions. They commonly occur in the 16S- and 23S-ribosomal RNAs, groups I and II self-splicing introns, ribonuclease P, and bacteriophage T4 messenger RNA. The majority of 16S-rRNA tetraloops are categorized into two sequence motifs: the UNCG motif and the GNRA motif. The GNRA tetraloop motif (the second nucleotide position (N) in this sequence motif may be any nucleotide and the third position (R) is any purine base) is the most prevalent tetraloop motif in naturally occurring RNAs.

Tetraloop receptors are RNA loop motifs that form tertiary interactions with the GNRA-type tetraloop. The structure of a tetraloop receptor consists of two Watson and Crick GC base pairs, a reverse Hoogsteen AU base pair, an adenosine platform, and a wobble GU base pair.

The interaction between the tetraloop and its receptor is responsible for diverse RNA three-dimensional structures. The GNRA tetraloop and its receptor interact in two ways. Firstly, the three adenosines of GAAA tetraloop stack upon the adenosine platform in the receptor and the resulting network of hydrogen bonds between the adenosines of the tetraloop and the minor groove of the receptor stabilize this tertiary interaction (Fig. 4.15). Alternatively, a GNRA tetraloop may bind to the
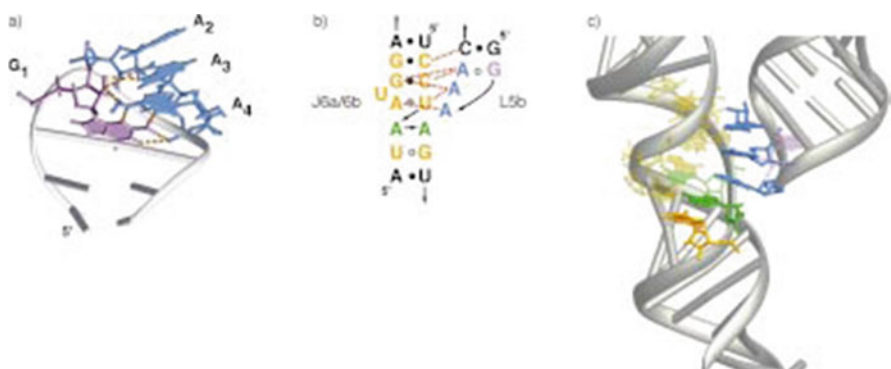
Fig. 4.15 Representation of the secondary structure interaction between the GAAA tetraloop and the tetraloop receptor
Reprinted from (Cate et al. 1996)

minor groove face of two tandem base pairs. For example, in the crystal structure of the hammerhead ribozyme, the GAAA tetraloop of one ribozyme is observed to dock against two tandem GC pairs in an adjacent molecule.

Biochemical studies of tetraloop–receptor interactions indicate that both the tetraloop and its receptor can tolerate a high degree of variability without sacrificing their binding affinity or specificity.

4.7   A-Minor Motif

The structural motif formed by insertion of adenosine into the minor grooves of RNA helices is termed as A-minor motif. The N1, N3, and 2′-OH atoms of the inserting adenosine nucleotide are available for hydrogen-bonding interactions (Fig. 4.16a). The receptor minor grooves are usually rich in GC base pair. In A-minor motif, the ribose–phosphate backbone of the adenosine is closer to one
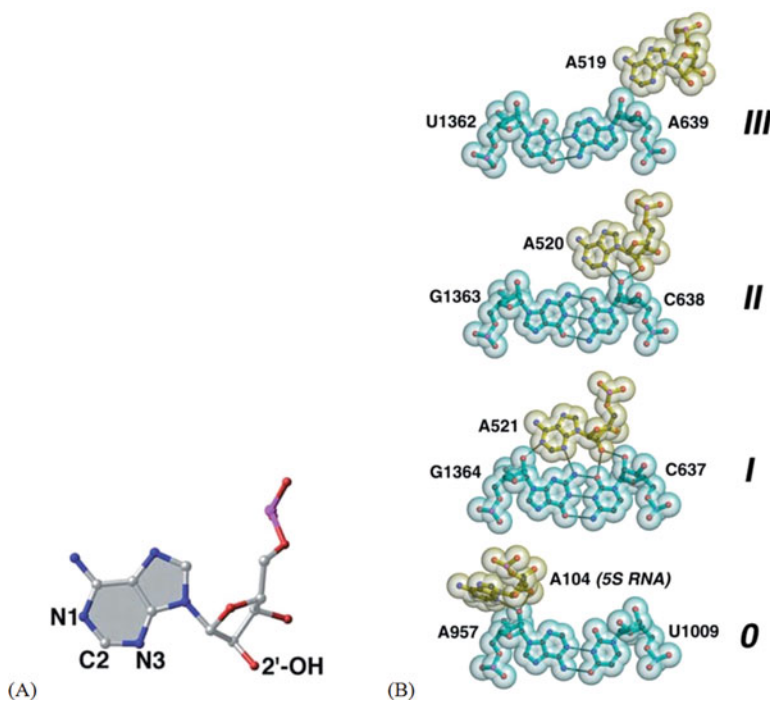
Fig. 4.16 (**a**) The smooth minor groove face of the adenosine nucleotide allows the base to pack tightly into the minor groove of a receptor helix. Its N1, N3, and O2′ atoms participate in hydrogen-bonding interactions. (**b**) Examples of the four major types of A-minor interactions found in *H. marismortui* 50S ribosomal subunit. In the surface representation, the inserted residue and the receptor helix base pair are shown in *gray* and *blue*, respectively
Reprinted from Nissen et al. (2001), Copyright (2001), National Academy of Sciences, USA

strand of the receptor helix than the other, and the orientation of the near strand is necessarily antiparallel to the strand to which the A belongs.

The A-minor motif is classified into four types depending on the position of the O2′ and N3 atoms of the A residue relative to the O2′ atom of the interacting base pair in the receptor helix (Fig. 4.16b). In type I, the most abundant A-minor motif type, both the O2′ and the N3 of the adenine residue are inside the minor groove of the receptor helix. In type II the O2′ of the adenine residue is outside the near strand O2′ of the helix, and the N3 of the adenine residue is inside the minor groove. In type III both the O2′ and N3 atoms of the adenine (or other) residue are outside the near strand O2′ of the receptor helix. And in type 0, the rarest form of the motif, the N3 of the adenine is outside the O2′ of the far strand of the receptor helix.

The type 0 and type III interactions are not adenine specific because it is the ribose of the inserted residue that fills the minor groove of the receptor helix, not the base. However, the interaction is optimized when the inserted base is an adenine. In contrast, both the type I and type II A-minor motifs are highly adenine specific because only adenine is able to fit comfortably into receptor minor groove and hydrogen bond with minor groove groups optimally.

A-minor motif is by far the most abundant RNA tertiary interactions in the large ribosomal subunit. Also, the interactions between tRNA and ribosomal large subunit is mediated by binding of the T stem of a tRNA to the A site of a ribosome in a way that allows A-motif formation.

4.8   Ribose Zipper

The ribose zipper is an RNA tertiary interaction characterized by at least two consecutive hydrogen-bonding interactions between ribose groups of two RNA helices that are running alongside each other in an antiparallel orientation. The two RNA helices are either two distinct segments of an RNA chain or two different RNA chains. Ribose zippers are created by inserting the backbone of one strand into the minor groove of another, bringing two backbone strands closer via shared hydrogen bonds formed between the 2′-OH of a base from one helix and the 2′-OH group and the O2 of a pyrimidine or the N3 of a purine in opposite helix.

The ribose zippers were first reported as an intermolecular interaction in ribozyme crystal structure and as two intramolecular interactions in the crystal structure of the P4–P6 domain of the group I intron (Fig 4.17). Since then ribose zipper elements have been identified in rRNAs of small and large ribosomal subunit, transfer RNA, riboswitches, RNA/ligand interactions, and signal recognition particle RNA. Ribose zippers tend to localize around tertiary interactions, such as tetraloop–receptor interactions and functions to reinforce the stability of entire tertiary substructures.
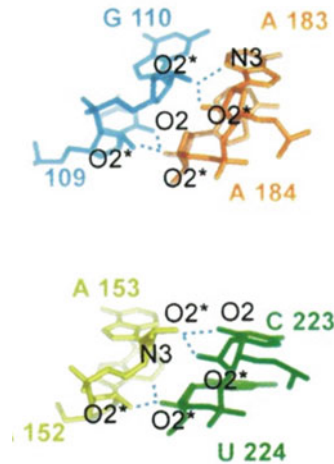
Fig. 4.17 Two ribose zippers in structure of the P4–P6 group I intron domain. The two RNA strands participating in the ribose zipper are arranged in antiparallel orientation. The riboses of two residues on each RNA strand interact by hydrogen bonding (*blue broken line*). Hydrogen bonds are formed between the 2′-OH of a base from one helix and the 2′-OH group and the O2 of a pyrimidine (C109, C223) or the N3 (G110, A152) of a purine in opposite helix
Reprinted from Tamura and Holbrook (2002), Copyright (2002), with permission from Elsevier

4.9   DNA Histone Interactions in Eukaryotic Cell

The eukaryotic genome is organized into a nucleoprotein complex called chromatin. Chromatin is further coiled into higher-order structures which allow compact and reversible packaging of the genetic material into the nucleus of a eukaryotic cell (Fig. 4.18). The principal protein components of chromatin are histones, a family of small basic proteins (H1, H2A, H2B, H3, and H4). The positively charged histones interact with negatively charged DNA (due to the phosphate groups in its phosphate–sugar backbone) via electrostatic interactions.

The basic structural unit of chromatin is the nucleosome, which consists of approximately 146 base pairs (bp) of DNA wrapped in 1.7 turns around an octameric histone core complex. The core complex consists of two molecules of each core histone (H2A, H2B, H3, and H4) and is organized as a central (H3–H4) tetramer flanked by two H2A–H2B dimers. Each nucleosome is connected to its neighbors by a linker DNA of approximately 10–80 bp length resulting in the formation of "beads on the string" structure, which is folded into a compact fiber with a diameter of approximately 30 nm. Further, linker histone H1 binds to DNA as it exits the nucleosome, interacts with the linker DNA, and stabilizes the 30 nm
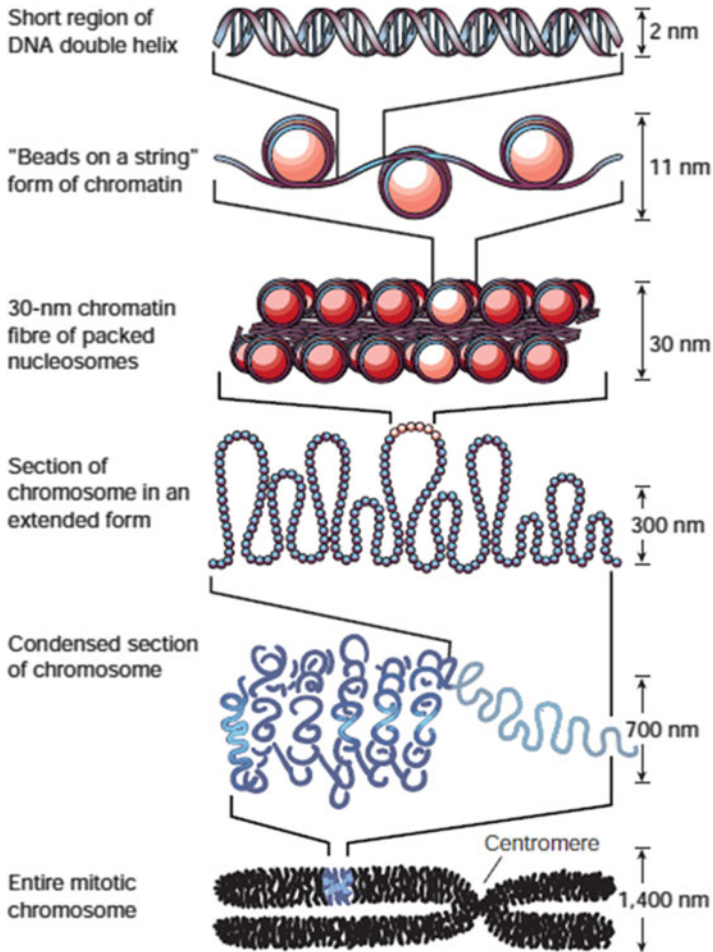
Fig. 4.18 The packaging of eukaryotic DNA
Reprinted by permission from Macmillan Publishers Ltd.: [NATURE] Felsenfeld and Groudine (2003), Copyright (2003)

fiber. In the presence of H1 histone, approximately 167 bp of DNA (in two helical turns) is associated with the nucleosome. As H1 histone binds to each nucleosome and to its adjacent linker DNA, loop structures with an average length of 300 nm are formed. These loop structures are compressed, folded, and tightly coiled into the chromatid of a chromosome.

4.10   DNA Supercoiling in Bacterial Cell

4.10.1 Introduction

Bacterial cells synthesize small DNA-binding proteins that participate in DNA supercoiling, resulting in compaction of the genetic material. These are collectively referred as histone-like proteins, as their biochemical properties resemble eukaryotic histones. The five different bacterial histone-like proteins include: the HU protein, integration host factor (IHF), protein H1, protein H, and FirA. Most bacterial species do not encode homologs of all the five proteins. However, HU proteins are present in almost all eubacteria.

HU is a heterotypic dimer consisting of two small basic proteins, HUα and HUβ, having similar amino acid sequences. HU binds to DNA in a nonspecific manner and wraps DNA into nucleosome-like structures. IHF is a heterodimeric basic protein composed of two subunits IHF-α and IHF-β. IHF exhibits substantial amino acid sequence homology with HU; however, unlike HU it binds specifically to the DNA sites containing the WATCARXXXTTR sequence, where W is A or T; X is A, T, C, or G; and R is A or G. IHF is thought to play a major role in nucleoid organization. It can fold a linear DNA molecule into a more compact arbitrarily twisted structure. The amino acid composition of another bacterial small DNA-binding protein, protein H1, differs significantly from the rest of the histone-like proteins. It is a neutral protein existing in three different forms H1a, H1b, and H1c having different isoelectric points, but same molecular weight. The protein binds very strongly to DNA and may be able to compact it. Little is known about the DNA-binding protein, Protein H and FirA. Protein H is known to interact with both double-stranded and single-stranded DNA up to a salt concentration of 0.1 M, and the basic protein, Fir A, is involved in transcription. However, it is not known if they also participate in packaging DNA.

4.10.2 Methods to Measure Degree of Supercoiling

4.10.2.1 Density Sedimentation

One of the earliest methods to measure supercoiling density involved centrifugation of a DNA sample in sucrose density gradient with increasing concentrations of ethidium bromide (Mirkin 2001). Principally, with an increase in DNA supercoiling, its compactness increases; hence, it sediments faster through the density gradient. The ethidium bromide in the density gradient intercalates between the stacked DNA base pairs and affects the DNA supercoiling. As the amount of intercalated ethidium bromide increases, the DNA supercoiling decreases until the relaxed form is attained, and further intercalation introduces supercoiling in opposite sense. The supercoiling density of a DNA sample can be calculated by measuring the critical dye concentration required for complete relaxation of the supercoiled DNA.

4.10.2.2 Gel Electrophoresis

Gel electrophoresis is a common and efficient method to determine the extent of DNA supercoiling. The technique employs gelling materials such as agarose and polyacrylamide that form three-dimensional mesh of channels. Under the influence of an electric field, the nucleic acid molecules loaded onto the gel matrix are separated on the basis of their molecular size or compactness. The degree of DNA supercoiling is directly proportional to its compactness. Thus, in gel electrophoresis a highly supercoiled DNA will move ahead of a less supercoiled DNA.

Topoisomers are topological isomers of a DNA molecule with different linking numbers. The topoisomers cannot be resolved on a standard agarose gel since they co-migrate as a single band. However, agarose gel electrophoresis performed in presence of an intercalator allows resolution of the highly supercoiled topoisomers. The commonly used intercalator is chloroquine, which functions to unwind supercoils of the topoisomers, thereby facilitating their better resolution in a gel.

References

Batey RT, Rambo RP, Doudna JA (1999) Tertiary motifs in RNA structure and folding. Angew Chem Int Ed 38(16):2326–2343

Blackburn EH, Gall JG (1978) A tandemly repeated sequence at the termini of the extrachromosomal ribosomal RNA genes in Tetrahymena. J Mol Biol 120(1):33–53

Cate JH, Gooding AR, Podell E, Zhou K, Golden BL, Kundrot CE et al (1996) Crystal structure of a group I ribozyme domain: principles of RNA packing. Science 273(5282):1678–1685

Chan PP, Glazer PM (1997) Triplex DNA: fundamentals, advances, and potential applications for gene therapy. J Mol Med 75(4):267–282

Day HA, Pavlou P, Waller ZA (2014) i-Motif DNA: structure, stability and targeting with ligands. Bioorg Med Chem 22(16):4407–4418

Devi G, Zhou Y, Zhong Z, Toh DFK, Chen G (2015) RNA triplexes: from structural principles to biological and biotech applications. Wiley Interdiscip Rev RNA 6(1):111–128

Donate LE, Blasco MA (2011) Telomeres in cancer and ageing. Philos Trans R Soc B 366 (1561):76–84

Dong Y, Yang Z, Liu D (2014) DNA nanotechnology based on i-motif structures. Acc Chem Res 47(6):1853–1860

Felsenfeld G, Groudine M (2003) Controlling the double helix. Nature 421(6921):448–453

Fricker J (1998) Triplex DNA as a novel diagnostic tool. Mol Med Today 4(4):140–141

Greider CW, Blackburn EH (1985) Identification of a specific telomere terminal transferase activity in tetrahymena extracts. Cell 43(2):405–413

Hayflick L, Moorhead PS (1961) The serial cultivation of human diploid cell strains. Exp Cell Res 25(3):585–621

Hou X, Guo W, Xia F, Nie FQ, Dong H, Tian Y et al (2009) A biomimetic potassium responsive nanochannel: G-quadruplex DNA conformational switching in a synthetic nanopore. J Am Chem Soc 131(22):7800–7805

Jain A, Wang G, Vasquez KM (2008) DNA triple helices: biological consequences and therapeutic potential. Biochimie 90(8):1117–1130

Laing C, Wen D, Wang JT, Schlick T (2012) Predicting coaxial helical stacking in RNA junctions. Nucleic Acids Res 40(2):487–498

Lane AN, Chaires JB, Gray RD, Trent JO (2008) Stability and kinetics of G-quadruplex structures. Nucleic Acids Res 36(17):5482–5515

Mergny JL, Lacroix L (2009) UV melting of G-quadruplexes. Curr Protoc Nucleic Acid Chem:17–11

Mirkin SM (2001) DNA topology: fundamentals. eLS

Murat P, Balasubramanian S (2014) Existence and consequences of G-quadruplex structures in DNA. Curr Opin Genet Dev 25:22–29

Murat P, Singh Y, Defrancq E (2011) Methods for investigating G-quadruplex DNA/ligand interactions. Chem Soc Rev 40(11):5293–5307

Nandakumar J, Cech TR (2013) Finding the end: recruitment of telomerase to telomeres. Nat Rev Mol Cell Biol 14(2):69–82

Nissen P, Ippolito JA, Ban N, Moore PB, Steitz TA (2001) RNA tertiary interactions in the large ribosomal subunit: the A-minor motif. Proc Natl Acad Sci 98(9):4899–4903

Olovnikov AM (1973) A theory of marginotomy: the incomplete copying of template margin in enzymic synthesis of polynucleotides and biological significance of the phenomenon. J Theor Biol 41(1):181–190

Rhodes D, Lipps HJ (2015) G-quadruplexes and their regulatory roles in biology. Nucleic Acids Res 43(18):8627–8637

Scaria PV, Will S, Levenson C, Shafer RH (1995) Physicochemical studies of the d (G3T4G3)* d (G3A4G3) d (C3T4C3) triple helix. J Biol Chem 270(13):7295–7303

Shafer RH (1997) Stability and structure of model DNA triplexes and quadruplexes and their interactions with small ligands. Prog Nucleic Acid Res Mol Biol 59:55–94

Simonsson T (2001) G-quadruplex DNA structures variations on a theme. Biol Chem 382 (4):621–628

Szostak JW, Blackburn EH (1982) Cloning yeast telomeres on linear plasmid vectors. Cell 29 (1):245–255

Tamura M, Holbrook SR (2002) Sequence and structural conservation in RNA ribose zippers. J Mol Biol 320(3):455–474

Topal MD, Fresco JR (1976) Complementary base pairing and the origin of substitution mutations. Nature 263(5575):285–289

Tyagi R, Mathews DH (2007) Predicting helical coaxial stacking in RNA multibranch loops. RNA 13(7):939–951

Macromolecular Interactions

5

Shipra Gupta and Arunima Verma

Abstract

Biomolecular interactions form the basis of life and orchestrate different biological pathways. Biological macromolecules including proteins, nucleic acids, enzymes and ligands mediate such biomolecular interactions and form basis of biochemistry. All the biological pathways are coordinated by these macromolecules. Thus, understanding the macromolecular interactions such as protein–protein interaction, protein–DNA interaction, protein–RNA interaction and protein–ligand interaction can help understand the blueprint of life. The present chapter explains the fundamental concepts on the major biomolecular interactions, the possible ways of interactions and different type of models for interactions. Thermodynamics reactions occur, whilst binding of macromolecule with small molecules and different types of factors govern these bindings such as free energy, binding kinetics, enthalpy and entropy and the forces and factors that govern the protein–ligand interactions followed by the entropy–enthalpy compensation and its influence on binding affinity. This chapter provides the reader knowledge about the overall picture of metabolic interactions occurring within any organism.

S. Gupta (✉)
Excelra Knowledge Solutions Pvt. Ltd, Hyderabad, Telangana, India
e-mail: libranshipra@gmail.com; shiprabioinfo@gmail.com

A. Verma
Autonomous Government PG College, Satna, Madhya Pradesh, India

5.1 Macromolecular Interactions

5.1.1 Protein–Protein Interactions

The fruition of the Human Genome Project (HGP) embodied the field of genetics to its present form where it is on pinnacle of significant theoretical and practical advances. The HGP also envisaged an inclusive understanding of the entire proteome content contained by an organism. Further comprehensive investigation into the expressed proteins and proteome of an organism led to emergence of new discipline of proteomics. Proteomics revolves around an ample variation of applications that explain complex biological processes occurring at a molecular level within a cell as well as how these processes differ in varying cell types. Further describing it succinctly, proteomics may be defined as a field that involves exploration of proteomes in terms of intracellular protein composition, structure and its own unique activity patterns. In the past decade, the researches involving proteomics have increased exponentially, and a scrupulous focus has been laid to the protein–protein interactions (PPIs) occurring within the organism. The daunting array of 'omics' data obtained from sequencing of the human genome in company with proteomics-based protein profiling studies served as a catalyst that caused renaissance in protein interaction analysis.

Studying the protein interactions is imperative for understanding the manner in which the proteins operate within the cells. Protein–protein interactions (PPIs) are pivotal to facilitate major biological process involving cell-to-cell interactions, cellular morphogenesis, cell division and propagation, cell motility and apoptosis. Further, it also provides useful insights into gene expression and transcriptional activation/repression; chromatin packaging, signal transduction, muscle contraction, regulation of gene expression and immune, endocrine and pharmacological signalling; and metabolic and developmental control. Hence, resolving the ins and outs of PPIs provides a thorough insight of functioning of any organism. Consequently characterising such interactions within a given cellular proteome would be a future landmark for understanding the basis of biochemistry of the cell.

The computable properties of PPIs are summarised by Phizicky and Fields (Phizicky and Fields 1995).

1. PPIs can transform the kinetic properties of enzymes as demonstrated by the altered binding of substrates, altered catalysis as well as changed allosteric properties of the protein complexes.
2. PPIs can promote substrate channelling by moving a substrate between or among diverse subunits of a protein complex as well as between different domains of a single multifunctional polypeptide, finally resulting in an intended end product.
3. PPIs can generate a novel binding site for small effector molecules.
4. PPIs can suppress or annihilate a protein.
5. PPIs can alter the specificity of a protein for its substrate recognition and even promote interaction of protein with diverse binding partners.

Various non-covalent interactions, for example, hydrogen bonds, ionic bonds, hydrophobic bonds and van der Waals forces, between the amino acid residue side chains form the basis for protein folding, protein assembly and PPIs (Ofran and Rost 2003). These bonds provoke multiplicity of associations among the proteins. On the basis of these associations, the PPIs can be classified in several ways. Firstly, on the basis of their mutual interaction surfaces, the PPIs may be either homo-oligomeric or hetero-oligomeric. Secondly, on the basis of stability, they may be obligate or nonobligate. Thirdly, based on their persistence, they may be transient or permanent. When only one type of protein assembles/associates together to form a macromolecular complex, it is termed as homo-oligomer. Their formation is assisted by contribution of non-covalent interactions in an existing quaternary structure of the protein. During formation of any homo-oligomer, energy accumulated at the interface of subunits serves to bind ligand or modify the protein conformation as per the reaction to the regulatory ligands. In order to return to their original monomeric form, denaturation of the complex is requisite. The most common examples of homo-oligomers are carrier proteins, transcriptional regulatory factors, scaffolding proteins, etc. Till date, haemoglobin is one of the finest illustrations of oligomeric protein. The thorough knowledge about the relationships between sequence, structure, dynamics, energetics and function of haemoglobin illustrates the protein to be a model for studying homo-oligomer protein system.

Stable interactions are characteristically depicted by proteins that are integral part of permanent multisubunit complexes and take long duration to interact together. The subunits of the complex protein can be identical or non-identical in nature. Such interacts are majorly seen on homo-oligomers (identical subunits) but can also be observed sometimes in hetero-oligomers (non-identical subunits). Most common examples of proteins showing stable interactions are cytochrome c, subunits of ATPase, haemoglobin and core RNA polymerase. These interactions are easily detected by co-immunoprecipitation and far-Western methods.

In contrast to stable interactions, proteins that interact momentarily and reversibly with other proteins show transient interactions. Such interactions orchestrate the majority of vital cellular processes, for instance, cell growth, cell cycle, metabolic pathways, protein modification, transport, folding, signalling, signal transduction, etc. They are on/off at any instant of time, entail specific set of conditions that determine the interaction, may be strong or feeble and may be rapid or slow. Such interactions can be identified by cross-linking or label transfer methods. The most common example of protein that shows such interaction is the G protein-coupled receptor (GPCR).

Proteins depicting covalent interactions are formed by disulphide bonds or electron sharing; hence, they have very strong associations. These interactions are rare in nature and principally observed in several post-translational modification events, like ubiquitination and SUMOylation. On the contrary to covalent associations, the non-covalent bonds are formed during transient interactions by amalgamation of weaker bonds, for example, ionic interactions, hydrogen bonds, van der Waals forces or hydrophobic bonds. Non-covalent bonds promote the operation of metabolic pathways, signal transduction, etc.

5.1.1.1 Protein–Protein Interaction Databases

The paramount amount of interaction identification of large-scale PPI experiments is stored in the form of biological databases known as protein interaction databases. The information stored in these databases is serving as basis for understanding the interactome of various organisms. These databases are popularly classified into three types, *viz.* primary databases, meta-databases and prediction databases.

Primary databases contain protein interactions from experimental validated methods and published literature. Meta-databases extract experimental data from primary databases, amalgamate all the extracted information and remove the redundant information to provide comprehensive set of data. Prediction databases are similar to meta-databases in that they also extract and integrate information from primary databases, but in addition to this, they also perform computational analysis in order to fill the gaps in interactome. For example, if we don't have information regarding two proteins interacting in mouse and similar orthologous proteins are found to interact with each other in humans, then we may presume that both the proteins will interact with each other in mouse also. The most common PPI databases are as follows:

STRING (Search Tool for the Retrieval of Interacting Genes/Proteins) is a biological database that contains information of known and predicted protein–protein interactions. The database is freely accessible and regularly updated and contains information integrated from multiple sources, such as experimental data, computational prediction methods and public text collections. The recent version of STRING contains information pertaining to 2031 organisms, 9.6 million proteins and 184 million protein–protein interactions (Szklarczyk et al. 2017).

The Database of Interacting Proteins (DIP) records experimentally determined interactions between proteins. It amalgamates information from a variety of sources, and the data stored within DIP is curated in three manners: (1) manually, (2) by expert curators and, automatically, (3) using computational methodologies that extract the information about the protein–protein interaction networks. DIP is a member of the International Molecular Exchange Consortium (IMEx), which is a group of the public providers of interaction data (Xenarios et al. 2000). The idea of documenting all the known molecular interactions in the form of a database was initially put forward by Tony Pawson (1998). A consortium involving Genome Canada, the Canadian Institutes of Health Research (CIHR), the Ontario Research and Development Challenge Fund, IBM and MDS Proteomics funded together to bring this idea into reality in the form of a database named Biomolecular Interaction Network Database (BIND). BIND is an open-access, freely distributed public proteomics resource that serves as a platform to enable data mining and present visualisations of complex molecular interactions. BIND archives three basic entries, *viz.* (1) biomolecular interactions, (2) molecular complex and (3) pathway information. Biomolecular interaction includes information about a molecule such as name, synonym of molecule and location of molecule such as in which cell and in which species it is found and outlines experimental conditions obligatory to scrutinise binding in vitro conditions. Molecular complexes depict stabilised aggregate of molecules interacting together and have a function when bound to each

other. Pathway record section includes network of interactions implicated to regulation of cellular processes. It may even comprise information pertaining to phenotypes and diseases related to the pathway. BIND includes entries from individual submissions, interaction data from PDB (https://www.rcsb.org/pdb/home/home.do) (Berman et al. 2000) as well as interaction and complex information obtained from yeast two hybrid, mass spectrometry, genetic interactions and phage display methodologies. In order to create entry for BIND, two minimal types of information are obligatory, *viz.* (1) a PubMed publication reference and (2) an entry in another database (e.g. GenBank). All the data submitted to BIND are first curated for quality assurance after which they are made publically available. Two types of records are observed during curation: high throughput (HTP) and low throughput (LTP). HTP records constitute publications that have listed more than 40 interaction results from one experimental methodology. In contrast, the LTP records report much lesser interaction results. BIND is based on a data specification written using the Abstract Syntax Notation 1 (ASN.1) language. ASN.1 language is used by NCBI to store its data in their Entrez system and hence BIND also uses similar standards for its data representation. Further, ASN.1 format is chosen since it can effortlessly handle complex data, can effortlessly get translated into other data specification languages and is applicable to all kind of biological interactions. After its conception in 1999, the first version was released which was further modified as per the user feedback. The enhanced later versions included versions 2, 3 and 3.5, and finally in 2006, BIND got integrated into Biomolecular Object Network Databank (BOND) where it continues to be rationalised and further improved (Bader et al. 2003).

5.1.1.2 Methods to Detect Protein–Protein Interactions

In order to regulate the biological process, the proteins coordinate together to interact in a network of complex molecular associations. These molecular associations can be detected by multifarious methods. These methods are broadly classified into three categories: (1) in vitro methods, (2) in vivo methods and (3) in silico methods. The most conventionally used methods are shown in the following figure. Out of these methods, the three most commonly used high-throughput methods are yeast two-hybrid screening, protein microarrays and affinity purification followed by mass spectrometry (AP-MS) (Fig. 5.1).

Yeast Two-Hybrid (Y2H) Screening

This system was originally designed in 1989 by Fields and Song. The method was used to identify protein–protein interactions using the GAL4 transcriptional activator in the yeast *Saccharomyces cerevisiae*. The basic principle behind Y2H is the activation of downstream reporter gene(s) by the binding of a transcription factor onto an upstream activating sequence (UAS). The transcription factor gets divided into two diverse portions, called the binding domain (BD) and activating domain (AD) for two-hybrid screening. The BD domain is responsible for UAS binding, and the AD domain plays an important role in the activation of transcription. The Y2H is thus a protein-fragment complementation assay. In spite of its effectiveness, the yeast two-hybrid system has some restrictions, such as moderately low

PPI interaction methods

In vitro methods
- Affinity chromatography
- Coimmunoprecipitation
- Protein microarrays
- Protein-fragment complementation
- Phage display
- X-ray crystallography
- NMR spectroscopy

In vivo methods
- Yeast 2 hybrid
- Synthetic lethality

In silico methods
- Ortholog based sequence approaches
- Domain –pairs-based sequence approach
- Structure based approach
- Gene neighbourhood
- Gene fusion
- *In silico 2 hybrid*
- Phylogenetic tree
- Phylogenetic profile
- Gene expression

Fig. 5.1 Different types of methods used for understanding protein–protein interactions

specificity, and the method uses yeast as the main host system, which proves to be difficult for studying other biological models; the number of PPIs predictable is usually low because of the loss of many transient PPIs during purification process (Ito et al. 2001; Zhang 2009) (Fig. 5.2).

Protein Microarray

Protein microarray is a potential technology that provides a supple platform for cataloguing of hundreds to thousands of proteins in a highly parallel and high-throughput fashion. A protein microarray (or protein chip) tracks PPIs on large scale, and a major benefit is that multiple proteins can be detected in parallel by the method. Furthermore, they are speedy, economical, mechanised and highly responsive, which utilise small proportions of samples and reagents. The chip consists of a supporting surface such as a glass slide, nitrocellulose membrane and microtiter plate, to which an array of capture proteins is bound. Fluorescent dye-labelled probe molecules are added to the array. Reaction between the probe and the immobilised protein emits a fluorescent signal that is detected by a laser scanner. Such detection gives a positive result for protein–protein interactions (Zhang 2009).

The huge majority of PPI interfaces reflects the composition of protein surfaces, rather than the protein cores which are rich in hydrophobic residues specially the aromatic residues (Fig. 5.3).

5.1.1.3 Interface Descriptors

A comprehensive analysis of the molecular structures that interact among each other provides intricate details about the interface between the interacting proteins. Whilst characterising the PPI surfaces, important parameters such as size, solvent-accessible surface area (SASA), complementarity between surfaces, shape, hydrophobicity, residue interface propensities, segmentation and secondary
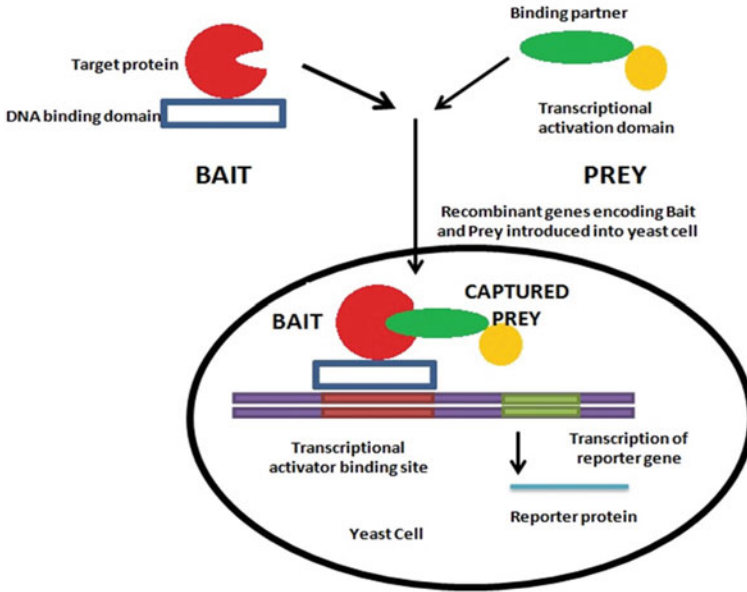
Fig. 5.2 Yeast two-hybrid system: The fusion of target protein to the DNA binding domain brings about formation of a dimer (together termed as BAIT). When BAIT fuses to the PREY, both together bind to promoter of reporter gene, thus causing transcription of activator binding site that further directs transcription of reporter gene to express the reporter protein

Fig. 5.3 Protein microarray: Correctly folded proteins get attached to surface of slide by help of BCCP and biotin. Misfolded proteins do not get attached to slide and are washed off. Such arrays of immobilised proteins are detected by labelled secondary antibodies. Fluorescent signals emitted by secondary antibodies are detected by microarray scanner
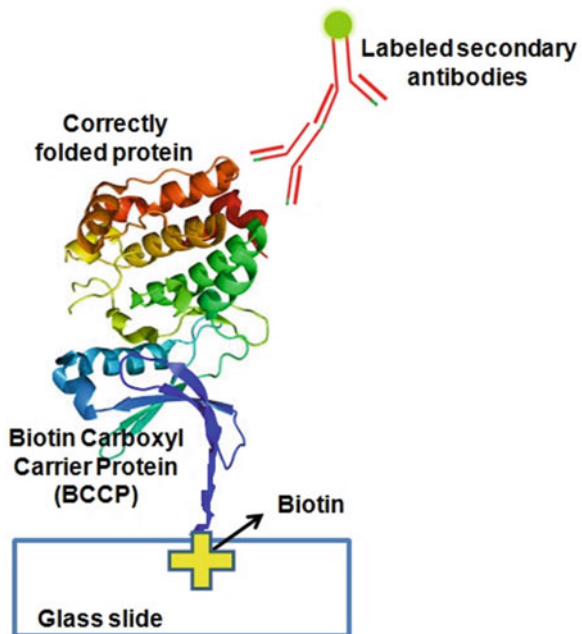
structure and conformational changes on complex formation influence the properties of PPI interfaces.

Thus, during a protein–protein interaction study, two conditions are necessary for a binding process to occur: (1) geometric complementarities between two proteins and (2) stability between both the proteins in terms of energetics (ΔG values). Furthermore, the protein surface is made up of many hydrophilic residues. The average charge density of native proteins is 1.4 charged groups per 100 A^2 of protein surface (Barlow and Thornton 1986). Due to these hydrophilic residues, the surface of protein has a natural tendency to attract water and get solvated. Thus, a proper binding occurs between two proteins only when both are complimentary in shape so that they can fit properly like a lock and key to facilitate binding between them. Another important criterion is balance between H-bonding and salt bridges occurring between two proteins as well as hydrophobic and hydrophilic effects occurring on protein surface. Thus, the hydrophobic effect, hydrogen bonds and salt bridges all play imperative roles in the energetics of the docked complex.

A hydrogen bond or a salt bridge provides favourable free energy for occurrence of the binding event between any two moieties (Xu et al. 1997). Hydrogen bonds are considered as potent contributors to strong physical interactions, and along with molecular surface shape complimentary between two proteins, the H-bonds are the significant component in the evaluation of binding (Meyer et al. 1996). Hydrogen bonds and salt bridges play a crucial role in protein binding (Xu et al. 1997) particularly in determining binding specificity (Fersht 1984; Fersht 1987). On the contrary, any unfulfilled/incomplete hydrogen bond donor/acceptor, or any isolated charge without forming a salt bridge, present on the interface of protein, could significantly destabilise binding, due to the desolvation effect caused by it. Thus the binding specificity depends on energetics contributed by the hydrogen bonds and salt bridges between proteins.

During molecular recognition, protein flexibility and dynamics of intermolecular interfaces determines the binding affinity and specificity. Also, structural stability and flexibility are influenced by the underlying binding energy landscape and are associated with functions, namely, specificity and permissiveness in recognition. Docking takes into consideration hierarchal approaches involving both ligand and protein flexibilities. Further, shape descriptors (depth, surface, extreme elevation, surface area, volume and shape complementarity) are used for the identification and comparison of various protein–ligand/protein–protein interactions and their binding sites. The PatchDock server uses the same descriptor for the binding analysis as in the case of bis(2-methylheptyl)phthalate showing maximum compatibility with PmRab7 and VP28.

5.1.2 Protein–Nucleic Acid Interactions

Proteins interact with DNA and RNA by means of analogous physical forces that comprise various interactions including electrostatic interactions (salt bridges), dipolar interactions (hydrogen bonding, H-bonds), entropic effects (hydrophobic interactions) and dispersion forces (base stacking). The forces contribute to either tight (sequence

specific) or loose (non-sequence specific) binding. An example of specific interaction may be when a specific protein recognises and inserts itself into the major groove of DNA double helix by means of α-helix motif through H-bonds and salt bridges. Additionally, the specificity and affinity of a particular protein–nucleic acid interaction may be amplified through protein oligomerisation or multi-protein complex formation (e.g. glucocorticoid receptor, mRNA splicing complexes, RISC, etc.).

5.1.2.1 Nucleic Acid Binding Domains

The tertiary structure of protein consists of distinct conserved domains that serve as important templates for binding of DNA and RNA into the proteins. These discrete conserved domains either may be found in the form of multiple repeats for the same nucleic acid binding domain or may be dispersed throughout the structure. The distinctiveness of these domains as well as their relative arrangement is important for functionality of the proteins. The most common DNA binding domains comprise zinc finger, helix-turn-helix, helix-loop-helix and leucine zipper, whilst the most studied RNA binding domains include zinc finger, KH, S1, PAZ and RNA recognition motif. Sometimes, the interaction between proteins and the nucleic acids may be quite complex. The proteins may directly bind to the nucleic acids or sometimes they may indirectly bind to the nucleic acids through other bound proteins. Some of these interactions are transient and may require chemical cross-linking for their stabilisation. Hence, in order to understand the comprehensive individual protein–nucleic acid complex and their role in cellular processes, we need to determine the type and structure of the protein involved in complex formation, identify the nucleic acid sequence and structure involved and further recognise the manner in which both components interact with each other.

The most common biological mechanisms during which the proteins/protein complexes interact with DNA are for maintenance of the structure of chromatin, for the transcription of DNA into RNA and for DNA repair mechanisms. The protein complexes slide along the genomic DNA till they locate precise docking sites, and then these proteins bind to DNA by means of their specific DNA binding domains such as helix-turn-helix and zinc finger domains. The protein–RNA interactions occur during transcription, post-transcriptional events, translation and post-translation events. The tools for protein RNA interactions are limited.

5.1.2.2 Databases

A concise information pertaining to databases have been illustrated in tabular form as below:

S. no.	Database	Description	Link	References
1.	3D-footprint	DNA–protein complexes	http://floresta.eead.csic.es/3dfootprint	Contreras-Moreira (2010)
2.	Protein–DNA Interface Database	DNA–protein interface	http://melolab.org/pdidb/web/content/home	Norambuena and Melo (2010)

(continued)

3.	Protein–RNA Interface Database	RNA–protein complexes	http://bindr.gdcb.iastate.edu/PRIDB	Lewis et al. (2011)
4.	Biological Interaction database for Protein–nucleic Acid	DNA–protein complexes	http://mordred.bioc.cam.ac.uk/bipa/	Lee and Blundell (2009)
		RNA–protein complexes		
5.	Protein–DNA complex structure analyser	DNA–protein complexes	http://bioinfozen.uncc.edu/webpda/	Kim and Guo (2009)
6.	Protein–DNA Recognition Database	Protein–DNA complexes	http://gibk26.bio.kyutech.ac.jp/jouhou/3dinsight/recognition.html	Prabakaran et al. (2001)
7.	Nucleic Acid Database	Structure of nucleic acid molecules	http://ndbserver.rutgers.edu/	Berman et al. (2003) and Coimbatore Narayanan et al. (2014)

5.1.2.3 Methods

Chromatin Immunoprecipitation (ChIP) Assays
The method is used to assess transcriptional regulation through epigenetics or transcription factor–DNA binding interactions. In order to evaluate DNA–protein interactions by the ChIP assay method, the living cells are treated by formaldehyde or other cross-linking reagents. A prior knowledge about the target protein and DNA sequence to be analysed is required. An antibody targeted against the protein of interest and PCR primers for the DNA sequence of interest are also required. The antibody selectively precipitates the protein–DNA complex from the other genomic DNA fragments. The PCR primers help in the detection of the desired DNA sequence and their amplification (Gade and Kalvakolanu 2012).

DNA Electrophoretic Mobility Shift Assay (EMSA)
The EMSA is used to assess proteins binding to known DNA oligonucleotide probes and determines the degree of affinity or specificity of the interaction. The basic principle behind EMSA is that protein–DNA complexes migrate slower than the free DNA molecules when subjected to native polyacrylamide or agarose gel electrophoresis. Since the rate of migration of DNA upon binding to the protein is retarded or shifted, EMSA is named as a gel shift or gel retardation assay. With an addition of protein-specific antibody, a larger complex (antibody–protein–DNA) is

created which migrated slower than the protein–DNA complex. The process is called supershift used to substantiate protein identities (Hellman and Fried 2007).

RNA Electrophoretic Mobility Shift Assay
The RNA–EMSA is a well-known and potential in vitro technique for the detection of RNA–protein interactions exploiting the changes in migration speed during gel electrophoresis. It is based on the fact that naked RNA has certain mobility on native gels, but if the RNA is complexed with protein, it results in the reduction of RNA mobility. The protein binding to RNA results in a distinctive upward shift in location of protein–RNA complex on the gel as depicted by the use of radiolabelled RNA. Majority of RNA–protein complexes especially the ones that have large affinity between the RNA and protein do not easily dissociate during long duration of electrophoretic separation. Such high-affinity interactions can be identified over a background of weak interactions. Therefore, EMSA is commonly used to detect complex mixtures of proteins such as cell extracts. EMSA is a very useful technique for investigating large-range RNA–protein interactions emerging from single protein-binding events to assemblage of large protein–RNA complexes such as spliceosome. Further, it helps in deriving kinetic parameters, for instance, affinity constants for RNA–protein interactions (Bak et al. 2015).

5.1.2.4 RNA Pull-Down Assay

RNA pull-down assays are used for selective extraction of the protein–RNA complex from a given sample. Classically, an RNA pull-down assay makes use of high-affinity tags, such as biotin or azido-phosphine chemistry. RNA probes are known to be biotinylated and form a complex with a protein from a cell lysate thereafter purified by means of agarose or magnetic beads. On the other hand, the protein may be labelled, or the RNA–protein complex may be detected using an antibody against the desired protein. The RNA can be detected by Northern blot or RT-PCR and the proteins using Western blotting or mass spectrometry (Marin-Bejar and Huarte 2015).

5.2 Small Molecular Interactions

Small molecule and protein interactions are important for advancement of basic science and drug development. There are a lot of approaches to understand the interactions from different prospectives.

5.2.1 Ligand Interactions at Equilibrium

The strength of association–dissociation of ligand binding is based on the ligand–receptor kinetics. The rate of molecular process is dependent upon the concentrations of the ligand and receptor involved.

$$\text{Ligand} + \text{Receptor} \rightleftharpoons \text{Ligand.Receptor}$$
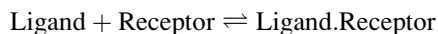
The rate of forward reaction is Kf (second-order rate constant), whilst the rate of reverse reaction is Kb (first-order rate constant). The rate of forward reaction equals the rate of reverse reaction at equilibrium (Sanders 2010).

$$(\text{Kf})\text{Ligand} + \text{Receptor} \rightleftharpoons \text{Ligand.Receptor}(\text{Kb})$$
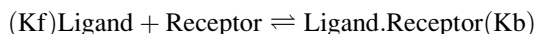
5.2.2 Binding of Small Molecules by Polymers

The binding of small compounds by synthetic polymers is the model of bimolecular interactions with substrate and has pharmaceutical significance. Polysoap, an amphiphilic polymer, is an important polymer of interest as it relates to the structure and function of globular proteins. Overall, strength of the synthetic macromolecule with small molecules is comparable to that of serum albumin. Polyvinylpyrrolidone, a polymer, binds to macromolecule much better than any other synthetic macromolecules and shows strong binding affinity to small molecules. Methyl orange is used as a binding probe, and due to its apolar and ionic group, it provides a suitable balance of hydrophobicity and hydrophilicity and is a very good reference anion (Salamone 1998).

5.2.3 Binding of Two Different Ligands

Binding of two different ligands to the macromolecules are of two types, allosteric and competitive binding. Allosteric binding is very common in biological systems, in which two ligands bind to the different binding sites of the macromolecule, whilst competitive binding is in which the two different ligands compete for the same binding site on the macromolecule.

The crystal structure of the human P2Y1R in complex with a nucleotide antagonist MRS2500 and with a non-nucleotide antagonist BPTU is a very good example of binding of two different ligands. This structure reveals two distinct ligand binding sites. MRS2500 recognises a binding site within the seven-transmembrane bundle of P2Y1R, whilst BPTU binds to an allosteric pocket located on the external receptor interface with the lipid bilayer (Zhang et al. 2015).

5.3 Models for Binding

Cooperative binding is one of the most interesting and not completely deciphered phenomena involved in control and regulation of biological processes. It was assumed that cooperative binding was observed in the substrates where multiple

binding of ligands (activators and inhibitors) is possible, and it is based on a particular structural design of the substrate.

5.3.1 Identical and Independent Site Model

Independent binding site model is the simplest model among the other models, where a single independent binding site forms a 1:1 ratio of macromolecule and ligand complex.

$$\text{Macromolecule} + \text{ligand} = Macromolecule.ligand$$
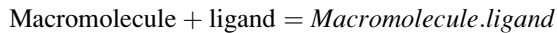
Binding sites may be identical when $\alpha \neq 1$, identical with negative cooperativity when $\alpha < 1$ or identical with positive cooperativity with values of $\alpha > 1$ (Riegel 1989).

5.3.2 MWC and Sequential Models

The Monod–Wyman–Changeux (MWC) model was given in 1965 for the conformational change mediating upon binding of indirect ligands. The central paradigm of the MWC model is followed by many classical regulatory proteins, namely, nicotinic acetylcholine receptor, Asp trans-carbamylase and haemoglobin. The conformational change mediating the allosteric interactions of the distinct sites on proteins led to a remarkable change in conformational pattern. The MWC model establishes the link between the regulatory proteins/substrates such as activators/inhibitors and cooperative binding substrate (Fig. 5.4).

In the early 1960s, only the crystallographic structures of two globular proteins, namely, myoglobin and haemoglobin, were solved. Initially, haemoglobin X-ray crystallographic studies proposed that equilibrium exists between high- and low-affinity states with a simplified MWC model. Later on, it is believed that the pH causes a reduction in the binding affinity of oxygen in haemoglobin. After some time, it came into notice that Bohr effect is required for the sequential break of hydrogen bonds in the transition state, which led to the Koshland–Nemethy–Filmer (KNF) model. KNF model suggested that the conformational change can be induced by ligand binding and can be transmitted to neighbour subunit intermediate conformations. Subunits can be in different conformations and can be changed subsequently, and the mechanism is called sequential model (Changeux, 2013).

5.3.3 Cooperative, Non-cooperative, Excluded Site Binding

CytR and cAMP receptor protein (CRP) binding facilitates both the negative and positive control of transcription from *Escherichia coli* deoP2. CRP activates transcription and forms multi-protein CRP–CytR–CRP complex, which is stabilised by
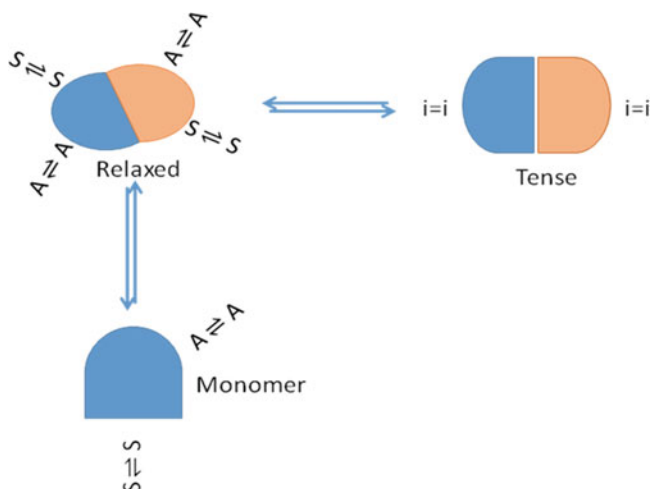
Fig. 5.4 Two-state concerted model of MWC model. The transition from relaxed to tense state of a dimer is shown here. A (activator), i (inhibitor) and S (substrate) are the three categories of molecules that interact with the enzyme and stabilise the relaxed and tense states, respectively

cooperative interactions between CRP and CytR. An additional non-cooperative binding site is specific to CytR binding and overlaps with CRP1 and CRP2 (Perini et al. 1996).

5.4   Energetics and Dynamics of Binding

Proteins play a very important role in the cell, including cell signalling (hormones) and mechanical (muscle), structural (cytoskeleton) and biochemical (enzymes) functions. The biological functions of the proteins are realised by direct interactions with other molecules such as membrane, substrates, nucleic acids, proteins and peptides and small-molecule ligands such as oxygen, solvent and metal (Perozzo et al. 2004). Ligand binding to protein involves multiple orientations. Sometimes in the binding process ligands (small molecules, waters, ions or cofactors) get deformed or have unconventional roles due to major contributions from conformational or solvation entropies. Here, the factors governing the molecular association of protein with small molecules along with relevant concepts such as free energy, binding kinetics, enthalpy and entropy and the forces and factors that govern the protein–ligand interactions followed by the entropy–enthalpy compensation and its influence on binding affinity will be discussed in detail.

5.4.1 Protein–Ligand Interaction: Physico-chemical Mechanisms

To understand the binding of the protein–ligand complexes, it is important to understand that the physico-chemical mechanisms play an important role in the protein–ligand interactions. The basic thermodynamics concepts, binding kinetics, binding driving forces/factors, enthalpy–entropy compensation and relationships relevant to protein–ligand interactions are introduced and rationalised in the present section.

5.4.2 Protein–Ligand Binding Kinetics and Thermodynamics Relationships

The thermodynamics complex system is made up of the solute (i.e. protein–ligand complex) and the solvent (i.e. buffer ions and liquid water). With the complex formation, heat exchange occurs among these molecules governed by the laws of thermodynamics. The driving forces that orchestrate the interactions between the protein and ligands are results of a variety of interactions and the energy transfer among the protein, ligand, water and buffer ions.

Gibbs free energy is the most important thermodynamics quantity for characterising these driving forces. The capacity of a thermodynamic system is measured by the Gibbs free energy, to do utmost or reversible work at a constant pressure and temperature (isobaric, isothermal) (Gilson and Zhou 2007). In the spontaneous process, binding of the protein–ligand occurs when the changes in the Gibbs free energy ($\Delta G°$) are negative in an equilibrium state at constant temperature and pressure. It should be observed that the free energy is a function of the states of a system and ΔG is therefore defined by the initial and the final state of the system, regardless of the pathway connecting these two states (Du et al. 2016).

5.4.3 An Affinity of a Protein for a Ligand Is Characterised by the Dissociation Constant, K_D

A ligand binds to a protein non-covalently. The general binding equilibrium for the ligand interacting with any protein is represented as follows:

$$\text{Protein} + \text{Ligand} \rightleftharpoons \text{Protein.Ligand}$$
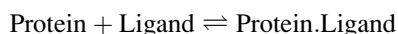
Protein–ligand represents the non-covalent complex. The equilibrium constant, K, for the reaction is shown as:

$$K_A = \frac{[\text{Protein.Ligand}]}{[\text{Protein}][\text{Ligand}]}$$

where K_A equilibrium constant is referred to as *association constant*. [Protein. Ligand] is the concentration of the protein in complex with the ligand, whilst [Ligand], [Protein] is the concentration of the free ligand and protein, respectively.

The *dissociation constant*, K_D, is the inverse of the association constant:

$$K_D = \frac{[\text{Protein}][\text{Ligand}]}{[\text{Protein.Ligand}]} \frac{1}{K_A}$$

The standard free energy (ΔG°) change upon complex formation is called the binding free energy of change, ΔG°_{bind}, and it is given by (Kuriyan et al. 2012):

$$\Delta G^o = -RT \ln K_A$$

$$\Delta G^o bind = -RT \ln K_A$$
$$\Delta G^o bind = +RT \ln K_D$$

where R is the universal gas constant with a value of 1.987 calK^{-1} mol^{-1} and T is the temperature in degrees Kelvin. ΔG consists of an enthalpy term (ΔH) and an entropy term (ΔS), related by another fundamental equation:

$$\Delta G = \Delta H - T\Delta S$$

The Gibbs free energy is dependent on temperature as represented by:

$$\Delta G(T) = \Delta H(T0) + \int_{T0}^{T} \Delta C_p dT - T\Delta S(T0) - \int_{T0}^{T} \Delta C_p d \ln T$$

where ΔC_p is the heat capacity change and $T0$ is an appropriate reference temperature. ΔC_p is independent of temperature in the range of interest as summarised below:

$$\Delta G(T) = \Delta H(T0) - T\Delta S(T0) + \Delta C_p \left[T - T0 - T \ln \frac{T}{T0} \right]$$

The enthalpy and entropy changes are dependent on temperature through the heat capacity change ΔC_p:

$$\Delta H(T) = \Delta H(T0) - \Delta C_p(T - T0)$$
$$\Delta S(T) = \Delta S(T0) - \Delta C_p \ln (T/T0)$$

The main objective of any thermodynamic analysis is to determine ΔG, ΔH, ΔS and their temperature dependence by using ΔC_p. These four parameters completely describe the energies governing molecular interactions (Perozzo et al. 2004).

5.4.4 Binding Driving Forces and Enthalpy–Entropy Compensation

To study novel ligand-binding modes and the key driving forces behind them, the absolute binding free energy has been calculated. Proteins bind with ligands, when binding free energy of the system is negative, whilst the magnitude of the difference in free energy between the bound and unbound state determines the stability of the complex. Reduction in the free energy of the system leads to the stability of the complex, i.e. protein–ligand binding and protein folding, although the folding and binding funnels as well as common driving forces used these two similar processes (Tsai et al. 1999a, b; Ma et al. 1999).

5.5 Structure of Protein–Ligand Complexes

Molecular recognition among various biological macromolecules is responsible for the functionality of any biological system. The molecular recognition employs collation/assembling of various biological macromolecules with each other through non-covalent interactions in order to form explicit complex/complexes. Various kinds of receptor–ligand interactions especially the protein–ligand interactions virtually form the basis of all the type of molecular recognition mediated within the biological system. All the protein–ligand interactions have two important components: proteins and ligands. Proteins serve as fundamental units of all living cells employed in all kind of structural, mechanical, biochemical and cell signalling functions. In order to mediate any cytoskeletal, muscular, enzymatic, hormonal function within the body, these proteins directly get associated with other proteins/peptides, nucleic acids, enzymes and even most importantly small-molecule ligands. A ligand can be termed as any small molecule that has the potential for protein binding with high specificity and affinity. The ligands associate with protein molecules by ionic bonds, hydrogen bonds, van der Waals interactions and hydrophobic effects. The complimentary binding site of protein provides a favourable site into which the ligand can fit properly to induce further cellular cascading. Further, the three-dimensional structures of protein–ligand complexes provide an in-depth understanding of protein–ligand interactions. These structures are exploited for structure-based drug designing of drugs used in various diseases (Seo et al. 2014).

5.5.1 Relationship Between Protein Conformations and Binding

Binding and dissociation between proteins and ligands are the two prime steps that mediate any ligand–protein interaction. The inherent conformational dynamics of proteins majorly influence ligand binding and dissociation (de Wolf and Brett 2000). Such conformational changes undergone by proteins include structural fluctuations, allosteric changes, domain motions within proteins, local folding–unfolding events, disorder-to-order transitions and many other changes within protein backbone and side chains. Several models have been recommended that

simplify the study of observed conformational changes. Some of the very prominent models include:

1. Lock-and-key model
2. The induced-fit model
3. The allosteric model
4. The protein trinity model
5. The conformational selection model
6. Population shift model

The average mobility analysis ratio of amino acids has revealed that some amino acids are highly fluctuating, some moderately fluctuating and some weak fluctuating (Sooriyaarachchi et al. 2010; Goh et al. 2004; Evenas et al. 2001). The classification of amino acids on basis of average mobility analysis is mentioned in table as follows:

S. no.	Amino acids	Mobility ratio	Types of fluctuation
1.	Gly, Ser, Ala, Asp, Pro	>1	Highly fluctuating
2.	Asn, Thr, Lys, Glu, Cys, Val, Gln, Arg	Between 0.7 and 1	Moderately fluctuating
3.	His, Met, Leu, Tyr, Ile, Phe, Trp	<0.7	Weakly fluctuating

Fascinatingly, the amino acids belonging to moderately and weakly fluctuating groups depict different degree of hydrophilicity. Group 2 majorly consists of polar/hydrophilic amino acid residues, whilst group 3 is mostly constituted by non-polar/hydrophobic residues. This difference in hydrophobic and hydrophilic nature is attributed to nonhomogeneous distribution of the amino acid residues within the proteins. Furthermore, polar residues primarily remain more exposed to water, whereas the non-polar residues tend to remain buried inside the protein in order to minimise the solvent-accessible surface area. In addition to this, any amino acid residue tend to experience greater fluctuation when exposed to surface rather than core because on the surface it has fewer nearest neighbours in comparison to core. The group 1 amino acids have a natural inclination to be part of protein loops rather than the standard secondary structure elements such as α-helices and β-strands. Apart from this, since the mobility of residue is directly proportional to the increase in temperature, hence it is assumed that nucleation event for unfolding of protein is commenced by highly fluctuating residues from the protein loop region. It is further proposed that substituting a highly fluctuating amino acid residue by a weakly fluctuating one can increase thermostability of protein. Group 1 residues have been recommended to contribute to local structure fluctuations in protein folding–unfolding event (Henzler-Wildman and Kern 2007; Boehr et al. 2009; Csermely et al. 2010; Kim et al. 2013).

5.5.2 Binding of Immunoglobulin and DNA-Binding Protein

The immunoglobulin domain (InterPro: IPR013783) consists of a beta-sheet structure with large connecting loops that recognises either DNA major grooves or antigens. This domain can be seen in Stat proteins of the cytokine pathway. The immunoglobulin domain contains a two-layered sandwich of 7–9 antiparallel β-strands arranged in two β-sheets with a Greek key topology, consisting of about 125 amino acids. The backbone constantly switches between the two β-sheets. Characteristically, the pattern is (N-terminal β-hairpin in sheet 1)-(β-hairpin in sheet 2)-(β-strand in sheet 1)-(C-terminal β-hairpin in sheet 2). The crossovers between sheets form an "X", so that the N- and C-terminal hairpins are juxtaposed to each other. These domains are frequently complicated in interactions, commonly with other Ig-like domains by means of their beta-sheets (Bork et al. 1994; Halaby et al. 1999; Potapov et al. 2004; Teichmann and Chothia 2000). There is overall structural similarity present in domains within this fold family despite the differences in their sequence. The classification of various Ig-like domains is based on their sequence characterising them in to V-set domains (antibody variable domain-like), C1-set domains (antibody constant domain-like), C2-set domains and I-set domains (antibody intermediate domain-like). For example, in the human T-cell receptor antigen CD2, domain 1 (D1) is a V-set domain, whilst domain 2 (D2) is a C2-set domain, both domains having the same Ig-like fold (Bodian et al. 1994).

Superfamily containing an Ig-like fold occurs in different types of proteins besides immunoglobulin molecules, for example, various T-cell antigen receptors, cell adhesion molecules, MHC class I and II antigens, as well as the haemolymph protein hemolin and the muscle proteins titin, telokin and twitchin.

5.5.3 Affinity and Specificity in Intermolecular Interactions

Biological function at the molecular level is realised by the interactions and recognition among biomolecules. The major factors governing the biomolecular recognition and binding process are the affinity that measures the stability of associating molecules, and another is the specificity of binding of one molecule to a specific binding partner (Wang amd Verkhivker 2003). The binding affinity describes the strength of interactions and can be experimentally measured by dissociation constant (K_d). K_d is a physico-chemical parameter that inspects the feasibility of interaction between molecules within a solution. The value of K_d is inversely proportional to binding affinity; thus, lower value of K_d depicts greater affinity between receptor and target proteins. Further, the binding affinity is subjective to non-covalent interactions such as hydrogen bonding, electrostatic interactions, hydrophobic bonding and van der Waals forces (Kastritis and Bonvin 2013). Some of the common methods to quantify binding affinity and dissociation constants *in vitro* are pull-down assays, gel shift assays, spectroscopic assays, equilibrium dialysis, isothermal titration calorimetry and analytical

ultracentrifugation. The most frequently used physico-chemical parameter to compute the binding affinity is the buried surface area (BSA). The drawback with BSA is that it cannot be employed to calculate binding affinity for flexible complexes; hence, entropic parameters are used for such complexes.

The binding of two proteins or a protein–ligand complex is a rapid reversible process and regulated by the law of mass action. For a specific receptor–ligand interaction, a receptor protein is fixed and present in limited amount, whilst the variable reaction component is termed as ligand protein. Certain assumptions are considered for a typical protein–ligand reaction:

1. All interactions are assumed to be reversible, and association reaction is considered to be bimolecular, whilst dissociation reaction is unimolecular.
2. Intramolecular interactions of the receptor protein are ruled out by keeping the receptor concentration fixed.
3. The interactions are computed at equilibrium.
4. The proteins and ligand are either in free or bound state with each other with no other chemical reactions between them.
5. The binding affinity (K_d) is directly proportional to the number of occupied receptor binding sites.

Considering all above conditions, a simple reversible reaction for a given receptor–ligand can be tabulated as follows:

$$A + B \rightleftharpoons AB,$$
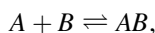
In detail it can be represented as:

$$[A] + [B] \underset{k_{off}}{\overset{k_{on}}{\rightleftharpoons}} [AB],$$
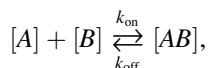
where

[A] and [B]: concentrations of the free reactants (protein and ligand)
[AB]: concentration of their bound complex (product)
k_{on}: the association rate constant and calculated in $M^{-1}\,s^{-1}$
k_{off}: the dissociation rate constant

At equilibrium K_d can be defined as follows:

$$K_d = \frac{[A][B]}{AB} = \frac{k_{off}}{k_{on}}.$$

Conventionally, high affinity has been used as the criterion for the stability and virtual screening of drug targets in the pharmaceutical industry. However, high affinity fails to always guarantee high specificity (Wlodawer and Erickson 1993), yet high specificity is crucial for molecular recognition and practice of drug design.

The conventional way of defining specificity is the capability of discrimination of a specific ligand against different receptors. To prove the specificity of a ligand to a receptor, one has to search all the related receptors. This is not always practical. For a specific ligand binding with different receptors, we are probing interactions between the ligand and different receptors through the change of sequences of the receptors (Wang and Verkhivker 2003; Liu et al. 2007). The process of a specific ligand binding with a specific receptor involves different intermediate binding modes exhibiting different structures with binding energies and different sets of contact interactions between the ligand and the receptor. By exploring different structures of various binding modes, the binding probes different interactions between the ligand and the receptor. If the receptor is large and there are sufficient number of contact interactions between the ligand and the receptor, probing interactions through different structures and sequences should be statistically equivalent (because exploring different binding structures mean exploring different spatial contacts and different contacts explore different sequences). The specificity can be explored by looking at the different intermediate binding modes between a ligand and a receptor, which is much easier to carry out, rather than looking at the whole universe of the receptors to test the specificity of a ligand, which is essentially impractical (Liu et al. 2009).

References

Bader GD, Betel D, Hogue CW (2003) BIND: the Biomolecular interaction network database. Nucleic Acids Res 31(1):248–250

Bak G et al (2015) Electrophoretic mobility shift assay of RNA-RNA complexes. Methods Mol Biol 1240:153–163

Barlow DJ, Thornton JM (1986) The distribution of charged groups in proteins. Biopolymers 25(9):1717–1733

Berman HM, Westbrook J, Feng Z, Gilliland G, Bhat TN, Weissig H, Shindyalov IN, Bourne PE (2000) The Protein Data Bank. Nucl Acids Res 28:235–242. doi:10.1093/nar/28.1.235

Berman HM et al (2003) The nucleic acid database. Methods Biochem Anal 44:199–216

Bodian DL et al (1994) Crystal structure of the extracellular region of the human cell adhesion molecule CD2 at 2.5 A resolution. Structure 2(8):755–766

Boehr DD, Nussinov R, Wright PE (2009) The role of dynamic conformational ensembles in biomolecular recognition. Nat Chem Biol 5(11):789–796

Bork P, Holm L, Sander C (1994) The immunoglobulin fold. Structural classification, sequence patterns and common core. J Mol Biol 242(4):309–320

Changeux J-P (2013) 50 years of allosteric interactions: the twists and turns of the models. Nat Rev Mol Cell Biol 14(12):819–829

Coimbatore Narayanan B et al (2014) The nucleic acid database: new features and capabilities. Nucleic Acids Res 42(Database issue):D114–D122

Contreras-Moreira B (2010) 3D-footprint: a database for the structural analysis of protein-DNA complexes. Nucleic Acids Res 38(Database issue):D91–D97

Csermely P, Palotai R, Nussinov R (2010) Induced fit, conformational selection and independent dynamic segments: an extended view of binding events. Trends Biochem Sci 35(10):539–546

de Wolf FA, Brett GM (2000) Ligand-binding proteins: their potential for application in systems for controlled delivery and uptake of ligands. Pharmacol Rev 52(2):207–236

Du X et al (2016) Insights into protein-ligand interactions: mechanisms, models, and methods. Int J Mol Sci **17**(2)

Evenas J et al (2001) Ligand-induced structural changes to maltodextrin-binding protein as studied by solution NMR spectroscopy. J Mol Biol 309(4):961–974

Fersht AR (1984) Basis of biological specificity. Trends Biochem Sci 9(4):145–147

Fersht AR (1987) The hydrogen bond in molecular recognition. Trends Biochem Sci 12:301–304

Gade P, Kalvakolanu DV (2012) Chromatin immunoprecipitation assay as a tool for analyzing transcription factor activity. Methods Mol Biol 809:85–104

Gilson MK, Zhou HX (2007) Calculation of protein-ligand binding affinities. Annu Rev Biophys Biomol Struct 36:21–42

Goh CS, Milburn D, Gerstein M (2004) Conformational changes associated with protein-protein interactions. Curr Opin Struct Biol 14(1):104–109

Halaby DM, Poupon A, Mornon J (1999) The immunoglobulin fold family: sequence analysis and 3D structure comparisons. Protein Eng 12(7):563–571

Hellman LM, Fried MG (2007) Electrophoretic mobility shift assay (EMSA) for detecting protein-nucleic acid interactions. Nat Protoc 2(8):1849–1861

Henzler-Wildman K, Kern D (2007) Dynamic personalities of proteins. Nature 450(7172):964–972

Ito T et al (2001) A comprehensive two-hybrid analysis to explore the yeast protein interactome. Proc Natl Acad Sci U S A 98(8):4569–4574

Kastritis PL, Bonvin AM (2013) On the binding affinity of macromolecular interactions: daring to ask why proteins interact. J R Soc Interface 10(79):20120835

Kim R, Guo JT (2009) PDA: an automatic and comprehensive analysis program for protein-DNA complex structures. BMC Genomics 10(Suppl 1):S13

Kim E et al (2013) A single-molecule dissection of ligand binding to a protein with intrinsic dynamics. Nat Chem Biol 9(5):313–318

Kuriyan J, Konforti B, Wemmer D (2012) The molecules of life: physical and chemical principles. Garland Science, New York

Lee S, Blundell TL (2009) BIPA: a database for protein-nucleic acid interaction in 3D structures. Bioinformatics 25(12):1559–1560

Lewis BA et al (2011) PRIDB: a protein-RNA interface database. Nucleic Acids Res 39(Database issue):D277–D282

Liu Z et al (2007) Molecular analysis of thymopentin binding to HLA-DR molecules. PLoS One 2(12):e1348

Liu Z et al (2009) Affinity and specificity of levamlodipine-human serum albumin interactions: insights into its carrier function. Biophys J 96(10):3917–3925

Ma B et al (1999) Folding funnels and binding mechanisms. Protein Eng 12(9):713–720

Marin-Bejar O, Huarte M (2015) RNA pulldown protocol for in vitro detection and identification of RNA-associated proteins. Methods Mol Biol 1206:87–95

Meyer M, Wilson P, Schomburg D (1996) Hydrogen bonding and molecular surface shape complementarity as a basis for protein docking. J Mol Biol 264(1):199–210

Norambuena T, Melo F (2010) The protein-DNA Interface database. BMC Bioinform 11:262

Ofran Y, Rost B (2003) Analysing six types of protein-protein interfaces. J Mol Biol 325(2):377–387

Perini LT et al (1996) Multiple specific CytR binding sites at the Escherichia coli deoP2 promoter mediate both cooperative and competitive interactions between CytR and cAMP receptor protein. J Biol Chem 271(52):33242–33255

Perozzo R, Folkers G, Scapozza L (2004) Thermodynamics of protein-ligand interactions: history, presence, and future aspects. J Recept Signal Transduct Res 24(1–2):1–52

Phizicky EM, Fields S (1995) Protein-protein interactions: methods for detection and analysis. Microbiol Rev 59(1):94–123

Potapov V et al (2004) Protein–protein recognition: juxtaposition of domain and interface cores in immunoglobulins and other sandwich-like proteins. J Mol Biol 342(2):665–679

Prabakaran P et al (2001) Thermodynamic database for protein-nucleic acid interactions (ProNIT). Bioinformatics 17(11):1027–1034

Riegel K (1989) When pediatric intensive care medicine becomes intensive. Padiatr Padol 24(3):181–187

Salamone JC (1998) Concise polymeric materials encyclopedia. *CRC press*. Am J Obstet Gynecol 1

Sanders CR (2010) Biomolecular ligand-receptor binding studies: theory, practice, and analysis

Seo MH et al (2014) Protein conformational dynamics dictate the binding affinity for a ligand. Nat Commun 5:3724

Sooriyaarachchi S et al (2010) Conformational changes and ligand recognition of Escherichia coli D-xylose binding protein revealed. J Mol Biol 402(4):657–668

Szklarczyk D et al (2017) The STRING database in 2017: quality-controlled protein-protein association networks, made broadly accessible. Nucleic Acids Res 45(D1):D362–D368

Teichmann SA, Chothia C (2000) Immunoglobulin superfamily proteins in Caenorhabditis elegans. J Mol Biol 296(5):1367–1383

Tsai CJ et al (1999a) Folding funnels, binding funnels, and protein function. Protein Sci 8(6):1181–1190

Tsai CJ, Ma B, Nussinov R (1999b) Folding and binding cascades: shifts in energy landscapes. Proc Natl Acad Sci U S A 96(18):9970–9972

Wang J, Verkhivker GM (2003) Energy landscape theory, funnels, specificity, and optimal criterion of biomolecular binding. Phys Rev Lett 90(18):188101

Wlodawer A, Erickson JW (1993) Structure-based inhibitors of HIV-1 protease. Annu Rev Biochem 62:543–585

Xenarios I et al (2000) DIP: the database of interacting proteins. Nucleic Acids Res 28(1):289–291

Xu D, Tsai CJ, Nussinov R (1997) Hydrogen bonds and salt bridges across protein-protein interfaces. Protein Eng 10(9):999–1012

Zhang A (2009) Protein interaction networks: computational analysis. Cambridge University Press, Cambridge, p 280

Zhang D et al (2015) Two disparate ligand-binding sites in the human P2Y1 receptor. Nature 520(7547):317–321

Lipid and Membrane Structures

6

Charul Sharma, Priya Vrat Arya, and Sohini Singh

Abstract

Lipids are small hydrophobic or amphipathic molecules that may entirely or in part originate by carbanion-based condensations of thioesters and/or by carbocation-based condensations of isoprene units. Further lipids are classified along with prominent examples. The concept of lipids, their molecular shape, macromolecular assembly and packing or shape parameter—surface area, hydrophobic volume and tail length is explained. Kinetically frozen micelles, inverted micelles, and supermicelles along with bilayers—has been explained. This explanation is supported by key features of formation and application aspect as well. Liposomes, vesicles, and GUV have been explained in detail along with related application in the different sectors. The aspect of visualization of various structures using typical visualization tools has been considered. The main focus revolves around X-ray, NMR, and microscopy both confocal and electron microscopy. A section on molecular dynamic simulations, to discuss about computational approach in better understanding, is also considered. The membrane phases, their transitions, and relative curvatures have been dealt in detail. The final section involves study of the role of membrane lipids in cellular process and human health. The aspect of immunotherapy and prospects in the future are also incorporated in the end.

C. Sharma (✉)
I. P. College, Bulandshahar, Uttar Pradesh, India
e-mail: drcharulsharma@gmail.com

P.V. Arya
Dyal Singh College, Delhi University, New Delhi, India
e-mail: aryapv@rediffmail.com

S. Singh
Amity University, Sector-125, Gautam Buddha Nagar, Noida 201313, Uttar Pradesh, India
e-mail: ssingh14@amity.edu

6.1 Lipid: Major Structural Classification

Lipids can be defined as naturally occurring greasy or oily organic biological molecules which generally are hydrophobic in nature (sparingly soluble in water) and usually dissolve in organic solvents like chloroform, ether, and benzene. They constitute a heterogeneous group of compounds encompassing fatty acids and include fats, oils, waxes, phospholipids, etc. Many more definitions are possible and probable for these compounds as the group is a very large and diverse one both in terms of structure and function, and yet many more definitions again are possible when their biosynthetic perspective is taken into consideration. Scientists have also included compounds that are related closely to fatty acid derivatives through biosynthetic pathways or by their biochemical or functional properties. So fatty acids and other compounds harboring similar biochemical and functional characteristics, which may or may not be derived via identical biosynthetic pathways, can be termed as lipids (http://www.lipidlibrary.co.uk). Due to this structural, functional, and biosynthetic diversity of lipids, many kinds of classifications based on various characteristics have been propounded and used over centuries, each system having its own pros and cons. Some systems classified lipids into two groups "simple" (those yielding two or less types of products on hydrolysis) and "complex" (those yielding three or more products on hydrolysis), while some others divided the group into three entities; this scheme of three types of lipids catered until quite recently and is still in use for the conventional classification. LIPID MAPS consortium provided a new insight into their structure and functionality and provided for a new systematic nomenclature for lipids in 2004 (Fahy et al. 2005). Under this new nomenclature, lipids are divided into eight major clear-cut categories, encompassing lipids from all living sources, i.e., eukaryotic, prokaryotic, archaeaic, and synthetic lipids as well. The classification given by the consortium categorizes lipids on the basis of their chemically functional backbone into polyketides, acylglycerols, sphingolipids, prenols, and saccharolipids, but a new category of fatty acyls was carved out from polyketides, the glycerophospholipids from the glycerolipids, and sterol lipids from prenols attributing to historical reasons and their bioinformatic advantages, thereby resulting in the formation of eight primary categories in total, rather than, the initial five. This scheme of classification is quite flexible and permits further subdivision of the major categories into classes and subclasses to accommodate all the present and newly discovered arrays of lipid structures. The structural, functional, and biosynthetic complexity of lipids make it almost impossible, for any classification scheme to group the lipids into clear water tight compartments, but then some kind of a demarcation is indispensable for the orderly arrangement of lipids into groups,

Table 6.1 List of general categories of lipids

Code	Category	Abbreviations	Example
01	Fatty acyls	FA	Dodecanoic acid
02	Glycerolipids	GL	1-hexadecanoyl-2-(9Z-octadecenoyl)-sn-glycerol
03	Glycerophospholipids	GP	1-hexadecanoyl-2-(9Z-octadecenoyl)-sn-glycero-3-phosphocholine
04	Sphingolipids	SP	N-(tetradecanoyl)-sphing-4-enine
05	Sterol lipids	ST	Cholest-5-en-3β-ol
06	Prenol lipids	PR	2E,6E-farnesol
07	Saccharolipids	SL	UDP-3-O-(3R-hydroxy-tetradecanoyl)-αD-N-acetylglucosamine
08	Polyketides	PK	Aflatoxin B_1

which is essential for their study, research, and lately for the development of new methodology for systematic data management. This new classification considered and discussed here is based on the chemical properties and mainly gains from the distinct hydrophobic and hydrophilic elements that are essential constituents of the lipids. Lipidomics is a system level analysis that involves complete characterization and profiling of the molecular structure of any lipid species and the biological part they play in any living entity vis-a-vis the expression of proteins involved in their metabolism and function (Wenk 2005). In lipidomics, levels and dynamic changes of lipids and lipid-derived mediators in cells or subcellular compartments are identified and measured quantitatively in the form of lipid profiles which can be further analyzed to yield biological insights.

The lipid categories proposed in this new system (Table 6.1 and Fig. 6.1) have names that were already in use and had been documented. The fatty acyls (FA) are a large group of molecules, heterogeneous in their structure and nature, which are synthesized by chain elongation of an acetyl-CoA primer adding on to malonyl-CoA (or methylmalonyl-CoA) groups comprising a cyclic functionality and/or are substituted with heteroatoms. This group is divided into two definite categories: the glycerolipids (GL), including acylglycerols and alkyl and 1Z-alkenyl variants, and the glycerophospholipids (GP), containing a phosphate (or phosphonate) group esterified to one of the glycerol hydroxyl groups. Though the sterol lipids (ST) and prenol lipids (PR) are quite different in their structure and function, both of them are formed by the polymerization of dimethylallyl pyrophosphate or isopentenyl pyrophosphate in a similar manner by the same biosynthetic pathway in all living organisms. Another category of is the sphingolipids (SP), with their core structure comprising of long-chain bases. One more category of this class is the "saccharolipids" (SL) in which the fatty acyl groups of the lipids are directly linked to the sugar backbone. The last category of the class is that of polyketides (PK), containing all metabolites of plant and microbes (Fahy et al. 2005).

(a) Fatty Acyls : hexadecanoic acid

(b) Glycerolipids : 1-hexadecanoyl-2-(9z-octadecenoyl)-*sn*-glycerol

(c) Glycerophospholipids : 1-hexadecanoyl-2-(9z-octadecenoyl)-*sn*-glycero-3-phosphocholine
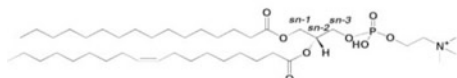
(d) Sphingolipds : N-(tetradecanoyl)-sphing-4-enine

(e) Sterol Lipids : cholest-5-en-3β-ol
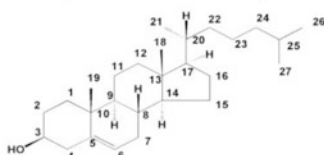
(f) Prenol Lipids : 2E, 6E-farnesol
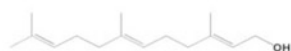
(g) Saccharolipids: UDP-3-O-(3R-hydroxy-tetradecanoyl)-αD-N-acetylglucosamine
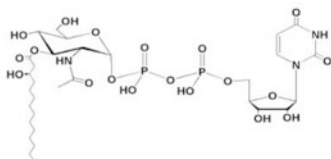
(h) Poluketides : aflatoxin B1

Fig. 6.1 Representative structures of lipid categories

6.1.1 Fatty Acyls (FA)

This basic term encompasses all fatty acids and their derivatives; this category of lipids shows considerable diversity. The synthesis of these acyls takes place by the addition of malonyl, or methylmalonyl-CoA groups, having cyclic functionality (which may be substituted by heteroatoms) to the basic acetyl-CoA primer. The

Table 6.2 Fatty acyl classes and subclasses

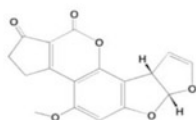| Designated ID Nos.	Fatty acyl classes and subclasses	Designated ID No.s	Fatty acyl classes and subclasses
FA01	**Fatty acids and conjugates**	FA0307	Hydroxyeicosapentaenoic acids
FA0101	Straight-chain fatty acids	FA0308	Epoxyeicosatrienoic acids
FA0102	Methyl-branched fatty acids	FA0309	Hepoxilins
FA0103	Unsaturated fatty acids	FA0310	Levuglandins
FA0104	Hydroperoxy fatty acids	FA0311	Isoprostanes
FA0105	Hydroxy fatty acids	FA0312	Clavulones
FA0106	Oxo fatty acids	**FA04**	**Docosanoids**
FA0107	Epoxy fatty acids	**FA05**	**Fatty alcohols**
FA0108	Methoxy fatty acids	**FA06**	**Fatty aldehydes**
FA0109	Halogenated fatty acids	**FA07**	**Fatty esters**
FA0110	Amino fatty acids	FA0701	Wax monoesters
FA0111	Cyano fatty acids	FA0702	Wax diesters
FA0112	Nitro fatty acids	FA0703	Cyano esters
FA0113	Thia fatty acids	FA0704	Lactones
FA0114	Carbocyclic fatty acids	FA0705	Fatty acyl-CoAs
FA0115	Heterocyclic fatty acids	FA0706	Fatty acyl-acyl carrier proteins (ACPs)
FA0116	Mycolic acids	FA0707	Fatty acyl carnitines
FA0117	Dicarboxylic acids	FA0708	Fatty acyl adenylates
FA02	**Octadecanoids**	**FA08**	**Fatty amides**
FA0201	12-Oxophytodienoic acid metabolites	FA0801	Primary amides
FA0202	Jasmonic acids	FA0802	*N*-acyl amides
FA03	**Eicosanoids**	FA0803	Fatty acyl homoserine lactones
FA0301	Prostaglandins	FA0804	*N*-acyl ethanolamides (endocannabinoids)
FA0302	Leukotrienes	**FA09**	**Fatty nitriles**
FA0303	Thromboxanes	**FA10**	**Fatty ethers**
FA0304	Lipoxins	**FA11**	**Hydrocarbons**
FA0305	Hydroxyeicosatrienoic acids	**FA12**	**Oxygenated hydrocarbons**
FA0306	Hydroxyeicosatetraenoic acids	**FA00**	**Other**

parent carbon chain constituting the FA's can be saturated or unsaturated and can be attached to functional groups or substituents containing oxygen, halogens, nitrogen, and sulfur. The fatty acyls are grouped into 13 classes (Table 6.2 and Fig. 6.2). The first class of the fatty acyls is the fatty acids and conjugates. A carboxylic acid with a long aliphatic saturated or unsaturated chain is called a fatty acid. Fatty acids occurring in nature are usually derived from triglycerides or phosphorous lipids and

(a) Straight chain fatty acid : hexadecanoic acid

(b) Methyl branched fatty acids: 17-methyl-6Z-octadecenoic acid
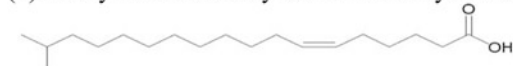
(c) Unsaturated fatty acids : 9Z-octadecenoic acid

(d) Hydroxy fatty acids : 2S-hydroxy-tetradecanoic acid

(e) Oxo fatty acids : 2-oxo-decanoic acid

(f) Epoxy fatty acids : 6R, 7S-epoxy-octadecanoic acid
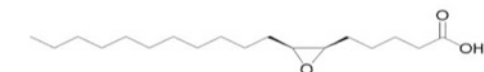
(g) Methoxy fatty acids: 2-methoxy-5Z-hexadecenoic acid

(h) Thia fatty acids : R-Lipoc acid: 1, 2-dithiolane-3R-pentanoic acid
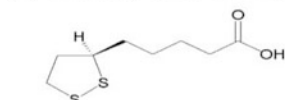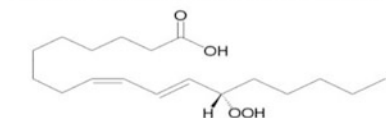
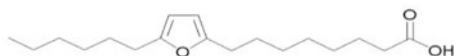(i) Hydroxy fatty acids : 13S-hydroperoxy-9Z, 11E-octadecadienoic acid

(j) Carbocyclic fatty acids : lactobacillic acid; 11R, 12S-methylene-octadecanoic acid

Fig. 6.2 Representative structures for fatty acyls

(k) Heterocyclic fatty acids : 8-(5-hexyl-furan-2-yl)-octanoic acid

(l) Amino fatty acids : 2S-amino-tridecanoic acid
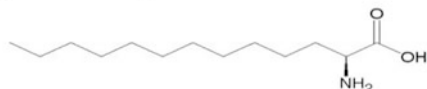
(m) Nitro fatty acids : 10-nitro, 9Z, 12Z-octadecadienoic acid

(n) Halogenated fatty acids : 3-bromo-2Z-heptenoic acid
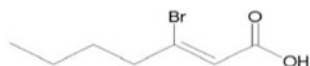
(o) Dicarboxylic acids : 1, 8-octanedioic acid
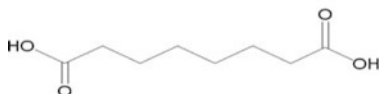
Fig. 6.2 (continued)

possess an unbranched chain of even number of carbon atoms ranging from 4 to 28. Naturally occurring fatty acids are important dietary sources as they release large quantities of fatty acids. These are further subdivided into 17 subclasses. The first subclass is the straight-chain saturated fatty acids and the last one the carboxylic acids. The components of this group are long-chain unbranched, branched, or cyclic fatty acids, which may be saturated or unsaturated with one, two, or more or double or triple bonds. Other than the chain types, various subclasses also differ from each other in their association with the heteroatoms (noncarbon atoms replacing carbon on the main chain of any organic compound) which may be oxygen, halogen, nitrogen, and sulfur. The longest straight chain in any branched-chain fatty acids is the main or parent chain and defines the chain length of that compound. Similarities, variations, and anomalies of this basic structure can be seen in nature all through the living world. Cyclic fatty acids with rings containing oxygen or nitrogen and carbon atoms ranging from three to six are also found in nature. *Octadecanoids* form the second class of the class fatty acyls; these are complex unbranched, polyunsaturated C18 fatty acids and skeletally related compounds, with multiple functional groups. These are divided into two subclasses and form important parts of the various pathways of plant hormone biosynthesis (Agrawal et al. 2004). The third subclass consists of *eicosanoids* which are polyunsaturated C20 fatty acids derived from arachidonic acid. These compounds include

prostaglandins, leukotrienes, thromboxanes, and other structural derivatives which make up 12 subclasses in all (Murphy and Smith 2002). These act as local hormones and play a role in inflammation, fever promotion, blood clotting, immune response, and some respiratory and reproductive processes. The *docosanoids* are oxygenated derivatives of C_{22} polyunsaturated fatty acids, such as docosapentaenoic acid (DPA) and docosahexaenoic acid (DHA). These are signaling molecules and also act as multifunctional regulators of neural cell integrity. The *fatty alcohols* with terminal hydroxy group and *fatty aldehydes* with their oxo group are another two subclasses of the fatty acyls, which play an important role in membrane attachment. N-fatty acylated amines, unsubstituted amides, and many other simple amides constitute another subclass of the fatty acyls, which is the *fatty amides*; these amides are responsible for essential biological activities in various living organisms. Other lipid classes in the fatty acyl category include *fatty acid esters, amides nitriles*, and *ethers*. Fatty esters also include the following categories of compounds which are fatty acyl thioester-CoA derivatives, fatty acyl thioester-acyl carrier protein (ACP) derivatives, fatty acyl carnitines (esters of carnitine), and fatty adenylates (mixed anhydrides); all of them are important biochemical intermediates playing essential roles in living systems. *Hydrocarbons* and *oxygenated hydrocarbons* form the last two subclasses of the fatty acyls on the virtue of their close similarity to six electron reduction products of fatty acids.

6.1.2 Glycerolipids (GL)

This category consists of all lipids which contain glycerols. But the phosphoglycerolipids were removed from this category and made into a new category of their own owing to their diversity, abundance, and functionality in the living systems. The lipids of the class possess a common glycerol backbone attached to at least one fatty acid-derived group. The class is divided into (Table 6.3 and Fig. 6.3) *monoradylglycerols*, *diradylglycerols*, *triradylglycerols*, and *other glycerolipids*, thus comprising of four subclasses. Mono-, di-, and trisubstituted glycerols constitute the largest part of this category, of which their fatty acid esters, acylglycerols, are the most abundant. Another subclass of the class is the glycerolglycans (glycosylmonoradylglycerols and glycosyldiradylglycerols) which contain the characteristic of glycosidic bonds where one or more sugar residues may be attached to the glycerol (Pahlsson, et al. 1998). Glycerolipids participate in the glycerolipids/free fatty acid β (GL/FFA) cycle, which plays a significant role in regulating several physiological processes including thermogenesis, insulin secretion, appetite control, and aging.

6.1.3 Glycerophospholipids (GP)

These compounds comprise of any glycerolipid containing a phosphate group ester-linked to the terminal carbon of glycerol backbone. All derivatives of

Table 6.3 Glycerolipids classes and subclasses

Designated ID Nos.	Glycerolipid classes and subclasses
GL01	**Monoradylglycerols**
GL0101	Monoacylglycerols
GL0102	Monoalkylglycerols
GL0103	Mono-(1Z-alkenyl)-glycerols
GL0104	Monoacylglycerolglycosides
GL0105	Monoalkylglycerolglycosides
GL02	**Diradylglycerols**
GL0201	Diacylglycerols
GL0202	Alkylacylglycerols
GL0203	Dialkylglycerols
GL0204	1Z-alkenylacylglycerols
GL0205	Diacylglycerolglycosides
GL0206	Alkylacylglycerolglycosides
GL0207	Dialkylglycerolglycosides
GL0208	Di-glycerol tetraethers
GL0209	Di-glycerol tetraether glycans
GL03	**Triradylglycerols**
GL0301	Triacylglycerols
GL0302	Alkyldiacylglycerols
GL0303	Dialkylmonoacylglycerols
GL0304	1Z-alkenyldiacylglycerols
GL0305	Estolides
GL00	Other

glycerophosphoric acid with at least one O-acyl, O-alkyl, or O-alk-1′-enyl residue attached to the glycerol moiety are grouped under this class. These organic compounds are also known as phospholipids. The glycerophospholipids are further subdivided into classes (Table 6.4 and Fig. 6.4), on the basis of the nature of their polar head group. Glycerophosphoglycerols and glycerophosphoglycerophosphates possess a second glycerol unit comprising a part of the head group, whereas a pseudosymmetrical molecule is created in the case of glycerophosphoglycerophosphoglycerols (cardiolipins) by the addition of a third glycerol unit, acylated at the sn-1′ and sn-2′ (sn denotes stereospecific numbering) positions. The head groups of the class are further characterized by the sn-1 and sn-2 substituents present on the glycerol backbone. The addition of a second carbon to the symmetrical glycerol backbone renders it asymmetric, and they thus act like a chiral "head group," *viz*., the addition of second carbon at the sn-3 position, in eukaryotes and eubacteria and on the sn-1 position in archaebacteria (Pereto et al. 2004). Chirality may also be induced when sn-1 and sn-3 carbons are substituted by different substituents. Usually, one or both of these hydroxyl groups present on the head are acylated with long-chain fatty acids. The category is divided into 20 classes and even more subclasses. The phospholipids form an integral part of the biological membranes, act as reservoir for lipid mediators which act as signal transductors and modulators of gene expressions, and also play a role in inflammatory reactions (Table 6.4 and Fig. 6.4).

(a) Monoradylglycerols : Monoacylglycerols : 1-dodecanoyl-*sn*-glycerol

(b) Diradylglycerols : Diacylglycerols: 1-hexadecanoyl-2-(9z-octadecenoyl)-*sn*-glycerol

(c) Diradylglycerols : Alkylacylglycerols: 1-O-hexadecyl-2-(9z-octadecenoyl)-*sn*-glycerol

(d) Diradylglycerols : 1Z-alkenylacylglycerols: 1-O-(1Z-tetradecenyl)-2-(9Z-octadecenoyl)-*sn*-glycerol

(e) Triadylglycerols: Triglycerols: 1-dodecanoyl-2-hexadecanoyl-3-octadecanoyl-*sn*-glycerol

(f) Diradylglycerols: Diradylglycerols glycans: 1,2 di-(9Z, 12Z, 15Z-octadecatrienoyl)-3-O-β-D-galactosyl-*sn*-glycerol

(g) Diradylglycerols:Di-glycerol tetraethers:caldarchaeol
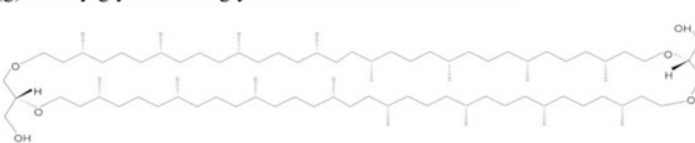
(h) Diradylglycerols: Di-glycerol tetraether glycans: gentiobiosyl-caldarchaeol:Glcβ1-6Glcβ-caldarchaeol

Fig. 6.3 Representative structures for glycerolipids

6.1.4 Sphingolipids (SP)

All compounds derived from the lipid sphingosine possessing a long hydrocarbon tail with a polar domain containing an amino group are called sphingolipids. This family of compounds is a complex one, with a common sphingoid base backbone

Table 6.4 Glycerophospholipid classes and subclasses

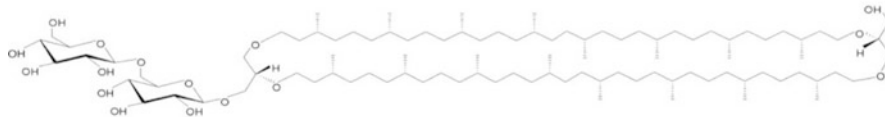| Designated ID Nos.	Glycerophospholipid classes and subclasses	Designated ID Nos.	Glycerophospholipid classes and subclasses
GP01	**Glycerophosphocholines**	GP0903	1Z-alkenyl,2-acylglycerophosphoinositol trisphosphates
GP0101	Diacylglycerophosphocholines	GP0904	Monoacylglycerophosphoinositol trisphosphates
GP0102	1-alkyl,2-acylglycerophosphocholines	GP0905	1-alkyl glycerophosphoinositol trisphosphates
GP0103	1Z-alkenyl,2-acylglycerophosphocholines	GP0906	1Z-alkenylglycerophosphoinositol trisphosphates
GP0104	Dialkylglycerophosphocholines	**GP10**	**Glycerophosphates**
GP0105	Monoacylglycerophosphocholines	GP1001	Diacylglycerophosphates
GP0106	1-alkyl glycerophosphocholines	GP1002	1-alkyl,2-acylglycerophosphates
GP0107	1Z-alkenylglycerophosphocholines	GP1003	1Z-alkenyl,2-acylglycerophosphates
GP02	**Glycerophosphoethanolamines**	GP1004	Dialkylglycerophosphates
GP0201	Diacylglycerophosphoethanolamines	GP1005	Monoacylglycerophosphates
GP0202	1-alkyl,2-acylglycerophosphoethanolamines	GP1006	1-alkyl glycerophosphates
GP0203	1Z-alkenyl,2-acylglycerophosphoethanolamines	GP1007	1Z-alkenylglycerophosphates
GP0204	Dialkylglycerophosphoethanolamines	**GP11**	**Glyceropyrophosphates**
GP0205	Monoacylglycerophosphoethanolamines	GP1101	Diacylglyceropyrophosphates
GP0206	1-alkyl glycerophosphoethanolamines	GP1102	Monoacylglyceropyrophosphates
GP0207	1Z-alkenylglycerophosphoethanolamines	**GP12**	**Glycerophosphoglycerophosphoglycerols (cardiolipins)**
GP03	**Glycerophosphoserines**	GP1201	Diacylglycerophosphoglycerophosphodiradylglycerols
GP0301	Diacylglycerophosphoserines	GP1202	Diacylglycerophosphoglycerophosphomonoradylglycerols
GP0302	1-alkyl,2-acylglycerophosphoserines	GP1203	1-alkyl,2-acylglycerophosphoglycerophosphodiradylglycerols
GP0303	1Z-alkenyl,2-acylglycerophosphoserines	GP1204	1-alkyl,2-acylglycerophosphoglycerophosphomonoradylglycerols
GP0304	Dialkylglycerophosphoserines	GP1205	1Z-alkenyl,2-acylglycerophosphoglycerophosphodiradylglycerols
GP0305	Monoacylglycerophosphoserines	GP1206	1Z-alkenyl,2-acylglycerophosphoglycerophosphomonoradylglycerols

(continued)

Table 6.4 (continued)

Designated ID Nos.	Glycerophospholipid classes and subclasses	Designated ID Nos.	Glycerophospholipid classes and subclasses
GP0306	1-alkyl glycerophosphoserines	GP1207	Monoacylglycerophosphoglycerophosphomonoradylglycerols
GP0307	1Z-alkenylglycerophosphoserines	GP1208	1-alkyl glycerophosphoglycerophosphodiradylglycerols
GP04	**Glycerophosphoglycerols**	GP1209	1-alkyl glycerophosphoglycerophosphomonoradylglycerols
GP0401	Diacylglycerophosphoglycerols	GP1210	1Z-alkenylglycerophosphoglycerophosphodiradylglycerols
GP0402	1-alkyl,2-acylglycerophosphoglycerols	GP1211	1Z-alkenylglycerophosphoglycerophosphomonoradylglycerols
GP0403	1Z-alkenyl,2-acylglycerophosphoglycerols	**GP13**	**CDP-glycerols**
GP0404	Dialkylglycerophosphoglycerols	GP1301	CDP-diacylglycerols
GP0405	Monoacylglycerophosphoglycerols	GP1302	CDP-1-alkyl,2-acylglycerols
GP0406	1-alkyl glycerophosphoglycerols	GP1303	CDP-1Z-alkenyl,2-acylglycerols
GP0407	1Z-alkenylglycerophosphoglycerols	GP1304	CDP-dialkylglycerols
GP0408	Diacylglycerophosphodiradylglycerols	GP1305	CDP-monoacylglycerols
GP0409	Diacylglycerophosphomonoradylglycerols	GP1306	CDP-1-alkyl glycerols
GP0410	Monoacylglycerophosphomonoradylglycerols	GP1307	CDP-1Z-alkenylglycerols
GP05	**Glycerophosphoglycerophosphates**	**GP14**	**Glycerophosphoglucose lipids**
GP0501	Diacylglycerophosphoglycerophosphates	GP1401	Diacylglycerophosphoglucose lipids
GP0502	1-alkyl,2-acylglycerophosphoglycerophosphates	GP1402	1-alkyl,2-acylglycerophosphoglucose lipids
GP0503	1Z-alkenyl,2-acylglycerophosphoglycerophosphates	GP1403	1Z-alkenyl,2-acylglycerophosphoglucose lipids
GP0504	Dialkylglycerophosphoglycerophosphates	GP1404	Monoacylglycerophosphoglucose lipids
GP0505	Monoacylglycerophosphoglycerophosphates	GP1405	1-alkyl glycerophosphoglucose lipids
GP0506	1-alkyl glycerophosphoglycerophosphates	GP1406	1Z-alkenylglycerophosphoglucose lipids
GP0507	1Z-alkenylglycerophosphoglycerophosphates	**GP15**	**Glycerophosphoinositolglycans**
GP06	**Glycerophosphoinositols**	GP1501	Diacylglycerophosphoinositolglycans

| ID	Name	ID	Name
GP0601	Diacylglycerophosphoinositols	GP1502	1-alkyl,2-acylglycerophosphoinositolglycans
GP0602	1-alkyl,2-acylglycerophosphoinositols	GP1503	1Z-alkenyl,2-acylglycerophosphoinositolglycans
GP0603	1Z-alkenyl,2-acylglycerophosphoinositols	GP1504	Monoacylglycerophosphoinositolglycans
GP0604	Dialkylglycerophosphoinositols	GP1505	1-alkyl glycerophosphoinositolglycans
GP0605	Monoacylglycerophosphoinositols	GP1506	1Z-alkenylglycerophosphoinositolglycans
GP0606	1-alkyl glycerophosphoinositols	**GP16**	**Glycerophosphonocholines**
GP0607	1Z-alkenylglycerophosphoinositols	GP1601	Diacylglycerophosphonocholines
GP07	**Glycerophosphoinositol monophosphates**	GP1602	1-alkyl,2-acylglycerophosphonocholines
GP0701	Diacylglycerophosphoinositol monophosphates	GP1603	1Z-alkenyl,2-acylglycerophosphonocholines
GP0702	1-alkyl,2-acylglycerophosphoinositol monophosphates	GP1604	Dialkylglycerophosphonocholines
GP0703	1Z-alkenyl,2-acylglycerophosphoinositol monophosphates	GP1605	Monoacylglycerophosphonocholines
GP0704	Dialkylglycerophosphoinositol monophosphates	GP1606	1-alkyl glycerophosphonocholines
GP0705	Monoacylglycerophosphoinositol monophosphates	GP1607	1Z-alkenylglycerophosphonocholines
GP0706	1-alkyl glycerophosphoinositol monophosphates	**GP17**	**Glycerophosphonoethanolamines**
GP0707	1Z-alkenylglycerophosphoinositol monophosphates	GP1701	Diacylglycerophosphonoethanolamines
GP08	**Glycerophosphoinositol bisphosphates**	GP1702	1-alkyl,2-acylglycerophosphonoethanolamines
GP0801	Diacylglycerophosphoinositol bisphosphates	GP1703	1Z-alkenyl,2-acylglycerophosphonoethanolamines
GP0802	1-alkyl,2-acylglycerophosphoinositol bisphosphates	GP1704	Dialkylglycerophosphonoethanolamines
GP0803	1Z-alkenyl,2-acylglycerophosphoinositol bisphosphates	GP1705	Monoacylglycerophosphonoethanolamines
GP0804	Monoacylglycerophosphoinositol bisphosphates	GP1706	1-alkyl glycerophosphonoethanolamines

(continued)

Table 6.4 (continued)

Designated ID Nos.	Glycerophospholipid classes and subclasses	Designated ID Nos.	Glycerophospholipid classes and subclasses
GP0805	1-alkyl glycerophosphoinositol bisphosphates	GP1707	1Z-alkenylglycerophosphonoethanolamines
GP0806	1Z-alkenylglycerophosphoinositol bisphosphates	**GP18**	**Di-glycerol tetraether phospholipids (caldarchaeols)**
GP09	**Glycerophosphoinositol trisphosphates**	**GP19**	**Glycerol-nonitol tetraether phospholipids**
GP0901	Diacylglycerophosphoinositol trisphosphates	**GP20**	**Oxidized glycerophospholipids**
GP0902	1-alkyl,2-acylglycerophosphoinositol trisphosphates	**GP00**	**Other**

(a) Diacylglycerophosphocholines: 1-hexadecanoyl-2-(9Z-octadecenoyl)-sn-glycero-3-phosphocholine
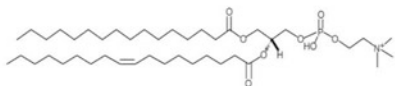
(b) Diacylglycerophosphonocholines: 1-hexadecanoyl-2-(9Z-octadecenoyl)-sn-glycero-3-phosphocholine
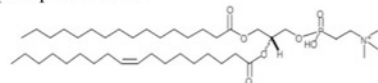
(c) Diacylglycerophosphoethanolamines: 1-hexadecanoyl-2-(9Z-octadecenoyl)-sn-glycero-3-phosphoethanolamine
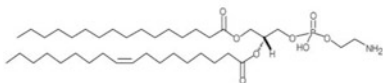
(d) Diacylglycerophosphoethanolamines : 1-hexadecanoyl-2-(9Z-octadecenoyl)-sn-glycero-3-phosphonoethanolamine
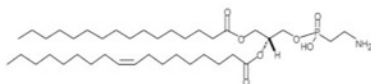
(e) Diacylglycerophosphoserines : 1-hexadecanoyl-2-(9Z-octadecenoyl)-sn-glycero-3-phosphoserine

(f) Diacylglycerophosphoglycerols : 1-hexadecanoyl-2-(9Z-octadecenoyl)-sn-glycero-3-phospho-(1'-sn-glycerol)
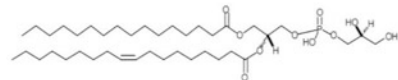
(g) Diacylglycerophosphoglycerophosphates : 1-hexadecanoyl-2-(9Z-octadecenoyl)-sn-glycero-3-phospho-(1'-sn-glycerol-3'-phosphate)
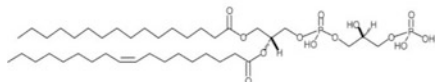
(h) Diacylglycerophosphoinositols : 1-hexadecanoyl-2-(9Z-octadecenoyl)-sn-glycero-3-phospho-(1'-myo-inositol);

(i) Diacylglycerophosphoinositolmonophosphates : 1-hexadecanoyl-2-(9Z-octadecenoyl)-sn-glycero-3-phospho-(1'-myo-inositol-3'-phosphate)

Fig. 6.4 Representative structures of glycerophospholipids
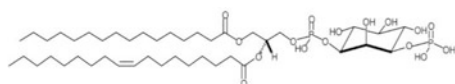
(j) Diacylglycerophosphates (phosphatidic acids): 1-hexadecanoyl-2-(9Z-octadecenoyl)-*sn*-glycero-3-phosphate

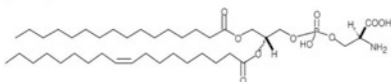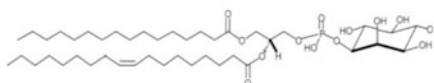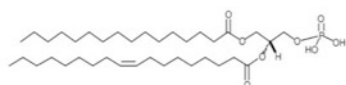(k) Diacylglyceropyrophosphates:1-hexadecanoyl-2-(9Z-octadecenoyl)-*sn*-glycero-3-pyrophosphate
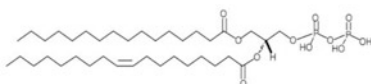
(l) CDP-diacylglycerols:1-hexadecanoyl-2-(9Z-octadecenoyl)-*sn*-glycero-3-cytidine-5'-diphosphate
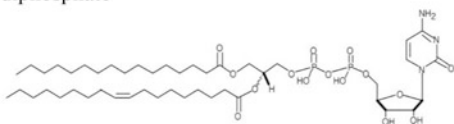
Fig. 6.4 (continued)

which is synthesized de novo from serine and a long-chain fatty acyl-CoA. This common backbone is then converted into other categories by subtle changes in the head group (Taniguchi et al. 2002) resulting in the formation of ceramides, phosphosphingolipids, glycosphingolipids, and other species, including protein adducts. This class comprises of ten major classes (Table 6.5 and Fig. 6.5) which are sphingoid bases and their simple derivatives (sphingoid base 1-phosphates), the bases with an amide-linked fatty acid (ceramides), complex sphingolipids with head groups attached with phosphodiester linkages (the phosphosphingolipids), or with glycosidic bonds (cerebrosides and gangliosides), and other groups (such as phosphono- and arseno-sphingolipids). The systematic nomenclature for sphingolipids has been recommended by IUPAC (IUPAC-IUB Commission on Biochemical Nomenclature (CBN)). Sphingolipids function as mechanical and chemical protectors of the cell membrane. They also play an essential part in cell recognition and signaling. They are also involved in pathways leading to apoptosis, proliferation, stress response, necrosis, inflammation, autophagy, differentiation, and senescence.

6.1.5 Sterol Lipids (ST)

All the steroids are derived from the same structure, which is a fused four-ring core, and they are further categorized into seven classes based (1) on the number of

Table 6.5 Sphingolipid classes and subclasses

Designated ID Nos.	Glycerophospholipid classes and subclasses
SP01	**Sphingoid bases**
SP0101	Sphing-4-enines (sphingosines)
SP0102	Sphinganines
SP0103	4-Hydroxysphinganines (phytosphingosines)
SP0104	Sphingoid base homologs and variants
SP0105	Sphingoid base 1-phosphates
SP0106	Lysosphingomyelins and lysoglycosphingolipids
SP0107	*N*-methylated sphingoid bases
SP0108	Sphingoid base analogs
SP02	**Ceramides**
SP0201	*N*-Acylsphingosines (ceramides)
SP0202	*N*-Acylsphinganines (dihydroceramides)
SP0203	*N*-acyl-4-hydroxysphinganines (phytoceramides)
SP0204	Acylceramides
SP0205	Ceramide 1-phosphates
SP03	**Phosphosphingolipids**
SP0301	Ceramide phosphocholines (sphingomyelins)
SP0302	Ceramide phosphoethanolamines
SP0303	Ceramide phosphoinositols
SP04	**Phosphonosphingolipids**
SP05	**Neutral glycosphingolipids**
SP0501	Simple Glc series (GlcCer, LacCer, etc.)
SP0502	GalNAcβ1-3Galα1-4Galβ1-4Glc- (globo series)
SP0503	GalNAcβ1-4Galβ1-4Glc- (ganglio series)
SP0504	Galβ1-3GlcNAcβ1-3Galβ1-4Glc- (lacto series)
SP0505	Galβ1 − 4GlcNAcβ1-3Galβ1-4Glc- (neolacto series)
SP0506	GalNAcβ1-3Galα1-3Galβ1-4Glc- (isoglobo series)
SP0507	GlcNAcβ1-2Manα1-3Manβ1-4Glc- (mollu series)
SP0508	GalNAcβ1-4GlcNAcβ1-3Manβ1-4Glc- (arthro series)
SP0509	Gal- (gala series)
SP0510	Other
SP06	**Acidic glycosphingolipids**
SP0601	Gangliosides
SP0602	Sulfoglycosphingolipids (sulfatides)
SP0603	Glucuronosphingolipids
SP0604	Phosphoglycosphingolipids
SP0600	Other
SP07	**Basic glycosphingolipids**
SP08	**Amphoteric glycosphingolipids**
SP09	**Arsenosphingolipids**
SP00	Other

(a) Sphinganines:sphinganine
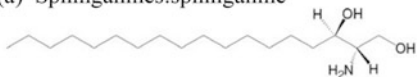
(b) Sphingosines:sphing-4-enine
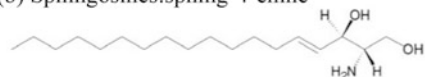
(c) Phytosphinganines: 4-hydroxysphinganine

(d) Sphingoid base homologs and variants: hexadecasphinganine

(e) N-mehtylated sphingoid bases: N,N-dimethylsphing-4-enine

(f) Spingoid base 1-phosphate: sphing-4-enine-1-phosphate

(g) N-acylsphingosine (ceramides): N-(tetradecanoyl)-sphing-4-enine

(h) Ceramide phosphocholines (sphingomyelins): N-(octadedcanoyl)-sphing-4-enine-1-phosphocholine

(i) Acylceramides: N-(30-(9Z,12Z-octadecadienoyloxy)-tricontanoyl)-sphing-4-enine
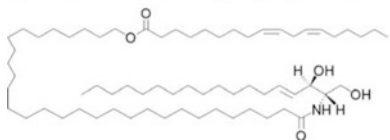
(j) Phosphosphingolipids: N-(tetradecanoyl)-sphing-4-enine-1-(2-aminoethylphosphonate)
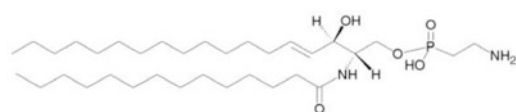
Fig. 6.5 Representative structures of sphingolipids

Table 6.6 Sterol lipid classes and subclasses

Designated ID Nos.	Sterol lipid classes and subclasses
ST01	**Sterols**
ST0101	Cholesterol and derivatives
ST0102	Cholesteryl esters
ST0103	Phytosterols and derivatives
ST0104	Marine sterols and derivatives
ST0105	Fungal sterols and derivatives
ST02	**Steroids**
ST0201	C_{18} steroids (estrogens) and derivatives
ST0202	C_{19} steroids (androgens) and derivatives
ST0203	C_{21} steroids (gluco/mineralocorticoids, progestogins) and derivatives
ST03	**Secosteroids**
ST0301	Vitamin D_2 and derivatives
ST0302	Vitamin D_3 and derivatives
ST04	**Bile acids and derivatives**
ST0401	C_{24} bile acids, alcohols, and derivatives
ST0402	C_{26} bile acids, alcohols, and derivatives
ST0403	C_{27} bile acids, alcohols, and derivatives
ST0404	C_{28} bile acids, alcohols, and derivatives
ST05	**Steroid conjugates**
ST0501	Glucuronides
ST0502	Sulfates
ST0503	Glycine conjugates
ST0504	Taurine conjugates
ST06	**Hopanoids**
ST00	**Other**

carbons in the core skeleton and (2) on their biological function. The classes are sterols, steroids, secosteroids, bile acids and derivatives, steroid conjugates, hopanoids, and others. The sterols, especially cholesterol and its derivatives, are the most commonly studied in the mammalian system (Bach and Wachtel 2003). Different subclasses have been allotted to the sterols from plant, fungal, and marine sources. The estrogen family forms a part of C18 steroids, whereas androgens like testosterone and androsterone constitute the C19 steroids. The C21 containing subclass, which contains a two-carbon side chain at the C17 position, comprises of the progestogens, glucocorticoids, and mineralocorticoids. The secosteroids, showing the characteristic B ring cleavage of the core structure, include various forms of vitamin D (Jones et al. 1998). Sterols play an important role in the physiology of eukaryotes; they are a part of membrane lipids thus play a role in membrane fluidity and cell signaling. They are also hormones and fat soluble vitamins and perform the of their respective classes (Table 6.6 and Fig 6.6).

(a) Cholesterol and derivatives: cholesterol; cholest-5-en-3**β**-ol
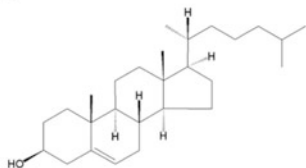
(b) Cholesterol esters: cholest-5-en-3**β**-ol dodecanoate
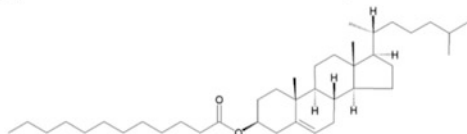
(c) C_{18} steroids (esterogens) and derivatives: β-estradiol; 1,3,5 [10]-estratriene-3, 17β-diol
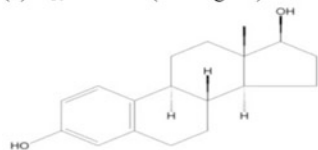
(d) C_{19} steroids (androgens) and derivatives: androsterone; 3α-hydroxy-5α-androstan-17-one
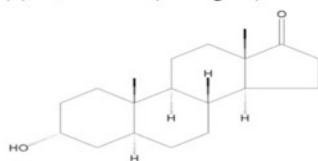
(e) C_{21} steroids and derivatives: cortisol; 11β, 17α, 21-trihydroxypregn-4-ene-3,20-dione
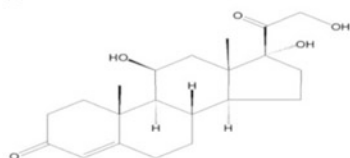
(f) Secosteroids: Vitamin D_2 and derivatives: vitamin D_2; (5Z, 7E, 22E)-(3S)-9, 10-seco-5,7,10 (19), 22-ergostatetraen-3-ol
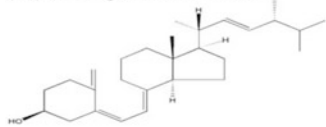
(g) Secosteroids: Vitamin D_3 and derivatives: vitamin D_3; (5Z,7E)-(3S)-9,10-seco-5,7,10(19)-cholestatrien-3-ol
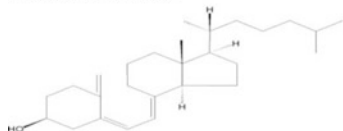
Fig. 6.6 Representative structures of sphingolipids

6.1.6 Prenol Lipids (PR)

These constitute alcohols represented by the general formula $H-(CH_2C$ $(Me) = CHCH_2)_nOH$. Their carbon backbone is made up of one or more isoprene units, synthesized via the mevalonic acid pathway, from the two five-carbon precursors, i.e., isopentenyl diphosphate and dimethylallyl diphosphate (Kuzuyama and Seto 2003), but in some bacteria (e.g., *Escherichia coli*) and a few plants, the formation of the isoprenoid precursors takes place through the methylerythritol phosphate pathway (Rodriguez-Concepcion 2004). The simple isoprenoids are synthesized by the addition of number of C5 units to the existing units. This number of the terpene units in an isoprenoid chain forms the basis of the classification of these simple isoprenoids (linear alcohols, diphosphates, etc.) (Table 6.7 and Fig. 6.7). All isoprenoids with 5 to 40 units are classified as different isoprenoids, and those with more than 40 isoprenoid subunits are grouped under polyterpene subclass (Porter and Spurgeon 1981). Vitamin A, its derivatives, phytanic acid, and pristanic acid (oxidation product of phytanic acid) are examples of C20 isoprenoids. Carotenoids are also essential simple isoprenoids which work as antioxidants and are precursors of vitamin A. The second class of the group is *quinones* and

Table 6.7 Prenol lipid classes and subclasses

Designated ID Nos.	Prenol lipid classes and subclasses
PR01	**Isoprenoids**
PR0101	C_5 isoprenoids
PR0102	C_{10} isoprenoids (monoterpenes)
PR0103	C_{15} isoprenoids (sesquiterpenes)
PR0104	C_{20} isoprenoids (diterpenes)
PR0105	C_{25} isoprenoids (sesterterpenes)
PR0106	C_{30} isoprenoids (triterpenes)
PR0107	C_{40} isoprenoids (tetraterpenes)
PR0108	Polyterpenes
PR02	**Quinones and hydroquinones**
PR0201	Ubiquinones
PR0202	Vitamin E
PR0203	Vitamin K
PR03	**Polyprenols**
PR0301	Bactoprenols
PR0302	Bactoprenol monophosphates
PR0303	Bactoprenol diphosphates
PR0304	Phytoprenols
PR0305	Phytoprenol monophosphates
PR0306	Phytoprenol diphosphates
PR0307	Dolichols
PR0308	Dolichol monophosphates
PR0309	Dolichol diphosphates
PR00	**Other**

(a) C_5 isoprenoids:dimethylallyl pyrophosphate; 3-methylbut-2-enyl pyrophosphate
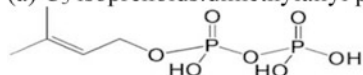
(b) C_{10} isoprenoids: 2E-geraniol
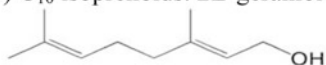
(c) C_{15} isoprenoids: 2E, 6E-farnesol
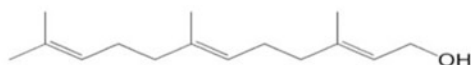
(d) C_{20} isoprenoids: retinol; vitamin A
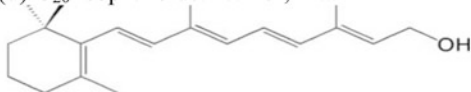
(e) C_{25} isoprenoids: manoalide
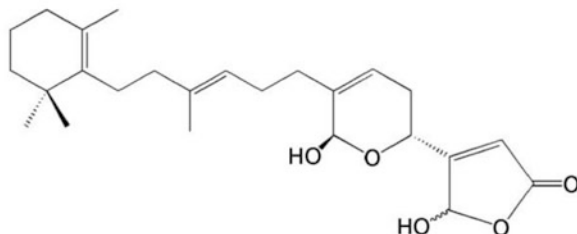
(f) C_{30} isoprenoids: 3S-squalene-2, 3-epoxide
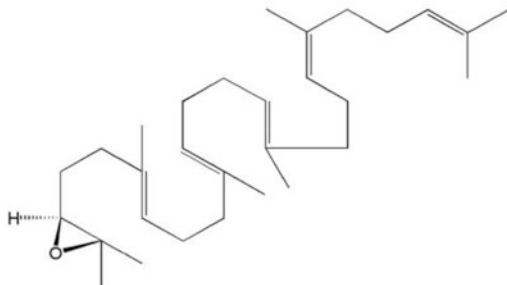
(g) C_{40} isoprenoids: β-carotene
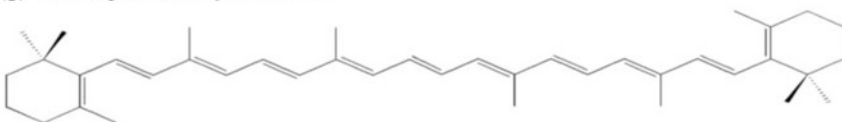
Fig. 6.7 Representative structures of prenol lipids

hydroquinones, having an isoprenoid tail attached to a quinonoid core of a nonisoprenoid origin (Ricciarelli et al. 2001). Vitamins E and K and ubiquinones belong to this class of the prenol lipids (Meganathan 2001a, b). Polyprenols and their phosphorylated derivatives belong to class polyprenols. They play an important role in oligosaccharide transport across biomembranes. Polyprenol phosphate sugars and polyprenol diphosphate sugars both belonging to different subclasses are extremely important for extracytoplasmic glycosylation reactions (Raetz and Whitfield 2002), extracellular polysaccharide biosynthesis (Lazar and Walker 2002), and eukaryotic protein N-glycosylation (Schenk 2001). This class is divided into subclasses on the basis of their biosynthesis and function. In bacterial polyprenols (bactoprenols), the terminal isoprenoid unit is unsaturated and is typically 10 to 12 units long (Meganathan 2001a, b). The animal polyprenols (dolichols) have a reduced terminal isoprenoid and usually consist of 18 to 22 isoprene units. The plant phytoprenols have three reduced distal units.

6.1.7 Saccharolipids (SL)

Saccharolipids are compounds of lipids where the fatty acids are directly linked to a sugar backbone, i.e., the glycerol backbone, present in glycero- and glycerophospholipids, is substituted by a sugar moiety, usually a monosacchride (Table 6.8 and Fig. 6.8). They may be present as glycans or as their phosphorylated derivatives. The most commonly found saccharolipids are the acylated glucosamine precursors of the lipid A, which is a constituent of the lipopolysaccharides in Gram-negative bacteria (Raetz and Whitfield 2002). Typical lipid A molecules are disaccharides of glucosamine, (Zähringer et al. 1999). The glucosamine backbone of lipid A is replaced by 2,3-diamino-2,3-dideoxyglucose, ("acylaminosugars") in the case of some bacteria (Sweet et al. 2004). This class further consists of Nod factors present in a few nitrogen-fixing bacteria, which are oligosaccharides of glucosamine derivatives possessing a single fatty acyl chain. Fatty-acylated

Table 6.8 Sacchrolipid classes and subclasses

Designated ID Nos.	Sacchrolipid classes and subclasses
SL01	**Acylaminosugars**
SL0101	Monoacylaminosugars
SL0102	Diacylaminosugars
SL0103	Triacylaminosugars
SL0104	Tetraacylaminosugars
SL0105	Pentaacylaminosugars
SL0106	Hexaacylaminosugars
SL0107	Heptaacylaminosugars
SL02	**Acylaminosugar glycans**
SL03	**Acyltrehaloses**
SL04	**Acyltrehalose glycans**
SL00	**Other**

(a) Acylaminosugars : Monoacylaminosugars: UDP-3-O-(3R-hydroxy-tetradecanoyl)-GlcN
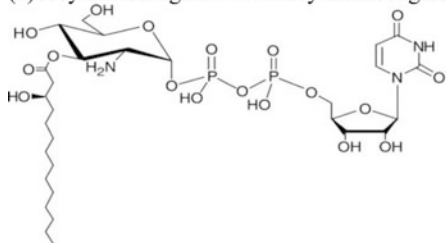
(b) Acylaminosugars : Diacylaminosugars: lipid X
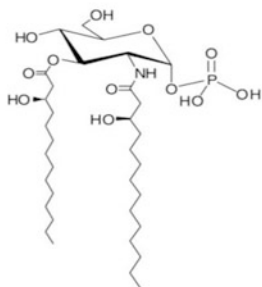
(c) Acylaminosugars : Tetraacylaminosugars: lipid IV_A
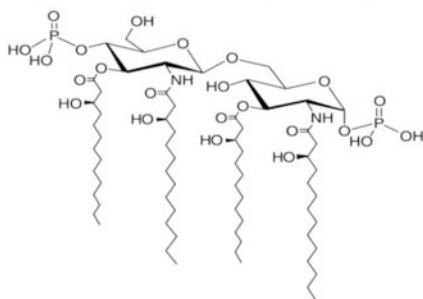
(d) Acylaminosugars glycans : Kdo_2lipid A
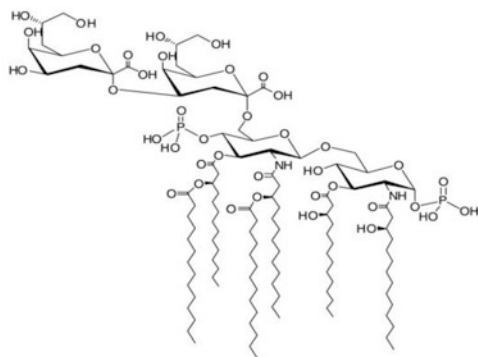
Fig. 6.8 Representative structures of sacchrolipids

derivatives of glucose (acylated trehalose units of some mycobacterial lipids) belong to the class acyltrehaloses. Many plants are known to possess acylated forms of glucose and sucrose.

6.1.8   Polyketides (PK)

Polyketides are natural metabolites that comprise the basic chemical structure of various anticancer, antifungal, anticholesteremic agents, antibiotics, parasiticides, and immunomodulators. They can be either synthesized by classic enzymes or by iterative and multimodular enzymes with semiautonomous active sites, which are similar to fatty acid synthases in their working mechanism and also in their involvement with the specialized acyl carrier proteins (Walsh 2004; Khosla et al. 1999).

Polyketide backbones undergo further modifications, via processes like glycosylation, methylation, hydroxylation, and oxidation, for various functional reactions. A few of the polyketides form hybrid scaffolds by forming linkages with nonribosomally synthesized peptides.

Many commonly used antimicrobial, antiparasitic, and anticancer agents are either polyketides or their derivatives; a few examples of the kind are drugs like erythromycins, tetracyclines, nystatins, avermectins, and antitumor epothilones.

Some polyketides may be potent toxins (Reeves 2003). The polyketides are divided into three classes (Table 6.9 and Fig. 6.9): (1) *Macrolides* consist of a large macrocyclic lactone ring to which one or more deoxy sugars are attached. The lactone rings usually contain 14, 15, or 16 members. They have antifungal and antibiotic activity. Some examples are azithromycin, clarithromycin, and erythromycin. (2) *Aromatic polyketides* basically possess polycyclic aromatic structures and are mostly present in bacteria, fungi, and plants. Most of them exhibit important biological activities and are imperative clinical agents. *Nonribosomal peptides (NRP)* are cyclic and/or branched chain containing peptide secondary metabolites, usually having cyclic and/or branched chain structures and are usually synthesized by microorganisms like bacteria and fungi. These may contain non-proteinogenic amino acids such as D-amino acids in their structures or may be modified and carry post-translational modifications like N-methyl and N-formyl groups or become glycosylated, acylated, halogenated, or hydroxylated. They are synthesized by *nonribosomal peptide synthetases*. Some important examples of the subclass are actinomycin, bacitracin, daptomycin, and vancomycin Table 6.10.

Table 6.9 Polyketide classes

Designated ID Nos.	Polyketide classes
PK01	Macrolide polyketides
PK02	Aromatic polyketides
PK03	Nonribosomal peptide/polyketide hybrids
PK00	Other

Fig. 6.9 Representative
structures of polyketides

(a). Macrolide polyketides : 6-deoxyyerythronolide B
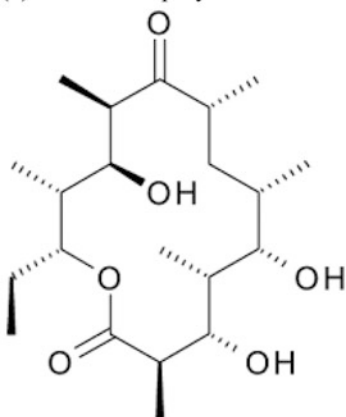
(b). Aromatic polyketides : griseorhodin A
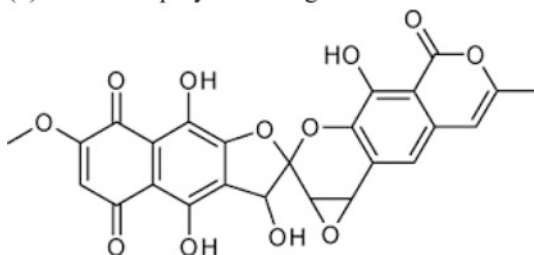
(c). Polyketide hubrids : epothilone D
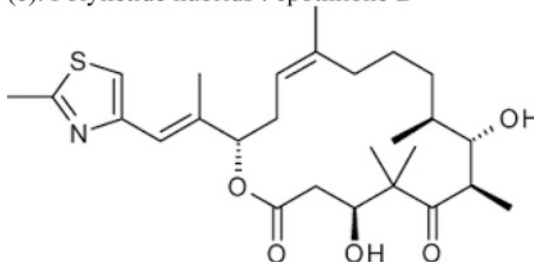
6.2 Lipids: Molecular Shape and Macromolecular Assemblies

Lipids exhibit large number of conformations and shapes. These three-dimensional conformations are attributed to a large number of associated factors in the surroundings. Lipids are amphipathic structures consisting of a polar head which is hydrophilic and a nonpolar hydrophobic tail region (Fig. 6.10).

Table 6.10 Summary of lipids and their location and key features

Sl	Lipids	Location	Key features/functions
A	Phospholipids	Membranes	Derivatives of **phosphatidic acid**
			The phosphate is esterified with the −OH of a suitable alcohol
			Important as an intermediate in the synthesis of triacylglycerols and phosphoglycerols
			Found only in small quantity in tissues
1	Phosphatidylcholines (lecithins)	Cell membranes (more abundant in the outer leaf of plasma membrane)	Most abundant phospholipid
			Cylindrical shape of molecules
			Can quickly organize into bilayers
			Stabilize the surface of lipid droplets in tissues where **triacylglycerols** are stored
			Choline is important in nervous transmission, as acetylcholine, and as a store of labile methyl groups
			Surface active agent and a major constituent of the **surfactant** preventing adherence, of the inner surfaces of the lungs
			Biosynthetic precursor of **sphingomyelin,** phosphatidic acid, lysophosphatidylcholine and **platelet-activating factor**, and **phosphatidylserine**
2	Phosphatidylethanolamine (cephalin) and phosphatidylserine	Most tissues (highest amount in myelin in brain tissue)	Less than 10% of the total phospholipids
			Component of cellular membranes
			Precursor of other phospholipids
			Essential cofactor of a large number of signalling proteins
			Blood coagulation
			Regulation of apoptosis

Table 6.10 (continued)

Sl	Lipids	Location	Key features/functions
3	Phosphatidylinositol	Membrane	Membrane trafficking
			Cell signalling and regulation
			Precursor of second messengers
4	Cardiolipin	Mitochondrial membranes	Integral component of mitochondrial complex III, IV and the ADP-ATP-carrier
			Essential for the stability of the quaternary protein of the ADP-ATP-carrier
			Part of mitochondrial creatine kinase and nucleoside diphosphate kinase
			Causes apoptosis in animal cells via death-inducing proteins
			Important cofactor for cholesterol translocation from the outer to the inner mitochondrial membrane
5	Lysophospholipids	Intermediates in phosphoglycerol metabolism	Phosphoacylglycerols containing only one acyl radical, e.g., **lysophosphatidylcholine (lysolecithin)**
			Important in the metabolism and interconversion of phospholipids
			Also found in oxidized lipoproteins
			Thought to promote **atherosclerosis**
6	Plasmalogens	Brain and muscle membranes	Plasmalogen-containing cell protect membranes are less fluid
			Store of polyunsaturated fatty acids
			May act as intracellular signalling compounds
			Membranes against oxidative stress
			Role in spermatogenesis and fertilization

Table 6.10 (continued)

Sl	Lipids	Location	Key features/functions
7	Sphingomyelins	Cells of brain and nervous system. Most abundant in plasma membrane and Golgi apparatus	Major source of the **ceramides**
			Substitute for phosphatidylcholine as a building block of membranes
			Form stable and chemically resistant outer leaflet of the plasma membrane lipid bilayer
			May control the distribution of cholesterol in cells
			Can be transported through the cytosol
			Promote raft formation
			Essential for the internalization of transferring signals
			Needed for the activity of a number of membrane-bound proteins
			Essential for chromatin assembly and dynamics integral component of the nuclear matrix
B.	Glycolipids (Glycosphingolipids)	In the cell membrane most abundant in nerve tissues	Major glycans of the vertebrate brain
			Not uniformly distributed but cluster as "lipid rafts,"
			Mediate cell-cell interactions via trans recognition, modulate activities of proteins in the same plasma membrane via cis regulation
			Essential for myelin-axon interactions
			Responsible for the epidermal permeability barrier
C.	Steroids (mostly cholesterol and its derivatives)	Membrane	Maintains the consistency of the cell membrane by preventing the membrane from becoming too fluid or too firm
			Stabilizes many membrane proteins in lipid rafts

Table 6.10 (continued)

Sl	Lipids	Location	Key features/functions
D.	Amphipathic lipids	Membrane Self-orient at oil-water interfaces. Forming membranes, micelles, liposomes, and emulsions	A bilayer of amphipathic lipids with the polar group in the water phase and the nonpolar group in the oil phase is the basic structure in biologic membranes
			Aggregations facilitate absorption of lipids from the intestine
			Carriers of drugs in the circulation, targeted to specific organs, e.g., in cancer therapy
			Gene transfer into vascular cells
			Carriers for topical and transdermal delivery of drugs and cosmetics

Fig. 6.10 Basic structure of lipids
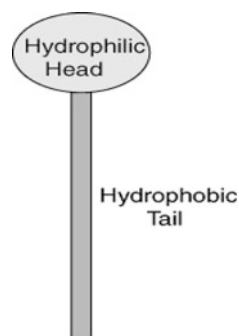
6.2.1 Packing or Shape Parameters: Surface Area, Hydrophobic Volume, and Tail Length

Biomembranes are essentially semipermeable. They may be impermeable to most of the polar or charged solutes but remain permeable to nonpolar compounds. Their thickness varies from 5 to 8 nm and appears trilaminar when viewed using an electron microscope. Phospholipids form a bilayer, wherein the nonpolar regions (hydrophobic tails) are directed toward the core of the bilayer and the hydrophilic head is present on the surface interacting with the aqueous phases.

Proteins get embedded in this lipid bilayer sheet and are held in place, by hydrophobic interactions, formed between the membrane lipids and hydrophobic domains present in the proteins. The orientation of proteins in the bilayer is asymmetrical providing essential "sidedness" to the two sides of the membrane.

Functional asymmetry is provided by the distinct protein domains present on each side of the bilayer. Thus, lipid and protein units in a membrane form a fluid mosaic pattern that, as its name suggests, is free to change continuously. The membrane fluidity is maintained because of the noncovalent interactions permitting the free lateral movement of lipid and protein molecules in the plane of the membrane. Longer fatty acid chains have higher surface areas than smaller ones, resulting in stronger Van der Waals interactions between long lipid chains. This leads to increasing Tm's with increasing chain length. In aqueous solutions, the hydrophilic "heads" of surfactant molecules, either as monomers or as part of a micelle, always remain in contact with water, whereas their lipophilic "tails" have less accessibility to water as constituent of a micelle. The molecular self-assembly in surfactant solutions can be predicted with the help of the micelle packing parameter equation $\{v_o/(a_e \times l_o)$ where v_o is the surfactant tail volume, l_o is the tail length, and a_e is the equilibrium area per molecule at the aggregate surface.

6.2.2 Micelles

It is a molecular assembly formed when the individual components achieve a thermodynamic equilibrium with monomers of the same species in the surrounding medium. It can also be defined as an aggregate (or supramolecular assembly) of surfactant molecules dispersed in a liquid colloid with the hydrophilic "head" regions in contact with the surrounding solvent, pushing the hydrophobic tail regions toward the center. It is brought about by the packing behavior of single-tail lipids present in the bilayer forming a normal-phase micelle (oil-in-water micelle). Inverse micelles are the exact opposites and have the hydrophilic head groups at the center with the hydrophobic tails extending out (water-in-oil micelle). They are mostly spheroid in shape, but other shapes, like ellipsoidal, cylindrical, and bilayers, are also possible, pertaining to other phases. The shape and size of a micelle are dictated by its molecular geometry and governed by the surfactant molecules and solution conditions, namely, concentration, temperature, pH, and ionic strength. Micelles are formed only when the surfactant concentration is greater than the critical micelle concentration (CMC), and the system temperature is greater than the critical micelle temperature, or Krafft temperature. The process of formation micelles is known as micellization. Free surfactant molecules in the system that are not part of a micelle are referred to as "monomers." The driving force for micelle formation in water is the hydrophobic effect, irrespective of the unfavorable thermodynamic parameters of enthalpy and entropy for surfactant assembly.

Micelle formation is necessary for absorption of fat-soluble vitamins and lipids in the alimentary canal. Bile salts bind with lipids and help in the formation of micelles and facilitating lipid (e.g., lecithin) and lipid-soluble vitamins (A, D, E, and K) absorption in the small intestine. In the stomach, proteases act on κ-casein (the soluble portion in caseins) resulting in the formation of an unstable micellar state, thereby causing the curdling of milk. Micelles find application in targeted drug delivery systems in case of gold nanoparticles and the like.

6.2.3   Inverted Micelles

These as their name suggests are totally opposite to the micelles in their structure with polar head groups directed toward the core and the hydrophobic tails pushed farther away from the center. Since hydrophilic sequestration creates highly unfavorable electrostatic interactions, the possibility of inverse micelles formation is quite low with increase in the charge of the head group.

6.2.4   Supermicelles

It is a supramolecular assembly of individual micelles also referred to as a hierarchical micelle and is formed by the self-assembly of long cylindrical micelles resulting in radial-, cross-, star-, or dandelion-like patterns in specially selected solvents. These structures are synthesized using a bottom-up chemical approach, i.e., by utilizing the chemical properties of single molecules to self-organize or self-assemble themselves into some desired useful conformations. Solid nanoparticles added to the solution serve as points of nucleation for the formation of the central core of the supermicelle. Covalent bonds connect the copolymers to form the stems of primary cylindrical micelles which may interact through weak hydrogen bonds or electrostatic or solvophobic interactions within the supermicelle structure.

6.2.5   Bilayers

The lipid bilayer forms the delimiting membrane of all the cells and is called the cell or plasma membrane. The structural units of this membrane physically constitute the barrier which forms the boundaries of any cell. These biological membranes are the perfect examples of lipid bilayers, the phospholipids organized into a bilayer, with polar hydrophilic heads toward the aqueous cytosol on one side and toward the tissue fluid on the other. The nonpolar, hydrophobic tail regions of the molecules lie on the inner side of the bilayer, where they face away from water. This bilipid layer thus forms a basic framework in and on which the other components of the membrane are embedded. Phospholipids typically tend to assemble in this manner, as this arrangement tends to satisfy the opposing tendencies of these amphipathic molecules (Fig. 6.11).

Fig. 6.11 Bipolar nature of layer
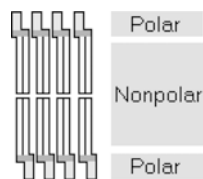
Fig. 6.12 Phospholipid
structure
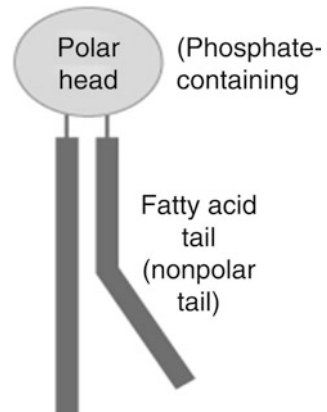
Fig. 6.13 Lipid bilayer
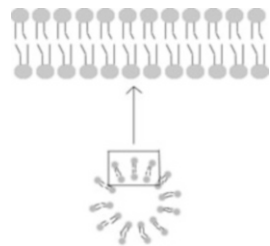
This whole structure, composed of two layers of phospholipid molecules, is termed as "lipid bilayer," is about 5 nm in thick, and is present in all living cells (Fig. 6.12).

Phospholipids are the most abundant lipid molecules that constitute the cell membranes. Their polar head group contains a phosphate group and contains two nonpolar fatty acid chains in its tail, which comprise of a string of carbons and hydrogens; one of the chains is kinked due to a kink in its double-bond structure. The phospholipids get arranged in bilayers with their hydrophobic tails toward the center and hydrophilic regions exposed to water, thus forming a structure that demarcates the inside and outside of the cell.

The lipid bilayer is asymmetrical with varied lipid and protein composition in each of the two bilayers. The lipid bilayer functions like a semipermeable membrane which prevents free passage of molecules across itself and allows only water and gases to easily pass through it (Fig. 6.13). It does not allow large molecules and small polar molecules to pass through. As discussed earlier it is a fluid mosaic structure of bipolar phospholipids, sterol lipids, etc. and proteins, which contribute to the fluidity of this membrane. Again, the "rigidity" and/or "fluidity" of the bilayer is dependent on its charge and the components. This fluidity along with confirmation of proteins is the key to membrane transport of the particles which can otherwise not cross the membrane.

6.2.6 Liposomes

These are small artificial vesicles which are spherical in shape. They may be formed of cholesterol and other natural nontoxic phospholipids. These may be formed of one or more lipid bilayers both surrounding and surrounded by aqueous units. Usually, liposomes are spherical vesicles with a large variation in their sizes. The size of the liposome can vary from very small (0.025 μm) to large (2.5 μm) vesicles. They are classified into two categories on the basis of their size and number of bilayers, multilamellar vesicles (MLV), and unilamellar vesicles which can again be further classified into two categories, large unilamellar and small unilamellar vesicles, LUV and SUV, respectively.

The unilamellar liposomes, as the name suggests, possess a single phospholipid bilayer, whereas the multilamellar liposomes are vesicles that have an onion-like structure with several unilamellar vesicles of decreasing sizes forming one inside the other, making a multilamellar structure of concentric phospholipid spheres separated by layers of water.

Liposomes are used in various industries for their properties. Their being biocompatible, biodegradable, less toxic, and their aptitude to trap both hydrophilic and lipophilic drugs and thus simplifying site-specific drug delivery to tumor tissues. They play an important role in investigational systems and drug delivery systems. Cosmetic and pharmaceutical industries use them as carriers for numerous molecule. Food and farming industries utilize them as delivery systems for unstable compounds, *viz*., antimicrobials, antioxidants, flavors, and other bioactive elements.

6.2.7 Vesicles and GUV

Unilamellar liposomes of the average diameter reaching up to 100 μm (two–three orders of magnitude greater than that of liposomes) are called giant unilamellar vesicles (GUVs). These are formed in appropriate conditions due to lipid swelling in aqueous media. This name was given as the size of these liposomes was much larger than those formed by other methods of sonification, extrusion, etc. They can be formed by the application of static (DC) electric field and by using a variety of lipid mixtures. Evans and Kwok, in 1982, studied the mechanical properties of the liposome membranes using the optical microscope. Studies showing the mechanisms of lipid swelling and liposome formation in aqueous media were done by Angelova and Dimitrov in 1986 and 1988. Proposed GUVs can be used as models for direct microscopic observation of DNA interactions with lipid bilayers (Angelova et al. 1992) and in the study on the interactions of non-membrane proteins like DNase and RNase with lipid bilayers (Fischer et al. 2000).

6.3   Visualizing Structures and Dynamics of Nano-assemblies

The lipid bilayers are simple models of biomolecules, but these systems are difficult to study because of fluctuations in their molecular and biological properties which vary with their size, position in the cell, charge, composition, chemical and physical nature, etc. A special class of macromolecular complexes reside in the lipid bilayer of the membrane, surrounding every cell or its compartments (organelles), like the nucleus, mitochondria, peroxisomes, or chloroplasts. Because of their amphipathic nature, their exterior surface is part hydrophilic and part hydrophobic, membrane proteins are difficult to deal with, and this is especially true of their complex assemblies. These fluctuations are very essential for the description of the structure of the bilayer as they affect the main force between bilayers. The visualization techniques usually involve a combination of methods, which include diffraction (at both low and wide angles), volumetric measurements, simulations, and analytical theory. A very important and accurate method of visualization is the technique of liquid crystallography, which provides a unique insight in the biophysics of lipid bilayers.

6.3.1   X-Ray and NMR Studies

X-ray diffraction on crystals of biological samples has been used to study the structures of the nano-assemblies of lipids. Max von Laue provided the X-ray diffraction pattern of crystals in 1912. A general equation, known as Bragg's law, was derived by William Lawrence Bragg to describe the founding principle of image formation by X-ray diffraction. Structural details of lipids have been observed using X-ray crystallography and NMR and have been instrumental in providing intricate details which can be further utilized in deciphering their properties. The structural details of the lipid bilayer and mechanism of primary and secondary messengers in the lipid layers have already been demystified using these techniques.

6.3.2   Microscopy: Confocal/EM

Confocal and electron microscopy are very good tools to visualize the structures and dynamics of various compounds in lipid chemistry. They provide a high-resolution visual structure which cannot be provided by other conventional methods. These advanced tools in microscopy have acted as facilitators in visualizing and exploring the components of cellular and subcellular environment in great detail. Confocal microscopy is used for the three-dimensional dissection of cellular organization, whereas the electron microscopy especially transmission electron microscopy is used extensively for the study of the whole internal structure in minute details. Cryo-electron microscopy, a type of electron microscopy, is used

for subcellular studies. Indirect references, using colloidal gold particles and/or other agents, are also used in electron microscopic studies.

6.3.3 Molecular Dynamic Simulation (A Computational Approach)

Biological membranes are selective barriers and check the indiscriminate to-and-fro passage of water, ions, and other polar molecules in and out of cells and cell compartments. Biomembranes are basically assemblies of lipid bilayers of phospholipids indiscriminately embedded with proteins and cholesterol. Lipids form the major part of the biological membranes and efficient energy storage compounds. They form flexible, semipermeable membranes that separate the cells from other cells and also form subcellular compartments due to their hydrophobic nature. Fat breakdown yields twice as much energy per gram than that yielded by carbohydrates or protein (Katsara and Gutberlet 2013). Molecular dynamic simulation is used to explore these structural, functional, and thermodynamic details at molecular level. The simulation have been used to view channel proteins in a thin slice of lipid bilayer, observe the channel proteins embedded in a lipid bilayer membrane, view the passage of water passing through the ion channel, and to illustrate water exclusion from the lipid bilayers, as a brief tutorial good for a quick look and last but not the least for the enlarged and detailed view of these molecular structures and functional dynamics of the structures being viewed.

6.4 Membrane Phase Transitions and Curvatures

Biological membranes are primarily composed of phospholipids, a large and diverse class of compounds composed of a hydrophilic head group covalently attached to a pair of hydrophobic fatty acids. This amphipathic nature of the phospholipids leads to the formation of bilayers when placed in water, as the phospholipids are driven to orient their head groups toward water and shield their fatty acid tails from it via the hydrophobic effect. Another significant characteristic of the lipid bilayer is that of its fluidity, which can be defined as the relative mobility of the particular lipid molecules, which again is dependent on the temperature, so the fluidity of the membrane is bound to change with any change in temperature.

This lipid bilayer can therefore exist in either a liquid or a solid gel phase. Each lipid has a characteristic transition temperature at which they undergo the transition from the gel to liquid phase. Though usually these bilayers tend to exist in a fluid phase under normal physiological conditions, their phospholipid components may undergo phase transitions under a given set of favorable environmental conditions. As in the case of transitions, between the liquid, solid, and gas phases of other simpler systems, these lipid phase transitions also represent changes in the entropy of the system, through reorganization of the system's components in response to changes in the free energy of the system. Lipids may exist in a number of phases, details of which are as follows:

6.4.1   The Liquid Disordered Phase (Lα)

The liquid disordered phase is a highly fluid state in which individual lipids can easily move laterally across the surface of the membrane in a relatively unhindered manner. This phase is characterized by the irregular packing of individual lipid molecules and also by the presence of kinks in unsaturated fatty acids which make up the given lipid molecule; this effectively reduces the surface area accessible to other fatty acid chains, weakening Van der Waals interactions, thus providing a large space for the movement of individual lipids.

6.4.2   The Gel Phase (Lβ)

Lipid bilayers enter a solid-like phase, i.e., the gel phase at temperatures less than T_m (melting temperature). Fatty acids with kinks usually undergo trans isomerization, which allows their kinked chains to extend fully which then leads to the strengthening of their van der Waals interactions, which as a result, leads to a more orderly lipid packing, preventing the lateral movement of lipids across the surface of the membrane.

6.4.3   The Liquid Ordered Phase (Lo)

The liquid ordered phase is actually a hybrid stage between the liquid disordered (Lα) and gel (Lβ) phases. This phase is characterized by constituent lipids possessing the right combination of sufficiently high, relative rigidity and membrane sterol concentration of sterol molecules. This characteristic state of the lipids leads to the formation of tighter packing of liquid phase membranes, while gel-phase lipids remain separated, thereby leading to a stage that lies somewhere between the liquid disordered (Lα) and gel (Lβ) phases.

6.4.4   The Ripple Phase (Pβ)

In this phase the lipid bilayer, at intermediate temperatures, arranges itself to form a series of ripples along the surface. The chain-packing structure in this phase is quite similar to the structure as seen in the gel phase.

6.4.5   The Pseudocrystalline Phase (Lc)

This phase is seen at low temperatures, where the lipid head-group interactions promote the packing of membrane lipids into a highly ordered superlattice.

6.4.6   Factors Affecting Lipid Phase Transitions

Van der Waals interactions among adjacent lipid molecules govern the phase behavior of lipid bilayers. The more the strength of van der Waals interactions between the lipid moieties, the tighter is the packing among them and the nearer they are to each other. The degree of this interaction in turn is determined by the length of the lipid tails and the strength with which they can pack together. Lipids with longer tails have more surface area to interact, thereby increasing the strength of these interactions and as a consequence decrease the lipid mobility. This phenomenon can be easily explained by the following example: paraffin wax, made up of long alkanes, is solid at room temperature, whereas octane (gasoline) a short alkane remains in liquid state at room temperature. Besides chain length, the degree of unsaturation observed in lipid tails also affects transition temperature as this unsaturation translates into a double bond and in turn produces a kink in the alkane chain, which disrupts its regular structure providing extra free space within the bilayer allowing more flexibility in the adjacent chains. This increase in the number of double bonds leads to lower transition temperatures, which in turn decrease the overall chain length by one carbon and typically alter the transition temperature of the lipid by 10 °C or less. But conversely, adding just one double bond decreases the transition temperature by 50 degrees or more. Tm is also affected by the presence of one or more double bonds in the tails of fatty acids, which alter the strength of van der Waals interactions between them. Unlike chain length, however, increasing unsaturation reduces the Tm of the lipid by reducing the accessible surface area of the fatty acid tail by forming kinks that prevent nearby tails from packing together as tightly, thus weakening inter-lipid van der Waals interactions and lowering the Tm of the lipid. The position of double bonds in the fatty acid chain influences the degree to which Tm is lowered, with double bonds closer to the middle of the chain producing larger kinks, thereby decreasing Tm more than double bonds located closer to either end of the chain. High local concentrations of membrane-associated proteins can decrease the Tm of sections of membrane through steric interactions between crowded proteins. Although elevated local protein concentrations can be critical for facilitating certain cellular processes, collisions between crowded proteins create lateral pressure that renders lipid domain separation more thermodynamically favorable—possibly leading to phase transitions, as shown.

6.4.7   Phase Separation

Membranes often contain a mixture of lipids of different lengths and degrees of unsaturation, resulting in differing Tm's. If such a membrane system is cooled, the resulting straightening of the fatty acid chains causes part of the gel phase lipids' chains to be exposed to water, resulting in a hydrophobic effect-driven aggregation of the long, newly formed gel-phase lipids. This results in the formation of patches of long, saturated, gel-phase lipids in the membrane. Phase separation between

lipids surrounding integral membrane proteins can briefly expose the hydrophobic residues of the middle of the protein to water. If enough other exposed proteins are nearby, this can result in a *hydrophobic effect-mediated protein aggregation* event. The differential rates of phase transition between lipids composing a membrane can lead to packing defects as gel-phase fatty acid chains straighten out, forming a short-lived gap between the now gel-phase chains and neighboring, still-liquid chains. Such gaps can allow cytoplasmic contents to leak out of the cell until they are plugged via lateral diffusion of neighboring lipids.

6.5   Role of Membrane Lipids in Cellular Processes and Human Health

Modulation of membrane protein functionality is an important biochemical function performed by the lipid bilayer. Some of the membrane proteins may require specific lipids for their activity, for example, phosphatidylethanolamine controls the transport activity of Ca^{2+} ATPase; that invariably means that active transport of calcium across the membrane by the Ca^{2+} ATPase depends on the presence or absence of phosphatidylethanolamine in the membrane (Cheng et al. 1986).

Cholesterol is specifically required for enzyme transport function in mammals and is irreplaceable as it cannot be substituted by any of the other sterols which may be present in the membrane (Yeagle et al. 1988). Thus, cholesterol is an important constituent of the membrane which is essentially required for cell growth and development in mammalian cells.

Another example of modulation of protein function is the enzyme lactose permease (LacY) of *Escherichia coli* which cannot function in a proper manner in the absence of phosphatidylethanolamine. This membrane lipid is essential for proper insertion and folding of LacY (Dowhan and Bogdanov 2012). The membrane lipid cardiolipin is essential for the carrier functions of mitochondrial adenosine diphosphate/adenosine triphosphate (ADP/ATP), and its absence diminishes the enzyme activity (Hoffmann et al. 1994; Jiang et al. 1997; Nury et al. 2005). These few examples emphasize the importance of cell membrane lipids binding to membrane proteins and regulating their biological function. Covalent bonds between lipids and proteins modulate protein function (Yeagle 2014).

Post-translational modifications of proteins such as acylation or prenylation make them more hydrophobic, causing their integration with lipid component of the bilayers and thereby their transfer from aqueous phase to the lipid bilayer.

Localization of these proteins to the membrane from the aqueous phase induces a new function into the protein that did not exist previously. Thus, these covalent modifications of proteins by lipids have regulatory implications in the cell. There is an asymmetric distribution of phospholipids across the plasma membrane as their polar head group doesn't allow them a free passage through the hydrophobic interior of the membrane (Yeagle 2014). Thus, flip-flop movement in pure phospholipid bilayers is limited. But, in the plasma membrane of the human RBC,

translocation of phospholipids from one side of the bilayer to the other takes place with the help of enzymes which complete the function at the expense of hydrolysis of ATP.

6.5.1 Membrane Lipid Metabolism

Cellular metabolic pathways are responsible for the synthesis of membrane lipids which then again become substrates for metabolic pathways. One pathway which shows a direct relevance to the "remodeling" of phospholipids by the exchange of fatty acids is observed in the phospholipase A2 cleavage. Phospholipase A2 cleaves the ester bond at the second position of the glycerol backbone resulting in the removal of one of the fatty acids. Reacylation of this position in phospholipids requires acyl-CoA. The original diacylglycerol is 16/0, but it is usually replaced by unsaturated fatty acids rationalizing the observed abundance of unsaturated fatty acids at position 2 and saturated fatty acids at position 1 of the glycerol backbone present in several phospholipids. Another example of remodeling occurs when unsaturated lipids are converted to cyclopropane-derivatized lipids to resist oxidation on the entry of organisms into dormant state. Examples of two major pathways showing the role of phospholipid as substrate in cells are the following: (1) One pathway is the synthesis of prostaglandins, using arachidonic acid (20/4) as the substrate for the reaction, this acid is found acylated to phospholipids in membranes at the second position of the glycerol backbone. Membrane activation leads to cleavage of the acid from the phospholipid by the action of phospholipase A2 making it available for prostaglandin biosynthesis.

(2) Another pathway is phosphorylation of phosphatidylinositol which is mediated by an intracellular kinase that adds phosphate groups to the sugar moiety within the cells of phosphatidylinositol resulting in the formation of a di- or triphosphorylated species playing an important role in signal transduction. Lipids such as phosphatidylethanolamine function as chaperons in protein folding helping in the insertion of bacterial membrane proteins into membranes during their biosynthesis (Dowhan and Bogdanov 2012).

6.5.2 Lipids as Signaling Molecules

Membrane lipids also act as second messengers within cells. On their activation by the ligands, the receptors located at the plasma membrane activate phospholipases which in turn cleave phospholipids. An example of this is phospholipase C which cleaves phosphatidylinositol and produces diacylglycerol and inositol phosphate. Two times previously phosphorylated phosphatidylinositol when cleaved will produce inositol triphosphate (IP3) as one of the cleavage products. The resultant cleavage products may function as secondary messengers. IP3 is instrumental in promoting

the release of stored intracellular calcium by interacting with the calcium channels present in the membrane of the endoplasmic reticulum.

This is an intricate part of a chain reaction, wherein a receptor activated at the cell surface in turn activates a phospholipase C, causing the release of IP3, which results in opening of a calcium channel in the endoplasmic reticulum. The phosphorylated form of PI is PIP2; it produces another messenger molecule, diacylglycerol, after hydrolysis by phospholipase C (Yeagle 2014).

6.5.3 Potential in Immunotherapy

Traditionally studied tumor-associated antigens are proteome and genome based, exhibiting lesser diversity as compared to less studied glycome complexity and diversity (Hakomori 2002, Durrant et al. 2006, Davidson et al. 1987, Zhang et al. 2010, Lewis et al. 1993, Hamilton et al. 1993a, b). This glycome diversity is an attribute of possible carbohydrate modifications and variation in lipid backbones (Hakomori 2002, Durrant et al. 2006, Helling and Livingston 1994). Glycolipids constitutes about 3% of outer monolayer of plasma membrane (Cazet et al. 2010); their association with membrane microdomains (Hakomori 2002, Durrant et al. 2006) represents a relatively unexplored world of tumor-associated antigens (Alberts et al. 2002 and Rabu et al. 2012). Glycans are complex carbohydrates, which are abundantly diverse and regulated. This abundant repertoire is produced by glycosylation, which forms glycoconjugates with proteins and lipids (Durrant et al. 2012). Glycan structures are known to be modified in pathogenic situations including cancers, particularly by modification in cellular glycosylation, which leads to expression of tumor-associated carbohydrate antigens (TACAs) (Helling and Livingston 1994) chiefly, by malignant transformation, tumor progression, survival, and evasion (Reis et al. 2010). Several glycans on the tumor surface and host elements mediate key pathophysiological events during ongoing tumor progression (Varki et al. 2009 and Narita et al. 1993). Glycoconjugate modification is now an established mark of cancer, presenting them as important biomarkers potentially used in clinics for tissue and serum assays (Ohtsubo and Marth 2006). The main TACAs expressed in breast carcinoma are mucin-type antigens, Lewis antigens, gangliosides (Helling and Livingston 1994), sialyl-Lewis[x] (s-Le[x]), sialyl-Lewis[a] (s-Le[a]), and sialyl-Thomsen-nouvelle (sTn) (Narita et al. 1993 and Soares et al. 1996). Their presence is usually correlated with poor prognosis and reduced overall survival (Ura et al. 1992). High expression of Lewis[y/b] is associated with decreased patient survival in lymph node-negative breast carcinoma using breast TMA (Miles et al. 1994). s-Le[x] is also an indicator of worst prognosis in TNBC (Madjd et al. 2005). Identification of unique tumor-specific targets that may be explored for therapy of cancer potentially holds the key for treatments against a variety of cancers.

References

Agrawal GK et al (2004) Rice octadecanoid pathway. Biochem Biophys Res Commun 317:1–15

Alberts B et al (2002) Molecular biology of the cell, 4th edn. Garland Science, New York

Angelova MI, Dimitrov DS (1986) Liposome electroformation. Faraday Discuss Chem Soc 81:303–311

Angelova MI, Dimitrov DS (1988) A mechanism of liposome electroformation. Prog Colloid Polymer Sci 76:59–67

Angelova MI et al (1992) Preparation of giant vesicles by external AC electric fields. Kinetics and applications. Prog Colloid Polymer Sci 89:127–131

Bach D, Wachtel E (2003) Phospholipid/cholesterol model membranes: formation of cholesterol crystallites. Biochim Biophys Acta 1610:187–197

Cazet A et al (2010) Tumor associated carbohydrate antigens in breast cancer. Breast Cancer Res 204(12):1–13. doi:10.1186/bcr2577

Cheng K et al (1986) The role of cholesterol in the activity of reconstituted Ca ATPase vesicles containing unsaturated phosphatidylethanolamine. J Biol Chem 261:5081–5087

Davidson NE et al (1987) Epidermal growth factor gene expression in estrogen-positive and negative human breast cancer cell lines. Mol End 1:216–223

Dowhan W, Bogdanov M (2012) Lipid-assisted membrane protein folding and topogenesis. In: Yeagle PL (ed) The structure of biological membranes. CRC Press, Boca Raton, pp 177–202

Durrant LG et al (2006) A new anticancer glycolipid monoclonal antibody, SC104, which directly induces tumor cell apoptosis. Cancer Res 66(11):5901–5909

Durrant LG et al (2012) Immunology in the clinic review series; focus on cancer: glycolipids as targets for tumour immunotherapy. Clin Exp Immunol 167(2):206–215

Evans E, Kwok R (1982) Mechanical calorimetry of large dimyristoylphosphatidylcholine vesicles in the phase transition region. Biochemistry 21:4874–4879

Fahy E et al (2005) A comprehensive classification system for lipids. J Lipid Res 46:839–862

Fischer A et al (2000) Giant vesicles as models to study the interactions between membranes and proteins. Biochim Biophys Acta 1467:177–188

Hakomori S (2002) Glycosylation defining cancer malignancy: new wine in an old bottle. Proc Natl Acad Sci U S A 99(16):10231–10233

Hamilton WB et al (1993a) Ganglioside expression on sarcoma and small-cell lung carcinoma compared to tumors of neuroectodermal origin. Proc Am Assoc Cancer Res 34:491

Hamilton WB et al (1993b) Ganglioside expression on human malignant melanoma assessed by quantitative immune thin layer chromatography. Int J Cancer 53:566–573

Helling F, Livingston PO (1994) Ganglioside conjugate vaccines. Mol Chem Neuropathol 21:299–309

Hoffmann B et al (1994) The reconstituted ADP/ATP carrier activity has an absolute requirement for cardiolipin as shown in cysteine mutants. J Biol Chem 269(3):1940–1944. http://biomodel.uah.es/en/model3/ac-gr.htm

Jiang F et al (1997) Cardiolipin is not essential for the growth of Saccharomyces cerevisiae on fermentable or non-fermentable carbon sources. Mol Microbiol 26(3):481–491

Jones G et al (1998) Current understanding of the molecular actions of vitamin D. Physiol Rev 78:1193–1231

Katsara J, Gutberlet T (2013) Lipid bilayers: structure and interactions. Springer sciences and Business Media, p 296

Khosla C et al (1999) Tolerance and specificity of polyketide synthases. Annu Rev Biochem 68:219–253

Kuzuyama T, Seto H (2003) Diversity of the biosynthesis of the isoprene units. Nat Prod Rep 20:171–183

Lazar K, Walker S (2002) Substrate analogues to study cell-wall biosynthesis and its inhibition. Curr Opin Chem Biol 6:786–793

Lewis GD et al (1993) Differential responses of human tumor cell lines to anti p185 HER2 monoclonal antibodies. Cancer Immol Immunother 37:255–263

Madjd Z et al (2005) High expression of Lewis y/b antigens is associated with decreased survival in lymph node negative breast carcinomas. Breast Cancer Res 7(5):780–787

Meganathan R (2001a) Biosynthesis of menaquinone (vitamin K2) and ubiquinone (coenzyme Q): a perspective on enzymatic mechanisms. Vitam Horm 61:173–218

Meganathan R (2001b) Ubiquinone biosynthesis in microorganisms. FEMS Microbiol Lett 203:131–139

Miles DW et al (1994) Expression of sialyl-Tn predicts the effect of adjuvant chemotherapy in node-positive breast cancer. Br J Cancer 1994(70):1272–1275

Murphy RC, Smith WL (2002) The eicosanoids: cyclooxygenase, lipoxygenase, and epoxygenase pathways. In: Vance DE, Vance JE (eds) Biochemistry of lipids, lipoproteins and membranes, 4th edn. Elsevier Science, New York, pp 341–371

Narita TH et al (1993) Association of expression of blood group-related carbohydrate antigens with prognosis in breast cancer. Cancer 71:3044–3053

Nury H et al (2005) Structural basis for lipid-mediated interactions between mitochondrial ADP/ATP carrier monomers. FEBS Lett 579(27):6031–6036

Ohtsubo K, Marth JD (2006) Glycosylation in cellular mechanisms of health and disease. Cell 126:855–867

Pahlsson P et al (1998) Characterization of galactosyl glycerolipids in the HT29 human colon carcinoma cell line. Arch Biochem Biophys 396:187–198

Pereto J et al (2004) Ancestral lipid biosynthesis and early membrane evolution. Trends Biochem Sci 29:469–477

Porter JW, Spurgeon SL (1981) Biosynthesis of isoprenoid compounds, vol 1. Wiley, New York

Rabu C et al (2012) Glycans as targets for therapeutic antitumor antibodies. Future Oncol 8(8):943–960

Raetz CRH, Whitfield C (2002) Lipopolysaccharide endotoxins. Annu Rev Biochem 71:635–700

Reeves CD (2003) The enzymology of combinatorial biosynthesis. Crit Rev Biotechnol 23:95–147

Reis CA et al (2010) Alterations in glycosylation as biomarkers for cancer detection;J. Clin Pathol 63:322–329

Ricciarelli R et al (2001) Vitamin E: protective role of a Janus molecule. FASEB J 15:2314–2325

Rodriguez-Concepcion M (2004) The MEP pathway: a new target for the development of herbicides, antibiotics and antimalarial drugs. Curr Pharm Res 10:2391–2400

Schenk B (2001) The ins(ide) and out(side) of dolichyl phosphate biosynthesis and recycling in the endoplasmic reticulum. Glycobiology 11:61R–71R

Soares R, Marinho A, Schmitt F (1996) Expression of sialyl-Tn in breast cancer. Correlation with prognostic parameters. Pathol Res Pract 192:1181–1186

Sweet CR, Ribeiro AA, Raetz CR (2004) Oxidation and transamination of the $3'$-position of UDP-N-acetylglucosamine by enzymes from Acidithiobacillus ferrooxidans. Role in the formation of lipid A molecules with four amide-linked acyl chains. J Biol Chem 279:25400–25410

Taniguchi N, Honke K, Fukuda M (2002) Handbook of glycosyltransferases and related genes. Springer, Tokyo

The Lipid Library.: http://www.lipidlibrary.co.uk

Ura Y et al (1992) Quantitative dot blot analyses of blood-group-related antigens in paired normal and malignant human breast tissues. Int J Cancer 50:57–63

Varki A, Cummings RD, Esko JD (2009) Essentials of glycobiology. Cold Spring Harbor Laboratory Press, Cold Spring Harbor

Walsh CT (2004) Polyketide and nonribosomal peptide antibiotics: modularity and versatility. Science 303:1805–1810

Wenk MR (2005) The emerging field of Lipidomics. Nat Rev Drug Discov 4:594–610

Yeagle PL (2014) Lipids. In: eLS. Wiley, Chichester. doi:10.1002/9780470015902.a0000711.pub3

Yeagle PL, Rice D, Young J (1988) Effects of cholesterol on (Na,K)-ATPase ATP hydrolyzing activity in bovine kidney. Biochemistry 27:6449–6452

Zähringer U, Lindner B, Rietschel ET (1999) Chemical structure of lipid A: recent advances in structural analysis of biologically active molecules. In: Brade H, Opal SM, Vogel SN, Morrison DC (eds) Endotoxin in health and disease. Marcel Dekker, New York, pp 93–114

Zhang G et al (2010) Suppression of human prostate tumor growth by a unique prostate-specific monoclonal antibody F77 targeting a glycolipid marker. Proc Natl Acad Sci U S A 107:732–737

Membrane Biophysics

7

Sushant Singh and Naresh C. Bal

Abstract

Membranes are the unique biological structures maintaining the intra- and extracellular partition. In unicellular organisms they define the living interior from the nonliving exterior. In case of eukaryotes, membranes also help in separation of different intracellular milieus. Membranes also play roles as the site of active exchange of information between intra- and extracellular environments in various ways. Here in this chapter, we first visit the structural aspects of biological membranes. Then, we discuss in details the various types of transport mechanisms that occur across membranes. We also describe the different types of ion channels and pumps with special emphasis of Na^+/K^+ ATPase and Ca^{2+} ATPases. We have paid special attention about diseases that are associated with dysfunction of ion channels and pumps. This chapter is designed for the readers to build a sound background on the functioning of biological membranes from the structural perspectives.

Keywords

Cell membrane • Membrane properties • Diffusion • Brownian motion • Membrane transport • Membrane lipids • Membrane ion-channels

S. Singh (✉)
University of Central Florida, Orlando, Florida, USA
e-mail: sushantsingh12@gmail.com

N.C. Bal
School of Biotechnology, KIIT University, Bhubaneswar, India
e-mail: naresh.bal@kiitbiotech.ac.in

183

7.1 Membrane Structure and Models

Cell membrane is the structure which separates intracellular components from other cells as well as protects it from the extracellular environment. Both prokaryotic and eukaryotic cells possess this cell membrane structure. In addition to cell membrane, the eukaryotic cells possess several intracellular membranes that help in the creation of partition inside the cell called "cell organelle" with specialized microenvironment to carry out sophisticated cellular functions. The major function of these intracellular membranes is to act as a selectively permeable barrier for the transport of different components through it. These membranes include the nuclear membrane, endoplasmic reticulum membrane, and membranes of mitochondria, Golgi complex, and lysosomes.

7.1.1 Physical Properties of the Membrane

Cell membrane is primarily made up of proteins and lipids. The protein portion can constitute up to 55% of the membrane, while the lipid component is usually around 45%, and this ratio between proteins and lipids varies in different cell types. Some of the physical properties associated with the cell membrane are:

- Acts as a selective barrier between intracellular milieu and external medium.
- Facilitate selective movements of different molecules across the membrane.
- Aids in cell-cell communication and interactions.
- Serves as a barrier to toxic and deleterious compounds.
- Roles of cell membrane have also been observed in cellular reproduction.
- Aids in mediating cellular motility.

7.1.2 Biophysical Properties of the Membrane

The cell membrane consists of unique biophysical properties that help in the survival and functioning of the cells. The different aspects in which the membrane has a role to play include transport and signaling, adhesion, migration, apoptosis, mitosis, etc. Some of these biophysical properties are explained below.

7.1.2.1 Surface Tension
In regard to the biological cell membrane, surface tension acts as an important attractive force that works on the cell surface and its associated molecules and enables them to assume the shape with the least surface area. The role of cell membrane surface tension was highlighted in 1969 by de Gennes and Papoular and in 1976 by Brochard et al. Cellular bilayer membrane without any concentration gradient across it was found to have negligible surface tension, indicating that with respect to membrane surface area, the free energy should be minimal. Also similar explanations were presented by Tanford (1979) and Israelachvili et al. (1977).

These explanations were of immense help in understanding shape fluctuations in red blood cell membranes. These arguments were also helpful in developing theories for single-layer or bilayer membranes. Theories of lipid molecule exchange assume that surface tension of a bilayer is zero, while that of a monolayer is nonzero. The surface tension is finite because of attractive forces among the hydrophobic interactions arising from the hydrocarbon chains and can minimize energy by reducing its area. This reduction in area can happen due to the dispersion of membrane in water, where it is free to expand or compress. However, the membrane cannot shrink infinitely because of the steric repulsions between the hydrated head groups and also electrostatic repulsions on the charge of the head groups. The membrane will adapt to this environment in such a state that the attractive interactions will balance out the repulsive forces. Attractive interactions among the hydrocarbon chains will neutralize the repulsive interactions of the charged head groups. Under these scenarios, with respect to area of the membrane, the free energy turns minimal. The outcome is that free energy with respect to area diminishes; the surface tension turns out to be zero with the bilayer membrane trying to adopt a state with optimal packing of liquid molecules. However, this situation is entirely different for a monolayer system where the membrane is at air-water interface. A finite surface tension arises into the system even with the packing of lipid molecule is optimal. In such system, these chains of hydrocarbon of lipids are in contact with air, surface tension is 30 dyn/cm, and this value holds good for fluid monolayer at optimal packing of lipids as reported by Nagle (1980) and Jahnig (1984).

7.1.2.2 Adsorption

Adsorption is a surface-based phenomenon and defined as the adhesion of different molecules (i.e., adsorbate) onto the surface (i.e., adsorbent), and this process creates a layer of molecules attached onto the surface. Adsorption is quite different from a similar process known as absorption in which the fluid (i.e., absorbate) gets dissolved in a liquid or permeates into the solid (i.e., absorbent). In biological system, adsorption phenomenon leads to the accumulation of compatible adsorbate, which mostly includes protein molecules onto the adsorbent, which is the cellular membrane. The adsorption of protein onto the surface of cell membrane plays a very important and significant role where different protein molecules remain attached onto the membrane surface. During the process of adsorption, the nature of bonding between the adsorbate and adsorbent depends upon the molecules involved ranging from physisorption, i.e., weak hydrogen bond or van der Waals force, to chemisorption, i.e., characteristic covalent force and the ionic interactions. Other factors affecting the adsorption phenomenon include the surface tension, intermolecular forces of adsorbate, and electrostatic interaction. The cell membrane does not adsorb molecules directly; these molecules first interact with the adsorb proteins onto the cellular surface.

7.2   Structure and Function of the Cell Membrane

The plasma membrane acts as boundary and separates the fluids within and outside the cell. It is composed chiefly of lipids and proteins where the lipids, usually phospholipids, provide backbone to the plasma membrane. The phospholipids are arranged in bilayer with hydrophobic fatty acid tails facing interior of the membrane, and on the inner and outer surfaces facing are the hydrophilic polar heads. Proteins are scattered usually heterogeneously throughout the membrane. Carbohydrate chains are also attached to some of these molecules, called glycolipids and glycoproteins. Cholesterol is an important lipid constituent found in plasma membranes of animals. The membrane is a viscous fluid, and its components can drift past one another in a restricted manner. Like the plasma membrane, the other intracellular membranes are also made up of both lipids and proteins. The proteins lying within the bilayer of phospholipids of the membrane carry out the several physiological functions, including selective transport of molecules, inter-organelle communication, and cell-cell interaction.

7.3   Membrane Structure

The current concepts in the plasma membrane have largely evolved through in detail analysis of structural and functional properties of plasma membrane. The red blood cell (RBC) plasma membranes of mammals have been extensively utilized to study the structure of biological membranes. This is because mammalian RBCs do not contain internal membranes and serve as a source of pure plasma membranes for biochemical analysis. It was the study on RBC plasma membrane that provided the first evidence of lipid bilayers. In 1925, two Dutch scientists, E. Gorter and R. Grendel, demonstrated that plasma membrane consists of lipid bilayer and not monolayer. Extraction of the membrane lipids from a known number of RBCs was done, corresponding to the known surface area of plasma membrane. They also determined the surface area of the extracted lipids as a monolayer upon being spread out to the interface of air-water. The surface area of the extracted lipid when arranged as monolayer turned out to be twice than in intact RBC membranes. This was the first experimental proof that the biological membranes are lipid bilayers in structure rather than being monolayers.

Further studies using high-magnification electron microscopy confirmed the bilayer structure of plasma membrane of the RBCs. The plasma membrane appears as parallel dense lines in electron micrographs, separated by an intervening space. Electron-dense heavy metals are being used in electron microscopy as stains for binding to polar head groups. The hydrophobic fatty acid chains do not bind the stains resulting in lightly stained interior portion which separates the dense lines, as seen in Fig. 7.1. The current concept of membrane structure was first proposed in 1972 by Jonathan Singer and Garth Nicolson. This membrane structure model is called "fluid mosaic model" of membrane structure. According to this, membranes are viewed as two-dimensional fluid and are made up of lipid bilayers with proteins
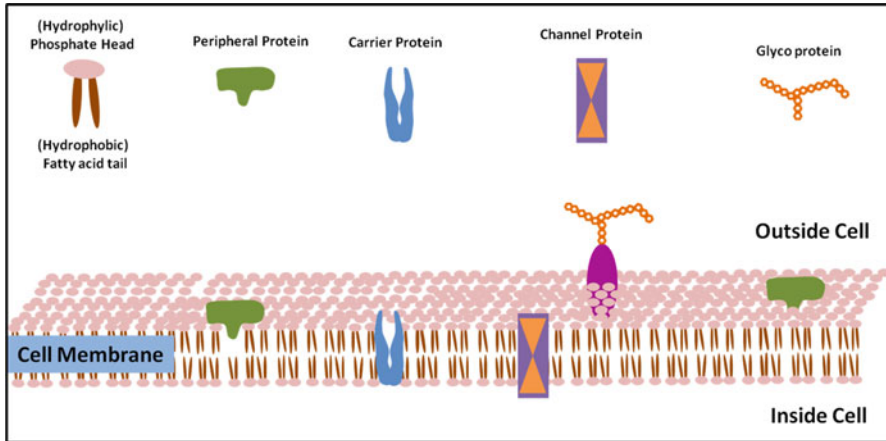
Fig. 7.1 Fluid mosaic model of the cell membrane. The membrane is composed of lipid bilayer with peripheral and intrinsic proteins embedded in it. The hydrophilic head is faced outside, while the hydrophobic head is immersed inside, into the interior of the membrane. Glycoproteins are attached onto the outside surface of the membrane

being inserted into it. Two classes of these membrane-associated proteins were distinguished by Singer and Nicolson, which they called as peripheral and integral membrane proteins.

7.3.1   Membrane Lipids

Four major kinds of phospholipids are present in plasma membranes of animal cells, which are phosphatidylcholine, phosphatidylethanolamine, phosphatidylserine, and sphingomyelin. In the case of membranes from most animal cells, these four types of lipids together account for about 70% of the total lipid content. Interestingly, these phospholipids are distributed disproportionately between the two layers of the membrane lipid bilayer. The outer plasma membrane layer consists largely of phosphatidylcholine and sphingomyelin. On the other hand, the inner layer mainly consists of phosphatidylethanolamine and phosphatidylserine. The inner half of plasma membrane also contains a fifth type of phospholipid, called "phosphatidylinositol." Even though phosphatidylinositol is relatively a minor component of the membrane, its vital role in cell signaling has been established with several decades of active research. The asymmetric distribution of lipid components in the membrane has functional significance. Both phosphatidylserine and phosphatidylinositol possess negatively charged head groups, and due to their greater abundance in the inner layer, they impart a net negative charge onto the plasma membrane cytosolic face.

Apart from phospholipids, glycolipids and cholesterol are also found in plasma membranes of animal cells. Although the glycolipids constitute about 2% of total

lipids and form a fairly minor component of the membrane, it provides very unique structure to the biological membrane. Glycolipids are found exclusively in the outer layer of the plasma membrane and are named "glyco" as they contain carbohydrate attached to their head group. The carbohydrate moieties of glycolipids are exposed to the surface of the cell and play an important role in the cellular interactions. Cholesterol is another unique constituent of membranes found mainly in the animal cells that is present in similar molar amounts as the phospholipids. Cholesterols get inserted into the phospholipid bilayer with their polar hydroxyl structure closely aligned to the phospholipid head groups. Cholesterol provides rigidity to the membrane and acts as an important regulator of fluidity of the membrane. On the one hand, cholesterol interferes with the fatty acid chain movement at high temperatures, resulting in outer part of the membrane being less fluid, while at low temperatures cholesterol interferes with fatty acid chains and prevents the membrane from freezing. Cholesterol is not present in most of the bacterial membranes. Although cholesterol is also absent in membranes of plant cells, they contain sterols which are structurally related compounds fulfilling the biological function of membrane fluidity.

In general, the phospholipid bilayers serve two important cellular membrane functions:

1. Phospholipid, being a basic component of membrane structure, also acts as barrier between two aqueous compartments due to the hydrophobic fatty acid chains present in the interior of the structure. Thus, it provides a highly impermeable boundary that limits movement of most water-soluble molecules such as ions and biomolecules.
2. The phospholipid bilayer is not solid but fluid. However, it is viscous enough to maintain its structural integrity: soft and flexible. Several natural phospholipids have one or more double bonds in their fatty acid tails, which introduces kinks into the hydrocarbon chains and contribute to the fluidity of the membrane.

Thus, both phospholipids and proteins are free to diffuse laterally within the membrane. Thus, this also becomes one of the critical biological properties for many membrane functions such as in signal transduction.

An emerging concept is that all lipid molecules do not diffuse freely into the biological membrane. Rather, few discrete membrane lipids enriched with cholesterol and sphingolipids (sphingomyelin and glycolipids) form more rigid structure than the other phospholipids. These clusters are termed as "rafts," and these structures move within the membrane and form associations with specific membrane proteins. Still, there remains a lot to understand about the functions of lipid rafts. Currently, it is suggested that these lipid rafts play important roles in biological processes including cellular signaling and the endocytosis-mediated internalization of extracellular molecules.

7.3.2   Membrane Proteins

Unlike lipids, proteins do not form the fundamental structural elements of membranes. However, membrane proteins execute specific biological functions that range from molecular transport to signal transduction, cell-cell interaction to cellular motility. In most plasma membranes, proteins constitute up to 40% by weight. As proteins are much larger than lipids, mostly the biological membranes ratio for protein and lipid molecule is around 1:100 numbers. Membrane proteins are usually differentiated into peripheral and integral. Peripheral membrane proteins get attached superficially to the lipid bilayer and do not get inserted into interior of the hydrophobic lipid bilayer. Indirectly these are associated by protein-protein interactions with the membrane usually involving ionic bonds. Peripheral membrane proteins can be dissociated from the membrane by treatment of polar reagents without disrupting phospholipid bilayer.

Integral membrane proteins present in the hydrophobic interior of the membrane can be released only after the disruption of the phospholipid bilayer. Small amphipathic molecules are commonly used as reagents for separating integral membrane proteins. Such molecules are basically detergents that possess both hydrophilic and hydrophobic moieties. Integral membrane lipids get displaced by the hydrophobic portions of the detergents, while the hydrophilic portions form soluble complexes in the aqueous solutions. Several of the integral membrane proteins are "transmembrane" as they span through lipid bilayer getting exposed to both sides of the membrane. High-magnification electron microscopy and freeze-fracture technique have been utilized to visualize these proteins. Onto the membrane internal portion, transmembrane proteins are exposed. These membrane-spanning parts of the proteins are made up of 20–25 hydrophobic amino acids usually organized into α-helices. The transmembrane proteins are inserted into the membrane during synthesis of the polypeptide chain on the endoplasmic reticulum. These nascent proteins evolved then get transported to plasma membrane through vesicles from endoplasmic reticulum and Golgi apparatus. Carbohydrate moieties are added into the maturing peptide in the endoplasmic reticulum and Golgi complex.

Several examples of peripheral and also integral membrane proteins exist in the nature. Spectrin is an ideal example of peripheral membrane protein and forms one of the major cytoskeletal protein components of the RBCs. Few other peripheral membrane proteins are found in the RBCs, and they are actin, ankyrin, and band 4.1. RBCs also contain integral membrane proteins such as glycophorin and band 3. Glycophorin is a small glycoprotein containing 131 amino acids having a molecular weight of about 30 kDa, the half of which is carbohydrate group. Glycophorin possesses a single membrane-spanning α-helix of 23 amino acids with the amino-terminal portion exposing the cell surface and is glycosylated heavily. The structural details of glycophorins are well characterized; however, its precise functional details still remain unknown. In contrast to this, the function of band 3 is well defined. Here, it's the anion transporter responsible for transport of bicarbonate (HCO_3^-) and chloride (Cl^-) ions across the RBC membrane. It has 929 amino acids and possesses 14 membrane-spanning α-helices. The protein band

3 remains in a dimeric state containing internal channel through which ion movements across the lipid bilayer take place.

Owing to their amphipathic nature, the crystallization of integral membrane proteins is very difficult. Hence, X-ray diffraction-mediated three-dimensional structural analysis is very hard. However, that has not deterred scientists to develop ways to apply X-ray crystallography on such proteins. The structure of photosynthetic reaction center of bacterium *Rhodopseudomonas viridis* was determined for the first time using X-ray crystallographic techniques in 1985. Three transmembrane proteins named L, M, and H (light, medium, and heavy) chains are present in the reaction center. The light (L) and medium (M) chain has five subunits each, while the heavy (H) transmembrane has one subunit. Also there exists fourth subunit of the reaction center, which is a peripheral membrane and is a cytochrome. With the help of protein-protein interaction, this fourth subunit gets bound to the photosynthetic complex. Although the membrane-spanning portion of most transmembrane proteins is α-helical, there are exceptions including the porins which are outer membrane channel-forming class of proteins of bacteria.

On a similar note, protein similar to porin protein of bacterial origin is also present onto the mitochondrial and chloroplast outer membrane. These protein structural analyses have revealed the β-barrel transmembrane-like structure, in which 16 β-sheets get folded into barrel-like structure with an aqueous pore enclosing into it. The polar amino acid side chain lines these pores, while the hydrophobic amino acids form the interior of the membrane and interact with it. Overall, the porin monomers form a stable trimmer where each contains three open channels which allow polar molecules to diffuse through the membrane.

In comparison to transmembrane proteins, several other proteins exist which are anchored by covalent interactions to the lipids and glycolipids of the inner layer of the plasma membrane. These types of protein are synthesized by the free cytosolic ribosomes, which get further modified with lipid addition. Some of these modifications include the addition of 14-carbon fatty acid chain, myristic acid, to the polypeptide chain on the amino terminus, and addition of palmitic acid (a - 16-carbon chain fatty acid) to the cysteine residue side chain. Another common lipid addition is "prenylation," which is the addition of prenyl group to the carboxy-terminal cysteine residue side chain. In most cases, these proteins behave as peripheral membrane proteins and are inserted into the membrane via positively charged polypeptide region or by the attached lipid structure. The positively charged domain of the protein provides surface to interact with the negatively charged phosphatidylserine head group on the cytosolic face of the plasma membrane. It is highly important to note that these anchored proteins into the inner layer of plasma membrane play an important functional role in signal transmission to intracellular targets, thereby signal transduction.

7.3.3   Composition, Function, and Membrane Transport

Cell membrane acts as a boundary, conserving the fluidic environment within and outside of cell. The major component of this cell membrane includes protein and phospholipids with these phospholipids being arranged in such a fashion that their fatty acid hydrophobic tail lies in the interior of the membrane with polar hydrophobic heads onto the outer and inner surfaces. Fundamentally, the entire cell membrane structure is termed as a phospholipid bilayer. There are four major phospholipids involved into lipid bilayer, i.e., phosphatidylcholine, sphingomyelin, phosphatidylethanolamine, and phosphatidylserine. Out of these, phosphatidylcholine and sphingomyelin form the major component onto the outer bilayer structure, whereas phosphatidylethanolamine and phosphatidylserine form the inner part. There is another phospholipid, i.e., phosphatidylinositol, which is a very minor component of the entire structure but plays a significant role in cell signaling. Also, in addition to phospholipids, the plasma membrane also contains a minor component in terms of carbohydrate, measuring around 2% in total onto the outer surface and playing a significant function. The two functional aspects associated with the phospholipids in this membrane structure include that, firstly, it keeps the outer and inner fluidic environment separated and, secondly, it does not allow the movement of water-soluble ions and molecules. In association with lipids, which play an important structural role in the cell membrane, proteins do play an important functional aspect in these membranes. With respect to its composition, the plasma membrane consists of an equal ration of lipids and proteins, i.e., 50% with minor percentage of carbohydrates ranging from 2 to 5%. The membrane proteins are categorized into two groups: residing on the outer side of membranes are known as peripheral membrane protein, while residing inside the lipid bilayer are known as integral membranes. The peripheral membranes are aqueous soluble and interact through protein-protein interaction; however, these are mainly ionic interactions and get disrupted by high salt as well as in extreme pH environment. Several integral membrane proteins are also known as "transmembrane proteins" as they span across the lipid bilayer and have parts exposed on either side of the membrane. These transmembrane proteins are helices of amino acids 20–25 in numbers, which are specifically hydrophobic. Also, certain carbohydrate groups are attached with the transmembrane polypeptide chains and exposed to the surface of cell membrane. These transmembrane proteins assist in the transport of certain ions and molecules through the cell membranes, thus acts as transporters. They play an active role in the selective permeability function of cellular membranes. These membrane transport proteins are categorized into two, i.e., channel transport proteins and carrier transport proteins. These proteins assist the different ions and molecules in either active or passive transport across cellular membranes.

7.3.3.1 Simple Diffusion and Brownian Motion
Simple diffusion and Brownian motion are associated with movement of atoms and molecules within a substance. It is the concept associated with the movement of particles and proves that each matter is composed of smaller particles and can be

separated from each other. Simple diffusion can be defined as movement of particles from the region of higher concentration toward the region containing lower concentration of particles. Diffusion forms a very important system in biological environment. It can also be defined as the movement of particles involved from the region of higher chemical potential toward its lower region. Osmosis is a type of diffusion, which is associated with the movement of water molecules. The movement of water is based on its potential gradient, which acts from higher potential gradient toward the lower gradient. In biological system, plants and animals distribute water, nutrients, and gases through diffusion phenomenon, and the best example is the movement of oxygen and carbon dioxide with blood capillaries.

In comparison to diffusion, Brownian motion is defined as the random movement of particles in a particular environment. Robert Brown gave the concept of Brownian motion in 1827. The movement of particle is directionless, and thus its movement is wayward and random, whereas in diffusion the particles move from higher concentration toward the lower concentration. The best example of Brownian motion is the movement of dust particles in the air. Thus Brownian motion is not governed by any concentration or direction factors other than particles of the medium.

7.3.3.2 Osmosis and Dialysis

Osmosis is a diffusion phenomenon where the movement of solute takes place across a semipermeable membrane. It involves movement of molecules of a solvent through the semipermeable membrane from its low-concentration solution toward the high-concentration solution, equalizing the two different solutions in terms of solute concentration. In comparison to osmosis, dialysis is different which involves the separation of molecules within themselves, i.e., separation of small molecules from the large ones. For understanding, osmosis is the movement of solvent (such as water molecule), while dialysis is the movement of solute (such as glucose molecule), and these are the two different processes, which occur continuously within our body at cellular level. To differentiate it further, osmosis allows only the solvent molecules to pass through the semipermeable membranes, while in case of dialysis, movement of solute, such as protein, glucose, and salt molecules, takes place through the semipermeable membrane. Application of this osmosis phenomenon is in the field of biochemistry and pharmacology, while dialysis applies to the field of medicine where it is performed to remove certain specific harmful molecules from the body, more specifically from the kidney removing the renal waste molecules.

7.3.3.3 Passive and Active Transport

Two different transport phenomena operate into the biological processes; they are active and passive transport mechanism. They help in the movement of different nutrients, water, and oxygen molecules into the cells, and they also help in the removal of waste products. These processes are categorized based on their utilization of energy resources for the transport of molecules. Active transport is an
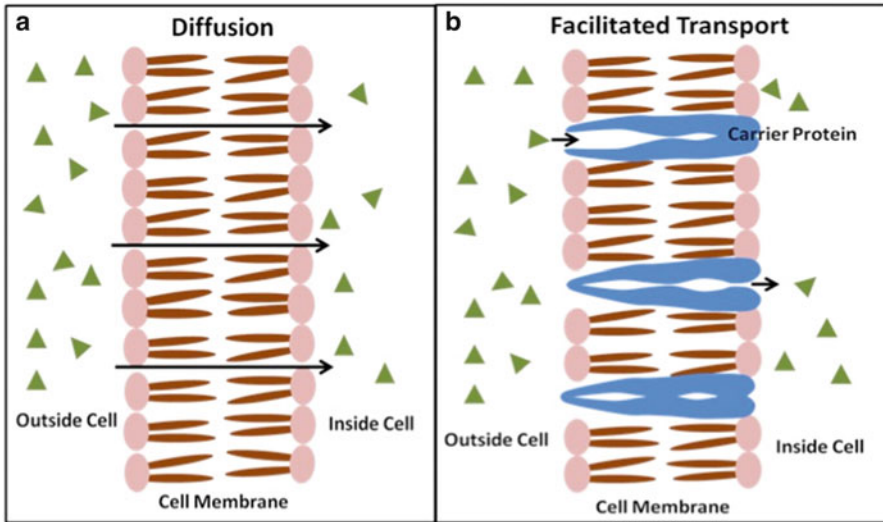
Fig. 7.2 (**a**, **b**) Represent passive diffusion process of the cell membrane. Diffusion is a sponta-neous process in which no external energy is required and the molecules move from the region of their higher concentration toward its region of lower concentration. However, when there is involvement of a specific carrier protein toward transfer of these molecules, it is called facilitated diffusion and still does not require energy for its transfer

energy-dependent process, which utilizes chemical energy molecules for its trans-port of molecules across the membranes. In comparison to energy-dependent process, passive transport does not require any energy molecules for its ion trans-port. It helps in the movement of ion and molecules based on their concentration gradient, such as from its high-concentration area toward its low-concentration areas, and thus does not require any energy input to derive its movement (Fig. 7.2). On the other hand, active transport utilizes cellular energy ATP molecules to drive the movement of different ions and molecules against the concentration gradient and thus helps in the transport of required molecules from its low concentration toward its high concentration. In eukaryotic cellular system, transport of amino acids, sugars, and lipids is processed through active transport mechanism. Cellular processes including endocytosis, exocytosis, and transport of ions through sodium-potassium pumps include this energy-driven transport mechanism (Fig. 7.3). In contrast to this energy-driven active transport processes, passive transport refers to the movement of ions based on the concentration gradient. Passive transport involves the movement of ions and molecules from the region of its higher concentration to lower concentration and thus using this passive transport mecha-nism, the cellular environments maintains the equilibrium without investing energy. It is important for a cellular system to maintain the equilibrium without utilizing much of the energy. Diffusion, facilitated diffusion, and osmosis of water and nutrients between cell and extracellular environment are some of the examples of passive transport mechanism.

Fig. 7.3 Represent active transport mechanism and this process involves energy for the transfer of molecules across the membrane. At the expense of energy molecules, in this mechanism molecules are transported from the region of lower concentration toward the region of higher concentration. Also based on the movement of ion molecules, it is divided into different categories
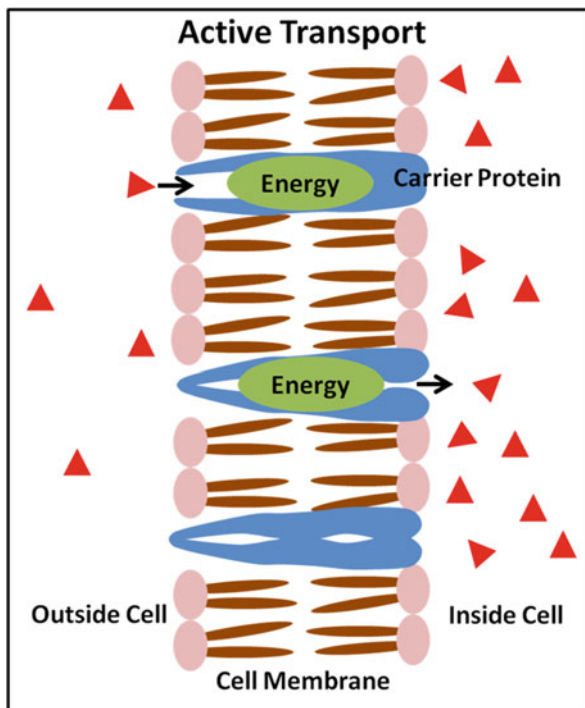
7.3.3.4 Secondary Active Transport

Based on the transport mechanism, active transport is further categorized into secondary active transport. In this category of active transport across cellular membranes, the transporter protein is coupled with the movement of ions across electrochemical gradient. The movement of ions takes place down its electrochemical gradient with subsequent uphill movement of other ions and molecules against the concentration gradient. These movements are also known as ion-coupled transport as both the ions are coupled with the transfer protein while moving in the direction together or against each other's concentration gradient (Fig. 7.4a, b). In the case of active transport, the driving energy for the ionic transport is provided by the hydrolysis of ATP. However, in the secondary active transport, the concentration gradient generates this driving energy across the membrane. A good example of this transport mechanism is the sodium (Na^+)/potassium (K^+) ATPase pumps where there is a very steep concentration gradient maintained across the cell membrane, i.e., extracellular Na^+ concentration is around 145 mM, while the intracellular is around 15 mM, and the free energy stored in this gradient is utilized by the Na^+-coupled transporters to drive the movement of ions across the membranes. Based on the direction of ion/molecule transfer, this secondary active transport is divided into symport and antiport. In symport type, it is a unidirectional transfer of the coupled ion and molecules, and the example is Na^+/glucose
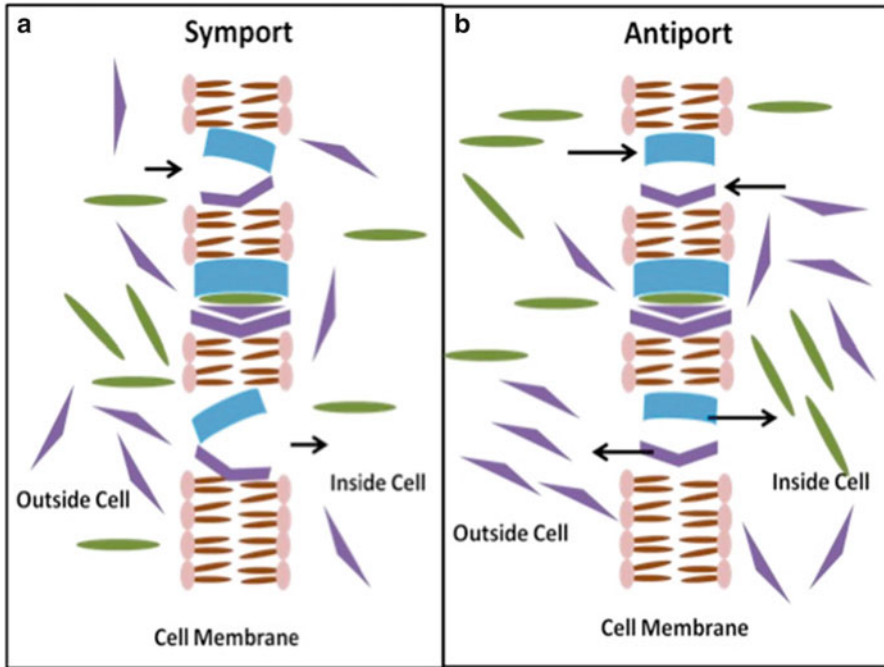
Fig. 7.4 (**a**, **b**) Represent secondary active transport mechanism. It is an energy-consuming process where molecules are transferred from the region of its low concentration toward the region of higher concentration at the expense of energy molecules. The movement of ions takes place down its electrochemical gradient with subsequent uphill movement of other ions and molecules against the concentration gradient. In symport type, it is a unidirectional transfer of the coupled ion and molecules, while in antiport type, the transfer of ions and molecules is just in opposite direction

cotransporter (SGLT1), which transfers two Na^+ ions and one glucose molecule together across the cell membrane, found in the proximal tubules of the kidney and small intestine, while in antiport type, the transfer of ions and molecules is just in opposite direction, respectively, and an example includes the Na^+/Ca^+ exchanger (NCX) which transfers three Na^+ ions inside against one Ca^+ ion outside the membrane, which are found in different muscle cells.

7.4   Transport of Ions and Molecules Through Membranes

The plasma membrane works as a selectively permeable barrier between the cellular interior and the cellular outer environment. The selectivity of the plasma membrane ensures that all the essentially required molecules enter the membrane easily, such as glucose, amino acids, and lipids into the cell. While it also ensures

that the metabolic intermediates remain inside the cell, waste compounds generated through the metabolic process leave the cell. Thus, it's the plasma membrane's entire responsibility toward maintaining a constant internal environment, and its selectivity for different molecules plays a key role in this process. The membrane lipid bilayer provides the impermeability to water-soluble molecules (glucose and amino acids and other ions). The membrane proteins serve as transporters of biomolecules and ions across the membrane. Because the requirement of different biomolecules varies between cells, the plasma membrane expresses a set of distinct transport proteins which uptake specific ion and molecules. Similarly, organelles with different internal milieu than that of the cytosol also contain unique transport proteins in their membrane to maintain this difference. There are several highly essential biological functions that require membrane transport. These processes include impulse conduction, signal transduction, nutrient uptake, cell proliferation, and tumor genesis. Epithelial cells form the inner lining of various tracts in animals that transport ions and small molecules across the other side. Epithelial cells lining the stomach secrete proton into the stomach lumen from a concentration of about micromolar range within the cell to a concentration of ~0.15 M inside the stomach, utilizing large amount of ATP. Those lining the absorptive small intestine transport products of digestion (such as glucose and amino acids) into the blood. The epithelial cells express different sets of transport proteins on two sides of the lumen. In addition, they express specialized membrane proteins that interconnect epithelial cells by protein-protein interaction, imparting strength and rigidity to the sheet at the same time, and help in preventing material transfer from one side to the other. Another common transmembrane transporter protein that utilizes energy is ATP-binding cassette (ABC) transporters that became hot area of research due to its role in multidrug resistance in cancerous cells. They are quite conserved among archaea, eubacteria, and eukaryotes and transport various substrates across cellular membranes. They have at one end the ligand-binding domain exposed while at other end an ATP-binding domain. In case of eukaryotic cells, ABC transporters usually function as pumps that extrude toxins and drugs out of the cell. Due to their importance, biology of membrane transport proteins is an increasing area of intense investigation by biopharmaceutical researchers to counter diseases.

7.4.1 Ion Channels: Unique Function in Physiology

We have discussed how membrane proteins play a very critical role in physiology as transporters (both active and passive) and co-transporters. There are another set of membrane proteins called "ion channels" which are often responsible for utilizing a gradient in ions upon a signal. While some channels are continuously open, most of them are gated, i.e., they can stay in open or closed state. According to the trigger for opening, they are classified into two types: voltage gated (gated by alterations in membrane potential) and ligand gated (when they open or close upon binding to a ligand). The ligand can be either external (like neurotransmitters, hormones) or intracellular (like Ca^{2+}, cAMP). Through the channel proteins,

molecules or ions move from the area of its higher to lower concentration, down the chemical gradient. Ion channels are essential for establishment and maintenance of resting membrane potential. Some of the ion channels are expressed in intracellular organelle like endoplasmic reticulum (inositol trisphosphate receptor, InsP3R) and mitochondria (voltage-dependent anion channels). Ion channels play a vital role in different biological processes including where it requires instant changes in ionic strength inside the cell such as cardiac, skeletal, and smooth muscle contraction, T-cell activation, and pancreatic β-cell insulin release. In recent years a whole field of channelopathy has come into existence to study diseases due to modification of the ion channel properties which can arise from genetic and autoimmune disorders.

7.4.2 Ion Transport Across Energy-Conserving Membranes

Every cell, prokaryotic as well as eukaryotic, has to acquire energy from the surrounding microenvironment. The major form of chemical energy inside every cell is ATP (adenosine triphosphate), which is synthesized on the specialized membranes usually termed as "energy-conserving membranes." This is found in bacteria as well as in eukaryotes. All of these membranes use proton-motive force to harness energy to drive ATP formation using ADP (adenosine diphosphate) and inorganic phosphate (Pi), which is a very high-energy-requiring process. The process of ATP synthesis is explained by "chemiosmotic theory" proposed by Peter Mitchell in the late 1960s who was awarded Nobel Prize in 1978. The process of ATP synthesis has been remarkably conserved through evolution. In bacteria it occurs on the cell membrane. But in eukaryotes this is carried out by specialized organelle, mitochondria in animal cells and chloroplast in plant cells. While most ATPase catalyze the decomposition of ATP into ADP and phosphate ion thereby releasing chemical energy to drive biological reactions, some ATPases work in the reverse direction, utilizing the energy derived from protein gradient to drive the ATP synthesis. These ATPases are termed as "ATP synthase" or "F-ATPases" and are the basis for the functioning of energy-conserving membranes. These are the major sources of ATP production by oxidative phosphorylation in eukaryotic mitochondria and through photosynthesis phenomenon in chloroplast. The ATP synthases are generally composed of two linked or coupled complexes, i.e., F1-ATPase complex and F0-ATPase complex. The F1-ATPase complex is the major catalytic core and consists of five different subunits, i.e., alpha, beta, gamma, delta, and epsilon. However, the F0-ATPase is embedded in the membrane and composed of three different subunits, i.e., A, B, and C, and additional subunits in mitochondria. Both of these complexes are coupled back-to-back with rotary motor function. The gamma subunit in the F1 complex forms the rotor inside the cylinder made up of alpha and beta subunits; however, in the F0 complexes, the rotor is formed of the C subunit, which is ring shaped. These rotors rotate in the opposite direction with F0 rotor being strong and using proton gradient force toward pushing F2 rotor in reverse direction and driving the ATP synthesis. The

same ATPases also work in similar reverse fashion in bacteria toward hydrolyzing the ATP energy and create the proton gradient.

7.4.3   Measurement of Driving Forces and Ion Transport

The flow of ions across the biological membrane regulates several important life processes including the heartbeat and nerve impulse. The measurement of these changes is very important toward understanding the normal and abnormality associated with the well-being of physiological states. All eukaryotic cells maintain a negative membrane potential on the inner side of surface compared to its exterior surface, which ranges between -20 and -90 millivolts (mV). In the case of electrically excitable cells such as neuron and skeletal muscle, it ranges from -70 to -90 mV. This field of study is referred to as "electrophysiology," and it includes analyzing the flow of ions and its associated effect. This field of study is of such importance that inventors of three electrophysiological techniques have been already awarded with Nobel Prize: Alan Lloyd Hodgkin and Andrew Fielding Huxley in 1963 for "voltage clamp," David H. Hubel and Torsten N. Wiesel in 1981 for "single neuron activity," and Erwin Neher and Bert Sakmann in 1991 for "patch clamp." In general, microelectrodes are used to measure the current either on the external or internal surface of the plasma membrane, and the intracellular electrical recoding provides the precise measurement of membrane potential. For the intracellular recording, the tip of a sharp microelectrode is inserted inside the cell, and another electrode called reference electrode is placed in contact with the extracellular fluid around the cell. The more recent patch clamp techniques can be used to measure ion flow through a group of ion channels or a single ion channel. The last several decades of research has resulted in the development of different variations of measurement of electrical current at the level of biological membrane. The patch clamp technique is an electrophysiological method that allows measuring ion flow across either a single or multiple ion channels in a membrane. This technique can be applied on a variety of cell types especially the excitable cells like muscle fibers, neurons, cardiomyocytes, etc.

7.4.4   Membrane Potentials and Concept of Redox Potential

Membrane potential of a cell is defined as the electrical potential difference between the inside of a cell with the surrounding extracellular environment. This electrical potential difference exists in all cell types with respect to its surrounding environment; however, this is especially important on the muscle and nerve cells as these changes associated results into the transfer of information across the cells. A typical cell membrane, for particular membranes of nerve cells, does maintain a small potential difference across its normal or resting state which is typically about -70 mV (millivolts). This voltage difference arises due to the difference in concentration of K^+ and Na^+ electrolyte ions present inside the cells and in the extracellular

environment. It is important to understand that to maintain the resting membrane potential, a very small number of negative and positive ion difference across the membrane are required. The two different factors influencing the movement of ions across the membrane are ion concentration gradient and the difference in electric potential. The concentration gradient applies to the uncharged molecules, while the charged ions are the basis of electric potential difference. Overall, the total energy change associated with the movement of ions across the membrane depends onto these two factors, and these two may act in the similar direction or the opposite. Reduction potential, also known as redox potential, is the measure of the tendency of chemical species to acquire electron, thereby getting reduced. Oxidation is the loss of electron, while reduction is the gain of it, and thus these oxidation-reduction reactions must occur simultaneously. Transfer of electrons takes place from reducing agent and toward oxidizing agent, in order that reducing agent gets oxidized, while the oxidizing agent gets reduced. In biological system, these oxidation reactions are always associated with the loss of hydrogen ion (H^+), which is known as dehydrogenation and, subsequently, the enzymes which catalyze these reactions grouped into dehydrogenases type. The overall oxidation-reduction reaction in a biological system can be differentiated into two halves, i.e., oxidation of the reduced species in one part while reduction of the oxygen species in the other part, and together, these constitute the conjugated redox pair reaction. A good example of these reactions is the functioning of nicotinamide adenine dinucleotide (NAD^+) and the nicotinamide adenine dinucleotide phosphate ($NADP^+$) in biological system. During reaction, the substrate, which undergoes oxidation, releases two hydrogen atoms. Subsequently, the oxidized nicotinamide of NAD^+ or $NADP^+$ accepts this hydrogen ion and gets reduced into nicotinamide. The NAD^+ is generally functional as oxidants in catabolic biological reactions, while the $NADP^+$ functions in anabolic reduction pathways. There are few enzymes, which can utilize the pool of NAD^+ or $NADP^+$ ions but mostly are quite specific for alone or the other, and this specific functionalization specialization retains the maintenance of pools of electron carriers having specific function.

7.4.5 Structure and Function of Na$^+$/K$^+$ ATPase and Ca^{2+} ATPase Pumps

In animal cells, it is observed that a lower concentration of Na^+ ion and a higher concentration of K^+ ion are observed, respectively, in the extracellular surrounding medium. These ion concentrations are maintained by the primary active transport pumps in the plasma membrane which is known as Na^+/K^+ ATPase pump. This process of moving Na^+ and K^+ ions across the plasma membrane is through an active transport mechanism and requires energy which is derived from the hydrolysis of ATP. The Na^+/K^+ ATPases involve the transfer of three Na^+ ions outside and two K^+ ions inside through the plasma membrane, and this unbalanced charge transfer contributes toward the maintenance and separation of charge across the plasma membrane. This pump also plays an important role in the action potential in

nerve cells. This pump also known as P-type ATPase as the phosphorylation of ATP is an important stem and leads to the conformational change of its structural units. This Na^+/K^+ ATPase pump also turns out to be an integral part of membrane protein and consists of two subunits spanning the membrane. The detailed mechanism for this Na^+/K^+ ATPase is still under debate; however, the current working model indicates two different conformations during the entire cycle of events. The conformation I is the dephosphorylation state with high affinity for Na^+ ion and low affinity for K^+, while the conformation II is the phosphorylated state with high affinity for K^+ ion while low affinity for Na^+ ion. The entire mechanism is electrogenic and creates a net separation of charge across the membrane as there is transfer of three Na^+ ions outside with respect to inner transfer of two K^+ ions. This results in the transmembrane potential of -50 to -70 mV, where the inside potential is negative with respect to outside and is essential for the conduction of action potential, especially in neuron cells. This mechanism of transferring the Na^+/K^+ ion across the membrane is an essential functioning of the cell, and almost 25% of the energy-yielding metabolism in human at rest is associated with these Na^+/k^+ ATPase functioning. The plasma membrane also contains different types of transmembrane protein channels that transfer Ca^{2+} ion into the cells. Two different systems for this Ca^{2+} transfer are Na^+/Ca^{2+} exchanger (NCX) with low affinity but with high capacity for Na^+ and Ca^{2+} ion transfer. Another one is the plasma membrane Ca^{2+} pump (PMCA), which is a high-affinity and low-capacity pump. Both of these transmembrane protein channel abundance vary with the cell types with NCX being highly abundant in the neuron and cardiac cells, i.e., excitable cell types. These pumps are being regulated through voltage gating or ligand-based interaction and also through the emptying of intracellular stores and allowing limited Ca^{2+} ion entry to the cell and transmitting the signals toward designated targets. Thus, this Ca^{2+} transient must be dissipated with its extrusion from the cell and is mediated by NCX and PMCA channels. Sarco-endoplasmic reticulum calcium pump (SERCA) found in the endoplasmic reticulum of skeletal muscle cells restores the basal level by sequestration of Ca^{2+} into the ER and into the mitochondria by the uniporter pumps. Overall in plasma membrane protein content, the PMCA pump has a very minor component in quantitative manner, and it is outnumbered by the NCX pump especially in excitable tissues. The PMCA pump is a fine-tuner of Ca^{2+} ion in the cytoplasm and even operates at the very low concentration. This PMCA pump was discovered by Schatzmann in 1966 in erythrocytes and was further characterized in numerous other cell types. Its purification and cloning studies revealed that it has the similar membrane topology of sarco-endoplasmic reticulum calcium (SERCA) pump found in the endoplasmic reticulum of skeletal muscle cells. Based on the SERCA template and with the help of molecular modeling work, the structural details were revealed with almost ten transmembrane domains with a large cytosolic head further being divided into three different components, i.e., A, N, and P domain, which are essential for functional activity. Overall, in the mammalian system, these PMCA pumps located onto the plasma membrane extrude the Ca^{2+} ion from the cells, while the SERCA pump sequesters these Ca^{2+} ions back into the intracellular organelle. Also there exist

several genes encoding these pumps, and for PMCA, four isoforms exist named PMCA1–PMCA4, which are based on their specific location within a cellular system. PMCA1 is distributed ubiquitously in cells and tissues and is one of the most abundant isoform. PMCA2 and PMCA3 are majorly abundant in the central nervous system; however, they are localized differently. PMCA2 is major component in Purkinje neurons, while PMCA3 is found abundantly in the cerebral cortex region. PMCA4 is distributed ubiquitously in cells and tissues and is around 80% of plasma membrane in erythrocytes.

7.4.6 Role of Ion Channels in Cellular Function

As discussed earlier, the ion channels facilitate the diffusion of different hydrophilic charged molecules and ions across the biological membranes. Ion channels are selective to specific ion and mediate very rapid flow of particular ions from high to low concentration, thus assist in the maintenance of cellular ionic equilibrium. Many of these ion channels respond to the extra- or intracellular signals by gating their opening, performing an important role in biology. The function of ion channels is essential for virtually all life processes including contraction-relaxation of excitable cells like skeletal and cardiac muscles, neural excitation, cell-cell communication, cell proliferation, and inflammation. A universal function of ion channels is to establish the resting membrane potentials in all cell types. Few of the examples are:

- Role of ion channels is well defined in conduction of impulse across motor neuron. K^+-channel with Na^+/K^+ pump (ATPase) establishes the resting membrane potential in the nerve cells, whereas Na^+-channel serves as the propagator of nerve impulse across the axon of the neuron. Voltage-gated Ca^{2+}-channels at the neuromuscular junction mediate release of acetylcholine leading to activation of the muscle. Acetylcholine (ligand)-gated channels on the muscle plasma membrane at the neuromuscular junction start depolarization of the muscle membrane. Further, Ca^{2+}-release channel located on the sarcoplasmic reticulum (ER of the muscle) initiates the muscle contraction process.
- In the gut and kidney, ion channels help in the maintenance of ionic polarity of the cell assisting in absorption of ions. In the stomach, K^+-channel helps in acid secretion by parietal cells in the gastric mucosa. In epithelial cells of the small intestine, K^+-channels are involved in ion uptake processes across the plasma membrane and also cell volume regulation. In the colonic epithelial cells, K^+-channels are engaged in maintenance of salt and water balance including secretory and reabsorptive processes. Na^+-channels (the isoform is called SCN3B) are found in the kidney and are important for maintenance of Na^+ level in the body. In addition, the kidney expresses another interesting channel called "aquaporin" which is highly permeable to water and plays a vital role in water reabsorption and regulation of urine volume.

- Unique sets of ion channels (K^+, Ca^{2+}, and Cl^-) are found to be involved in the activity of several types of immune cells. These channels are also involved in T-cell activation as well as its cell volume regulation. In lymphocytes, Cl^- channels trigger the homeostatic volume regulatory pathways which restore the cell to its normal following exposure to a dilute medium. Recent studies show that ion channels control a variety of physiological signaling events in the immune cells including gene expression, secretion of cytokines and chemokines mediating cell communication, cell migration, proliferation, and apoptosis.
- By regulating cytosolic Ca^{2+} concentration via release of Ca^{2+} from intracellular organelle, the Ca^{2+}-ion channels even regulate gene expression in many cells. Inositol 1,4,5-trisphosphate (IP3) receptor in non-excitable cells and ryanodine receptor (RyR) in excitable cells have been well established to release Ca^{2+} to the cytosol from the ER or SR, respectively, leading to alteration of gene expression.

7.5   Physiological and Metabolic Implications of Ion Pumps and Channels

In most cellular processes, ion pumps and channels are recruited for opposite functions, due to the fact that pumps drive ion flow uphill, whereas channels drive downhill the concentration gradient. For example, while K^+-pump on the plasma membrane facilitate movement of K^+ into the cytosol, K^+-channel drives extrusion of K^+ out of the cell. In the previous section, we have discussed that various membrane channels play in almost all the biological functions. In the recent years, there have been several disorders that have been linked to ion channels. These include cystic fibrosis, long QT syndrome, epilepsy, malignant hyperthermia, Bartter's syndrome, heart arrhythmia, diabetes, hyperinsulinemic hypoglycemia of infancy (HHI), familial hemiplegic migraine, episodic ataxia, myotonia, Dent's disease, congenital myasthenia, myasthenia gravis, hyperekplexia, polycystic kidney disease (PKD), Alzheimer's disease, Huntington's disease, and nephrolithiasis. Research in the last few decades has suggested role of ion channels in diabetes. Abnormalities of insulin secretion occur in many people with diabetes. K^+ and Ca^{2+} channels also play a role in the secretion of insulin in the beta cells of the pancreas. Altered function of these channels has been found in people with diabetes, suggesting a close link between ion channels and diabetes.

Ion pumps play an equally important role in cellular physiology and overall biological processes just as the ion channels. Na^+/K^+ ATPases play numerous roles including maintenance of high concentration of Na^+ outside and K^+ inside the cell. In all the cells, Na^+/K^+ ATPase helps in the maintenance of cell volume. In nerve and muscle cells, it aids the smooth propagation of electrical signal throughout the tissue. Ca^{2+}-pump in the muscle (both cardiac and skeletal) is the main mediator of the contraction-relaxation coupling which is essential for muscle activity. Mutations in Ca^{2+}-pump lead to diseases in humans including Brody's disease and Darier's disease. Similarly, alteration in its expression and activity has been

observed during several cardiovascular disorders. The H^+/K^+ ATPase in the gastric wall is the basis for secreting hydrochloric acid in the stomach. It is also expressed in late distal tubules and collecting ducts in the kidneys that mediate elimination of excess hydrogen ions from the body fluids.

Metabolic Implication Recent research has suggested that ion channels and pumps are involved in regulation of the whole-body energy demand and so metabolism. This is because maintenance of constant ion gradient across the membrane is a highly energy-demanding process utilizing ATP by the ion pumps. Most of the ion channels are leaky, meaning releasing some ions just due to high gradient. This activates the ATP-utilizing ion pumps. This leak-restabilization process is often a contributor to the basal metabolism of the individual. But during pathological situations, this process is differentially recruited leading to alteration in ATP usage, thereby affecting metabolic status of the individual which may lead toward a particular disease condition. It has been shown that mutation in proteins (like RyR, calsequestrin) of Ca^{2+}-releasing units in the skeletal muscle leads to metabolic diseases like malignant hyperthermia. Some studies have shown that SERCA-based ATP utilization by its regulators (like sarcolipin and phospholamban) has metabolic implication. Sarcolipin has been demonstrated to increase ATP utilization by SERCA leading to increase in the metabolic rate, and loss of this protein leads to diet-induced obesity and diabetes. These recent observations have excited the field of research. Further research defining the regulatory pathway will unravel the targets to utilize this mechanism to develop pharmaceuticals to increase energy expenditure, thereby providing protection against obesity and its associated metabolic disorders such as diabetes and muscle weakness.

Suggested Reading

Books and Book Chapters

Brett CMA, Oliveira Brett AM (1993) Electrochemistry. Principles, methods, and applications. Oxford university press, Oxford/New York/Tokyo

Einstein A (1956) Investigations on the theory of Brownian movement. Dover, New York

Glaser R (2001) Biophysics. Springer, Berlin/Heidelberg/New York

Hille B (2001) Ion channels of excitable membranes, 3rd edn. Sinauer, Sunderland

Takashima S (1989) Electrical properties of biopolymers and cell membranes. Adam Hilger, Bristol

Research Article

Ashcroft RG, Coster HGL, Smith JR (1981) The molecular organisation of bimolecular lipid membranes. The dielectric structure of the hydrophilic/hydrophobic interface. Biochim Biophys Acta 643(1):191–204

Bangham AD (1972) Lipid bilayers and biomembranes. Annu Rev Biochem 41:753–776

Benz R, Janko K (1976) Voltage-induced capacitance relaxation of lipid bilayer membranes. Effects of membrane composition. Biochim Biophys Acta 455:721

Branton D (1971) Freeze-etching studies of membrane structure. Philos Trans R Soc Lond Ser B Biol Sci 261(837):133–138

Bretscher MS (1972) Membrane structure: some general principals. Science 181:622–829

Bristol White SH (1973) The surface charge and double layers of thin lipid films formed from neutral lipids. Biochim Biophys Acta 323:343

Brochard F, de Gennes PG, Pfeuty P (1976) Surface tension and deformations of membrane structures. J Phys 37:1099–1104

Brown R (1828) A brief account of microscopical observations made in the months of June, July and August, 1827, on the particles contained in the pollen of plants; and on the general existence of active molecules in organic and inorganic bodies. Phil Mag 4:161–173

Chapman D, Gómez-Fernández JC, Goñi FM (1979a) Intrinsic protein–lipid interactions: physical and biochemical evidence. FEBS Lett 98(2):211–223

Danielli JF, Davson HJ (1935) A contribution to the theory of permeability of thin films. Cell Comp Physiol 5:495–508

de Gennes PG, Papoular M 1969 Volume jubilaire en l'honneurde A. Kastler. PUF, Paris

Edidin M (1974) Rotational and translational diffusion in membranes. Annu Rev Biophys Bioeng 3:179–201

Engelman DM (2005) Membranes are more mosaic than fluid. Nature 438(7068):578–580

Israelachvili JN, Mitchell DJ, Ninham BW (1977) Theory of self-assembly of lipid bilayers and vesicles. Biochim Biophys Acta 470:185–201

Jahnig F (1984) Lipid exchange between membranes. Biophys J 46:687–694

Nagle JF (1980) Theory of the main lipid bilayer phase transition. Ann Rev Phys Chem 31:157–195

Nicolson GL, Ash ME (2014) Lipid replacement therapy: a natural medicine approach to replacing damaged lipids in cellular membranes and organelles and restoring function. Biochim Biophys Acta 1838(6):1657–1679

RaziNaqvi K, Rodriguez JG, Cherry RJ, Chapman D (1973) Spectroscopic technique for studying protein rotation in membranes. Nat New Biol 245(147):249–251

Robertson JD (1959) The ultrastructure of cell membranes and their derivatives. Biochem Soc Symp 16:3–43

Singer SJ, Nicolson GL (1972) The fluid mosaic model of the structure of cell membranes. Science 175(4023):720–731

Tanford C (1979) Hydrostatic pressure in small phospholipid vesicles. Proc Natl Acad Sci U S A 76:3318–3319

Techniques in Biophysics

8

Vijay Kumar Srivastava

Abstract

The present chapter provides an understanding of the different techniques used in the field of biophysics. It includes UV–visible spectroscopy, circular dichroism (CD), nuclear magnetic resonance (NMR), X-ray crystallography, isothermal titration calorimetry (ITC), differential scanning calorimetry (DSC), fluorescence spectroscopy and optical rotatory dispersion (ORD). The UV–visible spectroscopy and fluorescence spectroscopy characterize the protein on the basis of their intrinsic as well as extrinsic properties. In addition to that ITC, ORD and DSC are a thermo-analytical technique that is based on the enthalpy, entropy and Gibbs free energy. CD spectroscopy is widely used to determine the protein fold, secondary and tertiary structures of protein. The more advanced technique to know the residue-specific information at the three-dimensional level is X-ray crystallography and NMR. These techniques have widespread usage in structure-based drug design in the pharmaceutical industry.

8.1 Structural Analysis by UV–VIS Spectroscopy

It is a method to determine the correlation between the particle and electromagnetic radiation. The light energy in the near-ultraviolet (UV) and visible (Vis) spectral region is approximately 150–400 kJ/mol. It is used to excite electrons from their ground state to higher energy states. Light absorption by molecules is monitored as

V.K. Srivastava (✉)
Indian Institute of Science Education and Research, Bhopal 462066, India
e-mail: vijaytechno@gmail.com

a function of frequency or wavelength generating an absorption spectrum. Particles with electrons in the delocalized aromatic systems frequently absorb light in the visible (400–800 nm) or near-UV (150–400 nm) region. Absorption spectroscopy is normally executed with particles suspended in liquid buffers. The solute absorbance shares a direct proportional relationship with its concentration contributing towards quantitative measurements. Molecular absorbance is dependent on various parameters such as on wavelength, chemical nature and molecular environment of the chromophores. Thus, absorption spectroscopy is a magnificent technique for studying various interactions involving ligands, enzyme catalysis and conformational changes in macromolecules (proteins and nucleic acids) on ligand binding. The nondestructive nature of the technique with high sensitivity makes it more useful for the analysis of even small quantity of samples (Cantor and Schimmel 1980).

8.1.1   Principle of Ultraviolet–Visible Absorption

It attributes to absorption in the UV–Vis spectral region. The principle behind the UV–visible spectrophotometer is the study of the interdependence between the radiation and matter which generates the transitions in the electrons present in an atom from its lower energetic, m, to a higher level, l, leading to absorption of energy from the atom equivalent to the energy difference between both the levels, $E_l - E_m$ (Fig. 8.1).

The change in energy level because of electronic transitions when plotted as a function of radiation wavelength generates the spectrum that provides knowledge about the energy difference associated with each electronic transition. Based on the wavelength of the incident radiation, there are different types of spectroscopy showed in Table 8.1.

It is most commonly implied in physical and analytical chemistry for molecule identification based on their emission or absorption spectrum (Skoog et al. 2007). The fundamental principle behind the technique is the Lambert–Beer law that determines the concentration of a given species.

Lambert–Beer Law
It defines the linear relationship between absorbance and concentration of an absorbing species. Experimental measurements are normally identified in terms of transmittance (T), which is represented as:

$$\log T = \log I/I_0 = \epsilon \mathrm{lc}$$

The incident and the transmitted beams are I and I_0, respectively. Transmission is related to absorbance (λ) as follows:
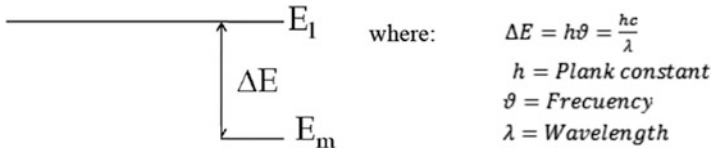
Fig. 8.1 Transition of energy from (m) to (l) (Skoog et al. 2007)

Table 8.1 Knowledge about the most external electrons atomic transition (Skoog et al. 2007)

$$A = -\log T$$

Lambert–Beer equation can be written as:

$$A = \epsilon l c$$

Experimental determination of transmittance is therefore possible using spectrometer. If the path length 'l', molar absorptive 'ϵ' and the absorbance 'A' are known, concentration of the substance 'c' can be measured. In a given set of experiment, both the parameters are fixed, so a straight line is generated on plotting the sample absorbance against the concentration of the absorbing substance. In general, a calibration curve can be calculated by drawing a graph with the measured absorbance values of a series of standard samples against their respective concentrations (Brown 1980).

Instrumentation Device measures light intensity as a function of wavelength. The essential component of a spectrophotometer is a light source, a sample holder, a monochromator for the separation of different light wavelengths and a detector (Fig. 8.2).

The tungsten filament (300–2500 nm) is most commonly used as a radiation source. The more frequently used visible wavelength is light emitting diodes (LED) and Xenon Arc Lamps. The detector is regularly a photodiode or a CCD, used with monochromators that allow the passage of a single wavelength of light to reach the detector. Diffraction beam splitter is associated with CCDs that help in the collection of light with different wavelengths on different pixels. A spectrophotometer
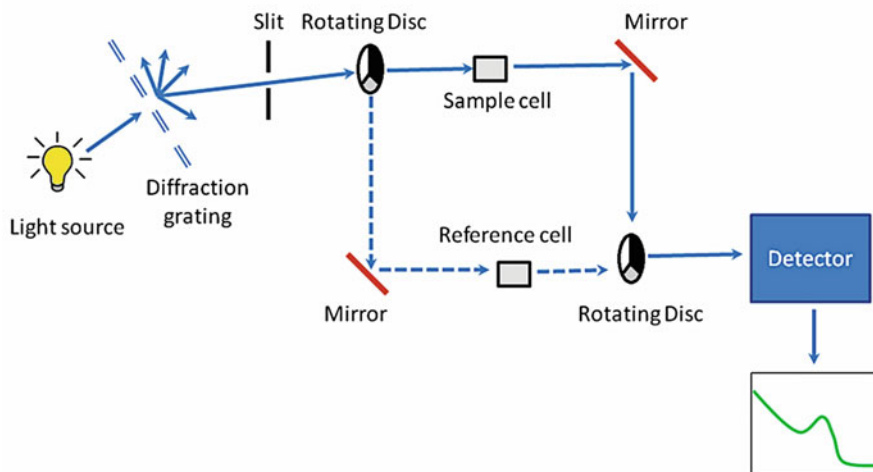
Fig. 8.2 Double beam UV–Vis spectrophotometer (Harris and Bashford 1987)

can be a single beam or double beam. In a single beam spectrophotometer, the complete light passes through the same sample cell. Reference *Io (usually solvent)* is measured before the sample. Double beam UV spectrophotometer is more commonly used in research nowadays (Harris and Bashford 1987). In this instrument, light is split into two beams before it reaches the sample. One beam is used for the reference cell and the other one for the sample cell. The reading for the reference and the sample is detected at the same time. Liquids are the most common samples used in UV/Vis spectrophotometer. Samples are placed in rectangular-shape cuvettes (made of either fused silica or quartz) with an internal width of 1 cm referred to as the path length, *l*, in the Lambert–Beer law. Glass and plastic cuvettes absorb in the UV range limiting their use for research purposes (Gore 2000).

8.1.2 Applications

It helps in the quantitative determination of various analytes, like transition metal ions, biological macromolecules and other conjugated organic compounds.

Recent Advancement in Ultraviolet–Visible Spectroscopy
Over the past few years, there is the development of many new techniques such as:

- Dual-wavelength spectroscopy
- Derivative spectroscopy
- Reflection spectroscopy

- Photoacoustic spectroscopy
- Photoluminescence spectroscopy
- Variable wavelength detectors for chromatography and enzyme kinetics studies

8.2   Circular Dichroism

8.2.1   Principle

The differential absorption of the right circularly polarized light (RCPL) and the left circularly polarized light (LCPL) components due to the presence of the chiral centres in the sample under study is responsible for the circular dichroism phenomenon (Atkins and Paula 2005, Solomon and Lever 2006). The spectra can be recorded at various wavelengths. Samples varying in shapes and sizes (including macromolecules) but containing chiral centre can be studied.

This technique is extensively used for studying protein conformation (both secondary and tertiary structures). CD spectrum is affected by changes in the sample environment, temperature, pH and ligand binding, proving it to be a useful technique for studying the effect of these conditions on the secondary structure (Nakanishi et al. 1994, Solomon et al. 2007 and Solomon and Lever 2006).

Electromagnetic radiation is a transverse wave consisting of an electric (E) and magnetic (B) field component oscillating perpendicular to each other (Rodger and Nordén 1997). Oscillation of electric field vector in one plane with changes only in magnitude produces linearly polarized light. On the other hand, circularly polarized light is the result of electric field vector rotating in the direction of propagation maintaining a constant magnitude (Fig. 8.3). Circularly polarized vector makes a circle over one period of the wave frequency at a particular space point. The behaviour of the electric vectors at a particular time point for different positions is shown below in Fig. 8.3 for both the linear and circularly polarized components of light. Circularly polarized electric vector follows a helical path along the direction of propagation (k). LCP electric vector exhibits counter clockwise rotation with propagation towards the observer unlike the RCP showing clockwise rotation (Solomon and Lever 2006).

Interaction of Circularly Polarized Light with Matter
CD instruments (also named as spectropolarimeters) measure the difference in absorbance between the L and R circularly polarized components ($\Delta A = A_L - A_R$) reported in terms of the ellipticity (θ) in degrees (Nakanishi et al. 1994). The electric field of a light beam causes a linear charge displacement on interaction with an electric dipole, while its magnetic field causes charge circulation (magnetic dipole). Both these dipoles cause electron excitation in a helical fashion including rotation, translation and their associated operators. The relationship between the sample's rotational strength (R) and the $\Delta\varepsilon$ is established as shown (Nakanishi et al. 1994):
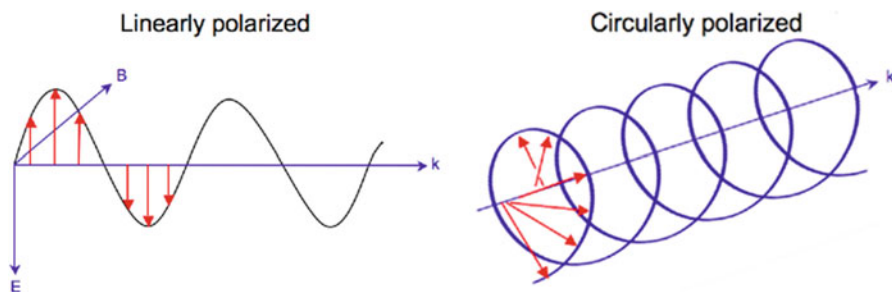
Fig. 8.3 Linear and circularly polarized light (Solomon and Lever 2006)

$$R_{\text{exp}} = \frac{3hc10^3 \ln(10)}{32\pi^3 N_A} \int \frac{\Delta\varepsilon}{v} \, dv$$

Theoretically, the rotational strength is determined as follows:

$$R_{\text{theo}} = \frac{1}{2mc} \text{Im} \int \Psi_g \widehat{M}_{(\text{elec.dipole})} \Psi_e d\tau \cdot \int \Psi_g \widehat{M}_{(\text{mag.dipole})} \Psi_e d\tau$$

The above two mathematical equations indicate that transformation of the electric and magnetic dipole moment components as the same irreducible representation results in non-zero $\Delta\varepsilon$ values. It can occur only at the Cn and Dn point groups, and it makes only chiral molecules optically active.

The circularly polarized light itself is 'chiral'; it differentially interacts with chiral molecules. In a CD experiment, the chiral sample is exposed with equal amounts of left and right circularly polarized light. The CD spectrum of the sample is produced because one of the components of the polarized light is absorbed more, than the other one resulting in characteristic CD spectrum (Solomon and Lever 2006). The interaction with the molecule causes the electric field to trace out an elliptical path. The ellipticity (θ) values are recorded. Symmetrical chirality of molecules is more important than the structural. CD spectra of any given protein/DNA sample are sensitive to its conformation.

Delta Absorbance
It is represented as:

$$\Delta A = A_L - A_R$$

ΔA (delta absorbance) is the difference between LCP and RCP light absorbances. ΔA is a function of wavelength, so knowledge of wavelength at which the experiment is performed is crucial (Rodger and Nordén 1997).

Molar Circular Dichroism
Beer's law depicts molar circular dichroism as below:

$$\Delta A = (\varepsilon_L - \varepsilon_R)C\,l$$

Here, ε_L and ε_R are the molar extinction coefficients for LCP and RCP light, C is the molar concentration and l is the path length in centimetres (cm).

$\Delta\varepsilon = \varepsilon_L - \varepsilon_R$ is the molar circular dichroism. The CD is the intrinsic property of any molecule. It is a function of wavelength (Rodger and Nordén 1997).

Extrinsic Effects on Circular Dichroism
The CD signals are very low in most of the biological samples, so in order to get the significant data, one has to pay considerable attention to the experimental conditions. The ellipticity range generally lies near to 10 mdeg.

Molar Ellipticity (θ)
By taking into consideration the cell path length and compound concentration (c), we can reach at a molar circular dichroism ($\Delta\varepsilon$).

$$\Delta\varepsilon = \varepsilon LCP - \varepsilon RCP = \Delta A/(C \times 1)$$

where εLCP and εRCP are the molar extinction coefficients for LCP and RCP light, respectively, C = molar concentration and l = path length in centimetres. The equation given below can be used for the interconversion of the molar circular dichroism and molar ellipticity, [θ] (Dodero et al. 2011).

$$[\theta] = 3298.2\,\Delta\varepsilon$$

The above equation was obtained by describing the ellipticity of the polarization as:

$$\tan\theta = E_{R-}E_{L/}E_{R+}E_L$$

where E_R and E_L resemble to the magnitudes of the electric fieldvectors of RCP and LCP, respectively.

When $E_R = E_L$, the θ is 0° and the light is linearly polarized. The θ become 45° when either E_R or E_L = to zero (Fig. 8.4).

Applications

- It is routinely used in the industry to know the effects of manufacturing, formulation, storage conditions on protein configuration and stability.
- The far UV range is used in CD to identify the percentage of different types of secondary structures in a protein (Dodero et al. 2011, Whitmore and Wallace 2008, Greenfield 2006).
- The tertiary structure of the protein can be measured in the near-UV CD spectrum (>250 nm).
- Changes in thermal stability of proteins/peptides on interaction with various ligands can be studied (Misra and Ramachandran 2009).
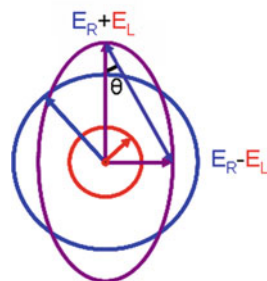
Recent Advancement in CD Spectroscopy The synchrotron radiation circular dichroism (SRCD) is a new advancement in the technique of CD (Sutherland et al. 1980, Snyder and Rowe. 1980 and Wallace 2000) that dates back to 20 years before (Sutherland et al. 1980, Snyder and Rowe 1980). The SRCD is helpful in studying the biological samples in more detail (Miles and Wallace. 2006). It was further refined with advancement in instrumentation and cross calibration (Miles et al. 2003, Miles et al. 2005) and enabling methods for study and interpretation of the results (Lees et al. 2004, Whitmore and Wallace 2004, Lees et al. 2006). SRCD in comparison to conventional CD is more advantageous as it provides finer details of the biological samples (Wallace and Janes. 2001).

8.3 NMR

8.3.1 Theoretical Principles of NMR

NMR stands for nuclear magnetic resonance: N (nuclear) is the magnetic moment of nucleus which is responsible for precision frequency, M (magnetic), because it involves the presence of external magnetic field, R (resonance) which is the resonance between the radio waves and nucleus which is responsible for signal or absorbance in this technique (Rabi et al. 1938).

Nuclear magnetic resonance results on placing the nuclei of atoms having spinning potential in a static magnetic field and exposed to a second oscillating magnetic field. The study of this resonance for inferring the structural, physical, chemical and biological properties of the molecules is known as NMR spectroscopy. NMR spectroscopy was based on the spin property of nuclei; hence it is very important to understand the spin.

The Basis of NMR
NMR is based on the principle that there is electric charge associated with all nuclei providing a spin to many nuclei. On the application of external magnetic field, an energy transfer takes place at a wavelength corresponding to the radio frequencies, resulting in the spin transfer from the base energy to a higher energy level. Return of
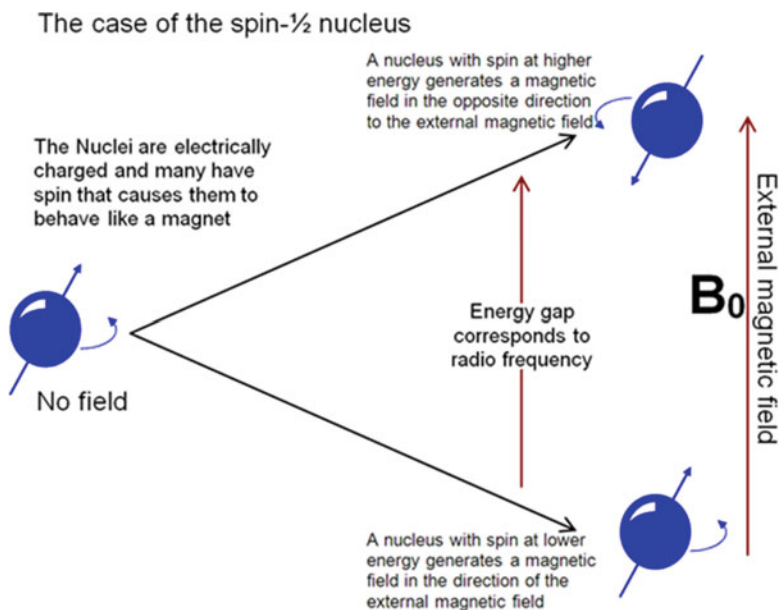
The case of the spin-½ nucleus

The Nuclei are electrically charged and many have spin that causes them to behave like a magnet

No field

A nucleus with spin at higher energy generates a magnetic field in the opposite direction to the external magnetic field

Energy gap corresponds to radio frequency

A nucleus with spin at lower energy generates a magnetic field in the direction of the external magnetic field

External magnetic field

B_0

Fig. 8.5 The basis of NMR (Source: http://chem.ch.huji.ac.il/nmr/whatis-nmr/whatisnmr.html)

the spin to its ground state causes energy emission at the same frequency (Galya and Rudnick 1988).

There are several ways to identify the signal that matches this transfer which is further processed to yield an NMR spectrum characteristic for the concerned nucleus (Fig. 8.5).

In simple words, NMR is the study of a molecule by the interaction of radio waves with the molecule placed in a high magnetic field. Nuclei are always in two states, α and β state at resonance, where α state absorbs energy and flips into β state. The difference of the energy in the two states is directly proportional to the external magnetic field. If the population of the nuclei in α and β state is equal, then there will be no NMR signal. Then β state relaxes back to α state by:

1. Spin–spin relaxation (T_2): energy transfer to the nearest nucleus
2. Spin–lattice relaxation (T_1): energy transfer to the surrounding

These relaxations produce decaying peak pattern which is after Fourier transformation converted into NMR signal (Fig. 8.6). The signal intensity relies on the population difference between α and β state which is further dependent upon the external magnetic field. This considers strong external magnetic field that produces a good NMR signal (Pranitha et al. 2011).

The accurate resonance frequency associated with energy transition relies on the effective magnetic field at the nucleus. The magnetic field is influenced by electron shielding that depends on the nuclei's chemical environment. Consequently,
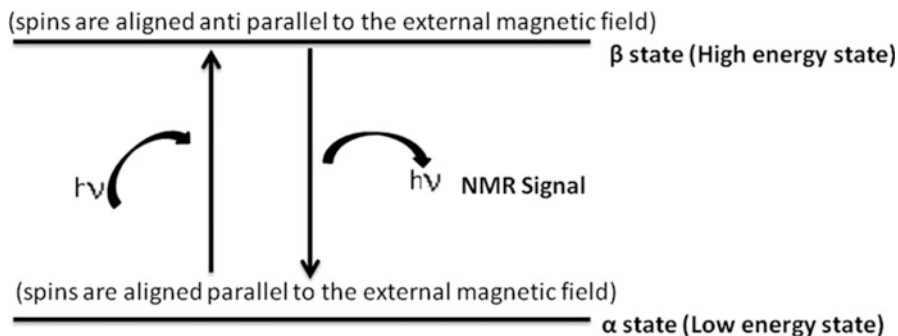
(spins are aligned anti parallel to the external magnetic field)

β state (High energy state)

hν

hν   NMR Signal

(spins are aligned parallel to the external magnetic field)

α state (Low energy state)

Fig. 8.6 Schematic representation of basis of generation of NMR signal chemical shift (Pranitha et al. 2011)

knowledge about the nucleus' chemical environment can be determined from its resonant frequency. The shift in the resonance due to the chemical environment is known as chemical shift (Cavanagh et al. 1996). Usually the resonant frequency is higher when the nucleus is more electronegative.

$$\delta = (\nu - \nu_0)/\nu_0$$

where:

δ = Chemical shift
ν = Magnetic field producing resonance per sample
ν_0 = Magnetic field producing resonance per reference

Chemical shift is independent of the magnetic field and is denoted in ppm. Tetramethylsilane is used as a reference (TMS). It is set to ν_0, thereby rendering a chemical shift of zero.

Spin–Spin Coupling
Orientation of neighbouring nuclei affects the effective magnetic field. This phenomenon is referred to as spin–spin coupling. It helps in understanding the atomic connections in a molecule. Nuclei experiencing the same chemical environment or chemical shift are called equivalent and others nonequivalent. Neighbouring nuclei exert a profound impact on each other's powerful magnetic field as visualized clearly in the NMR spectrum of nonequivalent nuclei. Distance between nonequivalent nuclei should be less than or equal to three bond lengths, to observe spin–spin coupling or J coupling. It occurs due to the mutual interaction of valence electrons of one nucleus with the proton of second nucleus and vice versa. This leads to the spin–spin splitting which was measured by looking at the peak of NMR (James and Oppenheimer 1994) Fig. 8.7.

For example, ethyl alcohol proton spectrum occurs when the methyl group splits to generate a *triplet* with an intensity ratio of 1:2:1 due to the presence of two

Fig. 8.7 Spin–spin coupling
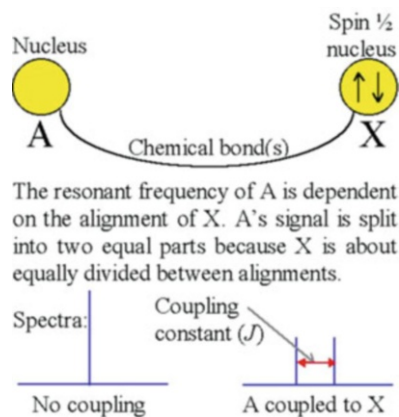
neighbouring CH_2 protons. On the same lines, the CH_2 is split into a *quartet* with an intensity ratio of 1:3:3:1 by the three neighbouring CH_3 protons. Principally, the two CH_2 protons will also divide again into a *doublet* to form a *doublet of quartets* by the hydroxyl proton, but this intermolecular exchange of the acidic hydroxyl proton causes loss of coupling information (Fig. 8.8).

Coupling Constant (J)
Coupling constant is the magnitude of the splitting effect, and it is measured by taking distances between peaks of multiples. The splitting size does not depend on the magnetic field and is measured as an absolute frequency (in hertz). Chemically bonded nuclei in the neighbourhood of the target nucleus can be identified using the splitting number (Blake et al. 1992).

8.3.2 Applications

- It is commonly known to study the three-dimensional structure of biomolecules in solution form.
- It is used to study interaction of macromolecules with ligands.
- It can be used to distinguish the cis and trans isoforms.
- It is used to study dynamics of protein folding.

Recent Advancement in NMR NMR spectroscopy continues to be an advance field in the structural determination of the proteins. Recent improvements in gradient technology and coupling the NMR techniques to different kinds of chromatographic methods will provide a new break in the process of drug discovery. These opportunities help in determining the receptor-bound conformations of small organic ligands (Hicks 2001).
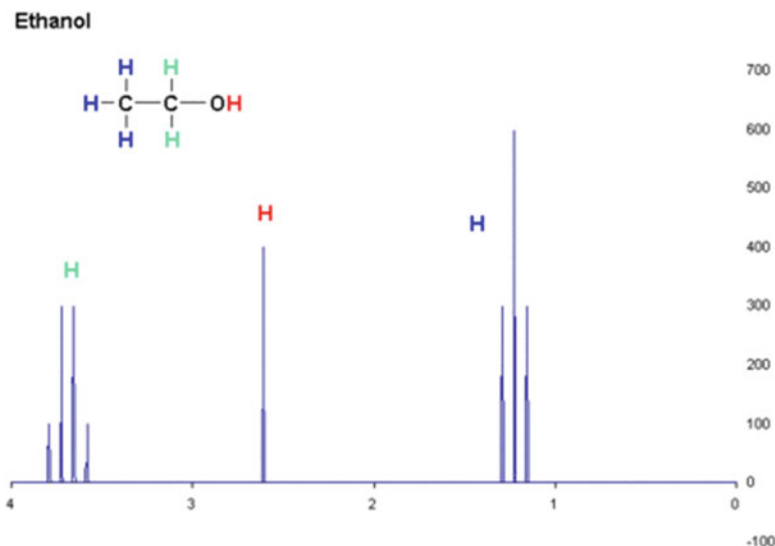
Fig. 8.8 Coupling information (Blake et al. 1992)

8.4   X-Ray Crystallography

8.4.1   Scientific History of Crystals and X-Rays

The first account of crystal symmetry in history comes across in the seventeenth century when Johannes Kepler put forward a hypothesis related to the hexagonal symmetry of snowflake crystals attributing to the regular packing of spherical water particles in his research work *Strena seu de Nive Sexangula* in 1611 (Kepler 1611).

The crystal symmetry was explored for the first time by Danish scientist Nicolas Steno in 1669. Steno showed that the angles between the faces are the same in each copy of a particular type of crystal (Steno 1669). Further René Just Haüy (1784) identified that each crystal face can be explained with the help of stacking patterns formed by the blocks of similar shape and size. Later on for identifying crystal faces, the term Miller indices was introduced by William Hallowes Miller in 1839. Haüy's study showed that crystals are made up of a single unit cell which is repeated several times in a three-dimensional space. In the nineteenth century, all the possible symmetries of a crystal was studied out by Johan Hessel, Auguste Bravais, Evgraf Fedorov, Arthur Schoenflies and William Barlow (1894). Barlow used all the available data and proposed several crystal structures in the 1880s that were validated later by X-ray crystallography (Barlow 1883). William Barlow's data in 1880s was too limited to accept his models as conclusive. The technique determined the position of hydrogen bonds (1) connecting the water molecules in ice (Fig. 8.9).

Fig. 8.9 X-ray crystallography determination of arrangement of water molecules in ice, revealing the hydrogen bonds (1) (Available at https://en.wikipedia.org/wiki/X-ray_crystallography)
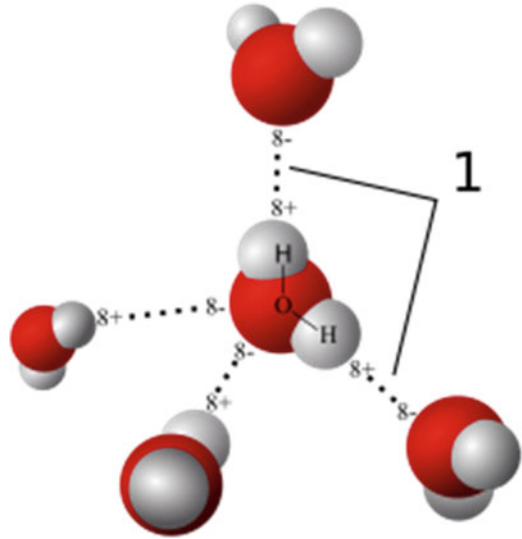
Scottish physicist James Clerk Maxwell predicted the existence of electromagnetic radiation that was accepted among scientists. The X-ray was discovered in 1895 by Wilhelm Roentgen. The nature of X-rays was uncertain, but soon physicists identified that X-rays were waves of electromagnetic radiation. Further, the experiments performed by Charles Glover Barkla identified the concept of transverse polarization. Single-slit experiments performed in the lab of Arnold Sommerfeld identified that X-rays had a wavelength of approximately 1 Å. Albert Einstein in 1905 introduced the photon concept but it was not broadly accepted. Later on in 1922 Arthur Compton confirmed the photon concept given by Albert Einstein by the scattering of X-rays from the electrons (Compton 1923). The X-rays were *not* electromagnetic radiation was argued by William Henry Bragg in 1907 (Bragg 1907, 1908, 1910). In contrast to Bragg's view later on in 1912, Max von Laue confirmed that X-rays were a form of electromagnetic radiation which was accepted by most of the scientist community.

8.4.2   X-Ray Diffraction and Scattering

Regular three-dimensional arrangement of atoms is defined as crystals. These atoms contain electrons that are responsible for scattering of incident X-ray waves. This phenomenon is referred to as elastic scattering with the electrons behaving as the *scatterers*. Destructive interference cancels the scattering effect in most directions, leaving few specific directions where constructive interference occurs as specified by Bragg's law (Fig. 8.10).

The diffraction pattern is produced by the X-rays because their wavelength λ resembles the magnitude (1–100 Å) as the spacing d between the crystal planes.
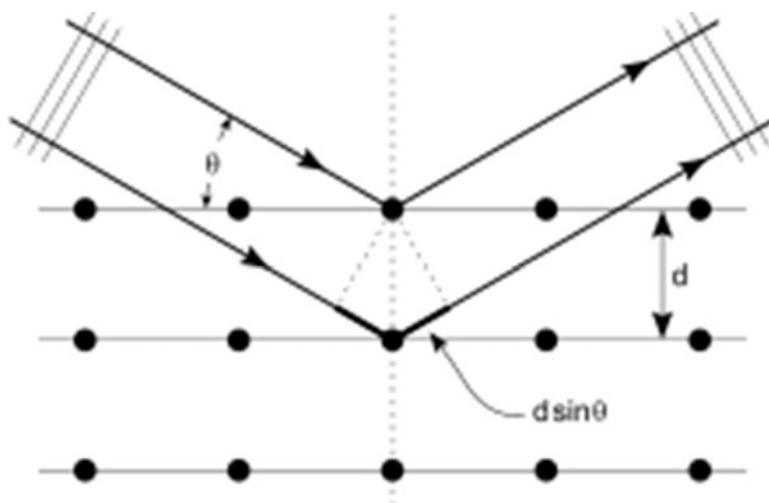
Fig. 8.10 The incident X-rays are scattered by electrons present in different planes. Symmetric arrangement of electrons in planes separated by distance d causes constructive interference where their path length difference 2d sinθ equals an integer multiple of the wavelength λ. Thus, a fraction of the incident beam is deflected by an angle 2θ, producing a reflection spot in the diffraction pattern

Diffraction could result from any wave interacting with a regular array of scatterers provided the spacing between the scatterers matches the wavelength of the incident wave. It was predicted for the first time by Francesco Maria Grimaldi in 1665. In 1821 David Rittenhouse in 1787, and Joseph von Fraunhofer showed the first artificial diffraction gratings for visible light. The idea that crystals could be used as a diffraction grating for X-rays came in 1912 by Paul Peter Ewald and Max von Laue in Munich. Ewald had proposed a resonator model of crystals for his thesis. The model proposed by Ewald could not be validated using visible light, because the wavelength was much larger than the spacing between the resonators. Later on von Laue realized that electromagnetic radiation of a shorter wavelength was needed to observe such small spacing. Further he suggested that X-rays might have a wavelength approximately equal to the unit-cell spacing in the crystals. von Laue worked with his two technicians, Walter Friedrich and his assistant Paul Knipping. They recorded the diffraction of a copper sulphate crystal by X-rays on a photographic plate. Once the photographic plate has been developed, they observed several well-defined circular spots arranged in a pattern of intersecting circles around the spot produced by the central beam. In 1914 von Laue was awarded the Nobel Prize in Physics for a law that connects the scattering angles and the size and orientation of the unit-cell spacing in the crystal (von Laue 1914).

Scattering Electron density within the crystal is responsible for the overall X-ray scattering. High energy of X-rays in comparison to the valence electrons causes

polarization of the scattered radiation. This process is described as Thomson scattering (Guinier 1952).

8.4.3 Crystallization Methods and Data Collection Strategies

Crystallization trials use various methods such as hanging drop and sitting drop vapour diffusion. Initially matrix formulations like those suggested by Jancarik and Kim (1991), Mazeed et al. 2003 and Cudney et al. 1994 will be used. This helps in the evaluation of a large number of combinations involving the pH, additives, precipitant and their ability to promote crystal growth for a given protein. The results of the initial screens are expected to hint at conditions that promote solubility, precipitation or crystal growth. Suitable conditions that give crystal growth obtained from initial matrix screen will be optimized. Parameters like precipitant, salt, protein concentration, pH and ambient temperature will be varied to produce suitable diffraction quality crystals. Details of the few prevalent methods are given below.

Hanging Drop Vapour Diffusion Method It is based on vapour diffusion method where a droplet containing purified protein, buffer and precipitant gradually equilibrates with a larger reservoir containing higher concentration of the similar buffers and precipitants. Initially, the precipitant concentration in the protein droplet is low, but as the water vaporizes from the drop and transfers to the reservoir, the precipitant concentration increases to a level that supports crystallization. Equilibrium status maintains the optimal conditions for crystallization till the completion of the process (Russo et al. 2013). The process is facilitated by making the system closed using high vacuum grease for sealing the space glass surfaces (Fig. 8.11).

Microbatch Oil Method A small drop of protein sample is mixed with the desirable crystallization buffer and pipetted under a layer of oil (paraffin oil, silicone oil or mixture of both) (Russo et al. 2013) so that the sample does not evaporate (Fig. 8.12).

Data Collection For the purpose of data collection, crystal will be mounted on quartz capillary (for room temperature) and/or transferred to harvesting cryosolution and flash-frozen in a liquid nitrogen stream. Protein crystals are picked up by a thin wire mesh containing loop, then flash-frozen with liquid nitrogen to avoid radiation damage on account of exposure to X-rays. It also decreases the noise in the Bragg peaks resulting from the thermal motion of atoms (the Debye–Waller effect) (Jeruzalmi 2006). The protein crystals usually get damaged in the absence of a suitable cryoprotectant (Helliwell 2005).

The capillary or loop with crystal is mounted on a goniometer head, aligned accurately within the X-ray beam and rotated. Kappa goniometers are popular as they can have three angles of rotation: the ω angle that permits rotation about an

Fig. 8.11 Hanging drop
vapour diffusion method
(Available at https://en.
wikipedia.org/wiki/Protein_
crystallization)
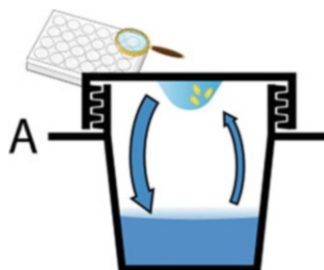
Fig. 8.12 Microbatch oil
method (Available at https://
en.wikipedia.org/wiki/
Protein_crystallization)
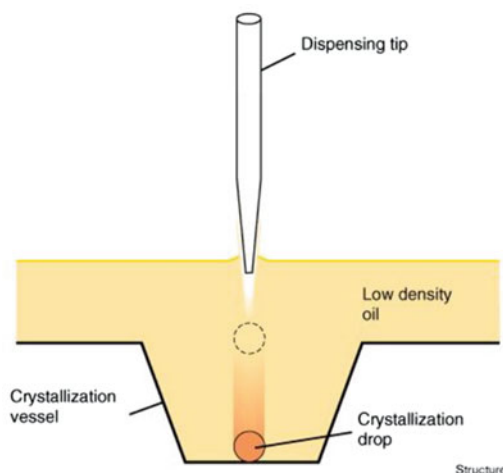
axis perpendicular to the beam, the κ angle that allows rotation about an axis at ~50°
to the ω axis and the φ angle helping in rotation about the loop/capillary axis. When
the value of κ angle becomes zero, it is considered that the ω and φ axes are aligned.
The κ rotation is the convenient method of mounting the crystal on the goniometer.
The oscillations conducted during the data collection as mentioned below take into
consideration only the ω axis (Garman ad Schneider 1997). There are different
types of goniometer, namely, the four-circle and the six-circle goniometer
(Fig. 8.13).

8.4.4 Structure Solution and Refinement

Structure Solution Once the intensity is obtained, the next step is the structure
solution. The structure factor, the square of which is the measured intensity, is a
complex number that consists of the information about the amplitude and the phase
of a wave. Calculation of the electron density distribution inside the crystal requires
both the amplitude F (hkl) and the phase α (hkl), but a diffraction experiment
provides only their magnitude |Fhkl|. The equation for electron density ρ (x, y, z) is
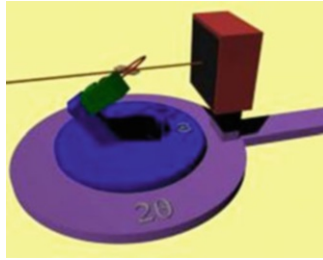
Fig. 8.13 Rotations about each of the four angles φ, κ, ω and 2θ align the crystal in X-ray beam. Position of the detector (*red box*) from the crystal is adjusted for better data resolution. A close positioned detector is useful for higher resolution, whereas the distanced position is required for better discernment of the Bragg peaks (Available at https://en.wikipedia.org/wiki/X-ray_crystallography#cite_note-105)

given by $\rho\,(x, y, z) = 1/V\,\Sigma hkl\,F\,(h\,k\,l)\,\exp.\,[-2\pi i\,(hx + ky + lz) + i\alpha\,(h\,k\,l)]$ where F (h k l) is the structure factor for the corresponding reflection and α (h k l) are the phases for each point xyz, in the unit cell. During a diffraction experiment, the measured quantity is the intensity, and the phase is lost. Initial phases can be estimated in a variety of ways which includes molecular replacement, Ab initio phasing (MAD or SAD phasing), anomalous X-ray scattering and heavy atom phasing (multiple isomorphous replacement).

Molecular Replacement (MR) This method allows the worker to obtain an initial set of phases using a homologous protein with known structure as a search model. The search molecule is further oriented and positioned in the unit cell of the molecule of interest. Thus, the related structure (phasing model) is used to obtain phase information after orienting the model in the unit cell of the protein. The main steps in MR are:

- The rotational search is carried out to know the orientation of the search model in the unknown crystal cell.
- Oriented model is placed in the unit cell relative to the crystallographic symmetry elements (translation search).
- Assessing the quality of the solution in visualization software.

In other words, the problem in molecular replacement is to find the six-dimensional search that includes the three rotational and three translational dimensions, which would place the search model in the unit cell of the crystal. In the first step the rotational parameters used to orient the model to that in the crystal are determined, while in the next step, translation parameters to place the now correctly oriented molecule in the asymmetric unit are calculated. The three-dimensional structure solutions can be obtained from the simple relation.

$$X = [R] \, M + [T]$$

where [R] is the appropriate rotation and [T] the required translation to correctly position the model in the unit cell. There are several programmes which are commonly used to solve the structure using molecular replacement calculation, and these are listed below.

Amore is a complete molecular replacement system in CCP4 suite, from Jorge Navaza (Navaza 1993, Navaza 1994, Navaza and Vernoslova 1995).

Beast brute-force molecular replacement is based on the maximum likelihood-based algorithm (Read 2001).

MOLREP is an automated programme for molecular replacement calculation, from Alexei Vagin (Vagin and Teplyakov 1997).

EPMR is a programme that uses an evolutionary search algorithm (Kissinger et al. 1999).

PHASER is a maximum likelihood-based approach for molecular replacement (McCoy et al. 2007). PHASER is the most common method used in the structure solution of macromolecular protein; hence a brief overview is given below.

This programme is used for phasing macromolecular crystal structures using maximum likelihood methods for its rotation and translation function searches. The programme has been developed by Randy Read and his group at the Cambridge Institute for Medical Research (CIMR) and is functional through the PHENIX and CCP4 software suites. PHASER employs the experimental data and the closest search model as input to generate positioned search model as shown below (Read 2001).

Rotation Likelihood Function It calculates the target function on a grid of orientations, and the one with the highest score is selected for the next step in MR. Here the Patterson map of the target is compared to Patterson map derived from the known homologue structure in different orientations. PHASER uses maximum likelihood algorithm to score the rotation function. The target and the model structures with the similar orientation provide the highest rotation score (Read 2001).

Likelihood Function for Translation It finds the absolute position(s) of the target in the unit cell after getting the orientation(s) from the RF. This is executed calculating a new Patterson map by moving the model and comparing it to the unknown-derived Patterson map (Read 2001).

Likelihood functions with partial ambiguity In cases where the contributions of different molecules lead to partial uncertainty of the relative phases, the orientation and/or position of the subset of the molecule is determined so as to use the information further for the complete molecule (Read 2001).

Refinement Once an initial estimate for the phase is obtained, either by molecular replacement or isomorphous replacement, calculation of electron density distribution inside the crystal is possible with the objective of fitting an initial molecular model into it. Refinement is the process of adjusting the model to find a closer agreement between the calculated and the observed structure factors. Molecular model coordinates x, y and z and thermal parameters are changed in order to improve the agreement between the calculated |Fc| and the observed |Fo|. Given the unfavourable ratio between the number of observations and the refined parameters, it is necessary to introduce some geometrical restrains (expected bond length, bond angle and torsional angle). The quality of the final model can be established on the basis of several quality indicators:

- Quality of the electron density maps
- R-factor/free R-factor (least square residual for the working and test dataset)
- Final model geometry

R-factor $= \Sigma hkl \mid |Fo| - k|Fc| \mid / \Sigma hkl \mid Fo|$ where Fo and Fc are observed and calculated structure factors for hkl reflections. Some programmes, which are used to refine the crystal structure, are:

REFMAC5 It is the process of refining the structure, using intensity or amplitude-based least squares or maximum likelihood refinement (Murshudov et al. 1997).

Arp/Warp of the automated refinement procedure (Perrakis et al. 1999). It implies the objective interpretation of crystallographic electron density maps and automatic construction and refinement of macromolecular models.

CNS Package for macromolecular structure determination and refinement (Brünger et al. 1989).

Phenix.Refine The maximum likelihood target function is incorporated in the PHENIX programme suite. This function provides the improved target for macromolecular refinement by accounting model incompleteness (missing and unmodelled atoms). Various reflection-data formats (e.g. CNS, MTZ and SHELX) in PHENIX are recognized in default, and the input experimental data are screened for any potential outliers (Read 1999).

Model Buildings on electron density maps and validation will be achieved using graphical programmes XtalView, COOT, PROCHECK, etc.

Applications High-throughput crystallography (HTC) and X-ray crystallography are adding a new dimension to the drug discovery process. These techniques give detail insights into the interaction between the proteins/nucleic acids and ligands. After getting the three-dimensional information, it is easy to make libraries of protein ligand complexes of different combination that can be further used in the drug discovery against infectious diseases (Knapman 2000).

Recent Advancement in X-Ray Crystallography A recent advancement is neutron macromolecular crystallography that has increased the pace of structure submission to the protein data bank (PDB). Efforts for improvisation of this technique include addition of new detectors such as the TOF Laue diffractometer 'NMX' at the European Spallation Source. The use of microfocus X-ray beams for crystal positioning helps in reducing the radiation damage, and efficient data merging from serial of images obtained from different sections of crystals has enhanced the advantage of this technique. The radiation damage caused by femtosecond pulses of X-ray FELs is continuously evaluated as in the case of cytochrome c oxidase and photosystem II crystal structures (Blakeley et al. 2015).

8.5 Isothermal Calorimetry (ITC)

8.5.1 Principle

It is the technique that quantitates the heat released or absorbed during a biomolecular interaction. As the name suggests, it is a titration method where the ligand is titrated to a molecule of interest in isothermal condition. The concept of the techniques is based on the very old fact that when substances interact, heat is either produced or absorbed depending on the type of interaction, exothermic or endothermic.

Instrumentation of ITC There are two cells in the instrument; one is main cell where the molecule of interest is kept and another is known as reference cell which is used to keep the buffer. Both the cells are kept in isothermal and adiabatic condition. The ligand is kept in syringe and titrated into the main cell. Depending on the interaction, the heat will be released or absorbed which will result in change in the temperature of the main cell. But the instrument tries to maintain the temperature of both the cells (reference cell and main cell) constant. In order to maintain the temperature, instrument provides more or less electric power to the main cell which is recorded as the raw heat of the interaction (Fig. 8.14). The raw signal in ITC is measured as power with the unit of mJsec^{-1}. This power is necessary to maintain the calorimeter cell from changing temperature as a function of time. In a typical ITC experiment, two reactants are titrated against each another, and whether the two reactants have any interaction is identified by measuring the change in the heat. It is the only method that gives the detailed information about
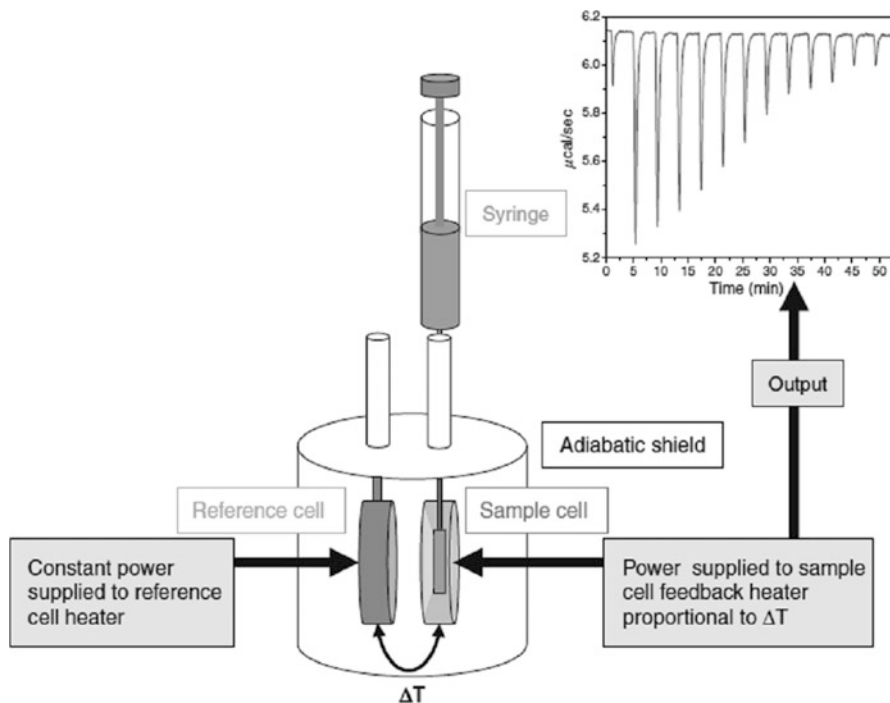
Fig. 8.14 Schematic representation of the instrumentation in ITC showing how the power adjusted by the instrument maintains the constant temperature difference between the sample and the reference cell upon successive addition of ligand molecule from the syringe resulting in the instrument signal

the various thermodynamic parameters such as binding constant (Kb), Gibbs free energy (ΔG), enthalpy (ΔH) and entropy (ΔS). (Wiseman et al. 1989).

Hence, the integrated power versus time curve gives the change in heat as the ligand is added to the sample cell containing the receptor solution. The release of the excess amount of heat at the beginning of the titration shows the substantial increase in complex formation at each step. All receptor binding sites are occupied towards the end of the experiment with no further change in the heat of dilution. Due to this reason always the heats of binding are determined by integrating the observed binding peaks and subtracting the heats of dilution. The heat of dilution of ligand is measured by injecting it into the buffer solution. Thermodynamic parameters can be identified by fitting the experimental data to an appropriate binding model (Indvk and Fisher 1998) using the ITC software. Nonlinear regression methods are very useful in fitting the output thermograms after the ITC experiments. The analysis yields binding stoichiometry (n), binding constant (K) and enthalpy of binding (ΔH) (Fig. 8.15). From these values, free energy of binding is calculated from the equation $\Delta G = -RT\ln K$ and entropy using the standard thermodynamic equation, $\Delta G = \Delta H - T\Delta S$.
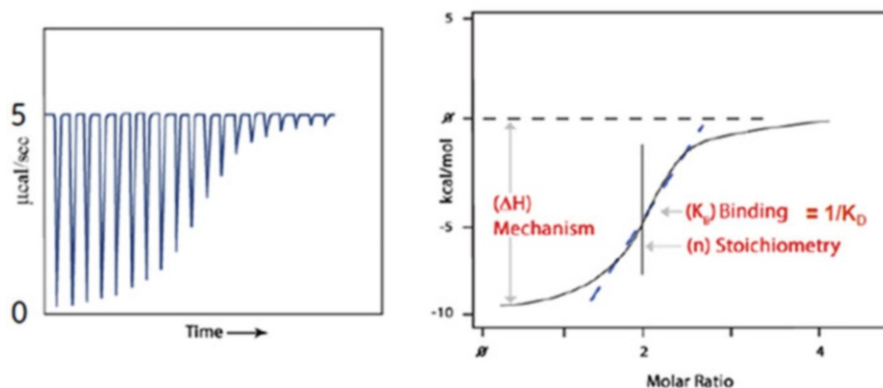
Fig. 8.15 Typical titration data: The *left panel* showing the change in heat and the *right panel* showing the graph after best fitting (Freyer and Lewis 2008)

The steepness of the curve is related to the affinity of the reaction, while the inflexion point of the curve denoted the stoichiometry of the reaction. The overall shape of the curve is dependent on the affinity as well as on the molar ratio of the concentrations of ligand and receptor molecule. This link between affinity and experimental design is best explained through the 'Wiseman c-parameter'.

$$c = n[M]^*K$$

It includes the y-intercept position with regard to $\Delta H°$ regardless of the absolute scaling along the x- and y-axes which is dependent on the value of c as depicted in Fig. 8.16. The curve is sigmoidal when the c-values are more than 10, and when it is less than 10, the stoichiometry is difficult to determine (Fig. 8.16). The important requirement for simultaneous determination of $\Delta H°$, K and n is $1 < c < 500$.

Experimental Considerations

In an ITC experiment, the macromolecule and ligand solution are titrated against each other, and the affinity is identified by the change in heat. The concentration of the ligand should be large enough (20–50-fold higher than receptor molecule) so that accurately measurable heat (>10 µcal) can be observed.

After determining the desired concentrations for the ligand and macromolecule molecule, the next important step is solution preparation. The final results of the ITC experiment can be determined by identifying the concentration of the macromolecule and the ligand solution. It is very important that the molar concentrations of the reactant molecules (macromolecule and ligand) be made as precise as possible. Both the solutions should be filtered and degassed properly before running the experiment and have the similar components, that is, solution having the same pH, buffer and salt concentration. If the two solutions are not exactly identical with each other, there may be heat of mixing (or dilution) signals that overcome the heat
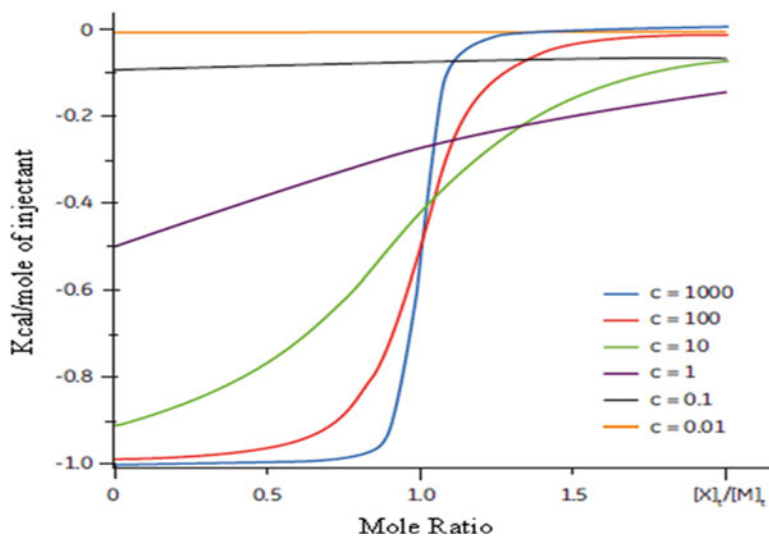
Fig. 8.16 Pictorial representation of the Wiseman isotherm (Freyer and Lewis 2008)

signals for the binding reaction. Finally, before analysing the data, proper control experiments should be run so as to eliminate the heats of dilution. This is known as correcting the raw data. It includes the subtraction of the heat of dilution of ligand as well as macromolecules from the heat of binding. Thus,

$$Q_{\text{correct}} = Q_{\text{measured}} - Q_{\text{dil:ligand}} - Q_{\text{dil:macromolecule}}$$

Before performing the ITC experiment, it is always good to identify the heat of dilution of the ligand. It can be measured, by titrating the ligand solution into buffer in the sample cell. It is always good to measure the heat of dilution for the macromolecule in the second blank experiment (Freyer and Lewis 2008).

8.5.2   Applications

- It is a technique that is used for the biophysical characterization of macromolecules in solution and is widely used in various scientific pursuits. It is also used to study the enzyme kinetics.
- Identification of the effect of molecular structural changes on binding mechanisms.
- Determination of biological activity.
- Nowadays ITC technique is very useful in drug industries. It is used for enthalpy screening to minimize drug resistance. Freire has proposed an elegant way to identify 'enthalpy' inhibitors, by simply screening at two temperatures and

selecting ligands that bind more tightly at lower temperatures (because $\Delta G = \Delta H - T\Delta S$) (Ababou and Ladbury 2004).

8.6 Differential Scanning Calorimetry (DSC)

8.6.1 Principle

It is a thermodynamic tool to identify the heat energy uptake. It occurs due to increase or decrease of temperature when the sample is injected. It is the most commonly used method to determine phase transition, that is, change in the molecule from one conformation to another (Van Holde et al. 2006). It is a useful method to determine the melting point of the samples (solid and liquid) or the combination of both known as suspension phases (Cooper et al. 2000).

In DSC experiments, energy is introduced together into sample and reference cell containing the target molecule and the solvent, respectively. The reference and the sample cell temperature increases as the time passes. In order to match the temperature of the sample to that of the reference cell, either the reaction will be endothermic or exothermic (Cooper et al. 2000, 2001, Cooper 2004). Due to the existence of the molecule of interest, excess energy is required to maintain the same temperature of the sample as the reference one (Fig. 8.17).

It is the most powerful technique to know the stability and folding of the macromolecules (Van Holde et al. 2006). The change in the value of specific heat capacity (Cp) is due to the interruption of forces that stabilizes the native protein structure, namely, hydrogen bonds, Van der Waals interactions, electrostatic interactions and solvent accessibility of the protein residues (Cooper 2000a, b). Therefore, in a DSC technique the shape, sharpness and position of DSC scans (thermodynamic parameters) are attributed to the structural conformation of the macromolecules.

Thermodynamic Terminology The heat-induced macromolecular transitions in a DSC experiment depend on the thermodynamic parameters which are as follows:

The Partial Cp of a Molecule Exact Cp value of the macromolecule in a sample cell is identified by taking the buffer in the reference cell. In DSC technique the sample can either be a protein, tRNA or the complex of protein with ligands (DNA and lipid) (Haynie 2008). The value of Cp at constant pressure is a temperature derivative of the enthalpy function [$Cp = (\Delta H/\Delta T)$p]. Integrating the values Cp [$H\,(T) \times \int T/T0\, Cp\,(T)\, dT + H\,(T0)$] will give the value for the enthalpy function (Privalov and Potekhin 1986).

ΔH, Change in Entropy (ΔS) and ΔCp of the Tm Seen in an aqueous solution, there exists balance between the folded and the unfolded condition of the macromolecules. The various thermodynamic parameters such as the ΔG of the
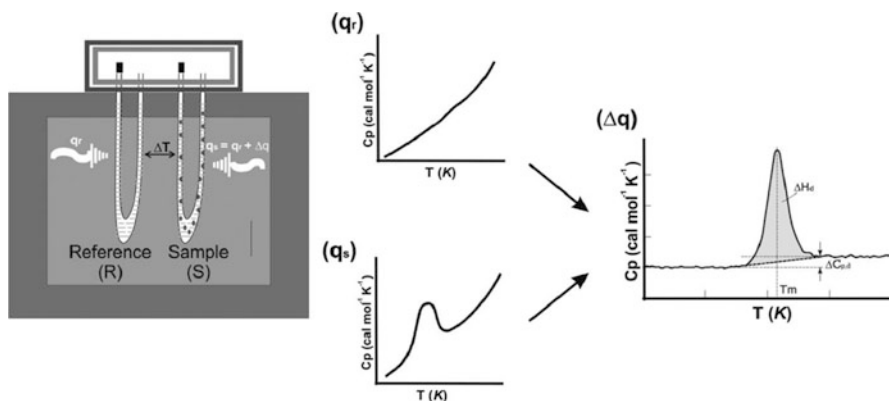
Fig. 8.17 Schematic diagram of a DSC technique

qs, qr and Δq represent the heat of the sample cell, reference cell and absorbed heat by the sample (Van Holde et al. 2006, Cooper 2004). T(K), ΔHd, ΔCp, d Cp and d denote the temperature in kelvin, change in enthalpy, change in specific heat capacity (Cp) and denatured (Cooper et al. 2000, 2001; Cooper 2004)

system, ΔH and ΔS dictate the stability of the folded or native conformation of the macromolecules (Ford and Willson 1999). The higher the stability the more will be the negative ΔG value. The unfolding of the protein becomes more when the forces holding the molecule break because the entropy factor overcomes the forces stabilizing the macromolecules (Sturtevant 1987, Haynie and Freire 1994). The temperature at which the protein is 50% folded is known as the melting temperature of protein depicted by Tm. More stability is indicated by higher Tm values. The DSC technique also measures the ΔCp value when the protein is denatured. This happens because in the denatured state the amino acids of the protein are accessible to the solvent molecule (Sturtevant 1987, Haynie and Freire 1994). Calorimetric enthalpy (ΔHcal) is considered as the integrated zone under the thermogram peak that gives total heat energy uptake by the sample after subtracting the baseline that affects the transition (Cooper et al. 2000). The Van't Hoff enthalpy (ΔH_{VH}) is not dependent on the transitional enthalpy (Cooper et al. 2000). It is identified by analysing the shape of an experimental graph of C_p^{ex} versus T. The transition state is determined by measuring both ΔH_{VH} and ΔHcal (Breslauer et al. 1992). The transition state exists in a two-state mode when the ΔH_{VH} and ΔHcal are equal to each other. The aggregation is identified when the ΔH_{VH} value exceeds than the ΔHcal pointing towards intermolecular cooperation on exposure to solvent. The curve of Cp against T can also be represented as Cp/T versus T after dividing the raw Cp value by T and plotting the results as a function of T.

Integrating the values, this curve gives the transition entropy (ΔS), expressed as $(\Delta S) = (\int Cp/T)\, dT$. Thus, each DSC thermogram provides quantitative measurements of ΔH, ΔS and ΔCp. Based on the above observation, transition-free energy (ΔG) can be calculated at each temperature (T) using the standard thermodynamic equation $\Delta G = \Delta H - T\Delta S$. Values of ΔS and ΔG obtained

from DSC results are not much reliable as compared to the direct determination of ΔH and ΔCp values owing to coupling and propagating of errors during experimentation (Krug et al. 1976).

Absolute Cp   In the sample cell the movement of the water by protein results in a negative value contributing towards the apparent Cp values. Correction for the water movement effect and normalization to a mole of protein gives the absolute Cp. This value can be identified by calculating the DSC values in a series of experiments using different protein concentrations (Kholodenko 1999). The advantage of absolute Cp values lies in understanding the long-range interactions and cooperative phenomenon prevalent in denatured proteins (Lin et al. 1993).

Recent Advancement in DSC   This technique is based mainly on the thermal identification of the macromolecules. The bottleneck of classical DSC is the weak transitions and overlapping events during the experiments. This can be resolved by using the modulated DSC (mDSC) that has several utilizations in the drug discovery (Knopp et al. 2016).

8.6.2   Applications in Biology

The thermal transitions of polymeric materials can be studied using DSC. These transitions can help in comparison with various materials but they do not identify the exact composition.

It is used to study the phase transitions in liquid crystals.

It is most commonly used for studying the curing processes in polymer industries.

It finds applications in understanding the oxidative stability of compounds to provide insights about its ideal storage conditions.

8.7   Fluorescence Spectroscopy

8.7.1   Basic Principles of Fluorescence Spectroscopy

It relates with the electronic and vibrational states. The molecules studied using this technique have a lower energy electronic and a higher energy excited state. There exist different vibrational states between these two states. The transition from ground to higher energy state after absorption of photon is traversed by various vibrational states. In between it loses the vibration energy upon interaction with the other molecules to achieve the lowest energy state. This process is depicted with the help of a Jablonski diagram (Fig. 8.18) (Brand and Johnson 1997).

The S0, S1 and S2 electronic states represent the ground, first and second energy state, respectively. In each electronic energy level, the fluorophore can reside in a number of vibrational energy levels, depicted as 0, 1 and 2. The quenching, energy

Fig. 8.18 Jablonski diagram
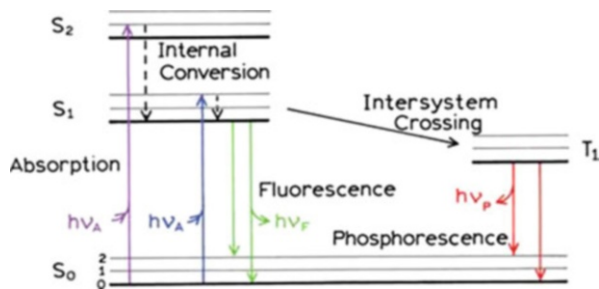
transfer and solvent interactions are the different types of interactions depicted in this Jablonski diagram (Jabłoński 1933), but the details are not discussed. The interstate transitions are shown with the vertical lines illustrating the instantaneous nature of light. According to the Franck–Condon principle, these transitions are too fast and occur within 10–15 s which is a short span of time that cannot cause significant displacement of nuclei.

The emission spectrum of perylene clearly depicts the energy spacing between the different vibrational energy states (Fig. 8.19).

The emission spectra of individual vibrational energy level are approximately 1500 cm^{-1} distant from each other. At room temperature, the thermal energy is more prevalent which is not enough to populate the excited vibrational states; therefore the absorption and emission usually occur from the molecules residing in the lowest vibrational energy states. Higher energy difference between the ground (S0) and excited (S1) state for thermal population of excited state is responsible for choosing the light not the heat for inducing the fluorescence. The fluorophore is excited and reaches to the S1 or S2 state after the absorption of light. The molecules relax and reach the lowest energy S1 state within 10–12 s prior to the fluorescence emission. Thus, the emission of fluorescence light usually occurs from the thermally equilibrated excited state with the lowest vibrational energy, i.e. S1 (Axelrod et al. 1992). Return to the ground state typically occurs to a higher excited vibrational ground state level, which then quickly (10–12 s) reaches thermal equilibrium (Fig. 8.19). Emission spectrum to reach higher vibrational ground states interestingly resembles the absorption spectrum of the S0 to S1 transition. The rationale behind this similarity is that electronic excitation does not modulate the nuclear geometry. This results in similar spacing between the vibrational energy levels of the excited states and the ground state. As a consequence, the vibrational structures observed in the absorption and the emission spectra are not different.

Spin conversion of molecules in the S1 state to the first triplet state T1 is possible. Emission from T1 is known as phosphorescence and is generally shifted to lower energy relative to the fluorescence. The modification of S1 to T1 is referred to as intersystem crossing. The transition from T1 to the S0 is closed due to which the value of rate constants for fluorescence is much higher in comparison to those for triplet emission. The heavy atoms support intersystem crossing increasing the phosphorescence quantum yields.
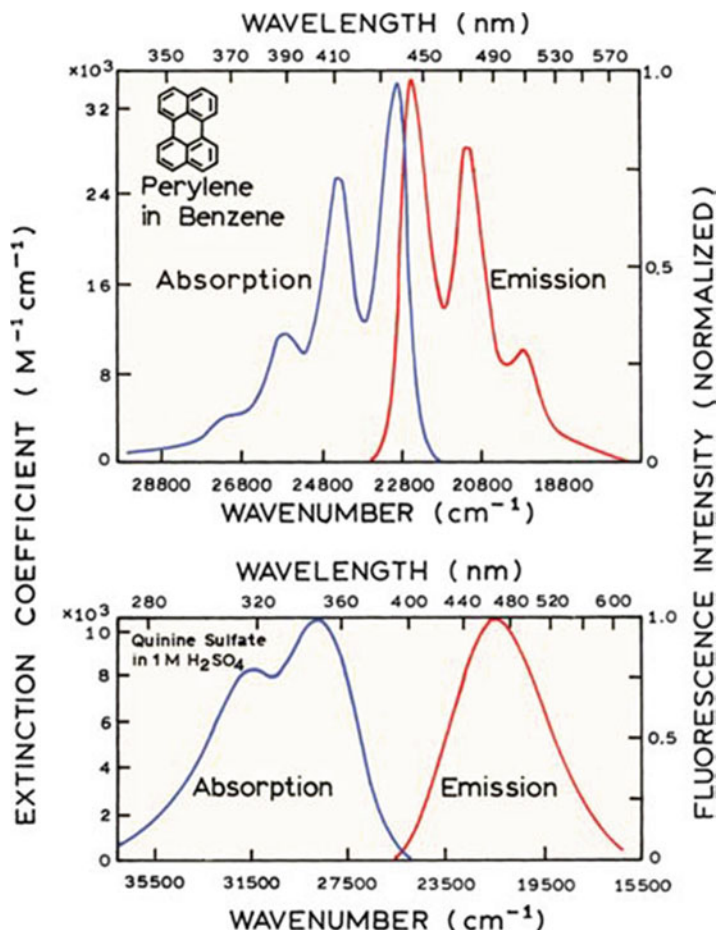
Fig. 8.19 Figure represents the absorption and fluorescence emission spectra of perylene and quinine (Jabłoński 1933)

8.7.2 Various Types of Fluorescence-Based Studies

8.7.2.1 Intrinsic Fluorescence

It is based on the three aromatic amino acids (tryptophan, tyrosine and phenylalanine). When all these residues are present in a protein known as class B protein (Weber 1960), the emission of tryptophan can be detected by selectively choosing the wavelength above 295 nm for excitation (Eftink 1991). Most widely used residue is tryptophan among the three aromatic amino acids, used for studying the intrinsic fluorescence of the proteins. The tryptophan fluorescence interferes with the fluorescence of the tyrosine and phenylalanine making the study complicated owing to the resonance energy transfer (Eftink 1991, Lakowicz 1999). Therefore, the intrinsic tyrosine fluorescence study is limited to the proteins

which do not have tryptophan. Contrary to this, a study by Ruan et al. has reported the use of tyrosine and phenylalanine in the fluorescence-based experiments in proteins (Ruan et al. 2002). Moreover, the tyrosine fluorescence remains unaffected by changes in several environmental factors including polarity and does not exhibit solvent chromism unlike the tryptophan fluorescence (Ross et al. 1992). This is the major disadvantage of using such a fluorescent reporter in biological samples. Phenylalanine fluorescence is very weak and hence rarely used in the study of proteins (Lakowicz 1999).

Thus, the 'natural protein fluorescence' term is regularly used for tryptophan fluorescence (Ladokhin 2000). The tryptophan fluorescence which is intrinsic and site-specific is considered as fluorescence probe for studying protein structure and dynamics (Eftink 1991). The frequency of tryptophan in proteins is about 1 mol% (Lakowicz 1999). Usually lower tryptophan content is considered to be good for the fluorescence studies in proteins as it prevents inter-tryptophan interactions preventing complications in data interpretation. Tryptophan-based fluorescence is sensitive to environmental components such as mobility and polarity. It can provide detailed information regarding change in protein conformations when it interacts with other molecules (Kirby and Steiner 1970, Beechem and Brand 1985). Hence, the use of tryptophan residues in fluorescence spectroscopic analysis of most of the peptides and proteins is well documented in literature (Misra and Ramachandran 2010). This is evident from the fact that more than 300 articles are published per year in which tryptophan fluorescence of the protein has been used (Vivian and Callis 2001). Tryptophan possesses certain spectral properties which are affected by several factors. As shown in Fig. 8.20, tryptophan residue contains a large indole ring consisting of two fused aromatic rings (Fig. 8.20).

Tryptophan emission spectrum shows red shift in polar environment and blue shift in surrounding nonpolar environment. This unique property of tryptophan to interact with both hydrophobic and polar groups makes it unique. It is the only amino acid with polar –NH group that forms a hydrogen bond and has the highest nonpolar accessible surface area (Chothia 1976). It is also capable of making π–π interactions due to its aromaticity and weak polar interactions (Burley and Petsko 1985, 1988). This amphipathic nature of tryptophan is responsible for its involvement in making unique hydrogen bonds and long-distance electrostatic interactions (Fonseca et al. 1992). This helps in the interfacial localization of Trp in membranes (Wimley and White 1996, Chattopadhyay et al. 1997). It is further strengthened by the motional and dielectric characteristics recognizable from the total fluid phase and the more isotropic hydrocarbon-like deeper regions of the membrane. Further, tryptophan helps in the maintenance of structural and function properties of both soluble and membrane proteins (Tang et al. 2002) as proved by mutational analysis where change in tryptophan residues leads to reduction or loss of protein functionality.

Fig. 8.20 Tryptophan
showing the 1La and 1Lb
transitions (Adapted and
modified from Ref. 32)
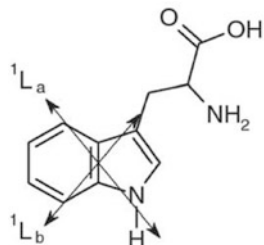
8.7.2.2 Extrinsic Fluorescence

The use of extrinsic fluorophores such as fluorescent dye is also well documented
for various protein analyses, namely, the study of folding and unfolding of proteins,
characterization of various intermediate stages of protein folding and study of
protein aggregation and fibrillation. Fluorescence properties of extrinsic
fluorophore depends upon the solvent relaxation process and intramolecular charge
transfer which in turn are affected by environment of dye as well as its interaction
with proteins. Nowadays various extrinsic fluorescence dyes are available for,
e.g. ANS, Bis-ANS, Nile red, Thioflavin T and many more. These dyes are
versatile, sensitive and suitable for studying high-throughput screening. ANS
(1-anilinonaphthalene-8-sulfonate) remains nonfluorescent in molten environment
but gives fluorescence in highly polar environment and organic solvents or upon
adsorption onto solid phases (Weber and Lawerence 1954). ANS interactions with
hydrophobic binding sites of apomyoglobin and apohemoglobin were earlier
reported. This interaction is associated with an increase in fluorescence and a
blue shift of the fluorescence peak maxima (Stryer 1965). ANS and its dimeric
analogue 4,4-bis-1-anilinonaphthalene-8-sulfonate (Bis-ANS) are the most widely
used dyes for studying protein interactions (Rosen and Weber 1969). The Nile red
which was initially used for detection of intracellular lipid droplets (Greenspan
et al. 1985) is also used for monitoring the conformational changes in several
proteins (Sackett and Wolff 1987). The use of dye DCVJ (9-dicyanovinyl)-
julolidine in understanding the tubulin structure and in the formation of hydropho-
bic microdomains, e.g. in protein aggregation, is reported by Kung and Reed
(1989). Congo red and Thioflavin T are well-studied dyes used for studying
fibrillation and amyloid fibril formation (Puchtler et al. 1961).

In conclusion, extrinsic fluorescent dye usage is well established for various
applications in the field of protein characterization, e.g. protein unfolding and
refolding processes (Acharya and Madhusudhana Rao 2003), to identify the molten
globule intermediates (Goto and Fink 1989), to study surface hydrophobicity
(Cardamone and Puri 1992), to determine active sites of enzymes (Takashi et al.
1977), to study aggregation and fibrillation (Vetri et al. 2007, Lindgren et al. 2005),
to assess conformational changes associated with chemical degradation (Anraku
et al. 2001), to study protein surfactant interactions and to analyse the macromole-
cule crystal. The development in the field of the use of external fluorophores has
gained attention due to the requirement of a sensitive detection method for

aggregation of proteins during the production, storage and management of biopharmaceuticals.

8.7.3 Data Analysis

The fluorescence intensity of a fluorophore is affected by the following factors:

1. Temperature: Fluorescence intensity is dependent on temperature. At high temperature the intensity falls off because electrons have more vibrational energy.
2. Exposure time: Usually the higher the exposure time, the lower is the fluorescence efficiency.
3. Quenching: Fluorescence quenching is possible either by internal sources, e.g. histidine residue, protonated amino acids like Glu or Asp, di-sulphide bonds, a heme group or by an external source such as solvent quenching due to proton transfer to polar molecules.

Firstly, the total integrated fluorescence intensity 'I' is calculated by integrating the area under the fluorescence curve with the following equation:

$$I = \sum_{\lambda} I(\lambda)$$

The integrated fluorescence intensity denotes the extent of protein unfolding. It integrates a nonlinear baseline slope with changes in togetherness of quenches, which can be attributed to an increase in the solvent accessible surface area of the protein resulting in the increase of external and internal quenching.

The behaviour of different proteins is differential in these circumstances. Generally, protein unfolding leads to an exposure of tryptophan amino acid towards solvent-exposed area that decreases the fluorescence intensity due to solvent-mediated quenching. Lorentzian function is used for modelling fluorescence emission. Fitting of this function to fluorescence in each spectrum yields a position of peak maxima. Alternatively, determination of wavelength at which the fluorescence intensity is maximum is a solution which is subjected to noise and under-sampling (Acharya and Madhusudhana Rao 2003).

8.7.4 Applications

- It is extensively used in various research purposes for the analysis of organic as well as biological samples. Recently it is implicated in differentiating malignant skin tumours from benign tumours.
- To study protein unfolding and refolding with respect to temperature as well as chemical reagents and characterization of its molten globular intermediates.

- To assess the protein aggregation.
- To study the amyloid fibril formation.
- To assess the hydrophobicity of proteins.
- Identification of protein ligand interactions.

8.8 ORD and CD

8.8.1 Principles of ORD and CD

Interaction of electromagnetic radiation with the matter results in changes both in the light and in matter. There are different parameters that are affected depending on the wavelength used for the experiments. Absorption by the sample results in a reduction in the intensity of light at any particular wavelength. Further, refractive index dispersion (scattering) causes change in the velocity of light when it interacts with the medium. When the plane-polarized light passing through the sample changes its plane of polarization depending on the wavelength of the incident radiation, the phenomenon is recognized as optical rotary dispersion (ORD). If the radiation becomes elliptically polarized at the absorption bands, then it is known as circular dichroism (CD). ORD and CD are distinct from normal absorption and dispersion phenomenon as the former requires the presence of chiral centres. ORD just changes the plane of polarization, whereas CD evaluates the differential absorption of right- (E_R) and left-handed (E_L) circularly polarized light by the molecules.

All the proteins contains amino acids having chiral centres except glycine, but individually contribution of amino acids to ORD and CD signals is low (Toniolo 1970). However, the protein consists of asymmetric and periodic arrangement of peptide units in space, which gives rise to their characteristic ORD and CD spectra.

8.8.2 Cotton Effect

A beam of linearly polarized light of wavelength λ can be considered as the addition of two components: beams of right- and left-handed circularly polarized light, with electric vectors E_R and E_L, respectively. When polarized light interacts with an asymmetric molecule (such as most biological macromolecules), two phenomena, CD and ORD, are observed, and the molecule is said to be optically active. These phenomena arise from the following events:

E_R and E_L travel at different speeds when they pass through the molecule. This difference in refractive index leads to optical rotation, the rotation of the plane of polarization, measured in degrees of rotation, αλ. ORD is the dependence of this rotation upon wavelength. In a region where the molecule does not absorb light, the rotation plotted against wavelength yields a plain curve. In the region of light absorption, however, the dispersion is anomalous. The rotation initially increases sharply in one direction, falling to zero at the absorption maximum, and then further
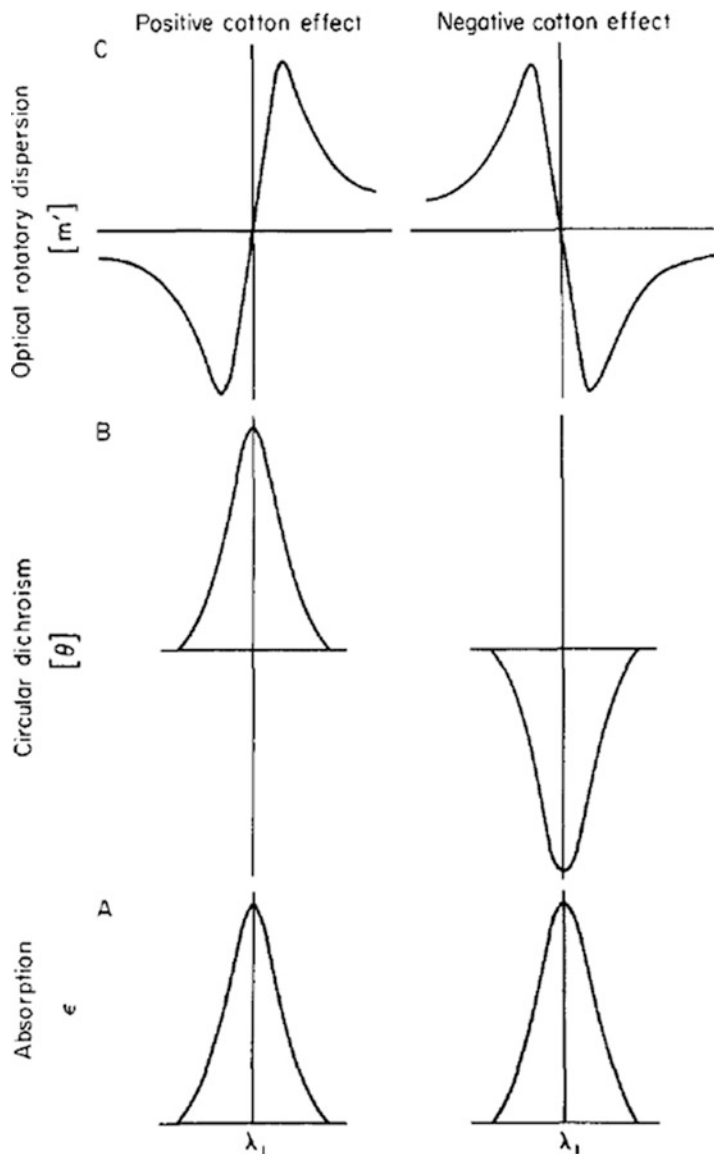
Fig. 8.21 A typical electronic absorption band (**a**) circular dichroism curve (**b**) and optical rotatory dispersion (**c**) curve

rising sharply in the opposite direction. This anomalous dispersion is called a Cotton effect (Fig. 8.21).

In the region of its Cotton effect, an asymmetric molecule which exhibits ORD will also show uneven absorption of left- and right-handed circularly polarized light; this difference in extinction coefficient ($\pounds_L - \pounds_R$) is known as circular dichroism and can be measured directly in some instruments as a differential

absorbance. When CD occurs the emerging light beam is no longer linearly polarized but instead is elliptically polarized. Thus, the ellipticity of the resulting light, θ_λ, is another measure of CD and is proportional to ($£_L - £_R$) typical absorption band with its associated ORD and CD Cotton effects shown in Fig. 8.21. Both dispersive and absorption phenomena are caused by the same charge displacements in a molecule; therefore, ORD and CD share close similarity. By means of the Kronig–Kramers transform equations developed by Moscowitz (Djerassi 1960), ORD curves can theoretically be computed from CD data and vice versa. This calculation is sometimes useful for evaluation of CD bands at very low wavelength.

8.8.3   Relation Between ORD and CD

CD and optical rotation are related (ORD), for the Kth optically active transition (Cotton effect), by the Kronig–Kramers relations (Kronig 1926, Kramers 1927). By means of these integral transforms, information contained in a complete ORD spectrum may be deduced, in principle, from a CD curve and vice versa. Computer programmes are available for calculation. Various methods of data manipulation can be compared in studies on d-10-camphor sulfonic acid. The transforms can be used to search for optically active transitions beyond the observable UV range (Cassim and Yang 1970). A generalization useful for qualitative calculation of band magnitude is that if a CD band is approximately Gaussian in shape, then

$$[M]peak - \big([M]trough\big)ORD \sim 1.2([\theta]maximum)CD$$

8.8.4   Applications

- CD is the most common method used for the identification of the secondary and tertiary structure of macromolecules specifically proteins. It further helps to investigate how the secondary structure in a protein changes due to mutations. It finds applications in studying protein folding, thermal stability and interaction studies.
- ORD spectroscopy technique shares similarity with electronic circular dichroism spectroscopy (ECD). It determines the optical rotation of a molecule which is chiral as a function of the wavelength of linearly polarized light.

References

Ababou A, Ladbury JE (2006) Survey of the year 2004: Literature on applications of isotherma titration calorimetry. J Mol Recognit 19(1):79–89

Acharya P, Madhusudhana Rao N (2003) Stability studies on a lipase from Bacillus Subtilis in guanidinium chloride. J Prot Chem 22:51–60

Anraku M, Yamasaki K, Maruyama T, Krangh-Hansen U, Otagiri M (2001) Effect of oxidative stress on the structure and function of human serum albumin. Pharm Res 18:632–639

Atkins P, de Paula J (2005) Elements of physical chemistry, 4th edn. Oxford University Press

Axelrod D, Hellen EH, Fulbright RM (1992) Total internal reflection fluorescence. In: Lakowicz JR (ed) Topics in fluorescence spectroscopy, vol 3: Biochemical applications. Plenum Press, New York, pp 289–343

Barlow W (1883) Probable nature of the internal symmetry of crystals. Nature 29(738)

Beechem JM, Brand L (1985) Time-resolved fluorescence of proteins. Annu Rev Biochem 54:43–71

Blake PR, Park J-B, Adams MWW, Summers MF (1992) Novel observation of NH–S (Cys) hydrogen-bond-mediated scalar coupling in cadmium-113 substituted rubredoxin from Pyrococcus furiosus. J Am Chem Soc 114(12):4931–4933

Blakeley MP, Hasnainb SS, Antonyuk SV (2015) Sub-atomic resolution X-ray crystallography and neutron crystallography: promise, challenges and potential. IUCrJ 2:464–474

Bragg WH (1907) The nature of roentgen rays. Trans R Soc Sci Australia 31:94

Bragg WH (1908) The nature of γ- and X-rays. Nature 77

Bragg WH (1910) The consequences of the corpuscular hypothesis of the γ- and X-rays, and the range of β-rays. Phil Mag 20(117):385

Brand L, Johnson ML. (1997) Methods in enzymology, Vol. 278: Fluorescence spectroscopy. Academic, New York

Breslauer KJ, Freier E, Straume M (1992) Calorimetry: a tool for DNA and ligand-DNA studies. Methods Enzymol 211:533–567

Brown SB (ed) (1980) An introduction to spectroscopy for biochemists. Academic, London

Brünger AT, Karplus M, Petsko GA (1989) Acta Crystallogr A 45:50–61

Burley SK, Petsko GA (1985) Aromatic-aromatic interaction: a mechanism of protein structure stabilization. Science 229:23–28

Burley SK, Petsko GA (1988) Weakly polar interactions in proteins. Adv Protein Chem 39:125–189

Cantor CR, Schimmel PR (1980) Biophysical chemistry, part II

Cardamone M, Puri NK (1992) Spectrofluorimetric assessment of the surface hydrophobicity of proteins. Biochem J 282:589–593

Cassim JY, Yang T (1970) Biopolymers 9:1475

Cavanagh J, Fairbrother WJ, Palmer AG III, Skelton NJ (1996) Protein NMR spectroscopy: principles and practice. Academic, San Diego

Chattopadhyay A, Mukherjee S, Rukmini R, Rawat SS, Sudha S (1997) Ionization, partitioning, and dynamics of tryptophan octyl ester: implications for membrane-bound tryptophan residues. Biophys J 73:839–849

Chothia C (1976) The nature of the accessible and buried surfaces in proteins. J Mol Biol 105:1–14

Compton A (1923) A quantum theory of the scattering of X-rays by light elements. Phys Rev 21(5)

Cooper A (2000a) Heat capacity of hydrogen-bonded networks: an alternative view of protein folding thermodynamics. Biophys Chem 85:25–39

Cooper A (2000b) Microcalorimetry of protein-DNA interactions. In: Travers A, Buckle M (eds) DNA-protein interactions. Oxford University Press, Oxford, pp 125–139

Cooper A (2004) Biophysical chemistry. Royal Society of Chemistry, London, pp 103–107

Cooper A, Nutley MA, Walood A (2000) Differential scanning microcalorimetry. In: Harding SE, Chowdhry BZ (eds) Protein-ligand interactions: hydrodynamics and calorimetry. Oxford University Press, Oxford, pp 287–318

Cooper A, Johnson CM, Lakey JH, Nollmann M (2001) Biophys Chem 93:215–230

Cudney R, Patel S, Weisberg K, Newhouse Y, McPherson A (1994) Screening and optimization strategies for macromolecular crystal growth. Acta Crystallogr D 50:414–423

de Kronig LR (1926) J Opt Soc Am 12:547

Djerassi C (1960) Optical rotatory dispersion. McGraw-Hill, New York; (a) Chapter by A. Moscowitz, p 150

Dodero VI, Quirolo ZB, Sequeira MA (2011) Biomolecular studies by circular dichroism. Front Biosci (Landmark Ed) 16:61–73

Eftink MR (1991) Fluorescence techniques for studying protein structure. In: Suelter CH (ed) Methods of Biochemical analysis, vol 35. Wiley, New York, pp 127–205

Einstein (1905) On a heuristic point of view about the creation and conversion of light. Ann Phys 17:132–148

Fonseca V, Daumas P, Ranjalahy-Rasoloarijao L, Heitz F, Lazaro R, Trudelle Y, Andersen OS (1992) Gramicidin channels that have no tryptophan residues. Biochemistry 31:5340–5350

Ford JL, Willson BR (1999) Thermal analysis and calorimetry of pharmaceuticals. In: Kemp R (ed) Handbook of thermal analysis and calorimetry, vol 4. Elsevier, The Netherlands, pp 923–1016

Freyer MW, Lewis EA (2008) Isothermal titration calorimetry: experimental design, data analysis, and probing macromolecule/ligand binding and kinetic interactions. Methods Cell Biol 84:79–113

Galya LG, Rudnick LR (1988) Am Chem Soc Div Pet Chem Prepr 33:382

Garman EF, Schneider TR (1997) Macromolecular cryocrystallography. J Appl Crystallogr 30 (3):211

Gore M (2000) Spectrophotometry & spectrofluorimetry. Oxford University Press, New York

Goto Y, Fink AL (1989) Conformational states of β-lactamase: molten-globule states at acidic and alkaline pH with high salt. Biochemistry 28:945–952

Greenfield NJ (2006) Using circular dichroism spectra to estimate protein secondary structure. Nat Protoc 1(6):2876–2890

Greenspan P, Mayer EP, Fowler SD (1985) Nile red: a selective fluorescent stain for intracellular lipid droplets. J Cell Biol 100:965–973

Guinier A (1952) X-ray crystallographic technology. Hilger and Watts LTD., London

Harris DA, Bashford CL (1987) Spectrophotometry and Spectrofluorimetry: a practical approach. IRL Press, Oxford

Haynie DT (2008) Biological thermodynamics. Cambridge University Press, Cambridge

Haynie DT, Freire E (1994) Estimation of the folding/unfolding energetic of marginally stable proteins using differential scanning calorimetry. Anal Biochem 216:33–41

Helliwell JR (2005) Protein crystal perfection and its application. Acta Crystallogr D 61:793–798

Hicks RP (2001) Recent advances in NMR: expanding its role in rational drug design. Curr Med Chem 8(6):627–650. http://en.wikipedia.org/wiki/Ultraviolet%E2%80%93visible_spectroscopy

Indvk L, Fisher HF (1998) Theoretical aspects of isothermal titration calorimetry. Methods Enzymol 64:295–350

Jabłoński A (1933) Efficiency of Anti-Stokes Fluorescence in Dyes. Nature 131:839–840

James TL, Oppenheimer NJ (1994) Nuclear magnetic resonance, part C. Methods in enzymology. Academic, New York, p 813

Jancarik J, Kim SH (1991) J Appl Crystallogr 24:409–411

Jeruzalmi D (2006) First analysis of macromolecular crystals: biochemistry and x-ray diffraction. Methods Mol Biol 364:43–62

Kepler J (1611). Strena seu de Nive Sexangula. Frankfurt: G. Tampach. ISBN 3-321-00021-0

Kholodenko V (1999) A simple method to measure the absolute heat capacity of proteins. Anal Biochem 270:336–338

Kirby EP, Steiner RF (1970) Influence of solvent and temperature upon the fluorescence of indole derivatives. J Phys Chem 74:4480–4490

Kissinger CR, Gehlhaar DK, Fogel DB (1999) Acta Crystallogr 55(Pt 1):247–255

Knapman K (2000) Chem Innov 30(2):46–52

Knopp MM, Löbmann K, Elder DP, Rades T, Holm R (2016) Recent advances and potential applications of modulated differential scanning calorimetry (mDSC) in drug development. Eur J Pharm Sci

Kramers HA (1927) Atti Congr. Int Fis Como 545

Krug RR, Hunter WG, Grieger RA (1976) Enthalpy-entropy compensation. Some fundamental statistical problems associated with the analysis of van't Hoff and Arrhenius data. J Phys Chem 80:2335–2341

Kung CE, Reed JK (1989) Fluorescent molecular rotors: a new class of probes for tubulin structure and assembly. Biochemistry 28:6678–6686

Ladokhin AS (2000) Fluorescence spectroscopy in peptide and protein analysis. In: Meyers RA (ed) Encyclopedia of analytical chemistry. Wiley, New York, pp 5762–5779

Lakowicz JR (1999) Principles of fluorescence spectroscopy. Kluwer-Plenum, New York

Lees JG, Smith BR, Wien F, Miles AJ, Wallace BA (2004) CDtool – an integrated software package for circular dichroism spectroscopic data processing, analysis and archiving. Anal Biochem 332:285–289

Lees JG, Miles AJ, Wien F, Wallace BA (2006) A reference database for circular dichroism spectroscopy covering fold and secondary structure space. Bioinformatics 22:1955–1962

Lin LN, Mason AB, Woodworth RC, Brandts JF (1993) Calorimetric studies of the N-terminal half-molecule of transferrin and mutant forms modified near the Fe(3_)-binding site. Biochem J 293:517–522

Lindgren M, Sörgjerd K, Hammarström P (2005) Detection and characterization of aggregates, prefibrillar amyloidogenic oligomers, and protofibrils using fluorescence spectroscopy. Biophys J 88:4200–4212

Mazeed S, Ofek G, Belachew A, Huang CC, Zhou T, Kwong PD (2003) Enhancing protein crystallization through precipitant synergy. Structure 11:1061–1070

McCoy AJ, Grosse-Kunstleve RW, Adams PD, Winn MD, Storoni LC, Read RJ (2007) J Appl Crystallogr 40:658–674

Miles AJ, Wallace BA (2006) Synchrotron radiation circular dichroism spectroscopy of proteins and applications in structural and functional genomics. Chem Soc Rev 35:39–51

Miles AJ, Wien F, Lees JG, Rodger A, Janes RW, Wallace BA (2003) Calibration and standardisation of synchrotron radiation circular dichroism (SRCD) amplitudes and conventional circular dichroism (CD) spectrophotometers. Spectroscopy 17:653–661

Miles AJ, Wien F, Lees JG, Wallace BA (2005) Calibration and standardisation of synchrotron radiation and conventional circular dichroism spectrometers. Part 2: factors affecting magnitude and wavelength. Spectroscopy 19:43–51

Misra G, Ramachandran R (2009) Biophys Chem 142:55–64

Misra G., Ramachandran R (2010) BBA Proteins Proteomics 1804:2146–2152

Murshudov GN, Vagin AA, Dodson EJ (1997) Acta crystallographica 53(Pt 3):240–255

Nakanishi K, Berova N; Woody R (1994). Circular dichroism: principles and applications

Navaza J (1993) Acta Crystallogr 49(Pt 6):588–591

Navaza J (1994) Acta Crystallogr A50:157–163

Navaza J, Vernoslova E (1995) Acta Crystallogr A51:445–449

Perrakis A, Morris R, Lamzin VS (1999) Nat Struct Biol 6(5):458–463

Pilch DS (2000) Calorimetry of nucleic acids. In: Egli M, Herdewijn P, Matsuda A et al (eds) Current protocols in nucleic acid chemistry. Wiley, New York, pp 7.4.1–7.4.9

Pranitha D, Parthiban S KD, Ghosh S, David Banji S (2011) Asian J Pharm Clin Res 4(4):9–14

Privalov PL, Potekhin SA (1986) Scanning microcalorimetry in studying temperature-induced changes in proteins. Methods Enzymol 131:4–51

Puchtler H, Sweat F, Levine M (1961) On the binding of Congo red by amyloid. J Histochem Cytochem 9:553–539

Rabi II, Zacharias JR, Millman S, Kusch P (1938) A new method of measuring nuclear magnetic moment. Phys Rev 53(4):318–327

Read RJ (1999) Acta Crystallogr 55(Pt 10):1759–1764

Read RJ (2001) Acta Crystallogr 57(Pt 10):1373–1382

Rodger A, Nordén B (1997) Circular dichroism and linear dichroism. Oxford University Press, Tokyo

Rosen CG, Weber G (1969) Dimer formation from 1-anilino-8-naphthalenesulfonate catalyzed by bovine serum albumin. A new fluorescent molecule with exceptional binding properties. Biochemistry 8:3915–3920

Ross JBA, Laws WR, Rousslang KW, Wyssbrod HR (1992) Tyrosine fluorescence and phosphorescence from proteins and polypeptides. In: Lakowicz JR (ed) Topics in fluorescence spectroscopy, Vol. 3, Biochemical applications. Plenum Press, New York, pp 1–63

Ruan K, Li J, Liang R, Xu C, Yu Y, Lange R, Balny C (2002) A rare protein fluorescence behaviour where the emission is dominated by tyrosine: case of the 33-kDa protein from spinach photosystem II. Biochem Biophys Res Commun 293:593–597

Russo Krauss I, Merlino A, Vergara A, Sica F (2013) Int J Mol Sci 14(6):11643–11691

Sackett D, Wolff J (1987) Nile red as polarity-sensitive fluorescent probe of hydrophobic protein surfaces. Anal Biochem 167:228–234

Skoog DA, Holler FJ, Crouch SR (2007) Principles of instrumental analysis, 6th edn. Thomson Brooks, Belmont

Snyder PA, Rowe EM (1980) The first use of synchrotron radiation for vacuum ultraviolet circular dichroism measurements. Nucl. Instr. Meth. 172:345–349

Solomon EI, Lever ABP (2006) Inorganic electronic structure and spectroscopy. Wiley-Interscience, New York

Solomon N, Wecksler AT, Schenk G, Holman TR (2007) Kinetic and spectroscopic studies of N694C Lipoxygenase: a probe of the substrate activation mechanism of a non-Heme ferric enzyme. J Am Chem Soc 129(24):7531–7537

Steno N (1669). De solido intra solidum naturaliter contento dissertationis prodromus. Florentiae

Stryer L (1965) The interaction of a naphthalene dye with apomyoglobin and apohemoglobin. A fluorescent probe of non-polar binding sites. J Mol Biol 13:482–495

Sturtevant J (1987) Biochemical applications of differential scanning calorimetry. Annu Rev Phys Chem 38:463–488

Sutherland JC, Desmond EJ, Takacs PZ (1980) Versatile spectrometer for experiments using synchrotron radiation at wavelengths greater than 100 nm. Nucl Instr Meth 172:195–199

Takashi R, Tonomura Y, Morales MF (1977) 4,4'Bis(1-anilinonaphthalene 8-sulfonate) (bis-ANS): a new probe of the active site myosin. Biochemistry 74:2334–2338

Tang Y, Zaitseva F, Lamb RA, Pinto LH (2002) The gate of the influenza virus M2 proton channel is formed by a single tryptophan residue. J Biol Chem 277:39880–39886

Toniolo C (1970) J Phys Chem 74:1390

Vagin A, Teplyakov A (1997) J Appl Cryst 30:1022–1025

Van Holde KE, Curtis Johnson W, Shing HP (2006) Thermodynamics and biochemistry. In: Principles of physical biochemistry, 2nd edn. Pearson Prentice Hall, Upper Saddle River, pp 72–105

Vetri V, Canale C, Relini A, Librizzi F, Militello V, Gliozzi A, Leone M (2007) Amyloid fibrils formation and amorphous aggregation in concanavalin A. Biophys. Chem 125:184

Vivian JT, Callis PR (2001) Mechanisms of tryptophan fluorescence shifts in proteins. Biophys J 80:2093–2109

von Laue M (1914) Concerning the detection of x-ray interferences (PDF). Nobel Lectures, Physics:1901–1921

Wallace BA (2000) Synchrotron radiation circular dichroism spectroscopy as a tool for investigating protein structures. J Syn chrotron Radiat 7:289–295

Wallace BA, Janes RW (2001) Synchrotron radiation circular dichroism spectroscopy of proteins: secondary structure, fold recognition, and structural genomics. Curr Opin Chem Biol 5:567–571

Weber G (1960) Fluorescence-polarization spectrum and electronic-energy transfer in proteins. Biochem J 75:345–352

Weber G, Lawerence DJR (1954) Fluorescent indicators of adsorption in aqueous solution and on the solid phase. Biochem J 56

Whitmore L, Wallace BA (2004) DICHROWEB, an online server for protein secondary structure analyses from circular dichroism spectroscopic data. Nucl Acid Res 32:W668–W673

Whitmore L, Wallace BA (2008) Protein secondary structure analyses from circular dichroism spectroscopy: methods and reference databases. Biopolymers 89(5):392–400

Wimley WC, White SH (1996) Experimentally determined hydrophobicity scale for proteins at membrane interfaces. Nat Struct Biol 3:842–848

Wiseman T, Williston S, Brandts JF, Lin LN (1989) Rapid measurement of binding constants and heats of binding using a new titration calorimeter. Anal Biochem 179(1):131–137

Advance Techniques in Biophysics

<div style="text-align:right;font-size:2em;font-weight:bold">9</div>

Mariana Fioramonte, Fabio Cezar Gozzo, Cristiano Luis Pinto de Oliveira, Rodrigo V. Portugal, and Marin van Heel

Abstract

Solution studies permit a direct investigation of the particles on a well-defined environment. A number of thermodynamic and spectroscopic methods can be used directly in solution providing important structural information. In this work, hydrogen deuterium exchange with mass spectrometry, useful for studying protein interactions, dynamics, and conformations, is explained with data analysis approaches having practical implications. Scattering methods, in particular small-angle X-ray scattering (SAXS), are described, and several applications are presented. As it will be shown, directly from the scattering data, it is possible to obtain size, shape, oligomerization state, and aggregation dynamics among several other parameters. We have further provided the details of cryogenic electron microscopy ("cryo-EM") where vitreous ice-embedded macromolecules, liposomes, nanoparticles, and three-dimensional structures are determined using several 2D projection images obtained from cryogenic TEM.

M. Fioramonte • F.C. Gozzo (✉)
Institute of Chemistry, University of Campinas, Campinas, Brazil
e-mail: marifioramonte@gmail.com; fabio@iqm.unicamp.br; fgozzo@gmail.com

C.L.P. de Oliveira
Institute of Physics, University of São Paulo, São Paulo, Brazil
e-mail: crislpo@if.usp.br

R.V. Portugal
Brazilian Nanotechnology National Laboratory (LNNano), CNPEM, Campinas, SP, Brazil

M. van Heel
Brazilian Nanotechnology National Laboratory (LNNano), CNPEM, Campinas, SP, Brazil

Leiden University – NeCEN, Leiden, The Netherlands

245

9.1 Hydrogen Deuterium Exchange with Mass Spectrometry

9.1.1 Introduction

Hydrogen deuterium exchange (HDX) is a technique that gained popularity in the last decade as a way to retrieve information about protein interaction, dynamics, and conformation. Its first applications dated back in 1954, when Kaj Ulrik Linderstrøm-Lang dissolved insulin in deuterated water and measured the density difference between the normal and deuterated insulin, thus inferring the amount of hydrogens exchanged per protein. The principle of HDX is very simple: when in contact with solvents with labile deuteriums, the labile hydrogens from the protein will exchange with deuterium from the solvent, and the rate at which this exchange occurs depends basically on two factors, solvent accessibility and the presence of intramolecular interactions, most commonly hydrogen bonds. The more exposed a hydrogen is, the higher the exchange kinetics, whereas unbound hydrogens will exchange faster than hydrogens involved in hydrogen bonds, for example. Thus, if a condition changes solvent accessibility or the intramolecular bonds pattern, these changes can be tracked measuring the change in deuterium uptake kinetics (DUK). Typical examples of applications include:

1. Interaction surface mapping: if a molecule (organic or protein) binds to a protein, the interaction region between the two molecules has its solvent accessibility decreased and, consequently, its DUK.
2. Conformational change: if a ligand or posttranslational modification causes a conformational change in a protein, some parts of the protein surface that were originally buried inside the protein will be exposed to the solvent, increasing its DUK. Conversely, some parts of the surface that were originally exposed may decrease its solvent accessibility, leading to a lower DUK.
3. Dynamics: upon ligand binding, parts of a protein may have its thermal movement decreased, leading to reduced dynamics on that specific region. Natural thermal movements usually imply in transient changes on the hydrogen bond pattern or at least in the weakening of these bonds: alpha helices that undergo swinging movements, for example, necessarily cause the hydrogen bonds of amidic hydrogens of the helices to be alternately weakened and strengthened. As the DUK increases for loosely bound hydrogens, increase in the dynamics of parts of the protein will lead to the increased DUK.

HDX is therefore very useful to track the structural changes described above. On the other hand, these structural changes are very difficult to follow by other techniques, and this fact is one of the reasons why HDX has gained so much popularity in the last decade. Besides its power and simple principle, several experimental difficulties have prevented its broad adoption by laboratories around the world. Nonetheless, in the last decade, these difficulties have been overcome, and HDX is nowadays a technique that can be easily implemented in any laboratory and can be even be automated to the point that very few human intervention is

needed. To understand these difficulties and how they were overcome, it is neces-
sary to understand how HDX experiments are performed and the fundamentals
behind it.

Measurements of DUK can be accomplished by either nuclear magnetic reso-
nance (NMR) or mass spectrometry (MS), but this chapter will focus only in the
HDX-MS principles and applications. It should be emphasized that HDX is mostly
a comparative technique as the absolute DUK is difficult to be rationalized, but on
the other hand, HDX is very reproducible when the necessary experimental care is
taken, thus being able to report very subtle differences in DUK between samples.

9.1.2   Overview of HDX Experiments

Several mechanisms can account for H/D exchange, depending on the pH of the
solution, but it is basically an acid-base reaction as depicted in Fig. 9.1.

To correlate the DUK with changes in protein dynamics or conformation, all
other factors that affect the DUK must be kept as constant as possible between
samples, and, among these factors, pH and temperature are by far the most
important ones. Figure 9.2 shows the dependency of several labile hydrogen
types present in proteins with pH. The first thing to be noticed is the huge difference
(>1010) in H/D exchange rate depending on the specific organic function, so
precise control over the solution pH is critical for reproducibility and sensitivity
of the experiment. Whereas alcohols, carboxylic acids, and amines exchange very
fast, the backbone amide hydrogen presents the slowest DUK. Another noteworthy
fact of Fig. 9.2 is that, at pH ~2.7, these backbone amide hydrogens present their
lowest rate, being 10.000 times slower than at physiological pH of 7.

Similarly, the DUK presents a large variation (>100×) depending on the
experiment temperature (Fig. 9.3). From room temperature to 0 °C, the DUK
decreases ~7 times, and along with pH, temperature must be precisely controlled
for a successful experiment.

To detect the amount of deuterium incorporated into a protein or peptide, a mass
spectrometry analysis is performed, requiring the exchanged sample to be dissolved
in H_2O. If MS analysis is performed under conventional conditions, i.e., pH ~3.5
and room temperature, a back exchange will occur, replacing the incorporated
deuterium by hydrogens from water. To quench this back exchange, the sample
must be conditioned at pH 2.7 and 0 °C, conditions that minimize the hydrogen
uptake kinetics. However, the same conditions that minimize the back-exchange
problems generate some experimental restrictions as the whole MS analysis
(including liquid chromatography) now needs to be performed ideally under these
situations. A typical HDX workflow is shown in Fig. 9.4.

The first limitation imposed by the HDX back-exchange quenching conditions is
the choice of protease. Only a few proteases are active in pH 2.7, and the most
commonly used is pepsin, although some alternatives have been recently used. The
second restriction is to perform the liquid chromatographic analysis in low temper-
ature (ideally 0 °C). The low temperature increases the solvent viscosity and,

Base catalysis

(a)
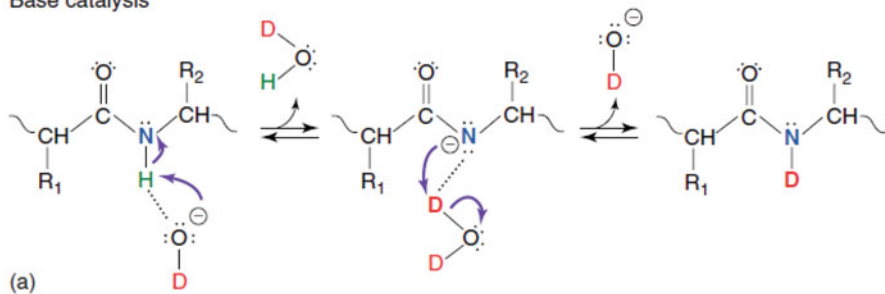
Acid catalysis

(i) N-Protonation

(ii) O-Protonation

(b)
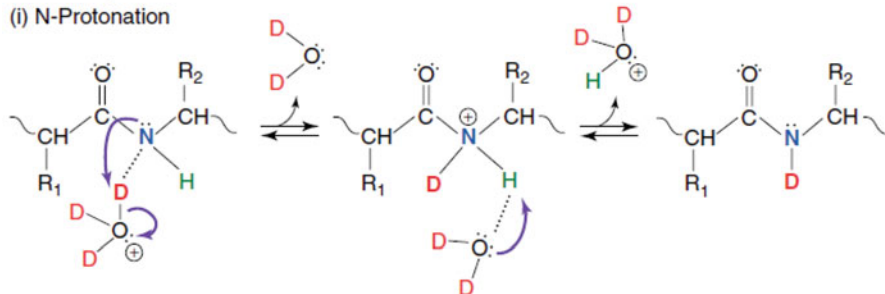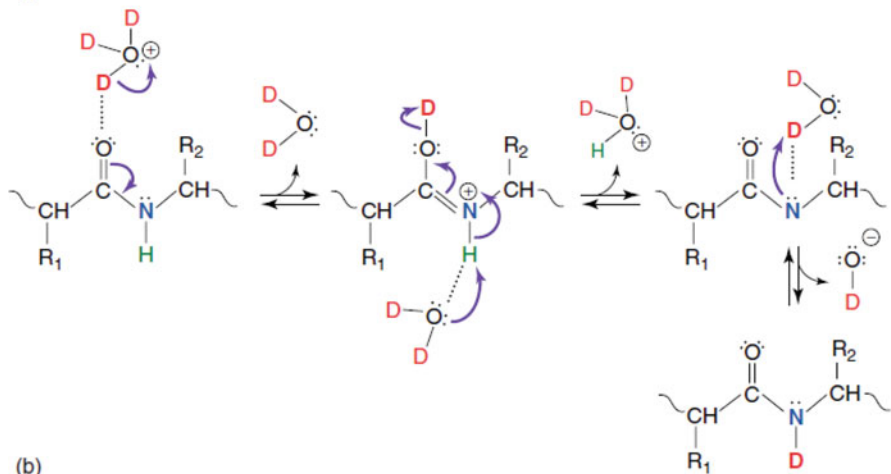
Fig. 9.1 Possible mechanisms for H/D exchange between water and amidic hydrogen depending on the pH of the medium (Reprinted from Engen, J. R., et al., *Encyclopedia of Analytical Chemistry*, 2011)
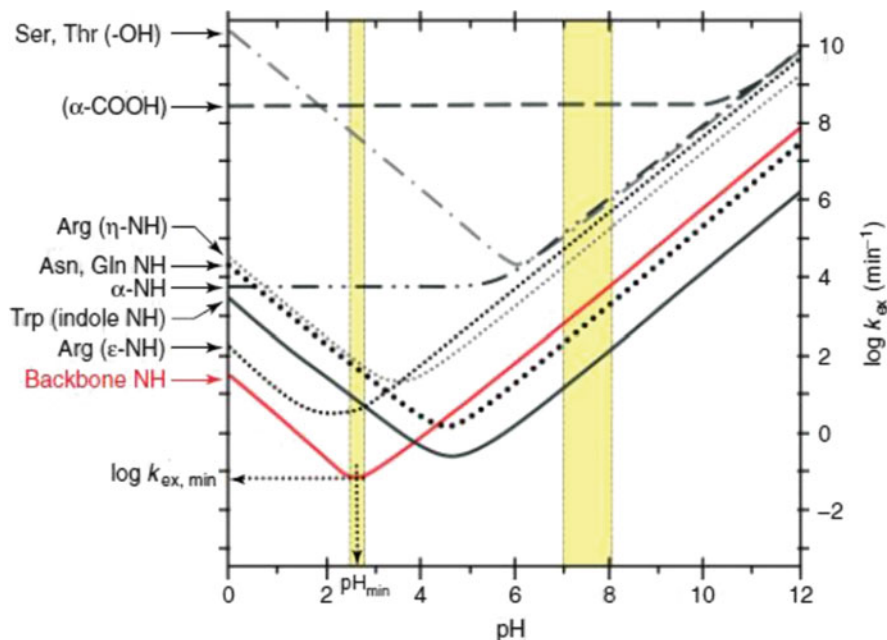
Fig. 9.2 Exchange rate constant (K_{ex}) in function of solution pH showing the dependency of labile hydrogen on different pH (Reprinted from Engen, J. R., et al., *Encyclopedia of Analytical Chemistry*, 2011)

Fig. 9.3 Temperature dependence of deuterium uptake kinetics on backbone amide (Reprinted from Engen, J. R., et al., *Encyclopedia of Analytical Chemistry*, 2011)

Fig. 9.4 Hydrogen deuterium exchange workflow. The target protein is originally solubilized at room temperature (25 °C) in its native, aqueous buffer. A > tenfold dilution (by volume) in D_2O buffer with the same compo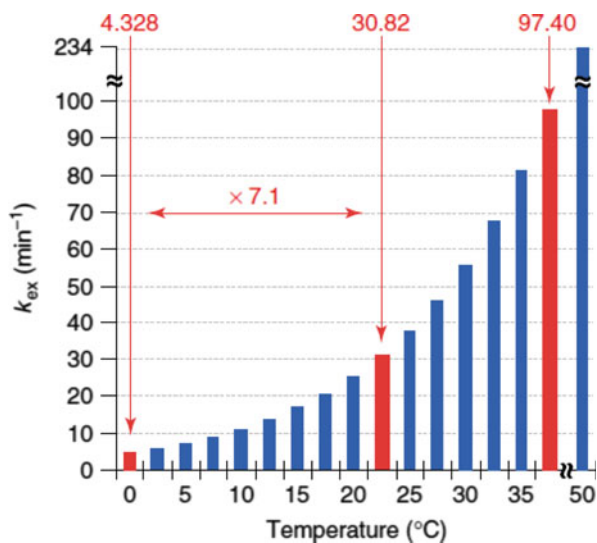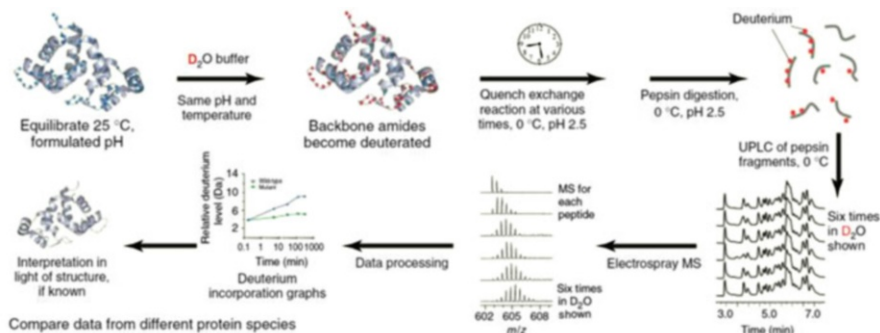sition starts the labeling experiment. A sample is collected in specified time intervals, and the exchange reaction is quenched by bringing the pH to 2.5 and the temperature to 0 °C. The protein in this condition is then digested with an acidic protease, usually pepsin. Peptide is then separated by reversed-phase chromatography, and each peptide has its mass measured by mass spectrometry. The difference in average mass between undeuterated and deuterated peptides is plotted as a function of exchange time. The data can be mapped into the protein structure if known (Reprinted from Engen, J. R., et al., Encyclopedia of Analytical Chemistry)

consequently, the system pressure. By changing the LC and MS conditions to perform the analysis under low pH and temperature, back exchange is minimized, and the most of incorporated deuteriums are detectable by MS.

The exchange of a hydrogen by a deuterium causes a change in mass of +1.0006 Da per exchange, thus measuring the mass of each peptide will return the amount of hydrogens exchanged. These measurements are then performed for each time point so that a kinetic curve is obtained for each peptide. The not so obvious point here is that for every peptide, the exact number of hydrogens exchanged will vary for each individual molecule so that the mass spectrum will show the overall distribution of exchanged species. This overall distribution appears as a broadening of the isotopic pattern as depicted in Fig. 9.5. The average deuterium uptake can then be calculated by the difference between the average mass of the exchanged peptide at each time point minus the average mass of original peptide. This relative deuterium level can be plotted against time to create the DUK. By measuring the DUK of the same peptide in two (or more) different samples, any difference in the DUK corresponds to a structural difference between the two samples, and the identity of the peptide reveals the location of this change in the protein.

9.1.3 Applications in Protein Dynamics and Interactions

Structure and protein conformation are intrinsically related to protein function and mechanism of action, and in most of the cases, this mechanism is occasioned by
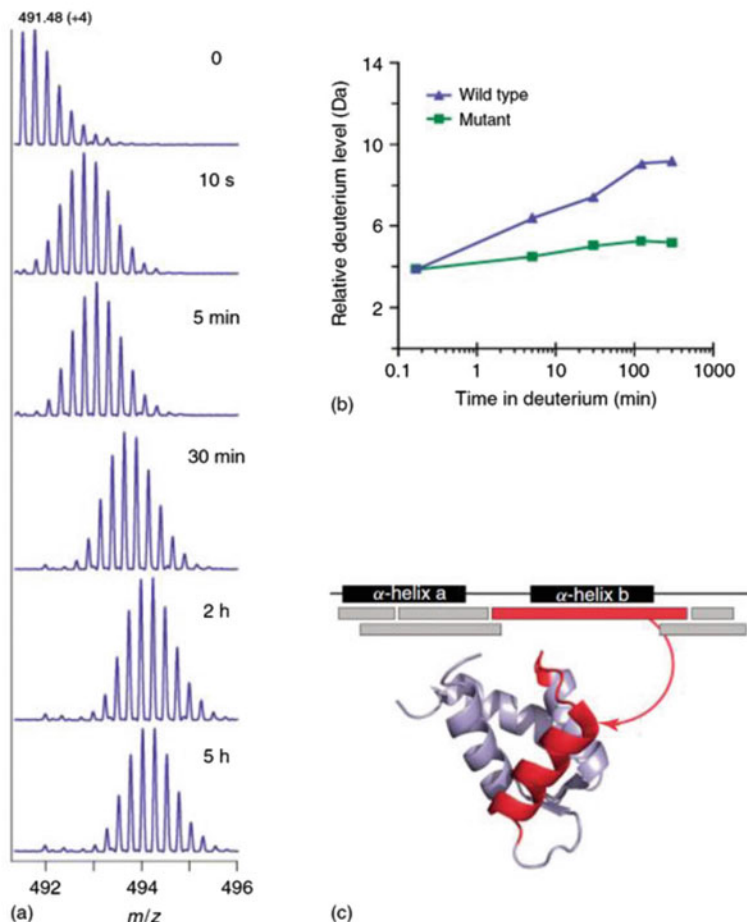
Fig. 9.5 Data analysis in HDX-MS. Example of HDX data analysis for a hypothetical peptide of m/z of 491.48, with +4 charge state. (**a**) ESI (+) mass spectra of undeuterated m/z 491.48 ion. The exchange time is shown in each spectrum. (**b**) Deuterium uptake graph for this peptide in the wild-type protein (*blue* triangles) and in the mutant protein (*green squares*). (**c**) The position of this peptide in the sequence and crystal structure of the protein. The peptide corresponding to this peptide m/z 491.48, +4 is shown in *red* in a peptide map (*top*) and in the structure (*bottom*) (Reprinted from Engen, J. R., et al., Encyclopedia of Analytical Chemistry, 2011)

protein binding to ligands and/or interaction with other proteins, leading to the necessary conformational for protein function accomplishment. Using HDX-MS it is possible to map protein interaction site with ligands and protein as well as the conformational changes caused by these interactions. For example, Goswami et al. employed HDX-MS to study the conformational changes in progesterone receptor B (PR-B) upon agonist (R5020) binding. They also showed that the interaction between TATA box-binding protein (TBP) with PR-B and R5020 occurs via

N-terminal activation function (AF) AF1, and these interactions impact the mobility on the C-terminal AF2. Another study performed by Zanphorlin and collaborators resorted to HDX-MS combined to chemical cross-linking to characterize the interaction site between the heat shock protein 90 kDa (Hsp90) and one of the translocate of the outer mitochondrial membrane (TOM) proteins, TOM70. It was known that Hsp90 has a C-terminal MEEVD motif which recognizes and interacts with co-chaperons. One of the HDX-MS experiments performed was the comparison between TOM70 on the presence/absence of MEEVD peptide and one scrambled peptide as control. Figure 9.6a illustrates the peptides that were protected, showing that scrambled peptide did not show any significant decrease on deuterium incorporation on TOM70. Figure 9.6b highlights the regions on TOM70 structure that presented deuterium uptake decreased by MEEVD peptide presence, indicating an interaction site. The authors compared this region to the interaction site observed on Hsp82/TOM71 crystallographic structure. HDX-MS of Hsp90/TOM70 protein complex was also performed. Figure 9.6c illustrates the deuterium uptake decreasing for Hsp90. The Hsp90 645–662 peptide showed very protected (4 Da decrease) in the presence of TOM70, and this region corresponds exactly to the interaction region identified by the chemical cross-linking experiment (Fig. 9.6d).

Scorsato et al. employed HDX-MS methodology to study the role of DYFL peptide on the structure of TOR signaling pathway regulator-like (TIPRL). TIPRL showed a new protein fold revealed by X-ray crystallography (Fig. 9.11, Chap. 1), which indicated that this protein interacts with the catalytic subunit of PP2A (PP2Ac), a known protein partner, by recognizing its conserved C-terminus. DYFL peptide is a mimic for the conserved C-terminal tail of PP2Ac. Using HDX-MS it was possible to define the protein regions that became more rigid upon peptide binding and, consequently, the regions that are very flexible in the absence of ligand. Interestingly, most of these flexible regions are not directly related to the peptide binding site, showing a long distance effect of the ligand and explaining why TIPRL does not crystallize in the absence of peptide.

Protein folding experiments can also be done under deuterium exchange conditions, and, by monitoring positions that become solvent protected or hydrogen bonded, it is possible to monitor the progression of protein folding. It is also possible to monitor the participation of other proteins during folding as Georgescauld and collaborators demonstrated using HDX-MS to study how GroEL/ES assists protein folding. This work compares assisted and unassisted folding of dihydrodipicolinate synthase (DapA) by GroEL/ES. DapA was unfolded with denaturant solution and then diluted into deuterium physiologic condition to fold into its native structure in the presence/absence of GroEL/ES. The study shows that upon GroEL/ES-assisted condition, the DapA folding changed by more than 30-fold faster and also changed the tetramer folding order (Fig. 9.7). Other studies also used HDX-MS to study how proteins as maltose-binding protein (MBP), cytochrome C, and phosphofructokinase-2 (Pfk-2) fold in solution.

HDX-MS can also be employed to study the mechanism of action of macromolecular protein complexes. Vahidi and collaborators showed the elegant employment of HDX-MS to interrogate the action mechanism of the molecular motor F0F1 to drive
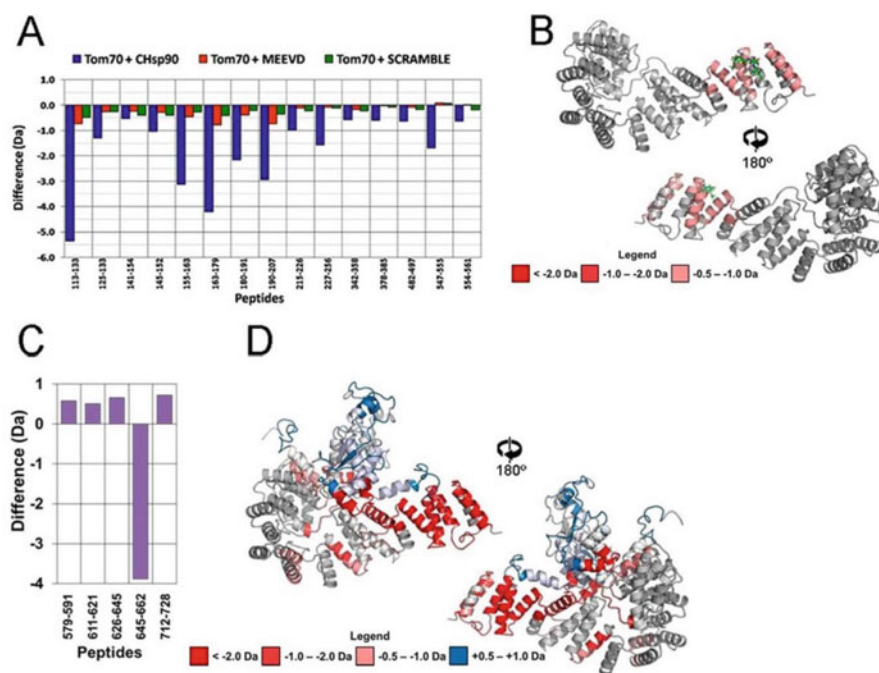
Fig. 9.6 (**a**) Deuterium uptake upon binding of peptides of Tom70 (scrambled peptide, *green*; MEEVD peptide, *red*; and C-Hsp90, *blue*). (**b**) Impacted regions in Tom70 by the presence of the MEEVD peptide are in *red*. (**c**) Tom70 deuterium incorporation upon binding of C-Hsp90. Only those with differences >0.5 Da are shown. (**d**) C-Hsp90/Tom70 model. The model was built considering the cross-linking and hydrogen deuterium exchange (Reprinted from Zanphorlin et al. 2016)

the synthesis of ATP from ADP and Pi. They showed that γ-helix shaft plays an important role in ATP synthesis. As showed in Fig. 9.8b, γ C-terminal helix has two different levels of deuterium exchange: dark red coloring highlights intensely enhanced deuterium uptake when the catalytically activated system is compared to the inhibited one, and the lighter red indicates also increased deuteration but in a less extensive way. These results could indicate that β-lever force is driving the rotation of γ-helix shaft inducing a torsional stress and then inducing destabilization of hydrogen bonds on the apical γ-helix that could act as a resistive force. Song and collaborators used HDX-MS to elucidate the mechanism by which factor VIIa (FVIIa), a trypsin-like protease, is upregulated by tissue factor (TF). In this study, it was employed electron transfer dissociation (ETD) fragmentation, resulting on deuterium uptake measurement at amino acid residue level. With this methodology, they showed that the enzyme transition to activated form induces conformation and local interactions pattern changes at key sites across the surface of the FVIIa domain spanning the TF-binding helix across the activation pocket to the calcium binding. They also showed that the conformational allosteric activation signal spreads to the EGF1 domain, underlining intra- and interdomain allosteric regulation of FVIIa.
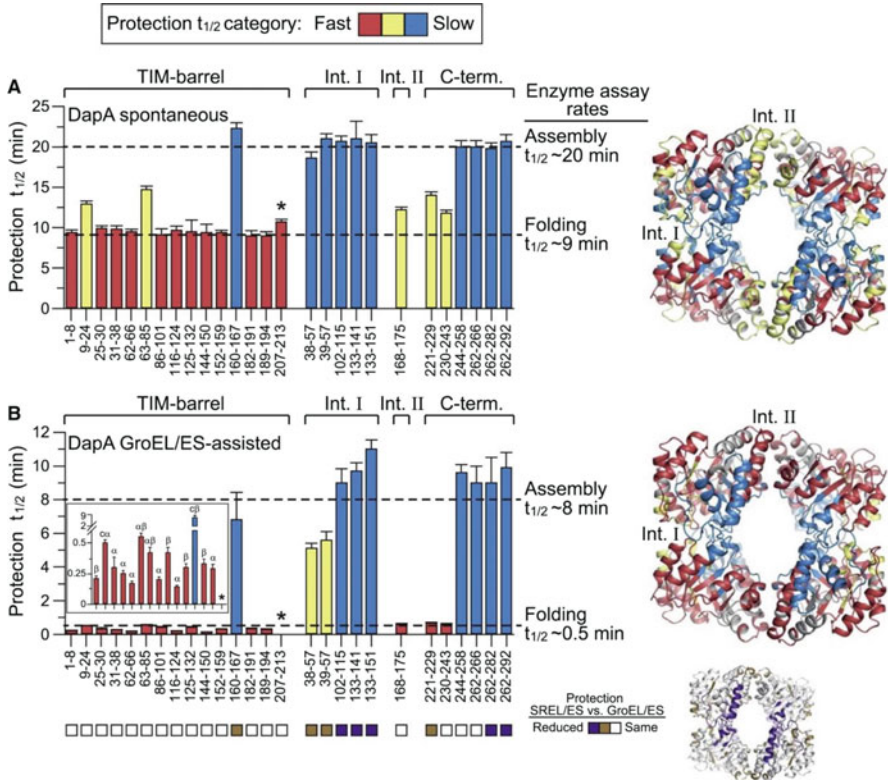
Fig. 9.7 Study of chaperone-assisted protein folding. DapA folding (**a**) in absence of GroEL/ES or (**b**) in the presence of GroEL/ES. Colors *red*, *yellow*, and *blue* represent protection half-time for each peptide (Reprinted from Georgescauld et al. 2014)

9.2 Small-Angle X-ray Scattering Investigations of Macromolecules in Solution

9.2.1 Introduction

Proteins are macromolecules essential for living systems. They are found in all cells and in all parts of the cells and are responsible for the many intricate and correlated biological processes (Voet et al. 2005). From a set of (only) 20 types of amino acid residues, a defined sequence of residues is build (known as primary sequence), and due to hydrophobic effects, this sequence folds forming the secondary and tertiary structures. The tertiary structure defines the shape of the protein in solution and is directly related to the protein function and dynamics (Otzen 2011). In several cases the proteins agglomerate on a well-defined manner (quaternary structure) forming functional supramolecular systems like, for example, the ribosome (Selmer et al. 2006). The knowledge on the structure of the macromolecule can be very useful to

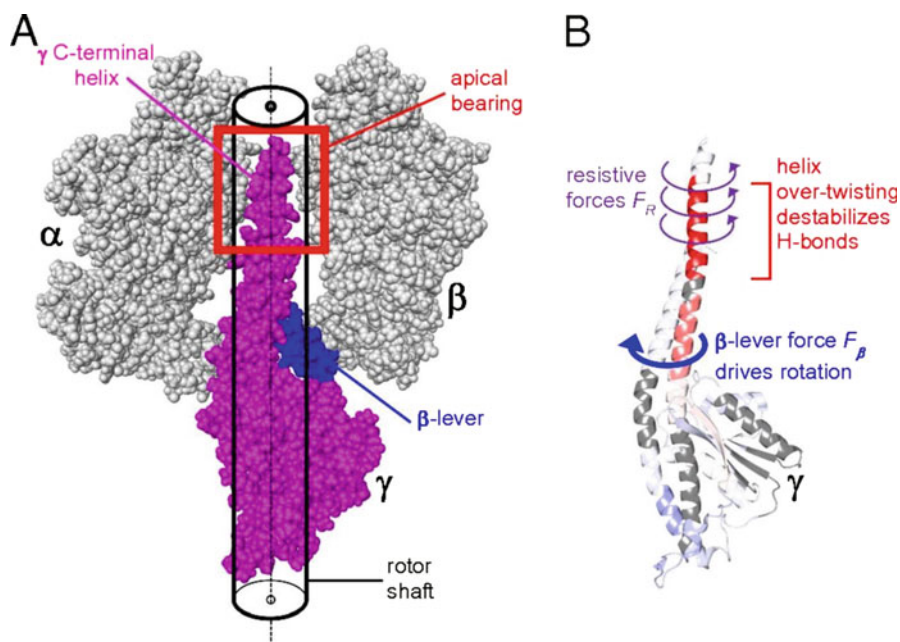**Fig. 9.8** (**a**) γ/α3β3-complex crystal structure (PDB ID 3OAA). (**b**) Deuterium incorporation levels on γ C-terminal helix during catalytic activity. The *dark red* coloring highlights intensely enhanced deuterium uptake when the catalytically activated system is compared to the inhibited one, and the *lighter red* indicates also increased deuteration but in a less extensive way (Reprinted from Vahidi et al. 2016)

understand its function on the system. There are several methods to investigate protein structure, function, and dynamics. When it is possible to crystalize the protein, protein crystallography methods can be used to retrieve atomic resolution information for the system. Nuclear magnetic resonance also permits atomic resolution information, but usually the measurements take a very long time and an elaborated data analysis. This technique permits the investigation of systems in solution but is limited to low molecular weight proteins (< 50 kDa). Electron microscopy techniques (TEM and cryo-EM) had an impressive advance on the recent years (Worrall et al. 2016) but still require elaborated sample preparation and are indicated for large complexes (of the order of hundreds of kDa or higher). Scattering techniques, namely, small-angle scattering, either using neutrons or X-rays, permit structural investigations directly in solution, with relative simple sample preparation, providing an experimental tool for real-time monitoring of the system and the retrieval of overall size, shape, and low-resolution structure (Oliveira 2011; Svergun et al. 2013). This technique is usually combined with complementary biochemical techniques like circular dichroism, calorimetry, fluorescence, sedimentation, etc., in order to obtain relevant information for the studied system. As will be presented in this section, SAXS can be used for real-time

monitoring of aggregation processes and retrieves internal structure information among several other parameters, directly from the scattering data.

9.2.2 General Principles

9.2.2.1 Small-Angle X-ray Scattering (SAXS)

The SAXS technique is very useful for the investigation of macromolecules due to the fact that it permits investigations for the system directly in solution, with a minimum interaction with the system and, in real time, can provide important information on the particle sizes, flexibility molecular weight, shapes, and aggregation state (Oliveira and Pedersen 2013).

A collimated beam of X-rays with, preferably, monochromatic wavelength λ strikes the sample, interacts with the electron clouds of the atoms, and is scattered. For a system of particles randomly oriented in space, embedded on a matrix with constant electron density, the measured scattering intensity is given by (Glatter and Kratky 1982):

$$I(q) = N\langle f^2(\vec{q})\rangle\langle S(\vec{q})\rangle \tag{9.1}$$

where $\vec{q}$ is the reciprocal space momentum transfer vector, with modulus given by $q = \frac{4\pi\sin\theta}{\lambda}$ (assuming 2θ as the scattering angle), N is the number of particles illuminated by the incident beam, $\langle f^2(\vec{q})\rangle = P(q)$ is the so-called form factor of the scattering particle, and $\langle S(\vec{q})\rangle$ is the structure factor of the system. The brackets can indicate averages over particle orientations, polydispersity, variation on contrasts, etc. As a result, the scattering intensity depends only on the modulus of the vector $\vec{q}$, which, essentially, leads to an important loss of information on the system (Oliveira 2011). From the analysis of the scattering intensity, important structural information can be obtained. When the system concentration is very low, one can neglect the interaction between the particles ($\langle S(\vec{q})\rangle \to 1$), and the measured intensity is given by:

$$I(q) = N P(q) = N I_1(q) \tag{9.2}$$

where $I_1(q)$ is the scattering from a single particle, randomly oriented. Equation 9.2 is very important because it indicates that it is possible to obtain information about the particle sizes and shapes even from a system of particles (Oliveira 2011; Svergun et al. 2013).

There are several modeling procedures that can be applied for the analysis of the scattering intensity. For monodisperse systems, a very useful procedure is the indirect Fourier transformation (IFT) method. In this approach, it is assumed that the form factor is the Fourier transformation of a real-space function, p(r), known as the pair distance distribution function. From the obtained p(r) function, it is possible to calculate the particle radius of gyration and retrieve the maximum size and the forward scattering I(0) (Glatter 1977; Semenyuk and Svergun 1991; Oliveira et al. 2009; Oliveira 2011). From the overall shape of the p(r) curve, it is also possible to directly infer the shape of the particle (Oliveira 2011). One of the major strengths of

this approach is the fact that any prior knowledge about the system is not necessary, only the assumption of monodispersity. On the last decades, important advances were made for the analysis and modeling of scattering data from monodisperse systems of macromolecules in solution. It is beyond the scope of this chapter to present a detailed review on this topic but is possible to obtain low-resolution 3D models for the particles in solution directly from the scattering intensity (Svergun 1997; Chacon et al. 1998; Svergun 1999; Walther et al. 2000), obtain protein-like low-resolution structures (Svergun et al. 2001), combine low- and high-resolution models to determine the conformation of proteins and complexes (Petoukhov and Svergun 2005) and model protein flexibility on domains (Bernado et al. 2007; Tria et al. 2015), include multiple sets of scattering and NMR data for the modeling (Wassenaar et al. 2012), combine scattering and hydrodynamic information (Solovyova et al. 2004; Tiroli et al. 2005), besides many other possibilities and methodologies (Kikhney et al. 2016; Tuukkanen et al. 2016). Some examples will be shown below, with the use of advanced modeling procedures.

9.2.3   Applications

9.2.3.1 In Situ Fibrillation Studies

Amyloid-like fibers or plaques are found on the development of several diseases. Alzheimer's, Parkinson's, and Machado-Joseph's diseases are devastating pathologies which affect mostly the brain with the formation of these types of aggregates. As a result to this systemic amyloidosis process, massive amounts of protein are deposited, leading to irreversible damages on the brain, cognitive afflictions, and death. In order to investigate the fibrillation and aggregation process, several model systems can be used. Under certain conditions, simple proteins like insulin and glucagon (Vestergaard et al. 2007; Oliveira et al. 2009) can form amyloid-like structures providing a very good template for structural investigation of this type of aggregates. Small-angle X-ray scattering can be used to monitor the in situ aggregation and fiber formation of these cases, directly in solution with a minimum influence on the process. One very interesting result is the investigation of the fibrillation of the protein glucagon in solution (Oliveira et al. 2009). Glucagon is a small peptide hormone, 29 residues/3.5 KDa, related to the control of blood sugar/glucose level in the human body. Interestingly, this molecule is a very good model system for fibrillation studies since it is known that, under low pH conditions, it can form large amyloid-like fibers, as seen in electron microscopy images (Dong et al. 2006). However, very little was known about the intermediate states that leave this small molecule to form very large fibers. From solution studies, using SAXS to monitor the system, it was possible to describe the full oligomerization process, in situ (Oliveira et al. 2009). For the sample preparation, the glucagon powder was dissolved in a 50 mM glycine/HCl buffer, on a pH close to 2.5. This low pH is crucial for the fibrillation process. The SAXS measurements were performed on a laboratory-based SAXS instrument NANOSTAR placed at the Institute of Chemistry, Aarhus University, in Denmark. Further details can be

Fig. 9.9 Initial state of glucagon agglomerates in solution. By varying the concentration, the formation of small aggregates is triggered (Reprinted from Oliveira et al. 2009 with permission from Elsevier)
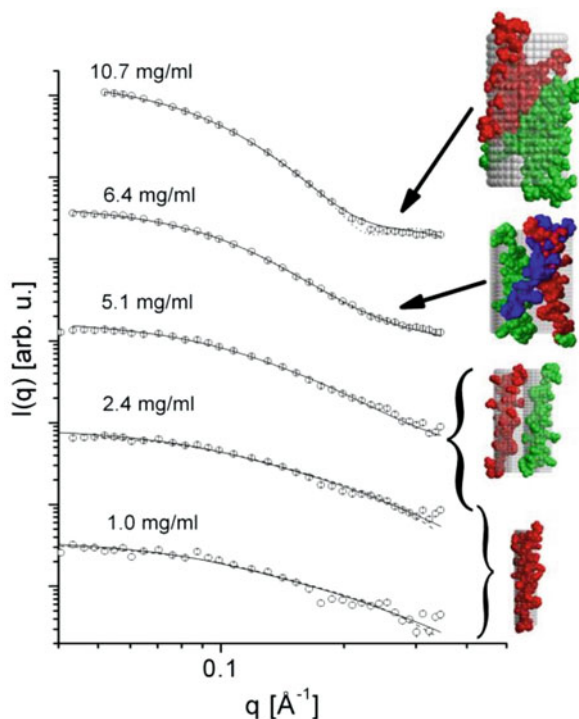
obtained on the original article (Oliveira et al. 2009). The initial investigation was the description of the system for a series of concentrations. The results are shown in Fig. 9.9. Interestingly, the variation of the concentration triggered the formation of small aggregates. This result was very important since it provided information on the initial states of the process. These initial states could be described by simple aggregates of the glucagon molecule, which has known atomic resolution model (1gcn.pdb) (Sasaki et al. 1975).

In acidic medium, the glucagon molecules show fibrillation, even for low or high concentrations (Pedersen et al. 2006). The only difference is on the so-called lag time, which is a period where there is no aggregation but changes on the secondary structure which then leads to the fibrillation process. In order to describe this process, an in situ investigation where the solution was monitored by SAXS under more than 50 h was performed. The series of SAXS curves is shown in Fig. 9.10a. As one can clearly see, there is a systematic change on the shape of the scattering curves.

Several model procedures were applied for this data, but one very important result was the demonstration that the whole series could be described by a three-component system: the initial state, small hexamers of glucagon, as shown in Fig. 9.9; a mature state, where thick rodlike fibers were formed; and an intermediate state where we demonstrate the presence of a thinner rodlike structure. By using this model, it was possible to follow the relative concentration of each species as shown in Fig. 9.10b.
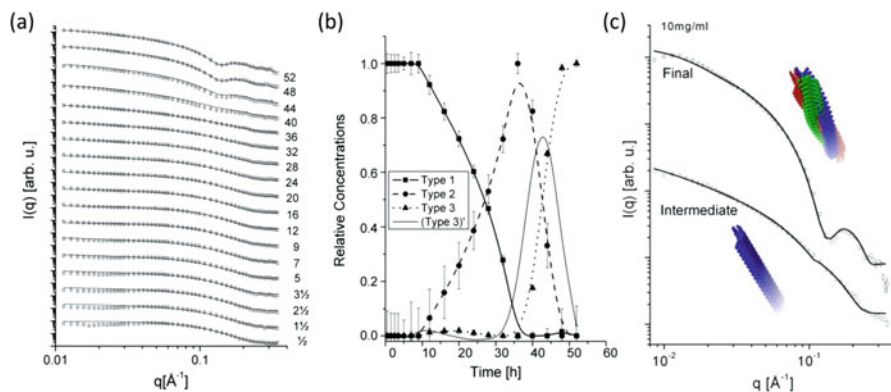
Fig. 9.10 Fibrillation of glucagon in solution. The sample at 10 mg/mL is incubated over several hours and monitored by SAXS. (**a**) Experimental SAXS data (circles) and the fitting (solid lines) for a three-phase system: initial agglomerate, intermediate fiber, and mature fiber. (**b**) Graph of the relative concentration of each species as a function of time. *Squares*, type 1 (initial); *circles*, type 2 (intermediate); *triangles*, type 3 (final); continuous *thin line*, derivative of type 3. (**c**) Real-space model for the glucagon fibers for sample at 10 mg/mL. The models next to the *curves* represent the best model result obtained from least-squares fitting. The *curves* are displaced for better visualization. *Bottom*, intermediate state; *top*, final state (Reprinted from Oliveira et al. (2009) with permission from Elsevier)

The concentration of small oligomers decreases at the same time where the intermediate state is formed (at ~9 h). The concentration of small oligomers goes almost to zero, the intermediate state evolves, and around ~40 h there is the formation of mature fibers, which become dominant at around ~50 h. Using real-space models based on the use of spherical beads on specific arrangements (Andersen et al. 2008; Oliveira et al. 2010; Alves et al. 2014), it was possible to propose low-resolution models for the intermediate and mature states, as shown in Fig. 9.10c. In this work, for the first time, the whole fibrillation process of the glucagon, starting from the single glucagon molecules up to the mature fibers, was presented and modeled, based principally on SAXS results.

9.2.3.2 Investigation of Lipoproteins
The plasma lipoproteins are responsible for the transport of cholesterol between cells. This is essential because the cholesterol molecules (highly hydrophobic) are involved in a number of processes like the structure of cell membranes, precursor or bile acids, vitamin D, and other steroids. Lipoproteins have overall sizes varying from 10 to 40 nm with lipid core composed of triglycerides and cholesterol esters, surrounded by a monolayer of phospholipids, free cholesterol, and apolipoproteins (apo), forming these quasi-spherical particles on different sizes and composition. They are classified in several types according to its size. Two important examples are the low-density lipoproteins (LDL) and the high-density lipoprotein (HDL). These two lipoproteins are related to atherosclerosis, having a key role in this pathology. Usually, the quantities of LDL and HDL, besides other indicators, are

used in lipid profile blood tests and used as indicators for risks of heart problems. However, recent works have shown that more important than the quantity of the lipoproteins on the blood are the oxidation levels of the lipoproteins (Alves and Figueiredo Neto 2014). Even though it is possible to visualize the structure of lipoproteins using microscopy techniques (Ren et al. 2010), solution studies can provide important information on the structural changes induced by the changes on the sample environment like oxidation levels and temperature.

The use of scattering methods for the investigation of lipoproteins was used already in the 1970s (Laggner et al. 1977), but the major problem on the use of these methods is the proper data analysis and modeling (Meyer et al. 1996). In recent works advanced methods were proposed for modeling the small-angle scattering data for lipoproteins in solution (Oliveira et al. 2014a, b; Maric et al. 2017), providing new possibilities for these studies. Two examples are shown in this section. The oxidation effects on the LDL and HDL structures were investigated by the dilution of those lipoproteins (concentration of ~2 mg/mL) in 10 mM PBS buffer with the respective addition of 20 μM $CuSO_4$/mg in order to trigger the oxidation by cupper. The oxidation reaction is stopped with the addition of 1 mM of EDTA to the sample solution. This in vitro oxidation is a very good approximation for the in vivo oxidation of lipoproteins (Gomez et al. 2008). In Fig. 9.11, the experimental SAXS data for LDL and HDL under oxidation stress is shown. The SAXS measurements for LDL were performed at the SAXS beamline of Brazilian Synchrotron Light Laboratory and for the HDL at the laboratory-based SAXS instrument NANOSTAR placed at the Institute of Physics of the University of São Paulo. More details on the sample environment can be obtained on the original article (Oliveira et al. 2014b). From the analysis of this data and the use of a new modeling procedure, it was possible to show that LDL structure is more affected by oxidation than HDL, which was in agreement with other works in the literature (Gomez et al. 2008). Interestingly, the electron density profile of LDL showed small changes, demonstrating that the overall internal structure of LDL is not drastically affected by oxidation. However, an important increase on the flexibility of the apoB protein, due to oxidation, was obtained (Oliveira et al. 2014b).

The effects on the LDL structure under temperature stress were also investigated (Oliveira et al. 2014a). In this case it was possible to follow the aggregation behavior and the temperature-induced changes in the internal structure of LDL over time, after subjecting the solution to a sudden temperature increase, from 22 °C to a higher value. The SAXS data were collected at the SAXS beamline of the Brazilian Synchrotron Light Laboratory, and more details on the sample environment can be obtained on the original article (Oliveira et al. 2014a). In Fig. 9.12a, it is shown the SAXS data for the sample at 42 °C. The systematic changes on the SAXS profile indicate the formation of aggregates of LDL and changes on its internal structure.

By the use of advanced modeling procedures, it is possible to model the scattering data (Fig. 9.12b) and retrieve the electron density profile (Fig. 9.12c), for each time interval. Interestingly, there is a systematic change on the profile, which is related to the melting of the internal lamellar structure of the LDL at this
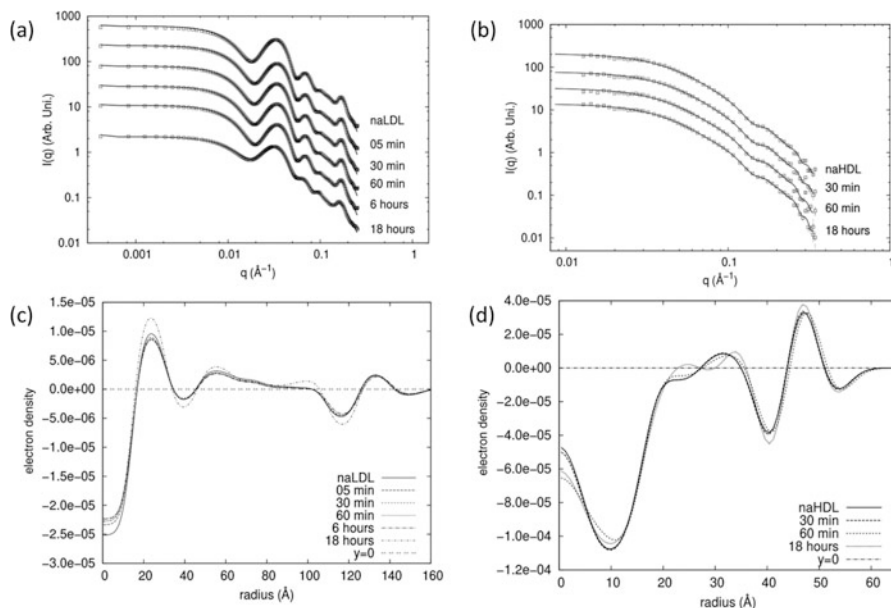
Fig. 9.11 SAXS data and average electron density profile for the oxidation of LDL and HDL over time. (**a**) LDL data and (**b**) HDL data. Experimental data (*open squares*) and model fit (*solid lines*) are shown. (**c**) LDL and (**d**) HDL electron density profiles obtained from the deconvolution modeling procedure (Reprinted from Oliveira et al. (2014b) with permission from Elsevier)
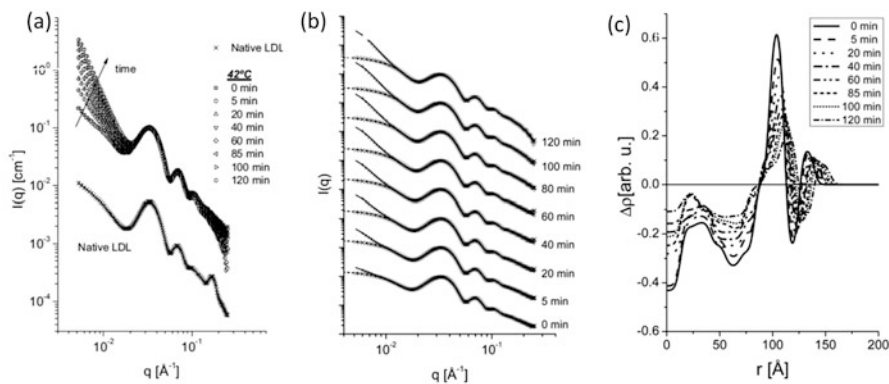
Fig. 9.12 SAXS data and modeling for sample at 42 °C. (**a**) Data series superimposed. The scattering data of the native LDL measured at 22 °C is shown for comparison. This curve is shifted for a better visualization. (**b**) SAXS experimental data for different times (*open circles*), theoretical fits using generalized indirect Fourier transformation (*solid lines*), decoupled form factor (*crosses*), and the fit of the form factor by using the deconvolution procedure (*dash lines*). (**c**) Radial electron density profiles obtained for each time (Reprinted from Oliveira et al. (2014a) with permission from Elsevier)

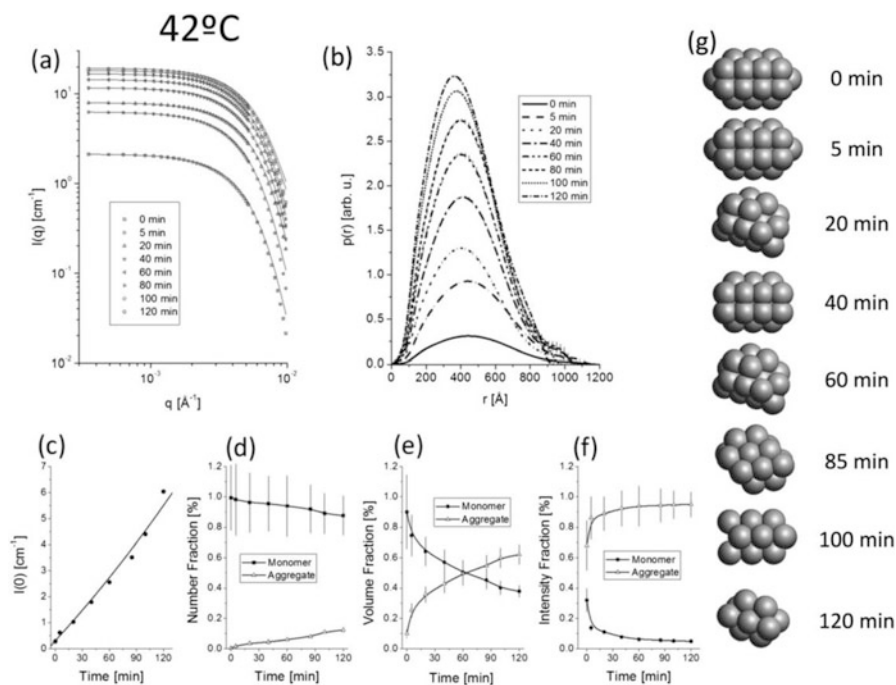**Fig. 9.13** Aggregation of LDL at 42 °C. IFT analysis: (**a**) scattering intensity for the aggregates (*circles*) obtained from the GIFT method. The corresponding p(r) function is shown in (**b**). Calculation of the fractions: (**c**) forward scattering for the data collected at 42 °C (*circles*) indicating a monotonic increase of the intensity. This indicates a systematic increase of the contribution of the aggregates. In this graph, the line is for eye guiding. (**d**) Number fraction of monomers (*circles*) and aggregates (*open triangles*). (**e**) Volume fraction of monomers (*circles*) and aggregates (*open triangles*). (**f**) Intensity fraction of monomers (*circles*) and aggregates (*open triangles*). In these graph, the lines are for eye guiding. Modeling of the aggregates: by using ab initio modeling, it is possible to fit the data (*solid lines* in **a**) and retrieve a 3D model for the aggregates, as shown in (**g**) for each time. Note that the spheres in (**g**) have a diameter of 350 Å (Reprinted from Oliveira et al. (2014a) with permission from Elsevier)

temperature (Oliveira et al. 2014a; Maric et al. 2017). Finally, from the analysis of the aggregation, behavior is also possible to retrieve the evolution of the aggregated species and also the overall size and shapes of LDL supramolecular aggregates, as shown in Fig. 9.13.

9.2.3.3 Conclusions

Scattering methods permit the investigation of the structure of macromolecules directly in solution. This allows the utilization of this technique for the description of a very broad range of systems and experimental conditions (Oliveira 2011; Oliveira and Pedersen 2013). In this chapter some general features of the SAXS technique and two selected applications were presented. The investigation of the

formation of amyloid-like fibers of glucagon in an in situ study demonstrated the full process, from the initial protein oligomers up to the formation of mature fibers. SAXS investigations on the low-density and high-density lipoproteins (LDL and HDL, respectively) provided interesting information on the internal structure, oxidation, and thermal-induced effects leading to aggregation and structural changes. In both cases, the combination of high-quality SAXS data, the use of advanced modeling procedures, and the correlation with additional results from complementary techniques permitted the retrieval of important structural details. Similar results are shown in a large number of applications in the literature, demonstrating the unique features of the use of scattering methods on the investigation of systems in solution (Petoukhov and Svergun 2013; Sun et al. 2017).

9.3 Cryogenic Electron Microscopy

9.3.1 Introduction

The transmission electron microscope (TEM) has played a pivotal role in visualizing the processes of life. Many different specimen preparation approaches have been developed to optimize the observation of different types of biological samples ranging from sectioned tissue and cellular organelles to individual macromolecules. Cryogenic electron microscopy ("cryo-EM") commonly refers to the observation of vitreous ice-embedded macromolecular complexes in a cryogenic TEM. It aims at elucidating the 3D structure of the complexes based on a large set of their extremely noisy 2D projection images.

The feasibility of obtaining a 3D reconstruction of a macromolecule based on a set of individual projection images in different orientations was demonstrated by De Rosier and Klug. At that time, the contrast needed to observe the macromolecules in a TEM was obtained by staining with heavy-atom salts (say, uranyl acetate), an approach known as "negative staining." The disadvantage of dry negative staining, which was primarily developed for direct visual interpretation of the images, is that it imposes resolution limits on the TEM observations, mainly due to specimen distortions and other interactions with the supporting carbon foil.

The advantages of rapidly freezing hydrated biological tissues in liquid helium for TEM studies were first noted by Fernandez-Moran. Taylor and Glaeser later demonstrated that high-resolution information could be obtained from frozen-hydrated (2D) protein crystals. Dubochet and colleagues developed the currently most used method of specimen vitrification for "single particles" by rapidly plunging the sample into liquid ethane. The sample is thus preserved in a close-to-native state in "vitreous ice," more appropriately described as "vitreous water." The vitrified specimen is kept at cryogenic temperatures throughout the process of transfer of the sample to the cryo-TEM and data collection. This protects the sample against the structural damage caused by recrystallization of the embedding medium and protects the sample somewhat against radiation damage by the electron beam. The vitreous water cryo-EM approach yields a superior structural preservation of

the sample compared to the earlier dry negative staining approaches by maintaining the hydration state of the molecules.

Originally, the computational methods, which were in part inherited from X-ray crystallography, could only deal with highly regular specimens, such as 2D crystals, helical fibers, and icosahedral assemblies. Proteins that did not exhibit such a high degree of repetition were not amenable to processing. Methodological developments during the 1980s led to a set of new computational tools allowing for the processing and 3D reconstruction of complexes of any given point group symmetry. Unsupervised MSA classification approaches were introduced, which allowed the unprejudiced grouping of very noisy molecular images. This overall methodology is now known as single-particle analysis (SPA) or single-particle cryo-EM when used for frozen-hydrated specimens.

Several further improvements in EM hardware were introduced over the last decades, which catapulted single-particle cryo-EM to a new level of sophistication. This includes new microscopes with better optics (parallel illumination, Cs correctors, energy filters), integrated computer-controlled sample transfer, and sample holders. In particular, highly efficient direct electron detectors have reached the market which can be operated in "movie mode" allowing to (a posteriori) compensate for local specimen movements. Finally, computational methods have been developed that allow one to distinguish between different states of a complex. This simultaneous processing of the complex in multiple structural states allows one to reveal a structure not only in 3D but also in 4D, where the fourth dimension represents the timeline or the "structure space" the complex follows in performing its function. Altogether, new methods and hardware formed the basis for the current "resolution revolution" we witness in the field.

9.3.2 Principles

9.3.2.1 Recent Technology Developments

Data processing has evolved over the last decades but equally important were the various technological developments that vastly improved the quality of the acquired "micrographs," the use of stable holders integrated into the microscopes, the automation of data collection, the use of energy filters, and finally the use of direct electron detectors:

1. *Integrated holders and microscope automation.* Modern cryogenic electron microscopes have fully integrated sample holders that can hold and store multiple specimens at liquid nitrogen temperatures. These holders are software controlled allowing for the automation of the data collection over different specimen areas and lasting from hours to days of unsupervised data collection. Automated data collection was introduced by Carragher and co-workers using a side-entry holder microscope, allowing for completely automatic data collection for single-particle cryo-EM. The only limitation was the amount of time that a cryo-holder could maintain a specimen at liquid nitrogen temperature and that

was limited by the size of the N_2 Dewar. The introduction of holders with automatic liquid nitrogen refiling capability allowed to extend the typical duration of a data collection session from hours to days. The stability of the new integrated holders was also significantly improved compared to the earlier side-entry holders.

2. *Energy-filtered images*. The electron gun accelerates electrons at a fixed voltage, typically 200 kV or 300 kV. The electrons will have an energy spread around that given value which will be smaller for a "field emission gun" (FEG) than for a conventional hairpin gun. The energy spread will be even smaller for a "cold" field emission gun. The electron microscope optics are designed to perform optimally at *one specific* acceleration voltage. The energy spread thus gives rise to some loss in resolution of the final image. A maybe even more important aspect is that *inelastic* interactions between the electron beam and the sample (including the interactions with the vitreous water) cause a significant fraction of the electrons recorded in the image to contribute to the background noise rather that to the image of the object thus deteriorating the quality of the images, especially at high resolution. The introduction of an energy filter in the microscope will significantly diminish these effects, significantly improving the micrographs.

3. *Direct electron detectors*. For decades, electron microscopy relied on silver-halide photographic film for recording the images. After a typical full-day acquisition session, exposing some 50 micrographs, the negatives needed to be developed and digitized. Optical diffractometer tests – to assess focus, drift, and astigmatism of the images – were part of the first evaluation step, eventually leading to digitized micrographs, ready for processing.

    At that time, CCD cameras had a size of up to 512×512 pixels, which was insufficient for competing with the approximately $8000 \times 12,000$ pixels that could be achieved in one go using scanned negatives. Furthermore, the sensitivity of the CCD cameras was also insufficient, leading to low signal-to-noise-dose images. When 4096×4096 cameras ($4\,k \times 4\,k$) were introduced, the specimen area covered improved massively, even though only about one-sixth of the area was covered by conventional film. The CCDs, however, had some advantages over film since the images were immediately available in digital form and could be directly assessed by power spectrum calculation, etc. Also, an "unlimited" number of micrographs could be collected, opening the path to automatic data collection. The camera technology evolved further to $8\,k \times 8\,k$ and even $10\,k \times 10\,k$ cameras, but, those high pixel count cameras did not achieve the same popularity as did the $4\,k \times 4\,k$ cameras.

The next – dramatic – development was the introduction of the direct electron detector, which did away with the scintillator used for converting the electron arrivals into photon bursts. This new generation of detectors counts electrons directly, without the conversion to photons, and does so much more efficiently in terms of detective quantum efficiency (DQE) than did the earlier CCD image sensor. These new detectors also have a much higher acquisition rate, allowing

for the collection of a rapid sequence of images from the same sample area: these images are referred to as "frames" of a "movie." The movie mode data collection approach allows us to handle the problem of beam-induced movement as was mentioned earlier.

9.3.2.2 Data Processing

In single-particle cryo-EM, a typical data collection experiment yields hundreds or even thousands of images ("micrographs"), with each micrograph containing anything from a few to a few hundred particles. The micrographs are necessarily all taken at somewhat different defocus, simply because we need to collect the data *guessing* the correct focus value to avoid damaging the radiation-sensitive biological material. The micrographs then need to be "CTF-corrected" to account for those different defocus values. Images of the same object taken at different defocus will show contrast reversals in their small details (dark-to-light and light-to-dark reversals). After CTF correction of the micrographs, the 2D particle images are extracted from the micrographs to form a "stack" of particles which constitutes the primary dataset. The 2D particle images are 2D projection images of the 3D structure we are after. To be able to calculate that underlying 3D structure, we need to find the relative orientation of all the 2D projection images. The position of each particle is determined by six parameters: three shift parameters (x, y, z) and three rotational parameters known as Euler angles (α, β, γ). The relative translational alignments and Euler angular orientations are optimized in an iterative process where the reconstruction is gradually refined toward higher resolution. Different strategies for this refinement have been implemented, but most follow a general reference-based alignment strategy. An exception is the "alignment by classification" ("ABC") approach which is reference-free and can also account for specimen heterogeneity ("ABC-4D") [unpublished work from M. van Heel's lab].

We will here not elaborate on how to take the best possible images in a cryo-EM, but we here provide a generic data processing pipeline for once good images have been collected:

1. *Correction of camera properties*. Each digital camera has its flaws and the manufacturer will try to correct those using some form of "flat field correction." What has not been generally appreciated is that large cryo-EM datasets themselves already contain enough information to precisely determine the characteristics of each of its pixels. This correction is highly effective, and a first processing of a newly collected large dataset will thus include a routine removal of extreme images and a normalization of the pixel characteristics.
2. *Movie processing*. With the latest generation of cameras, datasets can be collected as *movies*. Instead of collecting a single micrograph, a sequence of movie frames is collected, each taken with a fraction of the required overall dose. The final "micrograph" is then assembled as the sum of the 5–100 movie frames after those have been aligned with respect to each other. This alignment minimizes the effects of holder drift and beam-induced specimen movements and can even

be applied locally, around each recorded particle. Movie processing is currently a very active research field, and new developments are reported regularly.

3. *CTF correction*. It is important to correct the effects of the CTF as soon as possible at the level of the (movie-aligned) micrographs. This early CTF correction has the advantage that all images become directly comparable, allowing for all data to be processed simultaneously in a single batch. In most cryo-EM data processing, the CTF correction is performed on a micrograph-by-micrograph basis. A CTF processing based on the "principal components" (main eigenvectors) of all spectra in the dataset has the advantage that it focuses on Thon ring patterns that are found to prevail in the large dataset of micrographs. A very accurate and fast automatic "full dataset CTF correction" of very large dataset can thus be performed on standard desktop and notebook computers.

4. *Particle picking*. Having (camera and CTF) corrected the raw images, one will typically also filter the micrographs to emphasize the properties of the particles with respect to the average background. Automatic particle picking schemes can be a two-step procedure where one first un-discriminatively picks areas of the micrographs that have a higher local variance than the background. Once one has processed these first particle images, one obtains – from a preliminary 3D reconstruction (see below) – a good idea of what the different possible views of the structure would be, and one can then specifically search for those molecular views. This "cross-correlation"-based searching for specific molecular views in the micrographs can be very efficient yet may be prone to reference bias. One risks finding "Einstein" in random noise just because the reference image looks like Einstein. When searching for specific molecular views, a golden rule is that the results should yield reproducible high-resolution information that was not yet present in the low-resolution search images.

5. *Alignment and classification*. The stack of picked particles will contain molecular images in all possible positions (x, y) within the 2D image frame and in all possible in-plane rotational orientations (a). The required in-plane alignments are traditionally performed by cross-correlation function (CCF) maximization with respect to a set of preselected reference images. As is the case with CCF-based particle picking mentioned above, this process is inherently sensitive to reference bias. Multivariate statistical data compression and classification ("MSA") is then used to group the particles with different Euler angle orientations (β, γ). The MSA classification also strongly reduces the influence of individual references. One can avoid explicit alignments of individual molecular images altogether in a procedure known as alignment by classification (ABC) where the classifications are always performed *prior* to any form of alignment.

6. *Euler angles and 3D reconstruction*. Finding the translational alignments and Euler angular orientations of all particles relative to a common 3D structure is the ultimate goal of alignment and classification phase of the processing. A critical phase of the processing is assigning the first set of consistent Euler angle orientations (α, β, γ) to the good class averages obtained above. The first initial 3D structure can, for example, be obtained by "angular reconstruction." Again,

this is rapidly evolving field of research where new papers and methodological variants are appearing in rapid succession [unpublished work from M. van Heel's lab].

7. *Iterative refinements*. Once one has a consistent reliable low-resolution 3D structure (or more than one in the case of a heterogeneous dataset), the whole dataset starts to have a common coordinate system in terms of position (x, y, z) and Euler angles (α, β, γ). We then enter a phase of refinements aimed at optimizing all parameters with the aim to improve the reproducible high-resolution details. Various strategies exist for this refinement. A popular one is "projection matching" where molecular images are aligned with respect to all possible projections of the intermediate 3D structure. This approach has been very successful in recent years, but the approach is wasteful in terms of computational requirements and often needing special hardware ("GPU"). Refinements can also be performed using the angular reconstitution methodology mentioned above [unpublished work from M. van Heel's lab].

8. *Validation*. Of fundamental importance is the validation of the result by objective metrics. Although there exists a consensus in using the "Fourier shell correlation" (FSC) as a resolution metric, the threshold at which to define the absolute resolution value of the final refinement results is still the subject of ongoing discussion, although all fixed value threshold values have been argued to be incorrect more than a decade ago. Confusing topics have entered the polemics here where the FSC is said to be of "gold standard" when the interparticle alignments are performed in certain ways. The FSC, however, is merely a metric for comparing two 3D densities with each other in whatever field of science. A "gold standard" alignment is on the other hand an issue specific to the field of single-particle cryo-EM and not in any other field such as X-ray microscopy. The FSC is now being used in various fields of 3D data processing as a reliable reproducible resolution metric.

9.3.3 Applications

The vitreous ice specimen preparation approach has successfully been used for studying a wide range of samples other than macromolecules including: liposomes, micelles, emulsions, and nanoparticles. The major importance of vitreous ice-embedding approach has been the structural preservation of macromolecular complexes in a *quasi* in vivo buffer environment. Over the last years, many macromolecular structures have been elucidated by single-particle cryo-EM. High molecular weight structures like the Zika virus can now be solved to a resolution sufficient for de novo determination of its atomic coordinates. In X-ray crystallography, one can only see the *average* behavior of the molecules in their crystallography packing. In single-particle cryo-EM, in contrast, the dynamic information of the structural variability of each individual molecule remains available in the recorded raw data. The problem here is to extract that very noisy and complex information from the (huge) raw dataset. The larger the dataset, the better one can

characterize subtle variations among the recorded complexes, simply because more raw information is available to contribute to the statistical significance of the end results. The great challenge of cryo-EM is to precisely characterize the structural variations present in the sample. 4D cryo-EM, yielding multiple 3D structures per sample, often provides a basis for the functional interpretation of a biological system. 4D cryo-EM is thus undoubtedly one of the most rewarding challenges of current structural biology.

References

Adrian M, Dubochet J, Lepault J, McDowall AW (1984) Cryo-electron microscopy of viruses. Nature 308:32–36

Afanasyev P, Ravelli RBG, Matadeen R, De Carlo S, van Duinen G, Alewijnse B, Peters PJ, Abrahams JP, Portugal RV, Schatz M, van Heel M (2015) A posteriori correction of camera characteristics from large image data sets. Sci Rep 5:10317

Ahn J, Cao M-J, Yu YQ, Engen JR (2013) Biochim. Biophys. Acta 1834(6):1222–1229

Alves S, Figueiredo Neto AM (2014) Advances in the non-linear optical investigation of lyotropic-like low-density human lipoproteins in the native and oxidised states. Liq Cryst 41(3):465–470

Alves C, Pedersen JS, Pinto Oliveira CL (2014) Modelling of high-symmetry nanoscale particles by small-angle scattering. J Appl Crystallogr 47:84–94

Andersen FF, Knudsen B, Oliveira CLP, Frohlich RF, Kruger D, Bungert J, Agbandje-McKenna-M, McKenna R, Juul S, Veigaard C, Koch J, Rubinstein JL, Guldbrandtsen B, Hede MS, Karlsson G, Andersen AH, Pedersen JS, Knudsen BR (2008) Assembly and structural analysis of a covalently closed nano-scale DNA cage. Nucleic Acids Res 36(4):1113–1119

Bernado P, Mylonas E, Petoukhov MV, Blackledge M, Svergun DI (2007) Structural characterization of flexible proteins using small-angle X-ray scattering. J Am Chem Soc 129 (17):5656–5664

Brilot AF, Chen JZ, Cheng A, Pan J, Harrison SC, Potter CS, Carragher B, Henderson R, Grigorieff N (2012) Beam-induced motion of vitrified specimen on holey carbon film. J Struct Biol 177(3):630–637

Campbell MG, Cheng A, Brilot AF, Moeller A, Lyumkis D, Veesler D, Pan J, Harrison SC, Potter CS, Carragher B, Grigorieff N (2012) Movies of ice-embedded particles enhance resolution in electron cryo-microscopy. Structure 20(11):1823–1828

Castaño Díez D, Mueller H, Frangakis AS (2007) Implementation and performance evaluation of reconstruction algorithms on graphics processors. J Struct Biol 157(1):288–295

Chacon P, Moran F, Diaz JF, Pantos E, Andreu JM (1998) Low-resolution structures of proteins in solution retrieved from X-ray scattering with a genetic algorithm. Biophys J 74(6):2760–2775

Cheng Y, Grigorieff N, Penczek PA, Walz T (2015) A primer to single-particle cryo-electron microscopy. Cell 161(3):438–449

De Rosier DJ, Klug A (1968) Reconstruction of three dimensional structures from electron micrographs. Nature 217:130–134

Dong MD, Hovgaard MB, Xu SL, Otzen DE, Besenbacher F (2006) AFM study of glucagon fibrillation via oligomeric structures resulting in interwoven fibrils. Nanotechnology 17 (16):4003–4009

Evans P (2012) Biochemistry. Resolving some old problems in protein crystallography. Science 336(6084):986–987

Faruqi AR, McMullan G (2011) Electronic detectors for electron microscopy. Q Rev Biophys 44 (3):357–390

Fernandez-Moran H (1960) Low-temperature preparation techniques for electron microscopy of biological specimens based on rapid freezing with liquid helium II. Ann N Y Acad Sci 85:689–713

Fischer N, Konevega AL, Wintermeyer W, Rodnina MV, Stark H (2010) Ribosome dynamics and tRNA movement by time-resolved electron cryomicroscopy. Nature 466(7304):329–333

Frank J, Radermacher M, Penczek PA, Zhu J, Li Y, Ladjadj M, Leith A (1996) SPIDER and WEB: processing and visualization of images in 3D electron microscopy and related fields. J Struct Biol 116(1):190–199

Gasperini AAM, Puentes-martinez XE, Balbino TA, Rigoletto TDP, De Sa G, Corre C, Cassago A, Gaziola L, La Torre D, Cavalcanti LP (2015) Association between cationic Liposomes and low molecular weight Hyaluronic acid. Langmuir 31(11):3308–3317

Georgescauld F, Popova K, Gupta AJ, Bracher A, Engen JR, Hayer-Hartl M, Hartl FU (2014) Cell 157(4):922–934

Glaeser RM, Han B, Csencsits R, Killilea A, Pulk A, Cate JHD (2016) Biophysical perspective specimens. Biophys J 110(4):749–755

Glatter O (1977) New method for evaluation of small-angle scattering data. J Appl Crystallogr 10 (OCT1):415–421

Glatter O, Kratky O (1982) Small angle X-ray scattering. Academic Press, London

Gomez SL, Turchiello RF, Jurado MC, Boschcov P, Gidlund M, Figueiredo Neto AM (2008) The nonlinear optical response of human native and oxidized LDL: a new method to quantify their amount in the plasma. Atheroscler Suppl 9(1):154–154

Goswami D, Callaway C, Pascal BD, Kumar R, Edwards DP, Griffin PR (2014) Structure 22 (7):961–973

Grant T, Grigorieff N (2015) Particle cryo-EM using a 2.6 a reconstruction of rotavirus VP6. eLife 4:1–19

Harauz G, van Heel M (1986) Exact filters for general geometry three dimensional reconstruction. Optik 73(4):146–156

Henderson R (2013) Avoiding the pitfalls of single particle cryo-electron microscopy: Einstein from noise. Proc Natl Acad Sci U S A 110(45):18037–18041

Heymann JB, Conway JF, Steven AC (2004) Molecular dynamics of protein complexes from four-dimensional cryo-electron microscopy. J Struct Biol 147(3):291–301

Hu W, Kan Z-Y, Mayne L (2016) Englander. S W Proc Natl Acad Sci U S A 113(14):3809

Hvidt A, Linderstrøm-Lang K (1954) Biochim. Biophys Acta 14(4):574–575

Issman L, Brenner B, Talmon Y, Aharon A (2013) Cryogenic transmission electron microscopy nanostructural study of shed Microparticles. PLoS One 8(12):e83680

Jonić S (2016) Cryo-electron microscopy analysis of structurally heterogeneous macromolecular complexes. Comput Struct Biotechnol J 14:385–390

Kikhney AG, Panjkovich A, Sokolova AV, Svergun DI (2016) DARA: a web server for rapid search of structural neighbours using solution small angle X-ray scattering data. Bioinformatics 32(4):616–618

Klaholz BP, Myasnikov AG, Van Heel M (2004) Visualization of release factor 3 on the ribosome during termination of protein synthesis. Nature 427(6977):862–865

Kostyuchenko VA, Lim EXY, Zhang S, Fibriansah G, Ng T-S, Ooi JSG, Shi J, Lok S-M (2016) Structure of the thermally stable Zika virus. Nature 533(7603):425–428

Kühlbrandt W (2014) The resolution revolution. Science 343(March):1443–1444

Kuijper M, van Hoften G, Janssen B, Geurink R, De Carlo S, Vos M, van Duinen G, van Haeringen B, Storms M (2015) FEI's direct electron detector developments: embarking on a revolution in cryo-TEM. J Struct Biol 192(2):179–187

Kunath W, Weiss K, Sack-Kongehl H, Kessel M, Zeitler E (1984) Time-resolved low-dose microscopy of glutamine synthetase molecules. Ultramicroscopy 13(3):241–252

Laggner P, Degovics G, Muller KW, Glatter O, Kratky O, Kostner G, Holasek A (1977) Molecular packing and fluidity of lipids in human-serum low-density lipoproteins. Hoppe-Seylers Zeitschrift Fur Physiologische Chemie 358(7):771–778

Lengyel JS, Milne JL, Subramaniam S (2008) Electron tomography in nanoparticle imaging and analysis. Nanomedicine 3(1):125–131

Li X, Grigorieff N, Cheng Y (2010) GPU-enabled FREALIGN: accelerating single particle 3D reconstruction and refinement in Fourier space on graphics processors. J Struct Biol 172 (3):407–412

Li X, Mooney P, Zheng S, Booth CR, Braunfeld MB, Gubbens S, Agard DA, Cheng Y (2013) Electron counting and beam-induced motion correction enable near-atomic-resolution single-particle cryo-EM. Nat Methods 10(6):584–590

Lyumkis D, Brilot AF, Theobald DL, Grigorieff N (2013) Likelihood-based classification of cryo-EM images using FREALIGN. J Struct Biol 183(3):377–388

Mao Y, Wang L, Gu C, Herschhorn A, Désormeaux A, Finzi A, Xiang S-H, Sodroski JG (2013) Molecular architecture of the uncleaved HIV-1 envelope glycoprotein trimer. Proc Natl Acad Sci U S A 110(30):12438–12443

Maric S, Lind TK, Lyngsø J, Cárdenas M, Pedersen JS (2017) Modeling small-angle X-ray scattering data for low-density lipoproteins: insights into the fatty Core packing and phase transition. ACS Nano 11(1):1080–1090

Mastronarde DN (2005) Automated electron microscope tomography using robust prediction of specimen movements. J Struct Biol 152(1):36–51

McMullan G, Chen S, Henderson R, Faruqi AR (2009) Detective quantum efficiency of electron area detectors in electron microscopy. Ultramicroscopy 109(9):1126–1143

McMullan G, Faruqi AR, Clare D, Henderson R (2014) Comparison of optimal performance at 300keV of three direct electron detectors for use in low dose electron microscopy. Ultramicroscopy 147:156–163

Merk A, Bartesaghi A, Banerjee S, Falconieri V, Rao P, Davis MI, Pragani R, Boxer MB, Earl LA, Milne JLS, Subramaniam S (2016) Breaking Cryo-EM resolution barriers to facilitate drug discovery. Cell 165:1–10

Meyer DF, Nealis AS, MacPhee CH, Groot PHE, Suckling KE, Bruckdorfer KR, Perkins SJ (1996) Time-course studies by synchrotron X-ray solution scattering of the structure of human low-density lipoprotein during Cu2+−induced oxidation in relation to changes in lipid composition. Biochem J 319:217–227

Milne JLS, Borgnia MJ, Bartesaghi A, Tran EEH, Earl LA, Schauder DM, Lengyel J, Pierson J, Patwardhan A, Subramaniam S (2013) Cryo-electron microscopy – a primer for the non-microscopist. FEBS J 280(1):28–45

Nogales E (2016) The development of cryo-EM into a mainstream structural biology technique. Nat Meth 13(1):24–27

Oliveira CLP (2011) Investigating macromolecular complexes in solution by small angle X-ray scattering. In: Chandrasekaran DA (ed) Current trends in X-ray crystallography. InTech, Rijeka, pp 367–392

Oliveira CLP, Pedersen JS (2013) Structures of aggregating species by small-angle X-ray scattering. In: Otzen DE (ed) Amyloid fibrils and Prefibrillar aggregates. Wiley-VCH, Weinheim

Oliveira CLP, Behrens MA, Pedersen JS et al (2009) A SAXS study of glucagon fibrillation. J Mol Biol 387(1):147–161

Oliveira CLP, Juul S, Jorgensen HL, Knudsen B, Tordrup D, Oteri F, Falconi M, Koch J, Desideri A, Pedersen JS, Andersen FF, Knudsen BR (2010) Structure of nanoscale truncated octahedral DNA cages: variation of single-stranded linker regions and influence on assembly yields. ACS Nano 4(3):1367–1376

Oliveira CLP, Monteiro AM, Figueiredo Neto AM (2014a) Structural modifications and clustering of low-density lipoproteins in solution induced by heating. Braz J Phys 44(6):753–764

Oliveira CLP, Santos PR, Monteiro AM, Figueiredo Neto AM (2014b) Effect of oxidation on the structure of human low- and high-density lipoproteins. Biophys J 106(12):2595–2605

Otzen D (2011) Protein-surfactant interactions: a tale of many states. Biochimica Et Biophysica Acta-Proteins and Proteomics 1814(5):562–591

Pedersen JS, Flink JM, Dikov D, Otzen DE (2006) Sulfates dramatically stabilize a salt-dependent type of glucagon fibrils. Biophys J 90(11):4181–4194

Penczek PA, Frank J, Spahn CMT (2006) A method of focused classification, based on the bootstrap 3D variance analysis, and its application to EF-G-dependent translocation. J Struct Biol 154(2):184–194

Petoukhov MV, Svergun DI (2005) Global rigid body modeling of macromolecular complexes against small-angle scattering data. Biophys J 89(2):1237–1250

Petoukhov MV, Svergun DI (2013) Applications of small-angle X-ray scattering to biomacromolecular solutions. Int J Biochem Cell Biol 45(2):429–437

Ramírez-Sarmiento CA, Baez M, Zamora RA, Balasubramaniam D, Babul J, Komives EA, Guixé V (2015) Biophys J 108(9):2350–2361

Ren G, Rudenko G, Ludtke SJ, Deisenhofer J, Chiu W, Pownall HJ (2010) Model of human low-density lipoprotein and bound receptor based on CryoEM. Proc Natl Acad Sci U S A 107 (3):1059–1064

Rey M, Yang M, Burns KM, Yu Y, Lees-Miller SP (2013) Schriemer. D C Mol Cell Proteomics MCP 12(2):464–472

Rohou A, Grigorieff N (2015) CTFFIND4: fast and accurate defocus estimation from electron micrographs. J Struct Biol 192(2):216–221

Sasaki K, Dockerill S, Adamiak DA, Tickle IJ, Blundell T (1975) X-ray analysis of glucagon and its relationship to receptor-binding. Nature 257(5529):751–757

Scheres SHW (2014) Beam-induced motion correction for sub-megadalton cryo-EM particles. elife 3:e03665

Scheres SHW, Chen S (2012) Prevention of overfitting in cryo-EM structure determination. Nat Methods 9(9):853–854

Scheres SHW, Gao H, Valle M, Herman GT, Eggermont PPB, Frank J, Carazo J-M (2007) Disentangling conformational states of macromolecules in 3D-EM through likelihood optimization. Nat Methods 4(1):27–29

Scorsato V, Lima TB, Righetto GL, Zanchin NIT, Brandão-Neto J, Sandy J, Pereira HD, Ferrari ÁJR, Gozzo FC, Smetana JHC, Aparicio R (2016) Sci Rep 6:30813

Selmer M, Dunham CM, Murphy FV, Weixlbaumer A, Petry S, Kelley AC, Weir JR, Ramakrishnan V (2006) Structure of the 70S ribosome complexed with mRNA and tRNA. Science 313(5795):1935–1942

Semenyuk AV, Svergun DI (1991) GNOM – a program package for small-angle scattering data-processing. J Appl Crystallogr 24:537–540

Sigworth FJ (2016) Principles of cryo-EM single-particle image processing. Microscopy 65 (1):57–67

Sirohi D, Chen Z, Sun L, Klose T, Pierson TC, Rossmann MG, Kuhn RJ (2016) The 3.8 Å resolution cryo-EM structure of Zika virus. Science 352(6284):467–470

Smith MTJ, Rubinstein JL (2014) Beyond blob-ology. Science 345(6197):617–619

Solovyova AS, Nollmann M, Mitchell TJ, Byron O (2004) The solution structure and oligomerization behavior of two bacterial toxins: pneumolysin and perfringolysin O. Biophys J 87 (1):540–552

Song H, Olsen OH, Persson E, Rand KDJ (2014) Biol Chem 289(51):35388–35396

Stewart PL (2017) Cryo-electron microscopy and cryo-electron tomography of nanoparticles. Wiley Interdiscip Rev Nanomed Nanobiotechnol 9(2):e1417

Suloway C, Pulokas J, Fellmann D, Cheng A, Guerra F, Quispe J, Stagg S, Potter CS, Carragher B (2005) Automated molecular microscopy: the new Leginon system. J Struct Biol 151(1):41–60

Sun Y, Oseliero Filho PL, Oliveira CLP (2017) α-Lactalbumin and sodium dodecyl sulfate aggregates: denaturation, complex formation and time stability. Food Hydrocoll 62:10–20

Svergun DI (1997) Restoring three-dimensional structure of biopolymers from solution scattering. J Appl Crystallogr 30(2):792–797

Svergun DI (1999) Restoring low resolution structure of biological macromolecules from solution scattering using simulated annealing. Biophys J 76(6):2879–2886

Svergun DI, Petoukhov MV, Koch MHJ (2001) Determination of domain structure of proteins from X-ray solution scattering. Biophys J 80(6):2946–2953

Svergun DI, Koch MHJ, Timmins PA, May RP (2013) Small angle X-ray and neutron scattering from solutions of biological macromolecules. Oxford University Press, Oxford

Taylor KA, Glaeser RM (1974) Electron diffraction of frozen, hydrated protein crystals. Science 186(4168):1036–1037

Tiroli AO, Tasic L, Oliveira CLP, Bloch C, Torriani I, Farah CS, Ramos CHI (2005) Mapping contacts between regulatory domains of skeletal muscle TnC and TnI by analyses of single-chain chimeras. FEBS J 272(3):779–790

Tria G, Mertens HDT, Kachala M, Svergun DI (2015) Advanced ensemble modelling of flexible macromolecules using X-ray solution scattering. IUCrJ 2:207–217

Tuukkanen AT, Kleywegt GJ, Svergun DI (2016) Resolution of ab initio shapes determined from small-angle scattering. IUCrJ 3:440–447

Vahidi S, Bi Y, Dunn SD, Konermann L (2016) Proc Natl Acad Sci U S A 113(9):2412–2417

van Heel M (1984) Multivariate statistical classification of noisy images (randomly oriented biological macromolecules). Ultramicroscopy 13:165–184

van Heel M (1987) Angular reconstitution: a posteriori assignment of projection directions for 3D reconstruction. Ultramicroscopy 21(2):111–123

van Heel M (2013) Finding trimeric HIV-1 envelope glycoproteins in random noise. Proc Natl Acad Sci U S A 110(45):E4175–E4177

van Heel M, Frank J (1981) Use of multivariate statistics in analysing the images of biological macromolecules. Ultramicroscopy 6(1):187–194

van Heel M, Schatz M (2005) Fourier shell correlation threshold criteria. J Struct Biol 151 (3):250–262

van Heel M, Harauz G, Orlova EV, Schmidt R, Schatz M (1996) A new generation of the IMAGIC image processing system. J Struct Biol 116(1):17–24

van Heel M, Gowen B, Matadeen R, Orlova EV, Finn R, Pape T, Cohen D, Stark H, Schmidt R, Schatz M, Patwardhan A (2000) Single-particle electron cryo-microscopy: towards atomic resolution. Q Rev Biophys 33(4):S0033583500003644

Van Heel M, Portugal R, Rohou A, Linnemayr C, Bebeacua C, Schmidt R, Grant T, Schatz M (2012a) Chapter 19. 9. Four-dimensional cryo-electron microscopy at quasi-atomic resolution: IMAGIC 4D. Int Tables Crystallgraphy F:624–628

van Heel M, Portugal R, Rohou A, Linnemayr C, Bebeacua C, Schmidt R, Grant T, Schatz M (2012b) Four-dimensional cryo-electron microscopy at quasi-atomic resolution: IMAGIC 4D. Int Table Crystallog F:624–628

van Heel M, Portugal RV, Schatz M (2016) Multivariate statistical analysis of large datasets: single particle electron microscopy. Open J Stat 6(4):701–739

Vestergaard B, Groenning M, Roessle M, Kastrup JS, van de Weert M, Flink JM, Frokjaer S, Gajhede M, Svergun DI (2007) A helical structural nucleus is the primary elongating unit of insulin amyloid fibrils. PLoS Biol 5(5):1089–1097

Voet D, Voet JG, Pratt CW (2005) Fundamentals of biochemistry: life at the molecular level, 2nd edn. Wiley, New York/Chichester

Walters BT, Mayne L, Hinshaw JR, Sosnick TR, Englander SW (2013) Proc Natl Acad Sci U S A 110(47):18898–18903

Walther D, Cohen FE, Doniach S (2000) Reconstruction of low-resolution three-dimensional density maps from one-dimensional small-angle X-ray solution scattering data for biomolecules. J Appl Crystallogr 33:350–363

Wang Z, Hryc CF, Bammes B, Afonine PV, Jakana J, Chen D-H, Liu X, Baker ML, Kao C, Ludtke SJ, Schmid MF, Adams PD, Chiu W (2014) An atomic model of brome mosaic virus using direct electron detection and real-space optimization. Nat Commun 5:4808

Wassenaar TA, van Dijk M, Loureiro-Ferreira N, van der Schot G, de Vries SJ, Schmitz C, van der Zwan J, Boelens R, Giachetti A, Ferella L, Rosato A, Bertini I, Herrmann T, Jonker HRA, Bagaria A, Jaravine V, Guntert P, Schwalbe H, Vranken WF, Doreleijers JF, Vriend G, Vuister GW, Franke D, Kikhney A, Svergun DI, Fogh RH, Ionides J, Laue ED, Spronk C, Jurksa S, Verlato M, Badoer S, Dal Pra S, Mazzucato M, Frizziero E, Bonvin AMJJ (2012) WeNMR: structural biology on the grid. J Grid Comput 10(4):743–767

Worrall LJ, Hong C, Vuckovic M, Deng W, Bergeron JRC, Majewski DD, Huang RK, Spreter T, Finlay BB, Yu Z, Strynadka NCJ (2016) Near-atomic-resolution cryo-EM analysis of the salmonella T3S injectisome basal body. Nature 540(7634):597–601

Zanphorlin LM, Lima TB, Wong MJ, Balbuena TS, Minetti CASA, Remeta DP, Young JC, Barbosa LRS, Gozzo FC, Ramos CHIJ (2016) Biol Chem 291(36):18620–18631

Zheng SQ, Palovcak E, Armache J, Verba KA, Cheng Y, Agard DA (2017) MotionCor2: anisotropic correction of beam-induced motion for improved cryo-electron microscopy. Nat Publ Gr 14:4–5